The design of quantum dots and their conjugates as luminescent probes for analyte sensing

A thesis submitted in fulfilment of the requirements for the degree of

DOCTOR OF PHILOSOPHY

Of

RHODES UNIVERSITY

By

OLUWASESAN ADEGOKE

November 2013

DEDICATION

To my wife:

Mrs Aderonke Latifat Adegoke

and children:

Paul and Elizabeth Adegoke

and father:

Professor Gabriel Olaniran Adegoke

ACKNOWLEDGMENTS

"To everything there is a season, and a time to every purpose under the heaven"

Ecclesiastes 3:1

Firstly, I would like to thank God Almighty for the strength, enablement, wisdom, and intuitive understanding he granted onto me during the entire course of this project.

My sincere appreciation goes to my supervisor, Distinguished Prof Tebello Nyokong for believing in me and granting me the opportunity to carry out my PhD research under your supervision.

My dearest appreciation goes to my wife. You were indeed a God sent help meet. To my children, Elizabeth and Paul Adegoke, you were a source of blessing and encouragement. To my father Prof Gabriel Adegoke, many thanks for your support and fatherly care. You were indeed always there for us as a family.

I also express my gratitude to my host (Dr. Eugeny Ermilov and Dr Michael Höpfner) at the Charité - Universitätsmedizin, Institut für Physiologie, Berlin, Germany for your support during my stay in Berlin.

To all S22 colleagues, I wish you well. You will always be remembered. Also appreciated is the Chemistry department of Rhodes University, all staff members and postgraduate students.

Financial support from the Department of Science and Technology (DST)/MINTEK Nanotechnology Innovation Centre (NIC) sensor is gratefully acknowledged.

ABSTRACT

The design and applications of quantum dots (QDs) as fluorescent probes for analyte sensing is presented. Cadmium based thiol-capped QDs were employed as probe for the detection of analytes. Comparative studies between core CdTe and core-shell CdTe@ZnS QDs showed that the overall sensitivity and selectivity of the sensor was dependent on the nature of the capping agent and the QDs employed, hence making CdTe@ZnS QDs a more superior sensor than the core.

To explore the luminescent sensing of QDs based on the fluorescence "turn ON" mode, L-glutathione-capped CdTe QDs was conjugated to 4-amino-2,2,6,6-tetramethylpiperidine-N-oxide (4AT) to form a QDs-4AT conjugate system. The QDs-4AT nanoprobe was highly selective and sensitive to the detection of bromide ion with a very low limit of detection. Subsequently, metallo-phthalocyanines (MPcs) were employed as host molecules on the surface of QDs based on the covalent linking of the QDs to the MPc. Elucidation of the reaction mechanism showed that the fluorescence "turn ON" effect of the QDs-MPc probe in the presence of the analyte was due to axial ligation of the analytes to the Pc ring. Studies showed that the type of substituent attached to the MPc ring influenced the overall sensitivity of the probe. Additionally, a comparative investigation using newly synthesized phthalocyanine and triaza-benzcorrole complexes was conducted when these complexes were conjugated to CdSe@ZnS QDs for analyte sensing. Results showed that the triaza-benzcorrole complex can be employed as a host-molecule sensor but displayed a lower sensitivity for analyte sensing in comparison to the phthalocyanine complex.

CONTENT

LIST OF ABBREVIATIONS

•OH	=	Hydroxyl radical
4-AT	=	4-amino-2,2,6,6-tetramethylpiperidine-N-oxide
ASA	=	Acetylsalicylic acid
BSA	=	Bovine serum albumin
CNT	=	Carbon nanotubes
DFT	=	Density functional theorem
DMEM	=	Dulbecco's modified Eagle medium
DMF	=	Dimethylformamide
DMSO	=	Dimethyl sulfoxide
DPPH$^{\bullet}$	=	2,2-Diphenyl-1-picrylhydrazyl
DPPH-H	=	2,2-Diphenyl-1-picrylhydrazine
EDC	=	1-Ethyl-3-(3-dimethylaminopropyl)-carbodiimide
EDTA	=	Ethylenediaminetetraacetic acid
Eff	=	FRET efficiency
EPR	=	Electron paramagnetic resonance
FI	=	Fluorescence intensity
FRET	=	Förster resonance energy transfer
GSH	=	L-glutathione
HOMO	=	Highest occupied molecular orbital
HTDC	=	2-Hydroxyethyldithiocarbamate
L-cys	=	L-Cysteine
LOD	=	Limit of detection
LUMO	=	Lowest unoccupied molecular orbital
MAA	=	2-mercaptoacetic acid

MeOH	=	Methanol
MES	=	2-mercaptoethane sulphonic acid
MIP	=	Molecularly imprinted polymer
MPA	=	3- mercaptopropionic acid
MPc	=	Metallo-phthalocyanines
MSA	=	Mercaptosuccinic acid
NHS	=	N-hydroxysuccinimide
NIR	=	Near infra-red
$O_2^{\bullet-}$	=	Superoxide anion radical
ODE	=	1-octadecene
$ONOO^-$	=	Peroxynitrite anion
PBS	=	Phosphate buffered solution
Pc	=	Phthalocyanines
PMMA	=	Polymethylmethacrylate
Por	=	Porphyrin
QD	=	Quantum dot
RB	=	Rhodamine B
ROS	=	Reactive oxygen specie
TBHP	=	t-butylhydroperoxide
TFA	=	Trifluoroacetic acid
TGA	=	Thioglycolic acid
THF	=	Tetrahydrofuran
TOPO	=	Trioctylphophine oxide
XRD	=	X-ray powder diffraction

List of Symbols

τ_1	=	Longer lifetime
τ_2	=	Shorter lifetime
τ_3	=	Shortest lifetime
F	=	Fluorescence intensity
K_S	=	Static-Volmer quenching rate constant (static)
K_{sv}	=	Stern-Volmer quenching rate constant (dynamic)
α	=	Non-pheripheral position
β	=	Peripheral position
Φ_F	=	Quantum yield

LIST OF FIGURES

LIST OF SCHEMES

LIST OF TABLES

1. INTRODUCTION

This chapter provides a general overview of semiconductor quantum dots with emphasis on their synthesis, composition, surface chemistry, structural characterization and their reported applications as fluorescent-based sensors.

The synthesis of metallo-phthalocyanines and their conjugation to quantum dots to form nanoconjugates and the possible use of the conjugates is presented.

1.1. Quantum dots

The present technological age is witnessing an explosion of research in biotechnology, engineering and nanoscale science. Nanomaterials are basic building blocks for modern technological and scientific research. As the size of the organic or inorganic material becomes smaller on the nanometer scale, their electronic and optical properties vary largely from those of bulk materials, hence, they become size or shape dependent **[1]**. These properties of nanomaterials are the key to the success of nanoscience and nanotechnology. A particular type of semiconductor nanostructure that has found distinct applications in many areas is known as quantum dot (QD). QDs are semiconductor nanocrystals that exhibit unique electronic and optical properties that depend on the phenomenon known as "quantum confinement". The quantum confinement effect refers to the confinement of energetic levels to discrete values which results from the increase in the bandgap and decrease of the nanocrystal size to few nanometers. This effect enables the energy gap to be tuned with changes in the QDs size while the band-gap energy depends on the size and composition of the QDs. QDs are known to be zero dimentional and exhibit well separated and discrete quantized energy states due to their smaller number of atoms compared to bulk materials. During synthesis, the growth of the QDs is evident by an increase in its emission and absorption band to the lower energy region of the electromagnetic spectrum. Each aborption and emission band of a QD corresponds to a particular size of the QDs. The fluorescence of the QDs can be tuned from the UV to the far infra-red region. QDs are typically made up of a core of a semiconductor material and they are usually coated with a

shell of another semiconductor which exhibits wider band gap energies **[2-4].** QDs were first synthesized in 1982 for applications as probes for investigating surface kinetics **[5].** QDs core are usually composed of elements of groups II and VI of the periodic table, e.g., CdTe, CdHg, CdSe and CdS or groups III and V, e.g., InP, InAs and GaAs, while the shell material is typically ZnS (mostly used). The diameter of a typical QD is about 2 – 10 nm **[6].** The properties of semiconductor QDs are known to be unique when compared with fluorescent dye molecules. Organic dye molecules, despite their widespread availability in different colours and small size, are known to suffer from several limitations such as: broad fluorescence emission spectra, small Stokes shifts, narrow excitation spectra and photobleaching. Due to these limitations, organic dye molecules are less attractive for sensitive imaging and sensing applications. QDs on the other hand, have exceptional optical properties in comparison to organic dyes and these include: strong resistance to photobleaching, brighter fluorescence, size-dependent tunable emission and absorption in the visible and near infra-red (NIR) regions, narrow emission and broad absorption spectra and large and multiphoton absorption cross sections **[1,7-14].** Fig. 1.1 shows a representative size-tunable absorption and fluorescence spectra of CdTe QDs (used as an example).

1.1.1. Applications of QDs

Due to their unique properties, QDs have found myriad applications in a wide range of fields. They are exceptionally suitable for cellular assays, immunolabeling, live cell markers, in situ hybridization and as non-specific fluorescent stainers, etc, **[15-**

17]. The ability to excite several QDs at the same wavelength enables the opportunity for multiple applications which include: high-throughput screening of biological samples **[18]**. For example, multiple QDs labels can be used for optical bar coding **[19]**. Several groups have also employed QDs in Förster resonance energy transfer (FRET) technologies particularly when conjugated to biological molecules **[20,21]**, fluorescent dyes **[22]**, enzymes **[23],** organic compounds **[24]** and antibodies **[25].** QDs conjugates have been used in monitoring protein interactions **[26,27],** optical sensing **[28,29]** and imaging **[30,31].** Other applications of QDs includes: gene technology **[32],** pathogen and toxin detection **[33],** location of tumour **[34]** and detection of ions, organic compounds and biomolecules **[35-37].** Fig. 1.2 shows a representative schematic of the versatility of QD applications in different areas of science.

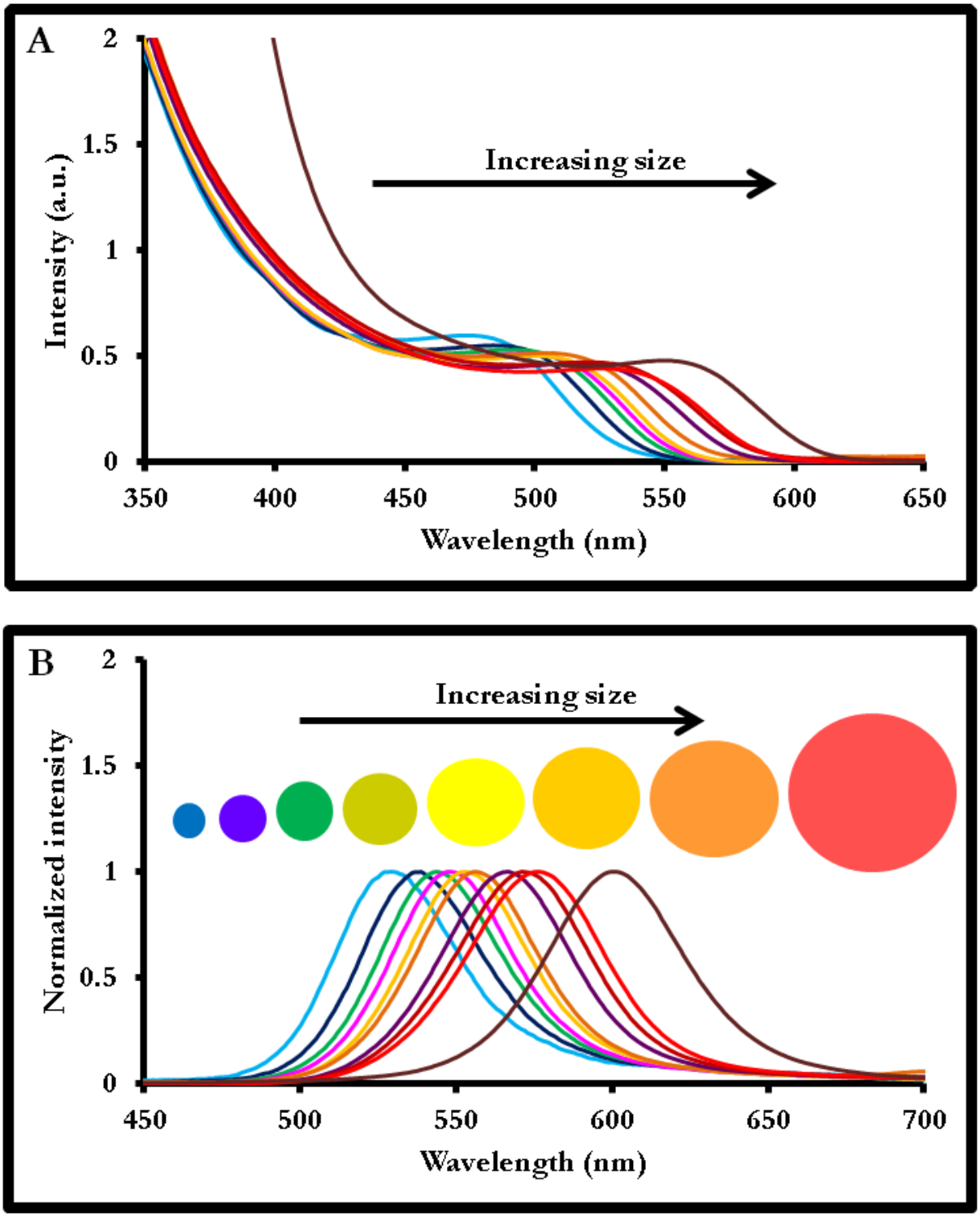

Fig. 1.1. Size-dependent absorption (A) and fluorescence emission (B) spectra of CdTe QDs [unpublished work].

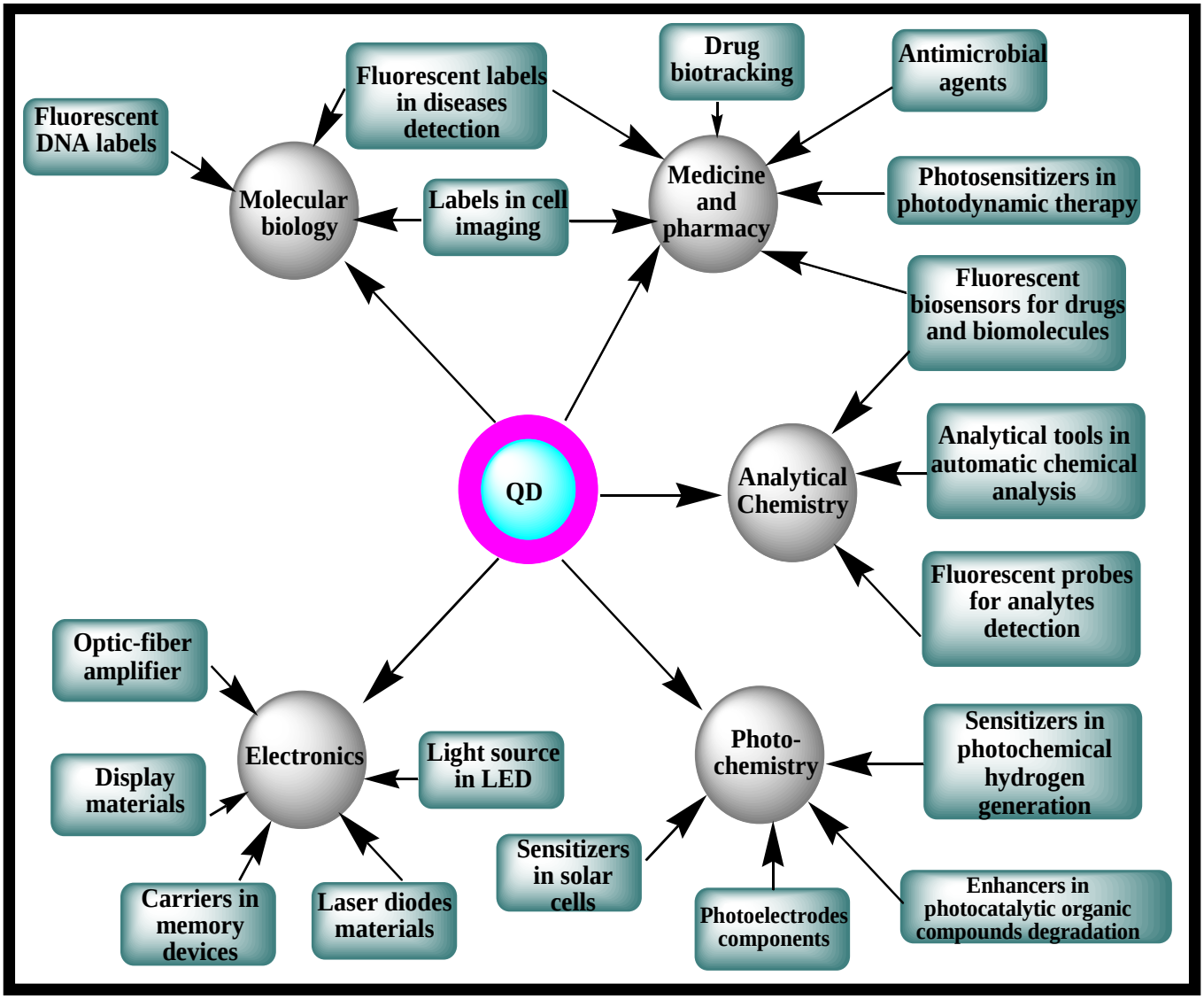

Fig. 1.2. The versatile applications of QDs in different facets of science [18].

1.1.2. Synthesis of water-soluble QDs

There are several methods reported in literature for synthesizing QDs with various properties in order to meet specific applications. To obtain water-soluble QDs required for chemical and biological applications, the two most frequently used methods includes: hydrothermal and organometallic synthetic routes **[38].** There are two major ways of obtaining water-soluble QDs via hydrothermal synthesis. The first involves the use of a cathode stripping electrode **[39]** containing the precursor

solution and a thiolated ligand under basic condition. The resultant QDs nuclei are formed in the presence of the thiolated bifunctional ligand and this results in the colour change of the electrolyte from colourless to red brown. The second approach (which was employed in this work) involves generating the QDs precursor (e.g. Te) in the presence of a reducing agent (e.g. $NaBH_4$) which is then mixed with another precursor (Cd) in the presence of a thiolated ligand under basic conditions **[40]**. Both procedures require the QD to grow at a temperature between 80 – 100 ^oC. In general, hydrothermal synthetic routes for QDs are much simpler, reproducible and can be scaled up. But often the QDs exhibits lower fluorescence quantum yields (Φ_F) and crystallinity.

To date, more than 70% of QDs reported in literature have been synthesized via the organometallic route which utilizes pyrolysis of organometallic precursors in organic solvents at a high boiling temperature (typically between 250 – 300 ^oC). It is known that high quality QDs are manufactured using this method. A hydrophobic surfactant is usually coated on the surface of the QDs resulting in the production of hydrophobic nanocrystals. In practice, these hydrophobic QDs are made water-soluble by several methods **[41].** For biological application, most of the methods rely on ligand exchange (Fig. 1.3) in which the hydrophobic coating is replaced with a hydrophilic ligand and thus enabling water solubility of the nanocrystal **[41,42].**

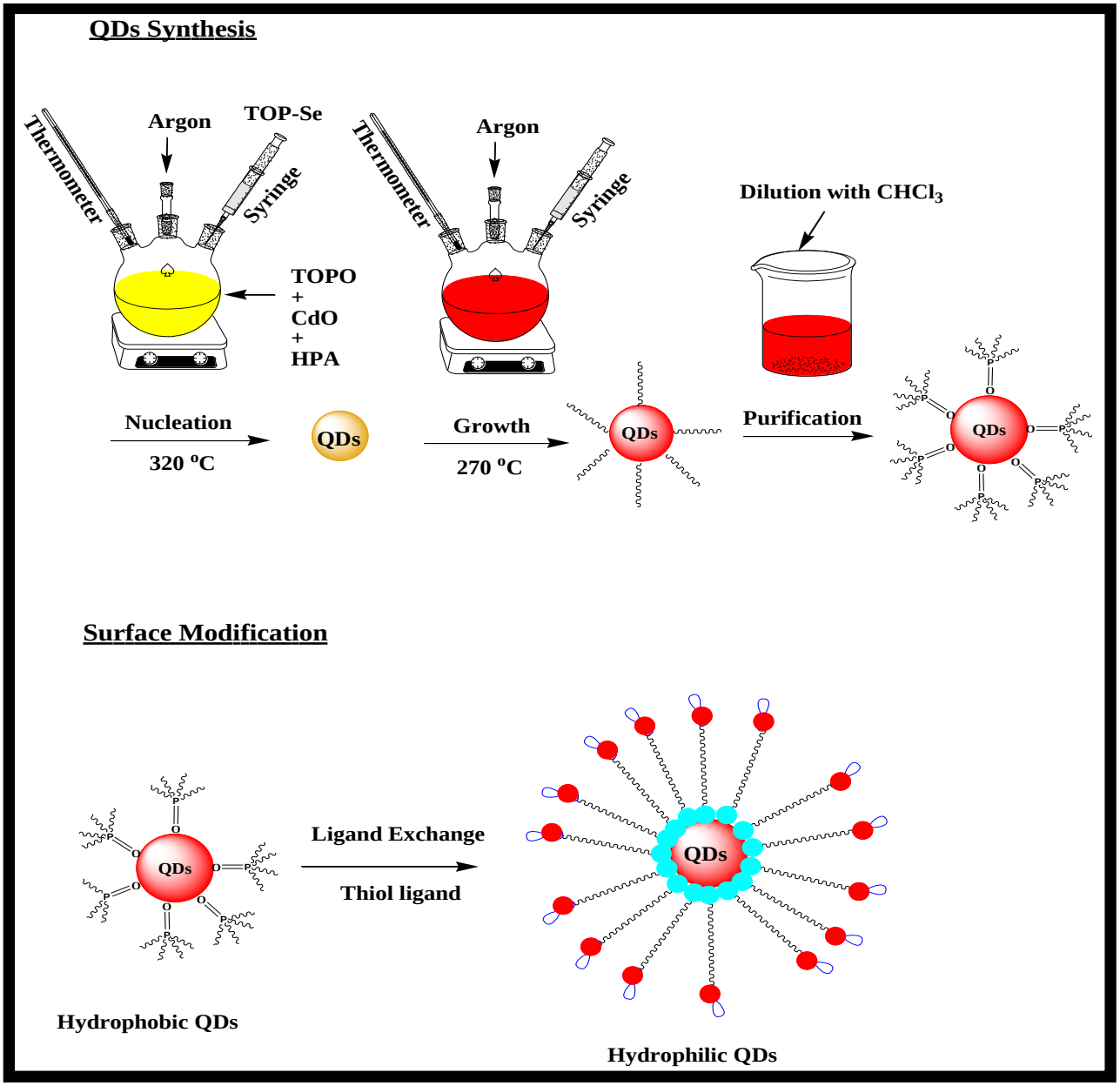

Fig. 1.3. Representation of a typical synthesis of QDs via the organometallic route and surface modification to obtain water-solubility. TOPO: Trioctylphosphine oxide; HPA: Hexylphosphonic acid.

Other molecules like organic dendrons, peptides, phospholipid block-copolymer micelles, copolymers with acrylic acids, dithiothretol and pyridine-modified polyethylene glycol have also been anchored onto the QDs surface to obtain water-

soluble nanocrystals **[41,43-46].** However, the transfer of hydrophobic QDs to hydrophilic QDs usually results in a drastic decrease in the fluorescence quantum yield of the QDs. This is presumably due to chemical reaction of water with surface states, a process which results in surface traps for conduction-band electrons. Hence, an efficient balance between the properties of the capping agent associated with the QDs and its effect on the photophysical properties of the nanocrystal need to be maintained to produce high quality QDs.

In this work, hydrothermal and organometallic synthetic routes were employed in manufacturing the QDs.

1.1.3. Core vs core-shell QDs

Core nanocrystal QDs have been extensively used in a variety of applications. In fact, most of the QDs probes reported in literature to date are mostly made up of core QDs. However, in terms of properties, they are of less quality compared to their core-shell counterparts for two major reasons: The first is that, core QDs are highly reactive as a result of their large surface area to volume ratio. This limitation results in an unstable structure which is highly prone to severe photochemical degradation **[47]**. Secondly, blinking and emission irregularities are examples of imperfections posed by the crystalline structure of the core QDs which results in switching between fluorescent and non-fluorescent states even under continuous illumination **[48].** Also, for core QDs it is difficult to obtain high quality near infra-red emitting QDs which are suitable for specific biological applications. The most commonly used core QDs are CdTe, CdS, ZnS and CdSe.

Core-shell QDs on the other hand are known to be highly stable and preferable to their core counterparts. The growth of the shell reduces the number of surface dangling bonds which is known to reduce the fluorescence quantum yield of the QD by acting as trap states for charge carriers **[49-50].**

In this work, both core CdTe and core-shell CdTe@ZnS and CdSe@ZnS are employed and their sensitivity and selectivity towards detection of analytes are studied.

1.1.4. Fluorescence quantum yield (Φ_F) and lifetime (τ_F)

The fluorescence quantum yield is usually employed as a tool in confirming the quality of individual QDs. Qu and Peng **[51]** have reported that the stoichiometric ratio of precursors, the composition of QDs and reaction time were important parameters that influenced the Φ_F of QDs. Also, it has been reported that as the particle radius increases, the Φ_F of visible emitting ZnO QDs decreased **[52].** In general, the coating of shell of wider bandgap energy on the core QDs has been extensively employed as a means of improving the Φ_F of QDs **[53].**

On the other hand, fluorescence lifetime measurements of QDs are usually used to elucidate interactions between the QDs and an analyte. τ_F values are known to be dependent on the structure, size of QDs, solvent and type of capping on the QDs **[54-57]**. QDs normally have decay lifetimes between 20 – 100 ns depending on the type of QDs **[9]**. They are also known to decay monoexponentially, biexponentially or triexponnetially, depending on the nature of the QD **[54,58,59]**. Wu *et al.*, **[54]** demonstrated that unfunctionalized CdS QDs decayed monoexponnentially while

their functionalized counterpart decayed biexponentially. In general, the coating of a shell on the core QDs is known to prolong the lifetime of the QDs **[48].**

1.1.5. The use of QDs in fluorescence sensing

Since the luminescence properties of QDs are very sensitive to their surface states, it is expected that upon interaction with an analyte, the QDs surface responds to changes in the efficiency of the electron-hole recombination **[60].** It is on this basis that several QDs optical-based sensors have been developed by exploiting either fluorescence enhancement or quenching modification strategies. Herein an overview on QDs probes which has been used to detect different classes of analytes is presented.

1.1.5.1. Fluorescence quenching

The fluorescence of QDs is drastically quenched through different mechanisms of interaction with the analyte. The fundamental principle of fluorescence quenching of QDs is as follows: upon excitation of QDs at a specific wavelength, electrons are promoted from the valence band to the conduction band. This results in the formation of free electrons in the conduction band and positively charged holes in the valence band of the QDs. Under appropriate conditions, the electron and hole will recombine leading to fluorescence. Upon interaction of the QDs with an analyte, the electron-hole recombination will be suppressed which leads to fluorescence quenching **[61,62].**

Quenching effect is also commonly observed in conventional QD-FRET systems in which several probes have been developed. This involves energy transfer from the QDs (which act as a donor) to an acceptor molecule, which is then accompanied by a decrease in the fluorescence of the QDs and a stimulated increase in the fluorescence of the acceptor **[63-65]**.

In general, fluorescence quenching processes, even though they are widely used, are known to be affected by pH, concentration, solvents, temperature, etc **[63]**. These factors, if not addressed or taken into proper consideration could compete with the analyte sensing in the detection system.

Table 1.1 summarizes a selection of analytes detected using CdTe, CdTe@ZnS and CdSe@ZnS QDs. Fluorescent QDs have been extensively utilized in the detection of several metal ions in aqueous solution. For example, Hou and Na employed the use of thioglycolic acid (TGA)-capped CdTe QDs for the detection of vanadium ion. They proposed that electron transfer from TGA to vanadium ion enabled the latter to bind to the QDs surface and thus facilitate the fluorescence quenching process for its detection **[66].** QDs-based sensors for Zn^{2+}, Ni^{2+} and Cu^{2+} have also been reported **[67,68]**, Table 1.1. QDs probes for the detection of other ions have been reported **[69-76].** Fluorescent QDs have also been used for the sensing of cardiolipin, vitamin B_6, nitro compounds, DNA and *Escherichia coli* etc **[77-81]**, Table 1.1. Other QDs-based fluorescence quenching sensor includes the detection of C_{60} **[82],** cholesterol **[83]**, peanol **[84]**, carnitine **[85]**, rifampicin **[86]**, ractopamine **[87],** lapochol **[88]**, glucose **[89]** and roxithromycin **[90]**, Table 1.1.

Table 1.1. A selection of CdTe, CdTe@ZnS and CdSe@ZnS QDs-based fluorescent probes for the detection of various anlytes.

QD type	QD capping or molecule attached	Analyte	Measuring signal	Ref
CdTe	TGA	V(V)	Fluorescence quenching	66
CdTe	TGA	Zn^{2+}, Mn^{2+}, Ni^{2+} and Co^{2+}	Fluorescence quenching/enhancement	67
CdTe	MPA	Cu^{2+}	Fluorescence quenching	68
CdTe	L-cysteine	Cardiolipin	Fluorescence quenching	77
CdTe	TGA	Vitamin B_6	Fluorescence quenching	78
CdTe	L-cysteine	Trinitrotoluene	Fluorescence quenching	79
CdSe@ZnS	Nucleic acid	DNA	Fluorescence quenching	80
CdSe@ZnS	Colistin	*Escherichia coli*	Fluorescence quenching	81
CdSe@ZnS	Calix[8]arene	C_{60}	Fluorescence quenching	82
CdSe@ZnS	MAA	Cholesterol	Fluorescence quenching	83
CdSe@ZnS	[a]PMMA	peanol	Fluorescence quenching	84
CdSe@ZnS	cysteine	Carnitine	Fluorescence quenching	85
CdTe@ZnS	GSH	Rifampicin	Fluorescence quenching	86
CdTe@ZnS	[b]MIP	ractopamine	Fluorescence quenching	87
CdTe	MPA	Lapachol	Fluorescence quenching	88
CdTe	GSH	glucose	Fluorescence quenching	89
CdTe	MPA	roxithromycin	Fluorescence quenching	90

CdSe	**ME**	**Ca^{2+}**	**Fluorescence enhancement**	**91**
CdS	**TGA**	**Melanine**	**Fluorescence enhancement**	**92**
CdSe@ZnS	**MAA**	**L-cysteine**	**Fluorescence enhancement**	**93**
CdTe	**S-βCD-MUA**	**Acetylsalicylic Acid**	**Fluorescence enhancement**	**94**
CdSe	**p-sulfonatocalix(n)arene**	**Phenylamine and methionine**	**Fluorescence enhancement**	**95**
CdTe	**CNT**	**H5N1 DNA**	**Fluorescence enhancement**	**96**
CdTe	**Neutral red**	**BSA**	**Fluorescence enhancement**	**97**
CdTe@CdS	**Glycophosphate**	**Cu^{2+}**	**Fluorescence enhancement**	**98**
CdSe@CdS	**Dithizone**	**Pb^{2+}**	**Fluorescence enhancement**	**24**
CdSe@ZnS	**Graphene oxide**	**Pb^{2+}**	**Fluorescence enhancement**	**99**
CdTe	**Spiky-Au**	**Anti-Neospora**	**Fluorescence enhancement**	**37**
CdTe	**Praseodymium(III)-rutin**	**DNA**	**Fluorescence enhancement**	**100**
CdTe	**Fluorescein isothiocyanate**	**Cd^{2+}**	**Fluorescence enhancement**	**101**

[a]Molecularly imprinted polymer
[b]2-Hydroxyethyldithiocarbamate
[c]Polymethylmethacrylate
TGA = Thioglycolic acid
MPA = 3- Mercaptopropionic acid
GSH = L-glutathione
MAA = Mercaptoacetic acid
ME = Mercaptoethanol
S-βCD-MUA = 11-[(Ethoxycarbonyl)mercapto]undecanoyl-β-cyclodextrin
CNT = Carbon nanotubes
BSA = Bovine serum albumin

1.1.5.2. Fluorescence enhancement

Fluorescence enhancement effect of QDs in luminescent sensor technology involves the activation of the non-radiative electron/hole recombination pathway of the QDs fluorescence in the presence of an analyte **[73]**. QDs sensors based on fluorescence enhancement are more difficult to develop and have been reported less in literature. They are more advantageous because factors which could compete with the detection system of a QD quenching sensor are less effective here. They can be classified into two main categories. The first involves analytes which interact directly with the QDs surface (without the QD being mixed, conjugated electrostatically or covalently to any molecule). Reports on this system are very few. Fluorescence sensing depends extensively on the chemical nature of the analyte and its interaction with the QDs surface.

For example, Mahmoud *et al* **[91]** (Table 1.1), interacted Ca^{2+} directly with the surface of 2-mercaptoethanol-capped CdSe QDs and developed a sensor based on the ability of Ca^{2+} to enhance the fluorescence of the QD. They proposed that the sensor works on the ability to form an analyte-capping ligand complex on the surface of the QD.

Wang *et al* **[92]**, Table 1.1, demonstrated in their work that melanine could directly enhance the fluorescence of TGA-capped CdS QDs. Hence, a sensor was developed for melanine. They proposed that the fluorescence enhancement process was due to the surface passivation of the surface states of the QDs by amine groups of melanine.

Detection of L-cysteine based on direct fluorescence enhancement has been reported using MAA-caped QDs **[93],** Table 1.1**.** The use of QDs as fluorescent sensors for the detection of drug and drug metabolites has been reported by Algarra et al., **[94].** 11-

[(Ethoxycarbonyl)mercapto]undecanoyl-β-cyclodextrin modified CdTe QDs was synthesized and employed for the detection of acetylsalicylic acid (ASA) **[94]**. The fluorescence enhancement process was based on the ability of ASA to form an inclusion complex with the QD.

The second classification of QDs sensors based on fluorescence enhancement involves analyte which interact with a QD bonded to a molecule or biomolecule of interest. In most cases, the molecule or biomolecule quenches the fluorescence of the QD and an analyte is introduced which restores the fluorescence in a concentration-dependent manner. This type of sensing is reported in this work.

Several QDs have been bonded to various molecules or biomolecules for the fluorescence enhancement sensing of specific analytes and this includes but not limited to: p-sulfonatocalix(n)arene (n =4 and 6) for the detection of phenylamine and methionine **[95],** carbon nanotubes for the detection of H5N1 DNA **[96]**, neutral red for the detection of bovine serum albumin **[97]**, glycophosate for the detection of Cu^{2+} **[98],** dithizone **[24]** and graphene oxide **[99]** for the detection of Pb^{2+}, gold nanoparticle for the detection of anti-*Neospora* antibodies **[37**], praseodymium(III)-rutin complex for detection of double-strand DNA **[100]**, and fluorescein isothiocyanate for the detection of Cd^{2+} **[101],** Table 1.1**.**

Some of the analytes detected in this work (as will be discussed later) have not been reported before for any QDs probe while those detected in this work and reported in literature were improved upon based on their detection sensitivity. Fluorescence enhancement sensing process of the QDs using phthalocyanines (Pcs) have not been reported before and it is therefore reported in this thesis.

1.1.6. QDs to be employed in this work

The QDs employed in this work were all water-soluble and cadmium-based. They were selected due to their wide applications in the chemical and biological fields and excellent fluorescence properties. The core QD used in this work is CdTe while the core-shell QDs used are CdTe@ZnS and CdSe@ZnS. The capping agents used in this work are thiol-based and are: thioglycolic acid (TGA), 3-mercaptopropionic acid (MPA) and L-glutathione (GSH). Fig. 1.4 shows the list of the QDs employed in this work. Thiol ligands were employed in this work to functionalize the QD surface because of their popularity in providing the greatest affinity to the QD surface compared to other functional groups **[102]**. The thiol ligands used have either an amino or carboxylic functionality which were employed for conjugation as will be discussed later. The QDs have been reported previously in literature but were re-synthesized in this work with slight modifications as will be presented later.

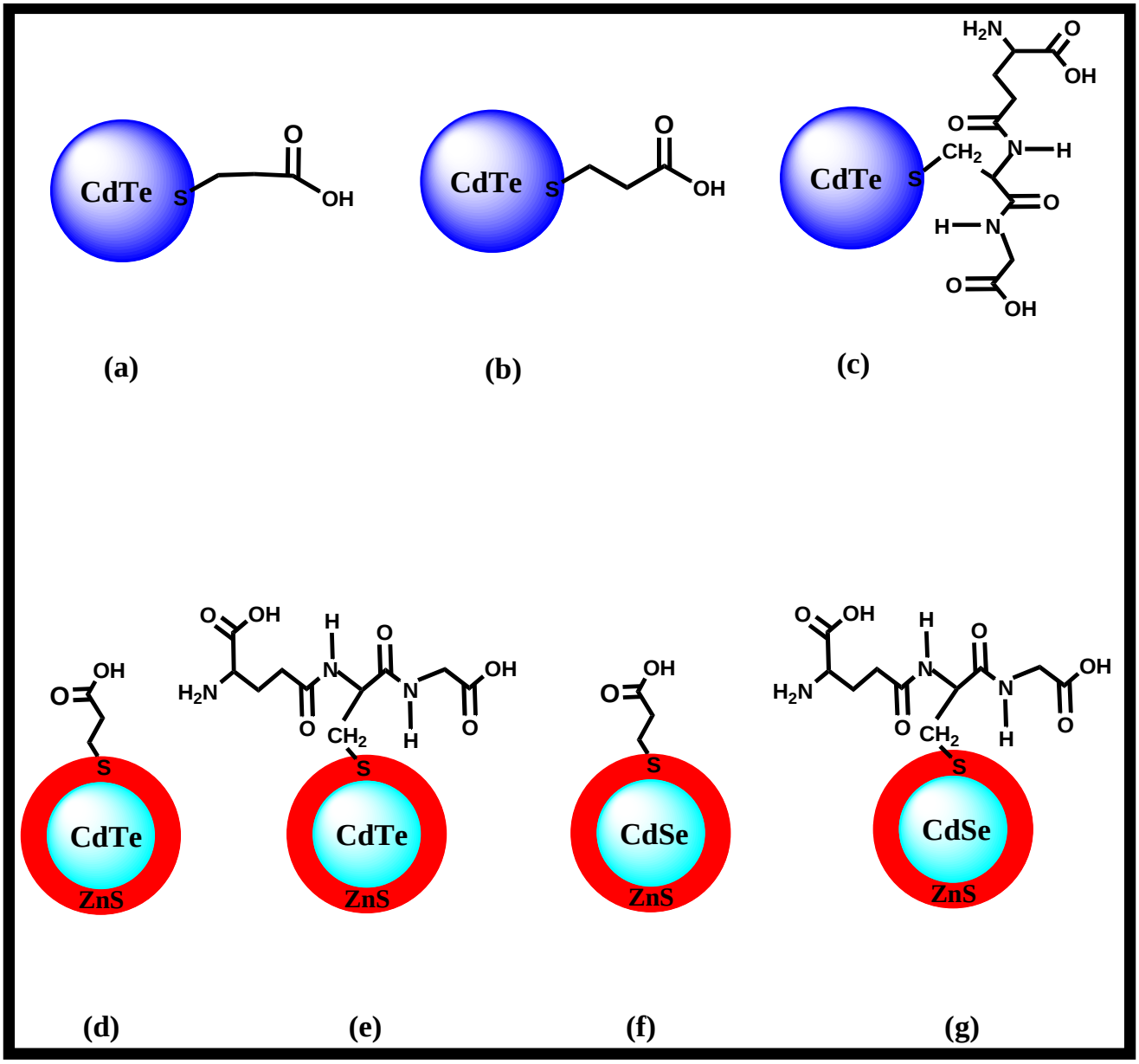

Fig. 1.4. List of QDs employed in this work. (a) TGA-CdTe, (b) MPA-CdTe, (c) GSH-CdTe, (d) MPA-CdTe@ZnS, (e) GSH-CdTe@ZnS, (f) MPA-CdSe@ZnS and (g) GSH-CdSe@ZnS respectively.

Sub-aim of the thesis

The aim of the thesis is to:

1. Employ the use of CdTe, CdTe@ZnS or CdSe@ZnS QDs (with or without conjugation) for the fluorescence sensing of analytes. Also, a comparative study on their sensitivity and selectivity will be carried out.

2. To link QDs phthalocyanines and related molecules for application as fluorescent-based sensors.

1.2. Use of 4-amino-2,2,6,6-tetramethylpiperidine-N-oxide (4AT) in sensing

4-Amino-2,2,6,6-tetramethylpiperidine-N-oxide (4AT) belongs to the class of nitroxyl free radicals which are often referred to as prefluorescent or profluorescent nitoxides because they are known to be effective quenchers of the fluorescence of pendent organic fluorophores **[103,104].** Profluorescent nitoxides have been studied for over 20 years and have been employed as sensors for free radical generation in polymer films **[105]**, cationic metals **[106]**, singlet oxygen in plants **[107]**, nitric oxide **[108]**, hydroxyl radical ($HO^{\bullet}$) **[109],** superoxide anion radical ($O_2^{\bullet -}$) **[110]** and antioxidants **[111].** 4AT has been reported to quench the fluorescence of CdSe QDs [**112,113**] and the possibility of using QDs-4AT as a sensor has previously been proposed **[113]**. Hence, Xu *et al.,* [**114**] reported the use of QDs-4AT for the fluorescence sensing of GSH. In this work, QDs-4AT conjugate was employed as a fluorescence probe for anion sensing for the first time.

1.3. Metallo-phthalocyanines

Phthalocyanines (Pcs) have attracted a great deal of interest in several fields of science and technology due to their numerous properties which arises from their electronic delocalization and extensive heteroaromatic π-conjugation. Their optical, electronic, structural and catalytic properties have induced applications in photovoltaic and solar cells, electrophotography, Langmuir-Blodgett films, molecular electronics, electrochromic display devices, photosensitizers, liquid crystals, optical disks, low-dimentional conductors and gas sensing **[115-124].** Pcs are two-dimensional 18 π-electron aromatic porphyrin synthetic analogues which are made up of four isoindole subunits linked together through nitrogen atoms (Fig. 1.5).

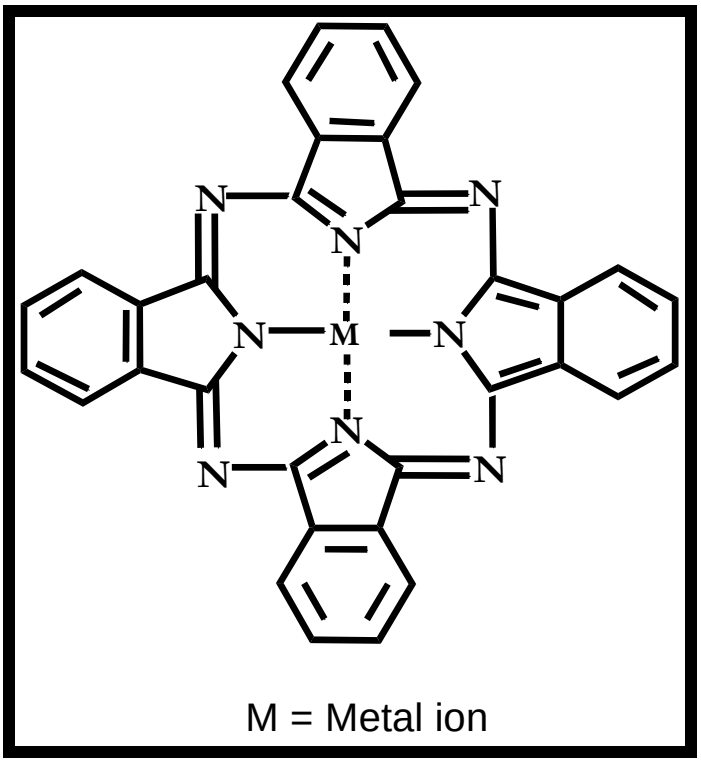

Fig. 1.5. General structure of phthalocyanine.

The chemical flexibility of Pcs and their metallo-phthalocyanine (MPc) derivatives enables the synthesis of a large variety of complexes containing different substituents (either axial, α-non-pheripheral or β-peripheral substitution). Also, the ability to incorporate up to 70 different metal ions into the Pc ring is a unique advantage in optimizing its physical responses which enables the design of a wide range of accessible chemical structures, capable of meeting specific needs **[125]**.

Properties which makes Pcs/MPcs significantly attractive is their high molar absorptivity, long triplet lifetimes with high triplet quantum yields (depending on the central metal), resistance to chemical and photochemical degradation and emission and absorption in the near infra-red region of the electromagnetic spectrum **[126]**.

1.3.1. Spectral behaviour

Fig. 1.6 shows the UV/vis spectrum of a typical MPc. The spectral region between 300 - 800 nm for Pcs has been grouped into two different regions based on theoretical calculations **[127]**. For a typical Pc (Fig. 1.6), the peak observed in the region 300 – 350 nm is recognized as the B-band (consisting of two bands) while the peak absorbing in the visible region 650 – 670 nm is known as the Q-band **[128].** The B-bands correspond to the a_{2u} to e_g and a_{2u} to e_g transitions while the Q-band has been reported to be due to excitation between the ground state a_{1u} highest occupied molecular orbital (HOMO) to e_g lowest unoccupied molecular orbital (LUMO) as decribed by Gouterman's four orbital model **[129].** In a vast number of Pcs, the Q-band is the most resolved and intense absorption band. The high molar extinction

coefficient (~ 10^5 L mol^{-1} cm^{-1}) of the Q-band is the basis of the depth of colour and purity of phthalocyanines. Unmetallated Pcs usually display a split Q-band as a result of their lower symmetry while metallated Pcs display a single Q-band in the visible region. This phenomenon is only valid for a symmetrically substituted Pc scaffold. Once the Pc complex is unsymmetrically substituted, the breaking of the symmetry results in the splitting of the Q-band for MPcs **[125]**.

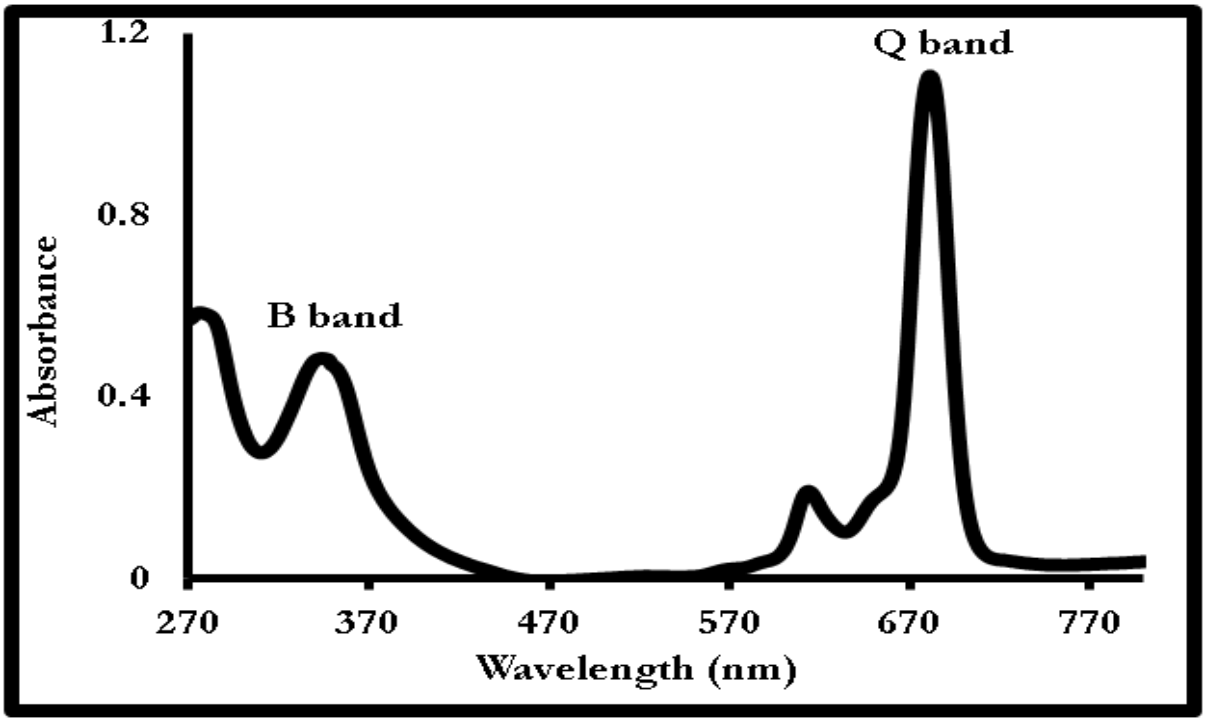

Fig. 1.6. Typical electronic absorption spectrum of metallo-phthalocyanine (unpublished work).

1.3.2. General synthesis of symmetrical and unsymmetrical A_3B type phthalocyanine

The general synthesis of symmetrical substituted Pc involves attachment of the same substituent into the Pc ring which can be achieved by condensation of mono-, di-, or tetra-substituted phthalonitriles to form the corresponding symmetrical tetra-, octa-

or 16-subtituted Pcs **[115].** The symmetrical tetra-substituted MPcs may be synthesized according to Scheme 1.1.

Recently, special attention has been focused on the design of unsymmetrical Pcs. This is because they exhibit better organization capabilities and improved physicochemical properties with valuable applications in photodynamic therapy, materials science, optical signal detection techniques and optical limiting applications **[130].**

Generally, statistical condensation is the most widely used method for the synthesis A_3B-type Pcs. The Pcs bear one different (B) isoindole subunits and three identical (A) subunits which usually affords a mixture of six compounds (Scheme 1.2). The ratios commonly employed are 3:1 and 9:1 which favours the formation of unsymmetrical Pcs (Scheme 1.2), **[131].** Sometimes, a ratio of 10:1 or even 40:1 is usually employed due to the different reactivities of substituents **[132].** Even though this method has been widely used for the formation of A_3B-type Pcs, it is often tedious due to difficulty in separating molecules with similar chemical structures.

Both tetra-substituted and mono-substituted MPcs were employed in this work. However, the use of mono-substituted MPc complexes allows for a more defined conjugation to QDs unlike the tetra-substituted MPc

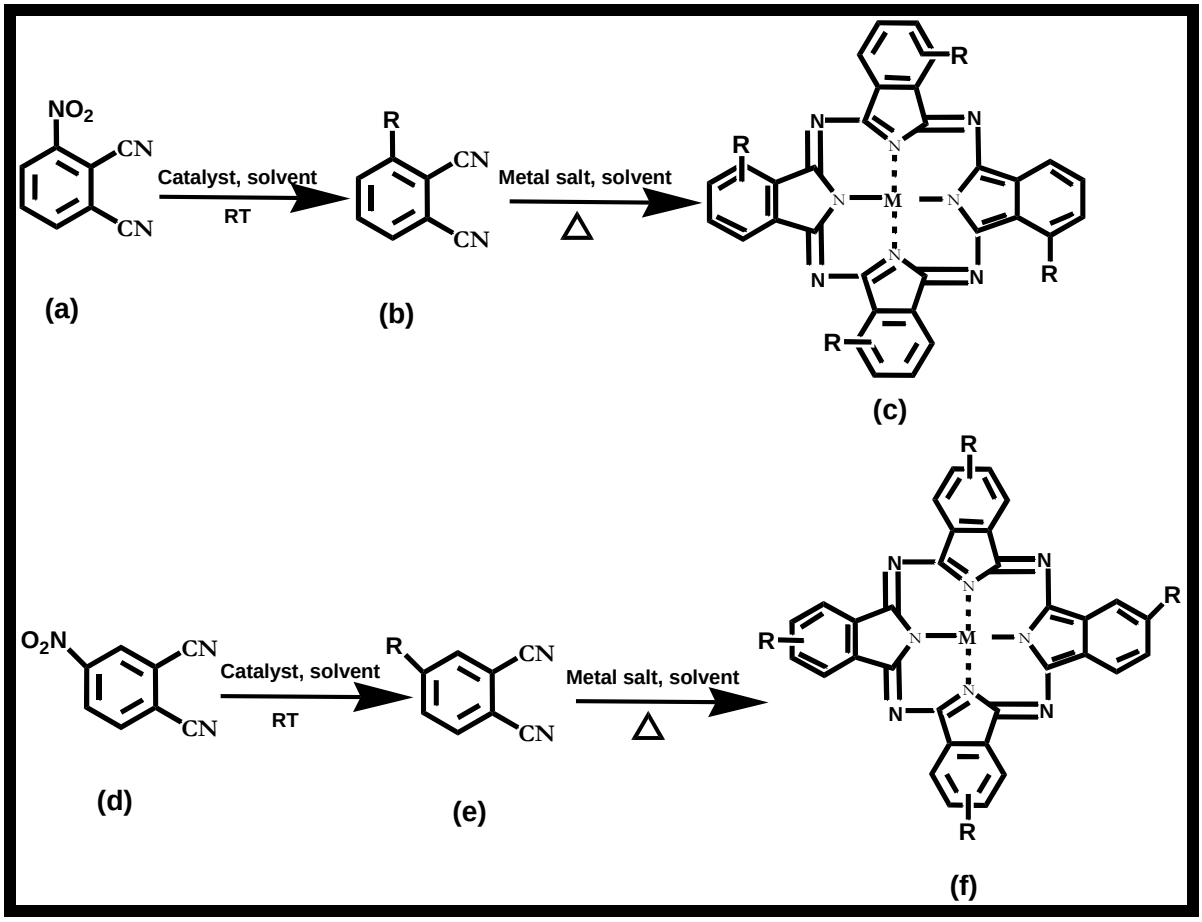

Scheme 1.1. Synthesis of non-peripheral (c) and peripheral (f) tetra substituted MPcs from monosubstituted phthalonitriles (a) and (d).

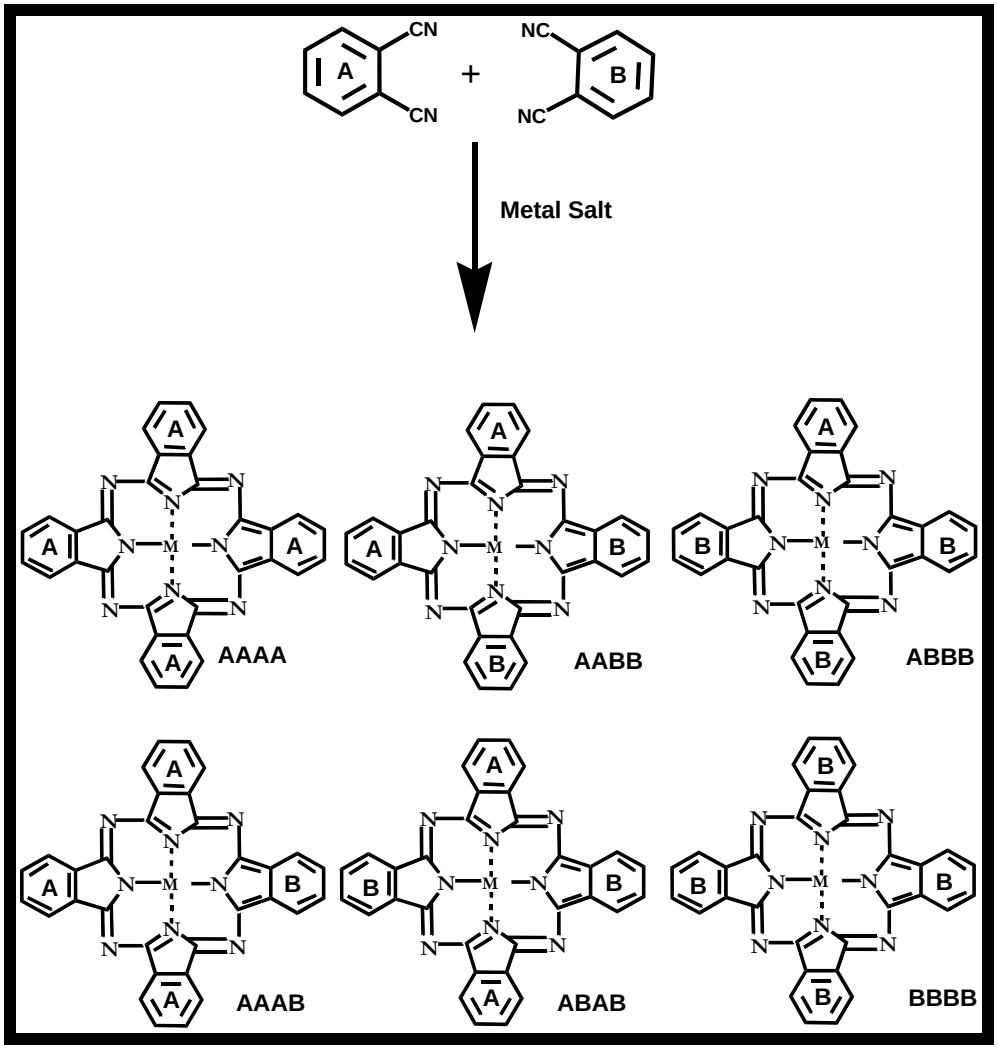

Scheme 1.2. Statistical condensation of two phthalonitriles to give 6 possible Pc structures [131].

1.3.3. Use of phthalocyanine in optical sensing

A number of reports have shown that Pcs can be effectively used as optical sensors. The variation of ring substituents and axial ligands, are known to influence different detection properties for gases **[133].** For example, Vanderkooi *et al*. reported a fluorescence quenching sensor for dioxygen using meso-tetra sulfonated and pyridyl porphyrin derivates **[134]**. A film of NiPc derivatives have been prepared by spin coating and employed as active layers for the detection of pentacholophenol and

semazine using Total Internal Reflection Ellipsometry **[135]**. Other Pc optical sensors include: detection of mercury ion (Hg^{2+}) using zinc tetraamino-phthalocyanine (ZnTAPc)-thymine conjugate **[136]**, monitoring of volatile organic compounds using (OH)CuPc thin films **[137]**, detection of NO_2 using surface plasmon resonance technique with CoPc as an active added layer **[138]** and detection of alcohol vapours using spin-coated films phthalocyanine-porphyrin blend **[139].**

In this work, an attempt was made for the first time in employing both symmetrical and unsymmetrically substituted MPc as fluorimetric sensors when coupled to QDs.

1.3.4. Phthalocyanine and related molecules synthesized in this work

The structures of the phthalocyanines that have been synthesized and used in this work are shown in Fig. 1.7. The synthetic route to obtain the metal tetra-amino phthalocyanines (MTAPc) containing the central metals: (Al (**1**), Co (**2**), Ni (**3**), and Zn (**4**) have been reported in literature **[140].** AlTAPc **(1)** has been reported for use as a fluorimetric sensor **[141,142].** CoTAPc (**2**) and NiTAPc **(3)** have mostly been used in electrocatalysis **[143,144],** while ZnTAPc **(4)** has been studied as photosensitizers **[145,146]** and in optical sensing **[136].** However, in this work, their use as fluorimetric sensors when covalently linked to QDs is reported for the first time.

Unsymmetrical aluminium mono-amino phthalocyanine (AlMAPc **(5**)) and the mono-aminophenoxy phthalocyanine derivative **(**AlMAPPc **(6))** were synthesized in this work for the first time. Similar derivatives of ZnMAPc and ZnMAPPc have previously been synthesized **[146,147].** The substituent was chosen to obtain an amide bond formation with the carboxylic group of the QDs.

Unsymmetrical nickel mono-mercaptosuccinic acid triazatetra-bencorrole (NiMMSATBC (**7**)) (which is characterized by the loss of a bridging nitrogen atom) and phthalocyanine **(**NiMMSAPc **(8))** complexes were also synthesized in this work for the first time and applied in fluorescence sensing application when coupled to QDs as was the case for the other phthalocyanines. The response of the fluorescence sensor with reference to the effects of central metals (Co, Ni or Zn) or the number of substituents (mono or tetra) on the Pc ring will be discussed.

1.3.5. Coating/conjugates of QDs with macrocyclic molecules and their use in optical sensing

The application of host-guest interactions in luminescent sensor technology has led to the use of a range of macrocylic compounds capable of recognizing analytes with excellent specificity. Macrocyclic compounds such as calixarene, cyclodextrin, crown ether and porphyrin (Por) have been conjugated or coated to QDs for sesning **[148].** Coating or conjugation, are two different routes of anchoring the macrocyclic compound onto the surface of the QD as depicted in Scheme 1.3. For the former, it involves synthesizing the QD together with the macrocylic compound with the sole aim of capping the compound directly onto the surface of the QD (Scheme 1.3A) **[149].**

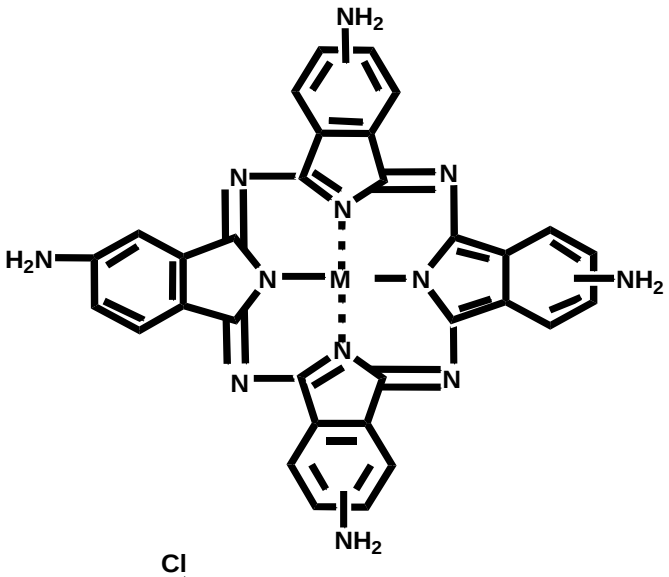

(1) ClAlTAPc: M = Al

(2) CoTAPc: M = Co

(3) NiTAPc: M = Ni

(4) ZnTAPc: M = Zn

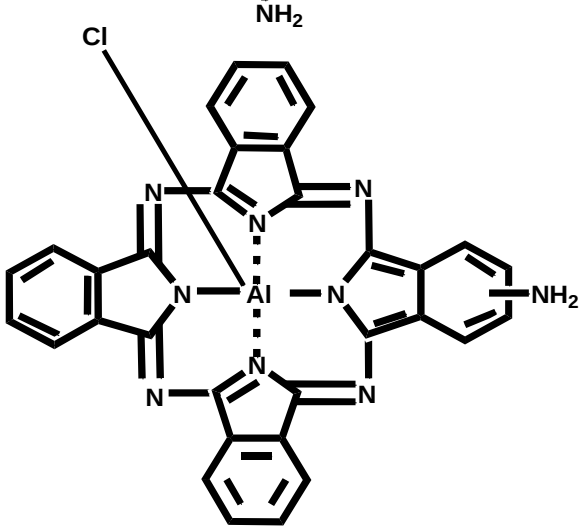

(5)
ClAlMAPc

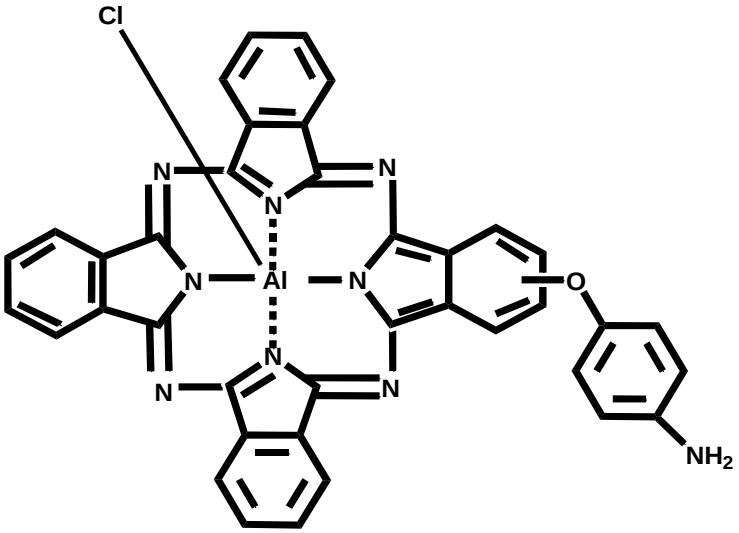

(6)
ClAlMAPPc

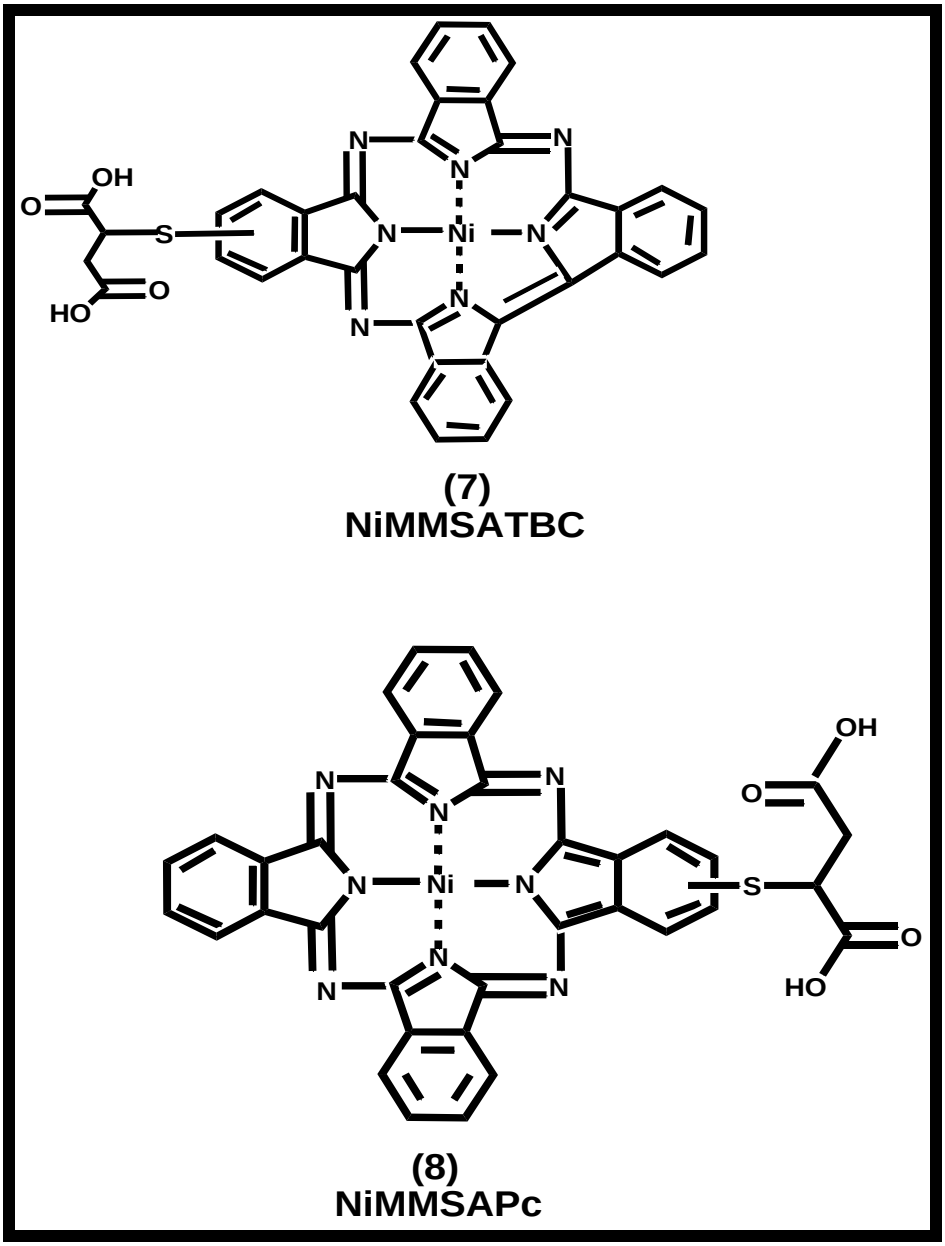

Fig. 1.7. Structure of MPcs used in this work.

Conjugation (which was employed in this work), involves synthesizing the QDs and macrocylic compound separately and covalently linking the two entities via a coupling agent to form an amide bond between the QD and the macrocylic compound **[146],** Scheme 1.3B. The combination of the molecular recognition properties of host molecules with the unique optical properties of QDs has

contributed to the design of sophisticated sensors. Table 1.2 **[94,150-162],** gives a summary of some reported host-molecule coated/conjugated QDs and their applications for analyte sensing. For example, *p*-Sulfonatocalix[4]arene-coated CdSe@ZnS QD was developed to detect acetylcholine **[152]**.

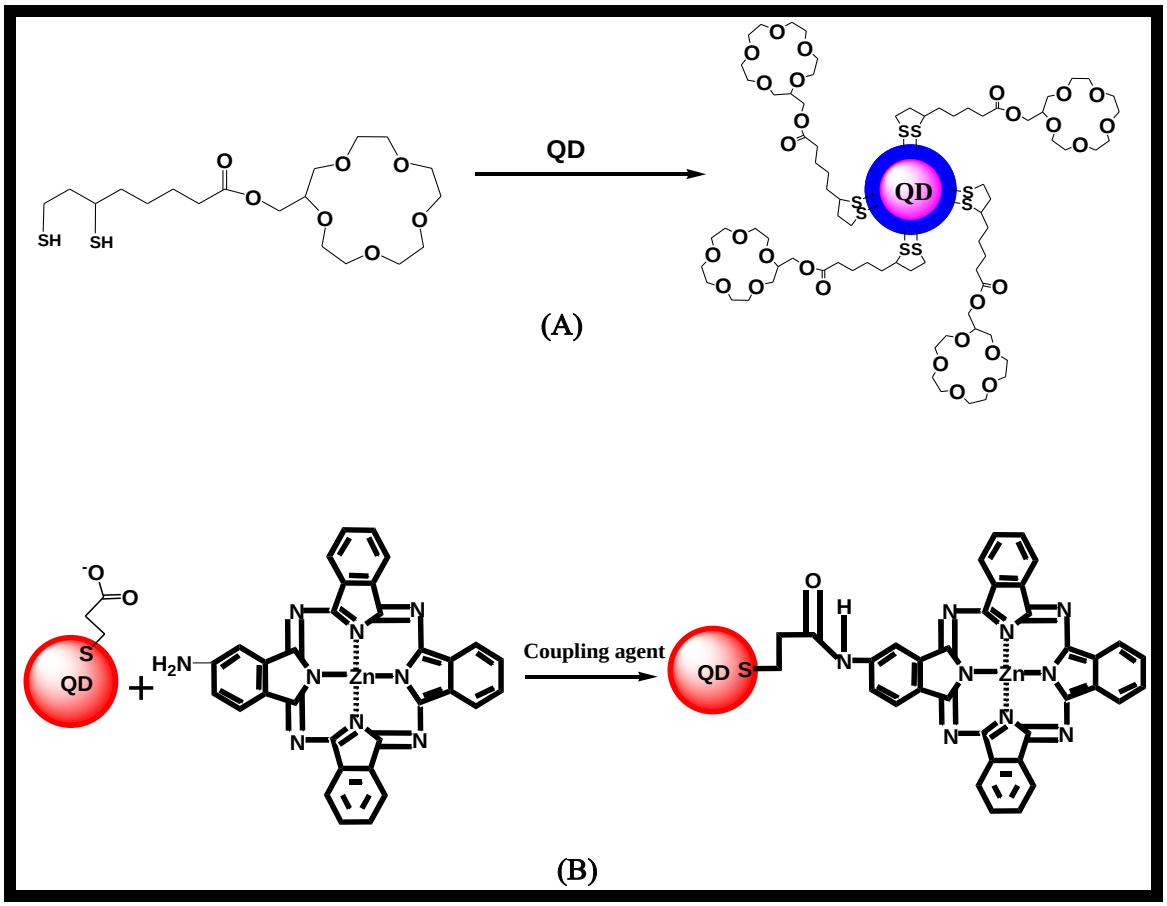

Scheme 1.3. Schematic showing the (A) coating of 15-crown-5 functionalized QD [149] and (B) conjugation of mono-substituted Pc to QD [146].

Table 1.2. Summary of QDs coated with macrocyclic compounds and their sensing systems.

Type of host-molecule coated QDs	Analyte Detected	Measuring signal	REF
β-Cyclodextrin-CdTe QDs	Acetylsalicyclic acid	Fluorescence enhancement	94
15-Crown-5-CdSe@ZnS QDs	K^+	FRET	149
a-Cyclodextrin-CdSe@ZnS QDs	*p*-nitrophenol	Fluorescence quenching	150
β-Cyclodextrin-CdSe@ZnS QDs	1-naphthol	Fluorescence quenching	150
S-calixarene-CdSe@ZnS QDs	Hg^{2+}	Fluorescence quenching	151
p-S-calix[4]arene-CdSe@ZnS QDs	Acetylcholine	Fluorescence quenching	152
calix[4]arene-CdTe@SiO_2 QDs	Methomyl	Fluorescence enhancement	153
calix[4]arene-CdTe@SiO_2 QDs	Anthracene	Fluorescence enhancement	154
calix[7]arene-CdTe@SiO_2 QDs	Pyrene	Fluorescence enhancement	154
p-S-calix[4]arene-CdSe QDs	L-Cysteine	Fluorescence enhancement	155
β-Cyclodextrin-CdSe@ZnS QDs	Anthracene	Fluorescence enhancement	156
β-Cyclodextrin-CdSe@ZnS QDs	*p*-nitrophenol	Fluorescence quenching	157
β-Cyclodextrin-CdSe QDs	$H_2PO_4^-$	Fluorescence quenching	158
[a]*β*-Cyclodextrin-CdTe-RB QDs	Amantadine	FRET	159
1,10-diaza-18-crown-6- QDs	Cd^{2+}	Fluorescence enhancement	160
Pyridyl-Por-CdSe@ZnS QDs	Zn^{2+}	Fluorescence enhancement	161
Mn, Fe, Co-TetraphenylPor-CdSe QDs	Nitric Oxide	Fluorescence quenching	162

[a]RB = Rhodamine B.

It was proposed that the binding of the ammonium cation of acetycholine with calixarene was responsible for the quenching of the fluorescence of the sensor **[152]**. The fluorescence enhancement effect of calix[4]arene coated QDs in the presence of anthracene was reported to be due to the ability of anthracene to induce ordered orientation by enhancing the conformational rigidity of the surface substituent and thereby suppressing the quenched fluorescence **[154]**. Cyclodextrins are also well known for forming inclusion complexes with several analytes due to their unique hydrophilic external surface and hydrophobic internal cavity **[163].** It has been reported that the fluorescence enhancement detection of anthracence using *β*-cyclodextrin modified CdSe@ZnS QDs was attributed to the formation of an efficient and new radiation path involving the modified anthracene-QDs system **[156]**. The sensing of *p*-nitrophenol using *β*-cyclodextrin coated CdSe@ZnS QDs has been reported to occur through electron transfer **[157]**. The electron transfer process was made possible, provided that *p*-nitrophenol binds directly to the receptor sites and thereby act as an electron transfer quencher of the fluorescence of the QD **[157].**

Two differently-sized 15-crown-5 coated CdSe@ZnS QDs were synthesized and employed as a sensor for K^+ **[149]**. It was demonstrated that upon addition of K^+, the two neighbouring QDs were bridged by a sandwich complex between K^+ and 15-crown-5, which resulted in the two QDs coming together in close proximity and thus engaging in FRET **[149]**. Also, the detection of Cd^{2+} using 1,10-diaza-18-crown-6 modified CdS:Mn@ZnS QDs was reported to occur via blocking of the electron transfer processes between the ligand and the QD owing to the complex formation between 1,10-diaza-18-crown-6 and Cd^{2+} **[160].**

Porphyrins belong to the class of heterocylic macrocyles that are characterized by the presence of pyrole subuints which are interconnected at the α carbon atoms through methine bridges **[164].** They are known to bind strongly onto the surface of QDs and thus can influence the optical properties of the QDs towards analyte sensing **[165]**. A classical example is the reported fluorescence enhancement sensor for Zn^{2+} using pyridyl porphyrin coated CdSe QDs **[161],** Table 1.2**.** The sensing mechanism was demonstrated to be due to the coordination of Zn^{2+} with the nitrogen from the pyridyl or pyrole rings **[161].**

The above discussions highlights some of the recent fluorescence sensing systems based on the coating or conjugation of macrocyclic compounds onto the surface of QDs prior to our own approach of incorporating phthalocyanines into the family of macrocyclic compounds bonded onto the surface of QDs for analyte sensing.

Sub-aim of the Thesis

It is important to note that MPcs have a similar structure to the porphyrins and have never been conjugated onto the surface of QDs for fluorescence sensing. Pcs are more stable than porphyrins and hence are employed in this work. We report for the first time in this work the design and applications of MPc-conjugated QDs as luminescent sensor for analyte sensing. Also, an attempt was carried out for the first time by conjugating the QDs to an organic radical (4AT) for use as a luminescent probe for ion sensing.

1.4. Analytes detected in this work

The analytes detected in this work are of the family of reactive oxygen species (ROS), metals ion, halides and amino thiol compounds. Their biological importance is summarized below.

1.4.1. Reactive oxygen species

Oxygen, while undoubtedly essential for life, can also pose destructive effects in tissue and/or impair its ability to function normally **[166]**. ROS such as hydrogen peroxide (H_2O_2), hydroxyl radical ($^{\bullet}OH$), peroxynitrite anion ($ONOO^-$), superoxide anion radical ($O_2^{\bullet-}$) and t-butylhydroperoxide (TBHP) are products of normal cellular metabolism. Based on estimation, it is reported that an average person has around 10,000 – 20,000 ROS attacking each cell body per/day **[167]**. In some cases, ROS are produced in the body to serve specific biological functions while in other cases they are produced as by-products of metabolic processes **[168].** Excessive production of these species in the body is known to induce age-dependent diseases such as arteriosclerosis, cancer, neurodegenerative disorders, oxidative stress and arthritis **[169].** Therefore, there is a need to develop probes capable of detecting ROS with high specificity.

Despite, the numerous analytes that have been detected using QDs, the utilization of QDs using fluorescence technique as a sensitive and selective probe for the detection of ROS has been less explored. Hence, novel probes for the detection of ROS are explored in this work.

1.4.2. Metal ion and halides

Several metal ions pose severe risk to human lives. It is for this reason that a selection of metal ions has been detected using CdTe-based QDs (Table 1.1) but not QDs-MPc conjugates. In this work, QDs-based probes for fluoride ion, bromide ion and mercury ion were developed.

Detection of fluoride ion is important since its excessive intake is of pathological concern and it could induce kidney and gastric disorder as well as dental and skeletal fluorosis **[170,171].** It has also been reported that brominated organic compounds were more toxic and mutagenic when compared with chlorinated ones **[172-174].** Alternatively, the toxicity of mercury in natural waters is a global concern **[175],** hence, its detection is of interest.

The design of a QD-based probe for Br^- is reported in this work for the first time. The use of QD-MPc probes for the detection of F^- and Hg^{2+} are also reported here for the first time.

1.4.3. Amino thiol-containing compounds

QDs probes for amino thiol-containing compounds of cysteamine and L-glutathione (GSH) were developed in this work. Cysteamine is of interest because its developmental and reproductive safety is an important concern for children suffering from cystinosis **[176].** GSH, a known tripeptide, is present in cells of many organisms and its ratio to disulphide is employed as a means for monitoring cellular oxidative stress **[177**], hence, its detection of paramount interest. Also, both have not been detected before using QDs-MPc conjugates.

1.5. Summary of aims of thesis

The aims of this thesis are summarized below:

1. Synthesis and characterization of semiconductor thiol-capped QDs.
2. Synthesis and spectroscopic characterization of MPc complexes.
3. Covalent linking of QDs to MPc complexes and subsequent characterization of the conjugate system.
4. Design and application of QDs (alone) as fluorescence sensor for analyte sensing.
5. Design and application of QDs-MPc and its related nanoconjugate as fluorescence sensor for analyte sensing.
6. Investigation of the efficiency of core and core-shell QDs (alone) towards analyte sensing (a comparative study).
7. Investigation of the effect of central metals on the Pc ring on the overall sensor sensitivity.
8. Investigation of the effect of ring substituents on the Pc ring on the overall sensor sensitivity.
9. Investigation of the efficiency of phthalocyanine and other macrocyclic compound (triazatetra-benzcorrole) towards analyte sensing (a comparative study).
10. Elucidation of the reaction mechanism of QDs-MPc probes towards analyte sensing.

2. EXPERIMENTAL

This chapter provides information on the materials, instrumentation and synthetic procedures used in this work.

2.1. Materials

2.1.1. QDs synthesis

Thioglycolic acid (TGA), mercaptopropionic acid (MPA), L-glutathione (GSH), cadmium chloride hemi-pentahydrate, tellurium powder (200 mesh), sodium borohydride, cadmium oxide, selenium powder, vegetable oleic acid, 1-octadecene and trioctylphophine oxide (TOPO) were obtained from Sigma-Aldrich..

2.1.2. MPc synthesis and conjugation to QDs

Mercaptosuccinic acid (MSA), trifluoroacetic acid (TFA), 1,2-dicyanobenzene, aluminium chloride, urea, sodium sulphide, 1-ethyl-3-(3-dimethylaminopropyl)-carbodiimide (EDC) and N-hydroxysuccinimide (NHS) were obtained from Sigma-Aldrich. 4-Nitrophthalic acid, ammonium chloride and ammonium molybdate were obtained from SAARCHEM.

2.1.3. Solvents and other reagents

Methanol, acetone, tetrahydrofuran (THF), dimethylformamide (DMF), ethanol, ethylenediaminetetraacetic acid (EDTA) and L-ascorbic acid, dulbecco's modified Eagle medium (DMEM), di-sodium hydrogen phosphate, 4-amino-2,2,6,6-tetramethylpiperidine-N-oxide (4AT) and dimethyl sulfoxide (DMSO) were obtained from Sigma-Aldrich.

2.1.4. Analytes

L-Cysteine, cysteamine, 2,2-diphenyl-1-picrylhydrazyl (DPPH•), hydrogen peroxide , t-butyl hydroperoxide (TBHP) were obtained from Sigma-Aldrich. Tris (hydroxyl methyl) amino methane, ferrous ammonium sulphate, sodium nitrite, sodium fluoride, sodium hydroxide, hydrogen chloride, manganese dioxide and salts of different ions: sodium chloride, calcium chloride, potassium chloride, aluminium chloride, iron (III) chloride, manganese chloride, chromium chloride, nickel chloride hexahydrate, zinc chloride, sodium nitrate, sodium sulphate, sodium sulphite, sodium acetate, sodium carbonate, potassium chloride, ammonium fluoride and potassium bromide were obtained from SAARCHEM. Sodium perchlorate hydrate was obtained from BDH chemicals.

All chemicals were of analytical grade and used without prior purification. All solutions were prepared with ultra pure water of resistivity 18.2 mΩ which was obtained from a Milli-Q Water System (Millipore Corp. Bedford, MA, USA). All other reagents were obtained from commercial suppliers and used as received. The experimental buffer solutions used in this work are: 50 mM Tris-HCl pH 7.4 and 10 or 50 mM phosphate buffer solution (PBS), pH 7.4, 9.4 and 12 (depending on the analyte). The pH was adjusted by addition of 0.1 M NaOH or HCl.

2.2. Instrumentation

1. Emission spectra were recorded on a Varian Eclipse spectrofluorimeter. The slit width (each 5 nm) was kept constant for all the experiments.
2. Ground state electronic absorption spectra were recorded on a Shimadzu UV-Vis 2550 spectrophotometer in the range 300-800/900 nm.
3. X-ray powder diffraction patterns were recorded using a Cu kα radiation (λ = 1.5405 Å, nickel filter), on a Bruker D8 Discover equipped with a proportional counter. Scanning was at 10 min^{-1} with a filter time-constant of 2.5 s per step and a slit width of 6.0 nm. The data were obtained in the range from $2\theta = 5^{o}$ to 60^{o}. A zero background silicon wafer slide was used for sample placement. The X-ray diffraction (XRD) data analysis was carried out using Eva (evaluation curve fitting) software. Subtraction of spline fitted to the curved background was used for baseline correction of each diffraction pattern and the full-width at half maximum values was obtained from the fitted curve.
4. A Metrohm Swiss 827 pH meter was used for pH measurements.
5. FT-IR spectra were obtained on a Perkin-Elmer spectrum 100 with universal attenuated total reflectance (ATR) sampling accessory.
6. Thermal gravimetric analysis (TGA) were recorded on a Shimadzu DTG-TG 60H with a gas flow of 120 ml/min and operated under nitrogen atmosphere.
7. Transmission electron microscopy (TEM) images were obtained using a Zeiss Libra TEM 120 model operated at 90 kV.
8. Energy dispersive spectroscopy (EDS) was carried out using an INCA PENTA FET coupled to a VAGA TESCAN using a 20 kV accelerating voltage.

9. ^{1}H nuclear magnetic resonance signals were recorded on a Bruker AMX 400 MHz NMR spectrometer or a Bruker Advance II+ 600 MHz NMR spectrometer.
10. Mass spectral data were collected with a Bruker AutoFLEX III Smart beam TOF/TOF Mass spectrometer. The spectra were acquired using α-cyano-4-hydroxycinnamic acid as the MALDI matrix, and a 355 nm Nd:YAG laser as the ionizing source.
11. Elemental analyses were carried out on a Vario EL III MicroCube CHNS instrument analyzer.
12. Fluorescence lifetime measurements were carried out using a time correlated single photon counting (TCSPC) setup (FluoTime 200, Picoquant GmbH). The excitation source was a diode laser (LDH-P-C-485 with 10 MHz repetition rate, 88 ps pulse width). Fluorescence was detected under the magic angle with a peltier cooled photomultiplier tube (PMT) (PMA-C 192-N-M, Picoquant) and integrated electronics (PicoHarp 300E, Picoquant GmbH). A monochromator with a spectral width of about 4 nm was used to select the required emission wavelength band. A scattering Ludox solution (DuPont) was used to measure the response function of the system and had a full width at half maximum (FWHM) of about 280 ps. To obtain good statistics, the ratio of stop to start pulses was kept low (below 0.05). Measurement of the entire luminescence decay curve (range 0 to 200 ns) was at the maximum of the emission peak. Data analysis was done using the program Fluofit (Picoquant GmbH). Estimation of the decay error times was carried out using the support plane approach.

13. Electron paramagnetic resonance (EPR) measurements were carried out using a Bruker EMX Plus EPR spectrometer, model number: EMP-9.5/12B/P. EPR settings were 0.632 mW for the microwave power, frequency 9.714 GHz, resolution 1024 points, centre field 3460 G and 100 G for the sweep width.
14. Gaussian 03 program using an Intel/Linux cluster was used for density functional theorem (DFT) calculations **[178]**.

2.3. Synthesis of QDs

2.3.1. Synthesis of TGA, MPA and GSH–capped CdTe QDs

Briefly, TGA, MPA and GSH-capped CdTe QDs were prepared via a procedure from the literature with some slight modifications **[179,180]** as follows: in a three-necked flask, 0.85 g (6.8 mmol) tellurium powder and 0.53 g (14.1 mmol) sodium borohydride were mixed with 20 ml of ultrapure Millipore water. The flask was fitted with a septum and the solution deaerated with argon gas and cooled by ice. After 8 h, white sodium tetra borate precipitate was formed at the bottom of the flask and the black Te powder fully disappeared, resulting in the formation of the clear supernatant NaHTe which was separated from the solution and was used as the Te precursor for QDs preparation. The QDs were grown by dissolving 1.0 g (4.4 mmol) $CdCl_2.2.5H_2O$ and 0.92 mL (11.7 mmol) TGA or 1.0 mL (11.5 mmol) MPA or 1.84 g (6 mmol) reduced GSH in ultrapure Millipore water (200 ml). The pH was adjusted to 11 with 1 M NaOH. Freshly prepared NaHTe solution was injected into the N_2-saturated precursor solution. The molar ratio used in our experiment were Cd:Te:TGA (1:1.5:2.7), Cd:Te:MPA (1:1.5:2.6) and Cd:Te:GSH (1:1.5:1.4) repectively.

To obtain QDs of different sizes, aliquots of the reaction mixture were taken at different time intervals for emission and absorption measurements. The resulting products were precipitated with ethanol and the unreacted precursors that did not participate in the reaction were removed via centrifugation at 3000 rpm. The resultant precipitate was re-precipitated with ethanol more than 3 times and dried under vacuum and kept in the dark for further use.

2.3.2. Synthesis of MPA and GSH-capped CdTe@ZnS QDs

The synthesis of CdTe@ZnS QDs was as reported before **[181]** with slight modifications. Briefly, 100 mg of purified TGA-CdTe QDs was added to 100 ml aqueous solution (pH = 8) containing 2 mmol $ZnCl_2$ and the capping ligands (4 mmol GSH or 4 mmol MPA). GSH or MPA were used as both the capping agent and sulphur source for the growth of ZnS shell on the respective CdTe cores. The solutions were heated to 100 ^oC in open-air and refluxed with time to control the sizes of the core-shell QDs. Aliquots of each reaction mixture were taken at different time intervals for emission and absorption measurements. The core-shell QDs were precipitated with ethanol, centrifuged and dried under vacuum.

2.3.3. Synthesis of MPA and GSH-capped CdSe@ZnS QDs

GSH and MPA-capped CdSe@ZnS QDs were synthesized via previously described methods **[182,183]** but with modifications. Briefly, 1.3 g (10.1 mmol) of CdO was added to a mixture of 30 mL oleic acid and 50 mL of octadecene in a three-necked flask. The solution was heated to ~260 ^oC under reflux and maintained under N_2

atmosphere to obtain a clear solution. The temperature of the solution was then lowered to 230 ^{o}C and a solution of Se powder (0.3 g (3.8 mmol) and 0.1 M TOPO in 25 ml of octadecene which was stirred for 24 h to obtain a homogeneous slurry under N_2 atmosphere) was added to the flask. The size of the core CdSe QDs was controlled by further lowering the temperature of the solution. Once the desired size of core CdSe QDs was obtained, solutions of Zn powder (0.407g, 6.2 mmol) in 20 ml oleic acid and 30 ml octadecene and 0.16 g (5.0 mmol) of sulphur powder dissolved in 20 ml oleic acid and 30 ml octadecene were alternatively injected into the TOPO-capped CdSe QDs solution to obtain the TOPO-capped CdSe@ZnS QDs. The QDs were then purified with the addition of methanol followed by acetone. The TOPO-capped CdSe@ZnS QDs are hydrophobic and therefore not suitable for aqueous analyte detection.

Water soluble MPA and GSH-capped CdSe@ZnS QDs were obtained via ligand exchange route. Firstly, MPA-KOH and GSH-KOH methanolic stock solution were prepared by adding 2 mL (23.0 mmol) of MPA or 2 g (6.5 mmol) of GSH separately to 3.0 g of KOH in 40 ml methanol. The purified TOPO-capped CdSe@ZnS QDs were then re-dispersed in chloroform and MPA-KOH or GSH-KOH methanolic solution was subsequently added followed by the addition of Millipore water. The solution was allowed to stir for 1 h. The obtained water-soluble QDs were precipitated out with methanol, washed and centrifuged several times with acetone and dried under vacuum.

2.4. Synthesis of peroxinitrite anion

$ONOO^-$ (an analyte detected in this work) was prepared by the method described previously in literature **[184].** Briefly, an aqueous solution containing freshly prepared 50 mM H_2O_2 (10 mL) and 50 mM $NaNO_2$ (10 mL) were cooled on ice for 30 min. The solution was then mixed vigorously and 1 mM of pre-cooled HCl (10 mL) was added followed immediately by addition of pre-cooled 1.5 mM NaOH (5 mL) to quench the reaction. The solution was stirred for 30 min, and some MnO_2 powder (2 g) was added to the reaction mixture to remove excess H_2O_2. Afterwards, the mixture was filtered and the solution containing $ONOO^-$ was stored at -20 ^{o} C. The concentration of $ONOO^-$ was determined from its absorbance at 302 nm (ε_{302} =1670 M^{-1} cm^{-1}) **[185]**.

2.5. Synthesis of phthalocyanine and related benzcorrole

2.5.1. Synthesis of symmetrical tetra-amono MPc derivatives

Symmetrical tetra-substituted MPc used in this work, are not new, hence, details are not provided. The synthesis of metal-free tetra-amino phthalocyanine (H_2TAPc), AlTAPc (**1**), CoTAPc (**2**), NiTAPc (**3**), and ZnTAPc (**4**) was followed based on previously described method reported in literature **[140].**

Unsymmetrical substituted MPc used in this work were synthesized for the first time and it is thus described below.

2.5.2. Synthesis of aluminium mono-amino phthalocyanine (Scheme 3.1 (Cl)AlMAPc(5))

The preparation of 4-nitrophthalonitrile has previously been described **[186].** Compound **9** was synthesized as follows: a mixture of 4-nitrophthalonitrile (0.25 g, 1.4 mmol) and 1,2-dicyanobenzene (0.55 g, 4.3 mmol) was loaded into a 3-necked round bottom flask and aluminium chloride (0.45 g, 3.4 mmol), DMF (10 ml) and 0.60 g, 10 mmol of urea were added. The reaction was heated up to 180 ^{o}C under argon atmosphere for 1 h and allowed to proceed for the next 24 h under a reduced temperature of 110 ^{o}C with vigorous stirring. The complex was precipitated out with methanol (MeOH) and washed repeatedly using centrifugation with 1 M HCl solution and dried. The product was then purified using silica gel column using MeOH:THF (2:1) solvent mixture as eluent. The desired product was eluted with DMF. Yield: 0.12 g, (54%). UV-Vis (DMF): λ_{max} (nm)(log ε) 670(4.06), 605(3.21), 338(3.63). IR [(ATR) ν_{max}/cm^{-1}] 1568 (NO_2 assym.), 1332 (NO_2 sym.), 1076 – 1119 (C-N), 727 (Al-N). ^{1}H NMR (DMSO-d_6): δ, ppm 9.44-9.66 (6H, m, Ar-H), 8.11-8.52 (8H, m, Ar-H), 7.88-8.05 (1H, m, Ar-H). *Anal.* Calc. for $C_{32}H_{15}N_9O_2ClAl.5H_2O$: C, 54.12; H, 3.52; N, 17.76. Found: C, 54.57; H, 3.66; N, 17.16. MALDI-TOF-MS *m/z:* Calc: 619.48. Found: 621.77 $[M+3]^+$ for $C_{32}H_{15}N_9O_2ClAl$.

AlMAPc **(5**) was prepared by reducing the nitro group of compound **9** using $Na_2S.9H_2O$. Briefly, 0.75 g (3.1 mmol) of $Na_2S.9H_2O$ was dissolved in 40 mL of water and 0.10 g (0.16 mmol) of compound **9** was added and the mixture allowed to stir for 24 h at room temperature. The solid product was separated and washed with 1 M HCl solution, acetone and diethyl ether. The product was further purified using a Phenomenex C_{18} Sep-Pak column using MeOH:THF (2:1) solvent mixture as eluent.

Yield: 0.02 g (9%). UV-Vis (DMF): λ_{max} (nm)(log ε) 674(4.73), 610(4.00), 352(4.39). IR [(ATR) ν_{max}/cm^{-1}] 3387 (NH_2 stretch), 1671 (NH bend), 1065 – 1188 (C-N), 843 (C-H stretch), 723 (Al-N). ^{1}H NMR (DMSO-d_6): δ, ppm 9.69-9.72 (7H, m, Ar-H), 8.46-8.59 (7H, m, Ar-H), 7.96 (1H, s, Ar-H). Anal. Calc. for $C_{32}H_{17}N_9ClAl.6H_2O$: C, 55.05; H, 4.16; N, 18.07. Found: C, 55.82; H, 3.53; N, 17.62. MALDI-TOF-MS m/z: Calc: 589.48. Found: 589.84 $[M+1]^+$ for $C_{32}H_{17}N_9ClAl$.

2.5.3. Synthesis of aluminium mono-amino phenoxy phthalocyanine (Scheme 3.2 (Cl)AlMAPPc(6))

Compound **10** has previously been synthesized and reported **[147].** The synthesis of compound **6** was the same for **9** except that compound **10** (0.5 g 2.1 mmol) and 1,2-dicyanobenzene (0.8 g, 6.4 mmol) were employed. The solid product was separated and washed with 1 M HCl solution, acetone and diethyl ether. The product was then purified using Phenomenex C_{18} Sep-Pak column. A solvent mixture of DMF:THF (10:1) containing a few drops of TFA was used to elute the desired product**.** Yield: 0.06 g (17%). UV-Vis (DMF): λ_{max} (nm)(log ε) 673(4.66). 606(3.89), 345(4.19). IR [(ATR) ν_{max}/cm^{-1}] 3043 (NH_2 stretch), 2927 (C-H), 1661-1601 (NH bend), 1496 (C=C), 1361 (C-O-C), 1009 – 1090 (CN), 832 (C-H stretch), 719 (Al-N). ^{1}H NMR (DMSO-d_6): δ, ppm 9.42-9.62 (2H, m, Ar-H), 8.98-9.33 (4H, m, Ar-H), 7.97-8.56 (11H, m, Ar-H), 7.69-7.74 (2H, d, Ar-H). Anal. Calc. for $C_{38}H_{21}N_9OClAl$: C, 66.91; H, 3.08; N, 18.49. Found: C, 67.65; H, 2.66; N, 18.20. MALDI-TOF-MS m/z: Calc: 681.48. Found: 687.23 $[M+6]^+$ for $C_{38}H_{21}N_9OClAl$.

2.5.4. Synthesis of nickel mono-mercaptosuccinic acid phthalocyanine and benzcorrole

2.5.4.1. Synthesis of 4-mercaptosuccinic acid phthalonitrile (Scheme 3.3 (11))

Compound **11** was synthesized by reacting 4-nitro phthalonitrile (1.5 g, 8.4 mmol) and mercaptosuccinic acid (1.2 g, 8.0 mmol) in 15 mL of dry DMSO at room temperature under Ar atmosphere for 30 min. After this time, K_2CO_3 (4.6 g, 33.3 mmol) was added portion wise for 2 hr. The reaction was allowed to stir and react for 24 h after which the product was washed several times with acetone, chloroform and diethyl ether.

Yield: 2.3 g, (96%). IR [(ATR)ν_{max}/cm^{-1}] 3324 (ν_{OH}), 2235 ($\nu_{C=N}$), 1541-1650 ($\nu_{C=O}$), 1345 (ν_{C-O}), 951 (ν_{C-S-C}). ^{1}H NMR (DMSO-d_6): δ, ppm 10.00 (1H, s, carboxy-H), 9.90 (1H, s, carboxy-H), 8.14 (3H, s, Ar-H), 4.02 (1H, s, methine-H), 2.50 (2H, s, methylene-H).

2.5.4.2. Synthesis of nickel mono-mercaptosuccinic acid triazatetra-benzcorrole (Scheme 3.3 (NiMMSATBC (7))

A mixture of $NiCl_2.6H_2O$ (0.34 g, 1.44 mmol), 4-mercaptosuccinic acid phthalonitrile (**11**) (0.25, 0.90 mmol), 1,2-dicyanobenzene (0.35 g, 2.7 mmol) and urea (0.30 g, 5 mmol) were stirred under Ar atmosphere in 20 mL of DMF at 180 ^oC for 1 h. After this time, the reaction temperature was lowered to 100 ^oC and the reaction was allowed to continue for 24 h. After cooling, the crude solution was washed sequentially with acetone, dichloromethane, hexane, THF:ammonia (1:1), chloroform:acetone (1:1) and diethylether. The desired product was then further purified using a Phenomenex C_{18} Sep-Pak column with a solvent mixture of

chloroform:MeOH (2:1) to remove the undesired product followed by DMF:THF (10:1) with few drops of TFA to elute the desired complex.

Yield: 0.013 g (8%). UV-Vis (DMSO): λ_{max} (nm)(log ε) 673(4.11), 623(3.71), 598(3.66), 456(3.93), 404(3.93). IR [(ATR) ν_{max}/cm^{-1}] 3197 (ν_{OH}), 1532-1666 ($\nu_{C=O}$), 1429 (ν_{C-OH}), 1334 (ν_{C-O}), 916 (ν_{C-S-C}), 755-800 (Ni-N). *Anal.* Calc. for $C_{36}H_{21}N_7O_4SNi.2H_2O$: C, 58.24; H, 3.37; N, 13.21. Found: C, 57.91; H, 3.24; N, 14.98. MALDI-TOF-MS *m/z:* Calc: 705.79. Found: 706.44 $[M]^-$ for $C_{36}H_{21}N_7O_4SNi$.

2.5.4.3. Synthesis of nickel mono-mercaptosuccinic acid phthalocyanine (Scheme 3.3 (NiMMSAPc (8))

The synthesis and purification of **8** was the same for **7** except that the amount of urea used was 1.20 g (20 mmol). The amount of all other reagents used was the same as that used for **7**. The desired product was eluted using a Phenomenex C_{18} Sep-Pak column with methanol:DMF (20:1) and few drops of TFA as eluent. Yield: 0.015 g (9%). UV-Vis (DMSO): λ_{max} (nm)(log ε) 672(4.70), 623(4.50), 588(4.45), 369(4.68). IR [(ATR) ν_{max}/cm^{-1}] 3024 (ν_{OH}), 1584-1649 ($\nu_{C=O}$), 1483 (ν_{C-OH}), 1332 (ν_{C-O}), 956 (ν_{C-S-C}), 752-828 (Ni-N). *Anal.* Calc. for $C_{36}H_{21}N_8O_4SNi.H_2O$: C, 58.55; H, 3.12; N 15.18. Found: C, 58.54; H, 3.23; N, 15.35. MALDI-TOF-MS *m/z:* Calc: 719.79. Found: 720.31 $[M]^-$ for $C_{36}H_{21}N_8O_4SNi$.

2.6. Conjugation

The conjugation procedures described in this section were performed and optimized in separate batches for specific detection of the analytes.

2.6.1. Conjugation of QDs to Pcs (1 – 6) (Scheme 3.4)

The method employed in this work was based on standard procedure described previously in literature for linking Pcs to QDs via an amide bond **[187,188]** but with some slight modification. Briefly, to a solution of QDs (10 mg or 15 mg or 20 mg, depending on the type) in PBS pH 7.4 buffer was added 1 mL of 0.1 M EDC (in water) to activate the carboxylate group of the QDs. The mixture was then stirred for 30 min – 2 h at room temperature, after which a mixture of 0.1 M NHS (in water) and 2 x 10^{-6} M of H_2TAPc, **1**, **3** or **4** in DMF:PBS pH 7.4 (3:2, , v/v), 8.1 x 10^{-6} M of **2** in DMF:PBS pH 7.4 (3:1, v/v) and 3.0 x 10^{-5} M of **5** and **6** in DMF:PBS pH 7.4 (5:1, v/v) were added and the stirring continued for 24 h. The resulting linked QDs-MPc conjugates were precipitated out from solution by the addition of ethanol and centrifuged repeatedly to remove free QDs and also washed repeatedly with DMF to remove free MPc. The QDs-MPc colloid is not soluble in the two solvents. The obtained QDs-MPc nanoconjugates were soluble in PBS buffer as a colloidal solution.

2.6.2. Conjugation of GSH-CdTe QDs to 4AT (Scheme 3.5)

GSH-CdTe QDs was conjugated to 4-amino-2,2,6,6-tetramethylpiperidine-N-oxide (4AT) for the fluorescence detection of bromide ion. The method employed in this

work is an adaptation of the procedure described in reference **[114],** but with some slight modification. Briefly, excess of EDC and NHS (1 mL each of 0.1 M solution) were added to a solution of colloidal CdTe QDs in ultrapure millipore water to activate the carboxylate group on the QDs. The mixture was then stirred for 2 h at room temperature with continuous gentle stirring. A solution of 3.9×10^{-3} M of 4AT was then added to the activated QDs and stirred at RT under argon flow for 24 h with continuous gentle stirring. The resulting QDs-4AT conjugate was precipitated out from solution to remove free 4AT and other unreacted molecules by the addition of ethanol followed by centrifuged at 3500 rpm for 10 min and drying under vacuum overnight. The resulting conjugate is represented as QDs-4AT.

2.6.3. Conjugation of GSH-CdSe@ZnS QDs to NiMMSATBC or NiMMSAPc

GSH-CdSe@ZnS QDs was conjugated to NiMMSATBC (**7**) and NiMMSAPc (**8**). The method followed is the same as described in section 2.6.2, except that EDC was used to activate the carboxylic groups of **7** and **8**. A solution of 10 mg of the QDs was dissolved in PBS pH 7.4 and 8.3×10^{-5} M of **7** and of 5.7×10^{-5} M **8** were dissolved in DMSO:H_2O (3:2, v/v) for conjugation. The purification steps were the same as described in section 2.6.2., except that methanol was employed to remove unconjugated QDs. The obtained QDs-MPc or QDs-TBC conjugates were soluble in PBS buffer as a colloidal solution.

2.7. Procedures for the preparation of solutions for fluorescence detection

2.7.1. DPPH•

QDs were mixed with a known concentrations of 2,2-diphenyl-1-picrylhydrazyl free radical (DPPH•). DPPH• has limited solubility in aqueous solution. Hence, this solvent mixture was employed to improve solubility. The fluorescence spectra of the QDs were recorded under an excitation wavelength of 400 nm. The working solutions were stirred vigorously prior to fluorescence measurements and all measurements were conducted at room temperature.

2.7.2. Hydroxyl radical

HO• radicals were generated from Fe^{2+}-EDTA/H_2O_2/ascorbic acid Fenton hybrid system that mimics the production of •OH for biological foot-printing of proteins **[189]** and were immediately added to a fluorescence cell containing colloidal solution of QDs in Tris-HCl buffer (50 mM) pH 7.4 (total volume = 3 mL). The solution was stirred vigorously for few seconds and the fluorescence measurement was taken afterward.

2.7.3. Peroxynitrite anion

As reported before **[190],** $ONOO^-$ is unstable around neutral pH and decomposes rapidly ($t_{½}$ < 1 sec) by protonation to its conjugate acid; peroxynitrous acid (ONOOH). The later rapidly isomerizes to nitrate by a first-order decay, and thus making the detection of $ONOO^-$ difficult. However, at alkaline pH, $ONOO^-$ is

relatively stable with a much longer half life. Moreover, *in vivo* and *in vitro* studies have shown that $ONOO^-$ is best detected in human serum at pH 9.2 **[191],** Hela cells at pH 9.4 **[192]** and other sensors for $ONOO^-$ has been developed at pH 10.5 **[193],** pH 11.5 and 12 respectively **[194]**. Thus, we studied the spectrofluorimetric detection of $ONOO^-$ by comparing two different pHs; 9.4 and 12 using 50 mM phosphate buffer solution. Phosphate buffer was chosen because it has previously been reported not to interfere in $ONOO^-$ reactions. Other commonly known buffers such as Tris and HEPES have been reported to react with $ONOO^-$ leading to secondary radical intermediates and $^{\bullet}NO$-donors **[195]**. In a separate set of vials containing 3 ml of selected QDs in buffer solution, varying concentrations of $ONOO^-$ were added and the mixture was shaken for a few seconds before taking the fluorescence measurements. The excitation wavelength was set at 400 nm.

2.7.4. Superoxide anion

Firstly, superoxide anion $O_2^{\bullet-}$ was generated in alkaline DMSO according to literature methods **[196,197],** and was stable for about 24 h **[198]**. The concentration of $O_2^{\bullet-}$ was determined according to its molar absorptivity (20061 M^{-1} cm^{-1} at 271 nm) in DMSO **[197,198]**. The selected nanoconjugates were dissolved in DMF:PBS pH 7.4 (3:1) and ultrasonicated for 15 min to disperse the colloidal nanoconjugates after which various concentrations of $O_2^{\bullet-}$ were added. All the steps for fluorescence measurements with the $O_2^{\bullet-}$ were performed sequentially. It was observed that in the presence of $O_2^{\bullet-}$, the enhancement of the fluorescence of the QDs in the conjugate was dependent on time. Hence, the colloidal mixture was allowed to equilibrate for

30 min before recording the fluorescence signal for each concentration of $O_2^{\bullet-}$. All measurements were recorded at room temperature.

2.7.5. Detection of the rest of the analytes

All fluorescence measurements were conducted under the same conditions. The QDs or nanoconjugates were dissolved in pH 7.4 buffer and ultrasonicated for 15 min to disperse the colloidal solution which was then allowed to stabilize for 5 to 60 min, depending on the conjugate solution. The solution containing the analytes and conjugates were mixed thoroughly and allowed to equilibrate for approximately 5 - 15 min (depending on the analyte) before taking the fluorescence measurements. The equilibration period was needed in order to obtain a stable fluorescence signal and homogeneous solution. The concentrations of analytes employed will be presented in figure captions for the detection of each analyte in chapter 4, 5 and 6.

2.7.6. Detection of fluoride ion in real samples

The detection of F^- ion in real samples was carried out in cell culture medium (Dulbecco's modified Eagle medium, DMEM) and tap water. Both were spiked with a known concentration of F^- ion and aqueous solution of QDs-**6** nanoconjugate (as an example) was employed to detect the analyte. Tap water was freshly collected from the laboratory and filtered through a 0.22 μM membrane filter before spiking with F^-. The concentration of F^- in DMEM and tap water was evaluated by comparing the resulting fluorescence enhancement response (from DMEM and tap water samples) with the linear regression plots obtained for F^- detection in PBS buffer.

2.8. Fluorescence quantum yields

Fluorescence quantum yield of the QDs were determined by the comparative method, according to Eq. 2.1 **[199]**:

$$\Phi_F = \Phi_{F(Std)} \frac{F \,.\, A_{Std} \,.\, n^2}{F_{Std} \,.\, A \,.\, n_{Std}^2} \qquad (2.1)$$

where A and A_{Std} are the absorbance of the sample and reference standard at the excitation wavelength respectively. F and F_{Std} are the areas under the fluorescence curve of the QDs and the standard, respectively and n and n_{Std} are the refractive indices of the solvent used for the sample and standard, rhodamine 6G in ethanol having a Φ_F = 0.94 **[200]** was used as the reference standard. The excitation wavelength for both the sample and standard was 400 nm and the absorbance was in the range of 0.05 and 0.1.

The fluorescence quantum yield of the QDs in the conjugates ($\Phi_{F(QD)}^{conjugate}$) were calculated according to Eq. 2.2:

$$\Phi_{F(QD)}^{conjugate} = \Phi_{F(QD)} \frac{F_{QD}^{conjugate}}{F_{QD}} \qquad (2.2)$$

$\Phi_{F(QD)}$ represents the fluorescence quantum yield of the QDs alone, and was used as the standard. $F_{QD}^{conjugate}$ is the fluorescence intensity of the QDs in the conjugated form and F_{QD} is the fluorescence intensity of the QD alone.

RESULTS AND DISCUSSIONS

3. **Synthesis and characterization**
4. **Dectection of analytes using QDs alone**
5. **Fluorescence detection of analytes using QDs-4AT**
6. **QDs-MPc conjugates for analyte detection**

PUBLICATIONS

The results presented in the following chapters have either been published or submitted for publication. These articles are not referenced in this thesis.

1. **Oluwasesan Adegoke**, Wadzanai Chidawanyika, Tebello Nyokong, Interaction of CdTe quantum dots with 2,2-diphenyl-1-picrylhydrazyl free radical: a spectroscopic, fluorimetric and kinetic study. *J. Fluoresc* 22 (2012) 771.
2. **Oluwasesan Adegoke**, Eric Hosten, Cedric McCleland, Tebello Nyokong, CdTe quantum dots functionalized with 4-amino-2,2,6,6-tetramethylpiperidine-N-oxide as luminescent nanoprobe for the sensitive recognition of bromide ion. *Anal. Chim. Acta* 721 (2012) 154.
3. **Oluwasesan Adegoke**, Tebello Nyokong, A comparative study on the sensitive detection of hydroxyl radical using thiol-capped CdTe and CdTe@ZnS quantum dots. *J. Fluoresc* 22 (2012) 1513.
4. **Oluwasesan Adegoke**, Tebello Nyokong, Probing the sensitive and selective luminescent detection of peroxynitrite using thiol-capped CdTe and CdTe@ZnS quantum dots. *J. Lumin*. 134 (2013) 448.
5. **Oluwasesan Adegoke**, Edith Antunes, Tebello Nyokong, Nanoconjugates of CdTe@ZnS quantum dots with cobalt tetraamino-phthalocyanine: characterization and implications for the fluorescence recognition of superoxide anion. *J. Photochem. Photobiol. A: Chem.* 257 (2013) 11.

6. **Oluwasesan Adegoke**, Tebello Nyokong, Fluorescence "switch on" of conjugates of CdTe@ZnS quantum dots with Al, Ni and Zn tetraamino-phthalocyanine by hydrogen peroxide: characterization and applications as luminescent nanosensors**.** *J. Fluoresc* 23 (2013) 963.
7. **Oluwasesan Adegoke**, Tebello Nyokong, Fluorescence "turn on" probe for bromide ion using nanoconjugates of glutathione-capped CdTe@ZnS quantum dots with nickel tetraamino-phthalocyanine: characterization and size-dependent properties. *J. Photochem. Photobiol. A: Chem.* 265 (2013) 58.
8. **Oluwasesan Adegoke**, Tebello Nyokong, Effects of analytes on the fluorescence property of CdTe@ZnS quantum dots decorated with cobalt tetraamino-phthalocyanine. *J. Lumin.* 146 (2014) 275-283**.**
9. **Oluwasesan Adegoke**, Tebello Nyokong. Unsymmetrically substituted nickel triazatetra-benzcorrole and phthalocynanine complexes: conjugation to quantum dots and applications as fluorescent "turn ON" sensors. *J. Fluoresc.* In press: DOI 10.1007/s10895-013-1317-4.
10. **Oluwasesan Adegoke**, Tebello Nyokong, Conjugation of mono-substituted phthalocyanine derivatives to CdSe@ZnS quantum dots and their applications as fluorescent "turn ON" sensors. *Synthetic Metals* **188** (2014) 35-45.

3. SYNTHESIS AND CHARACTERIZATION

This chapter reports on the synthesis and characterization of QDs, MPcs and QDs-MPc conjugates.

3.1. QDs

Thiol-capped QDs employed in ths work were synthesized via the hydrothermal and organometallic synthetic routes. For the former, water soluble and highly luminescent CdTe or CdTe@ZnS QDs were formed by mixing NaHTe (formed from the reaction of $NaBH_4$ and Te) with cadmium precussors in the presence of capping agents (TGA, MPA or GSH) and subsequently coating with ZnS shell to form the corresponding core-shell QDs. The reaction time and temperature were controlled to obtain the desired QDs size. To remove excess surfactant, the QDs were purified by mixing with an excess amount of ethanol followed by centrifugation.

It is widely known that CdSe@ZnS QDs remain among the widely used QDs for biological applications **[41].** However, to obtain high quality mono-dispersed QDs, they are usually synthesized via the organometallic route, which utilizes high temperature coordinating precursors. In this work, the as-synthesized CdSe@ZnS QDs were firstly capped with trioctylphophine oxide (TOPO) which gives hydrophobic QDs that are unsuitable for biological applications. Ligand exchange with MPA or GSH (which exhibit terminal carboxylic groups) was carried out to obtain water-soluble CdSe@ZnS QDs. Table 3.1 shows the list of QDs employed in this work.

3.1.1. XRD measurements

X-ray powder diffraction (XRD) was employed to provide useful information about the crystal structure and size of QDs used in this work, Fig. 3.1 shows the XRD patterns of TGA-CdTe and GSH-CdTe@ZnS QDs as representatives for the rest of

the QDs. The peaks for TGA-CdTe QDs were at 26.6, 44.0 and 52.1 and GSH-CdTe@ZnS QDs were at 28.60, 47.60 and 56.20 respectively. Following the growth of ZnS shell on the core CdTe, the peak position shifted to higher angles and thus confirms the formation of CdTe@ZnS core-shell QDs.. A typical zinc blend crystal structure **[77]** was obtained. The sizes of the QDs were also determined using XRD, according to the Scherrer Eq. (3.1) **[201]**.

$$\boldsymbol{d(\text{Å}) = \frac{k\lambda}{\beta \cos\theta}} \qquad \mathbf{3.1}$$

where λ is the wavelength of the X-ray source (1.5405), k is an empirical constant equal to 0.9, β is the full width at half maximum of the diffraction peak, and θ is the angular position. The sizes of the QDs were found to range from 2.2 to 4.7 nm (Table 3.1) for QDs employed in this work.

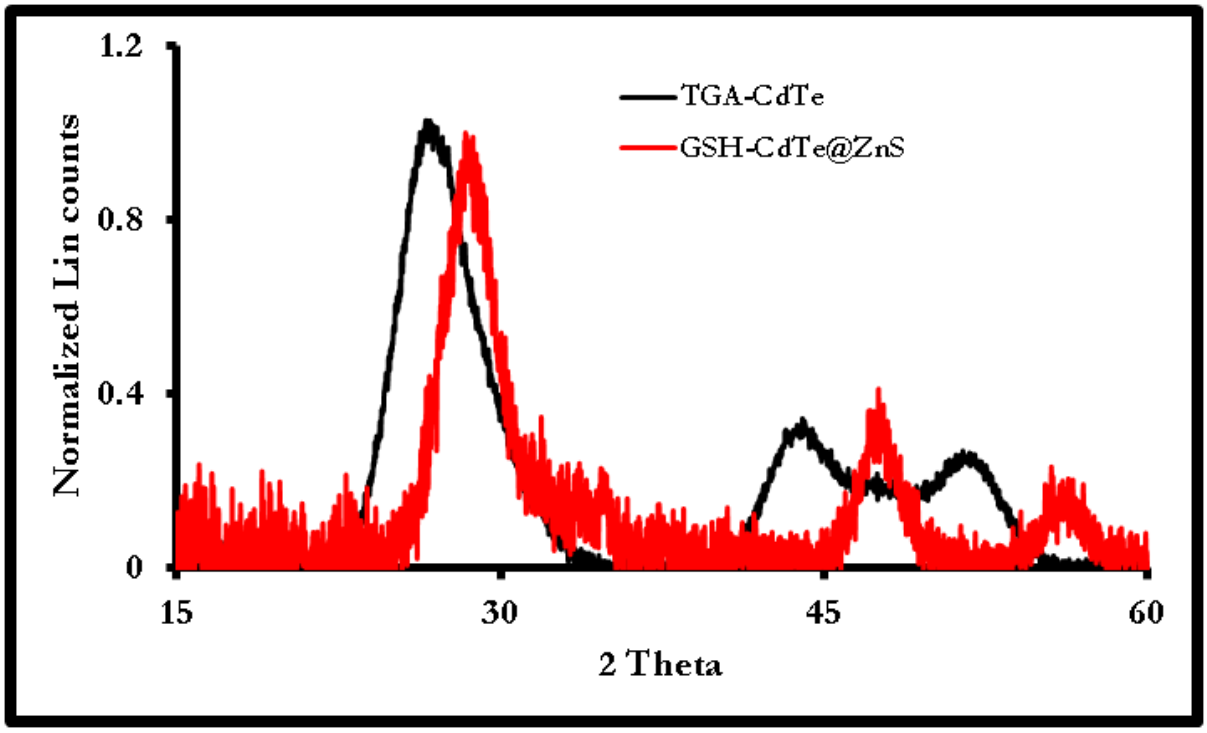

Fig. 3.1. Powder XRD spectra of TGA-CdTe and GSH-CdTe@ZnS QDs.

Table 3.1. List of QDs employed in this work showing their size, maximum absorption and emission wavelength and fluorescence quantum yields. Solvent: pH 7.4 buffer. Sizes of QDs obtained using XRD are shown in brackets.

QDs(nm)	[a]Abs max (nm)	[a]Emi max (nm)	Φ_F
TGA-CdTe(2.2)	477	555	0.14
TGA-CdTe(2.3)	503	549	0.80
TGA-CdTe(2.6)	521	568	0.57
MPA-CdTe(2.7)	509	566	0.47
GSH-CdTe(3.9)	602	632	0.34
MPA-CdTe@ZnS(3.0)	525	587	0.57
MPA-CdTe@ZnS(3.1)	510	557	0.72
MPA-CdTe@ZnS(3.4)	560	626	0.46
GSH-CdTe@ZnS(2.6)	510	562	0.62
GSH-CdTe@ZnS(3.0)	562	600	0.39
GSH-CdTe@ZnS(3.4)	530	602	0.14
GSH-CdTe@ZnS(3.6)	546	619	0.07
MPA-CdSe@ZnS(4.6)	568	597	0.52
GSH-CdSe@ZnS(4.7)	585	609	0.24

[a]Abs max = Absorption maximum and Emi max = Emission maximum.

3.1.2. TEM measurements

TEM was used to study the surface morphology of the QDs. Fig. 3.2A and 3.2B shows an example of the TEM images of the QDs. The TEM images of MPA-CdSe@ZnS QDs (Fig. 3.2A) and GSH-CdSe@ZnS QDs (Fig. 3.2B) shows that the QDs are nearly mono-dispersed with majority of the particles being almost spherical in shape as observed for the rest of the QDs. The sizes obtained from TEM for MPA-CdSe@ZnS QDs (4.4 nm) and GSH-CdSe@ZnS QDs (4.6 nm) (as examples) were similar to the values obtained from XRD, Table 3.1.

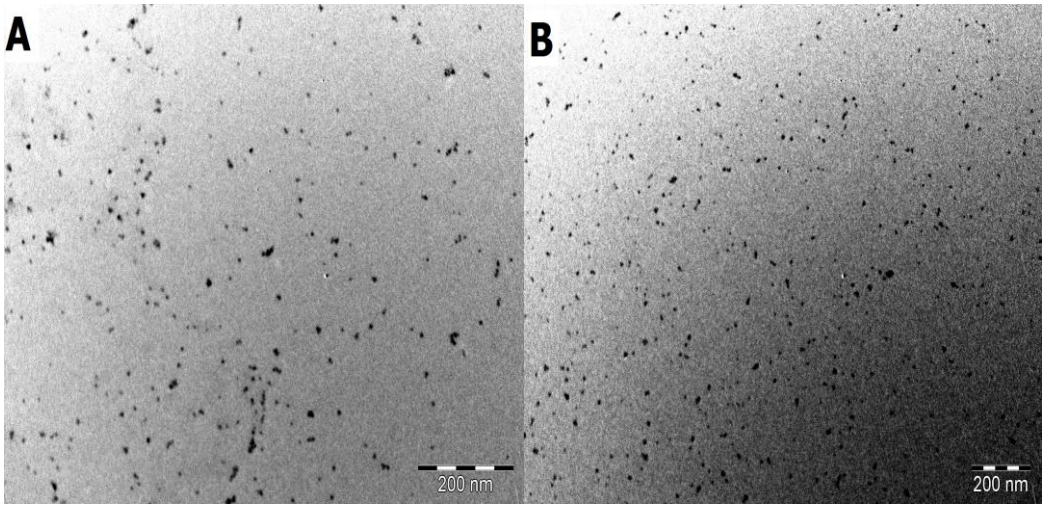

Fig. 3.2. TEM images for (A) MPA-CdSe@ZnS QDs and (B) GSH-CdSe@ZnS QDs.

3.1.3. UV/vis absorption and fluorescence emission spectra

Fig. 3.3 shows the typical fluorescence and absorption spectra of two different-sized TGA-capped CdTe QDs (used as examples) taken at different refluxing times. The fluorescence data of the QDs are listed in Table 3.1. The QDs exhibit broad absorption and well-resolved narrow emission spectra which shift to longer wavelengths with reaction time (hence increase in size). The relatively narrow emission spectra as observed in Fig. 3.3 may be attributed to elimination of surface

related recombination defects. The Φ_F of the QDs used in this work, range from 0.14 – 0.80. The Φ_F values of the QDs seem to be generally higher for smaller QDs compared to their larger counterparts. For example, the Φ_F values obtained for the differently-sized GSH-CdTe@ZnS (0.62, 0.14 and 0.07) (which were obtained from the same batch) were found to decrease remarkably with increase in the size of the core-shell QDs (Table 3.1). Different batches of QDs could have different defect states which could influence its Φ_F values. Similar trend in decrease of the Φ_F with size has been observed in literature **[202]** with the optimum Φ_F value being dependent on the capping agent. It has been reported that the lower Φ_F of larger QDs is due to larger non-radiative decay probabilities **[203].** Also, core-shell QDs are expected to increase Φ_F values and as shown in Table 3.1, the improvement is highly dependent on the size of the QDs. Thus, in this work, both the increase is size and the nature of the substituted could be responsible for decrease in Φ_F values.

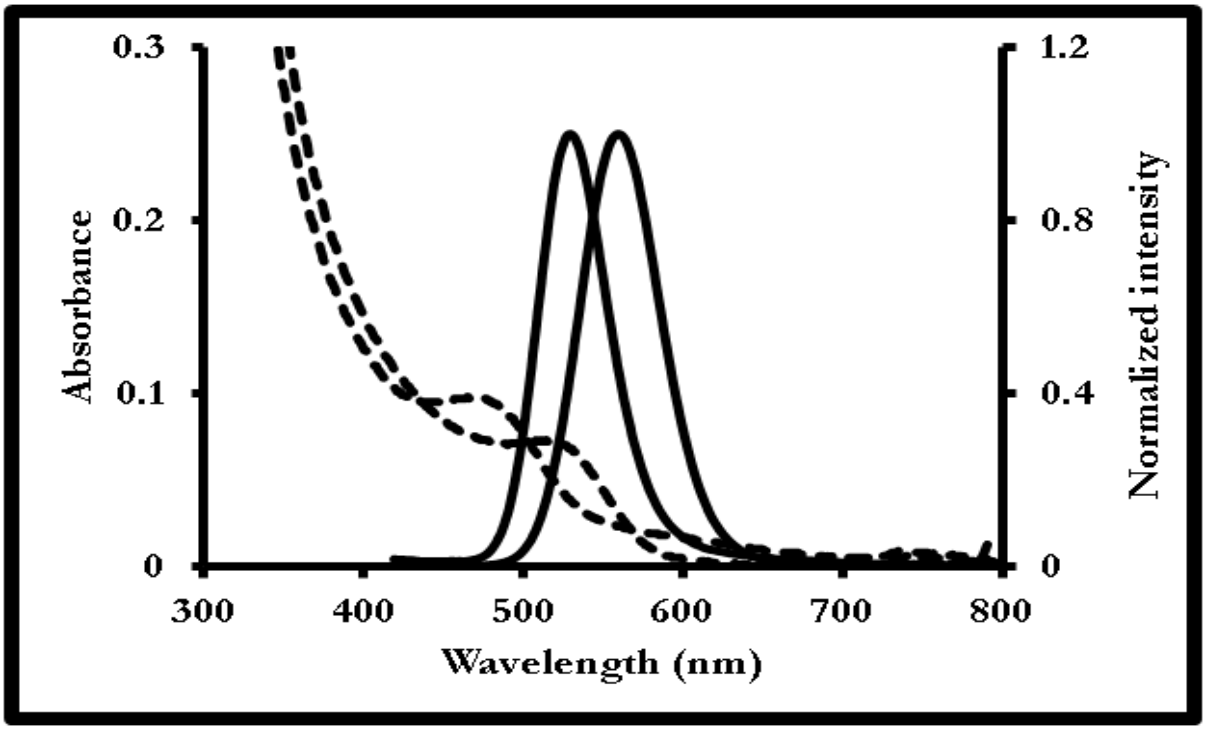

Fig. 3.3. Absorption spectra (dotted line) and fluorescence emission spectra (solid line) of TGA-capped CdTe QDs at room temperature. λ_{exc} = 400 nm.

3.1.4 Fluorescence lifetime measurements

In this work, fluorescence lifetimes were employed as a vital tool in elucidating possible interactions between the QDs and analytes of interest. They can provide key information on the recombination of photoinduced carriers in the nanocrystal QDs. Fig. 3.4 shows an example of the fluorescence decay curves of TGA-CdTe QDs. Similar decay curves were observed for the rest of the QDs. The QDs exhibit triexponential decays, Table 3.2. The longer lifetime τ_1, is associated with the involvement of surface states in the carrier recombination process **[204],** the shorter lifetime τ_2 could be as a result of intrinsic recombination of initially populated core states **[205]** while the shortest lifetime τ_3 is associated with radiative depopulation due to band edge recombination at the surface **[205**]. The differences in fluorescence

lifetimes observed could be due to the nature of the QDs (i.e., core or core-shell), their size and type of capping agent attached to its surface. The solvent medium could also influence the fluorescence lifetime values of the QDs. τ_F values (considering the same solvent media) are generally longer for larger QDs of the same type, contrary to observation for the Φ_F values (which decreased for QDs of the same batch (GSH-CdTe@ZnS (2.6, 3.4 and 3.6 nm)) in Table 3.1. Similarly, Zhimin et al., **[206]** carried out a study on the Φ_F and τ_F properties of different-sized CdTe QDs, capped with either TGA or MPA and observed that the Φ_F values increased for both QDs while the corresponding τ_F values increased for TGA-CdTe and decreased for MPA-CdTe. This was attributed to different degree of surface passivation of QDs by the thiol ligands **[206]. In general, fluorescence lifetime measurements provided explanations into the type of mechanism observed for the fluorescence quenching sensor by distinguishing between dynamic and static processes. For the fluorescence enhancement sensor, it was employed to confirm the enhancement effects observed for the QDs-MPc sensors in the presence of the analytes.**

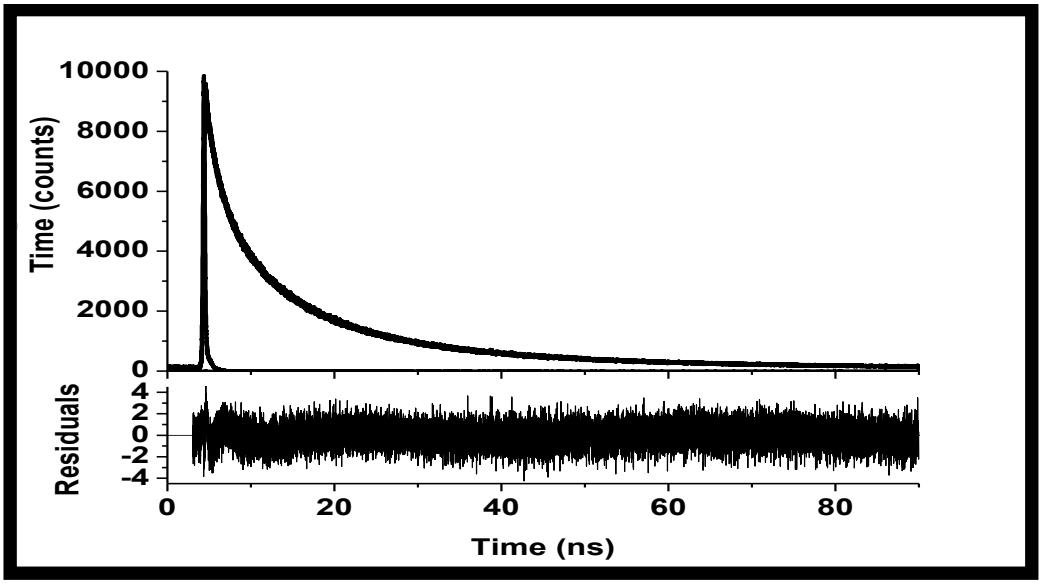

Fig. 3.4. Fluorescence decay curves of TGA-CdTe QDs (shown as an example).

Table 3.2. Triexponential fluorescence lifetime values for all the QDs employed in this work. The size of the QDs (nm) has been included to distinguish similar QDs. Solvent: pH 7.4 buffer.

QDs(nm)	τ_1 (ns) [a] (±0.10)	τ_2 (ns) [a] (±0.06)	τ_3 (ns) [a] (±0.01)	Mean τ_F(ns) (±0.1)
TGA-CdTe(2.2)	20.1 (0.66)	6.1 (0.30)	0.9 (0.04)	9.0
TGA-CdTe(2.3)	24.0(0.79)	7.3(0.19)	0.9(0.02)	10.7
TGA-CdTe(2.6)	22.5 (0.75)	7.8 (0.23)	1.1 (0.02)	10.5
MPA-CdTe(2.7)	29.0(0.83) 26.2(0.73)	7.0(0.15) 8.3(0.24)	0.8(0.02) 1.5(0.03)	12.3 12.0
GSH-CdTe(3.9)	65.0(0.91)	15.1(0.08)	2.8(0.01)	27.6
MPA-CdTe@ZnS(3.0)	33.8(0.68) 34.8(0.86)	12.0(0.30) 7.1(0.12)	1.4(0.02) 1.5(0.02)	5.7 14.5
MPA-CdTe@ZnS(3.1)	43.8(0.50)	14.9(0.44)	2.8(0.06)	20.5
MPA-CdTe@ZnS(3.4)	46.4(0.62)	15.8(0.34)	2.9(0.04)	21.7
GSH-CdTe@ZnS(2.6)	45.6(0.54)	15.7(0.40)	2.6(0.06)	21.3
GSH-CdTe@ZnS(3.0)	60.6(0.89) 55.1(0.93)	16.0(0.09) 11.0(0.06)	1.5(0.02) 1.0(0.01)	26.0 22.4
GSH-CdTe@ZnS(3.4)	57.3(0.88)	11.2(0.07)	0.9(0.05)	23.1
GSH-CdTe@ZnS(3.6)	66.1(0.86)	11.7(0.12)	0.8(0.08)	26.2
MPA-CdSe@ZnS(4.6)	13.5(0.53)	4.4(0.38)	0.7(0.9)	6.2
GSH-CdSe@ZnS(4.7)	19.1(0.58)	6.3(0.34)	1.3(0.8)	13.4

[a]**Relative abundance in brackets.**

3.2. MPc

3.2.1. Characterization of MTAPcs (1 – 4)

The UV/vis absorption spectrum of compound **3** (as an example for MTAPc) with a Q-band maximum at 723 nm is displayed in Fig. 3.5. It was observed that the Q band position of the MTAPc (M = Al, Co, Ni and Zn) were all red shifted. The red shifting is typical of MTAPc, due to the electron donating nature of the NH_2 substituents **[163]**. The MTAPc complexes are not soluble in aqueous media, hence, the solvent mixture of DMF:PBS was employed for the MTAPc complexes in order to ensure the presence of aqueous environment used for conjugation.

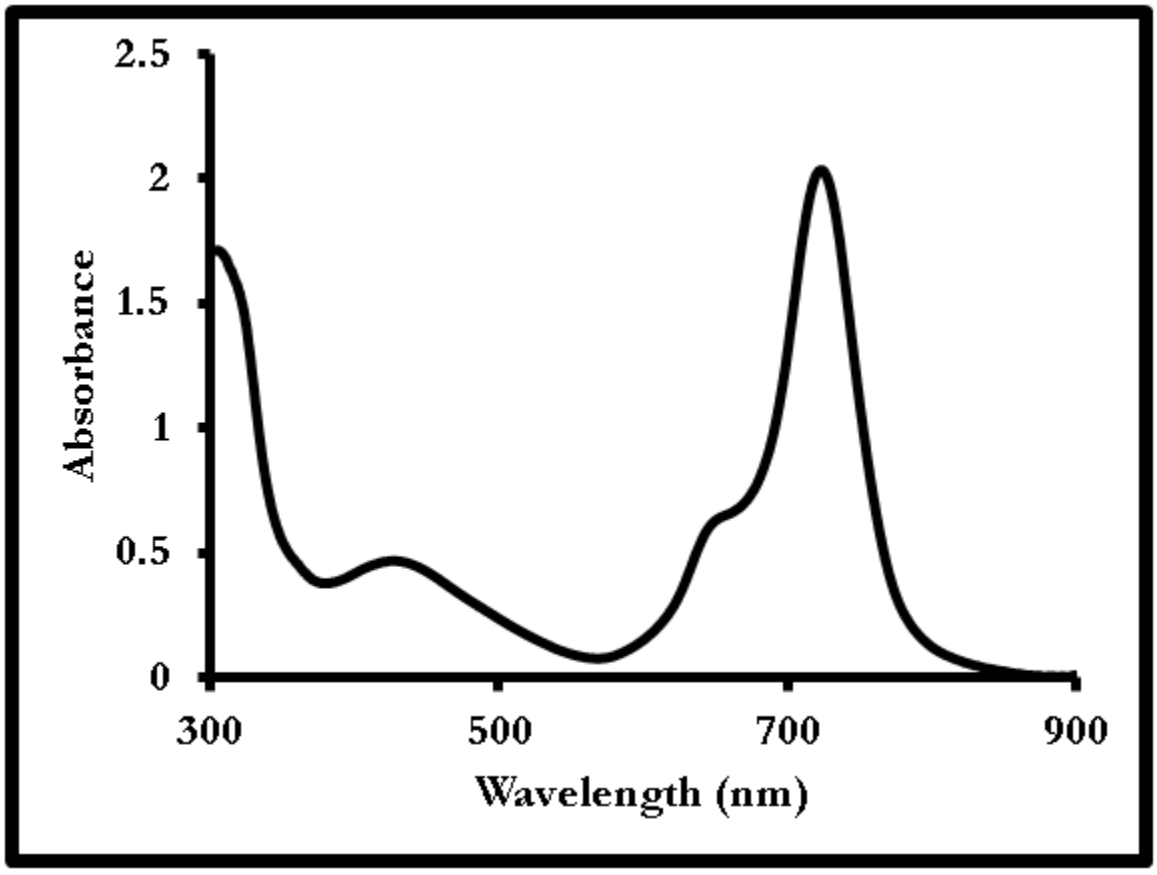

Fig. 3.5. UV/vis spectrum of compound 3 measured in DMF:PBS buffer pH 7.4 (2:1, v/v).

3.2.2. Synthesis and characterization of monoamino Pcs (5) and (6)

The synthetic procedures employed for compound **5** (Schemes 3.1) was achieved by firstly synthesizing (Cl)AlMNPc (**9**) in which the nitro group was reduced to obtain compound **5**. Scheme 3.2 was employed for the synthesis of **6**. Both **5** and **6** require extensive separation due to the presence of a number of compounds. All the compounds were characterized by UV/vis, IR, ^{1}H NMR, elemental analysis and MALDI-TOF mass spectroscopy, all of which showed agreement with the expected results.

The UV/vis spectra of compound **5** and compound **6** in DMF are displayed in Fig. 3.6. Both spectra exhibited a monomeric Q band maximum with excellent solubility in DMF.

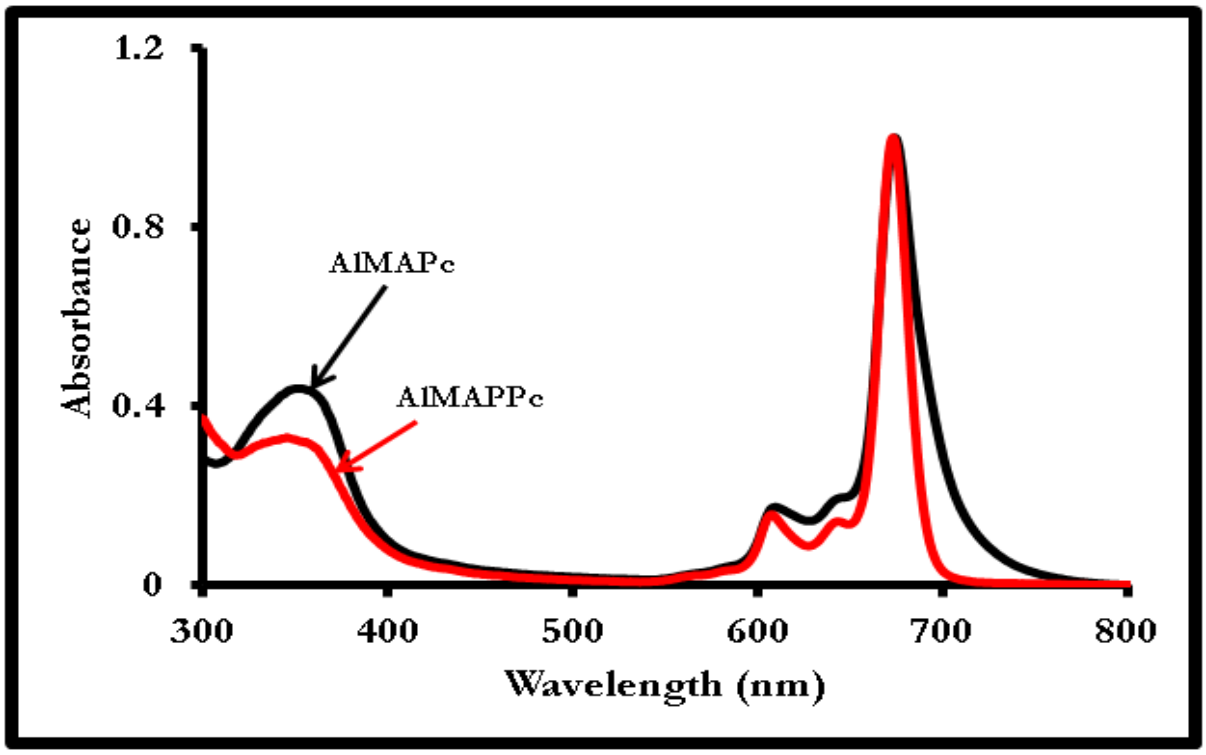

Fig. 3.6. UV/Vis spectra of as-synthesized (Cl)AlMAPc (5) and (Cl)AlMAPPc (6) in DMF.

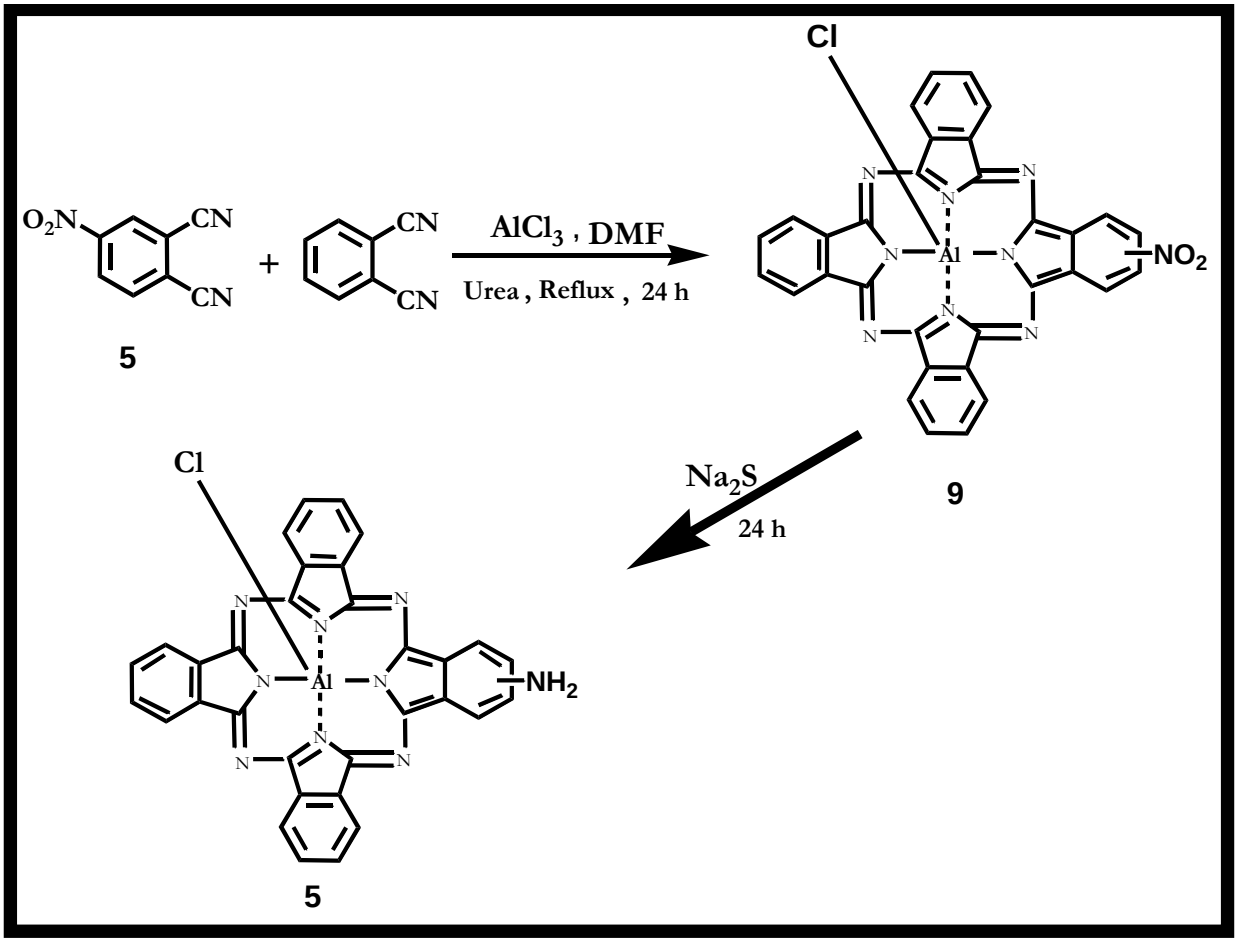

Scheme 3.1. Synthesis of ClAlMAPc (5) derivative.

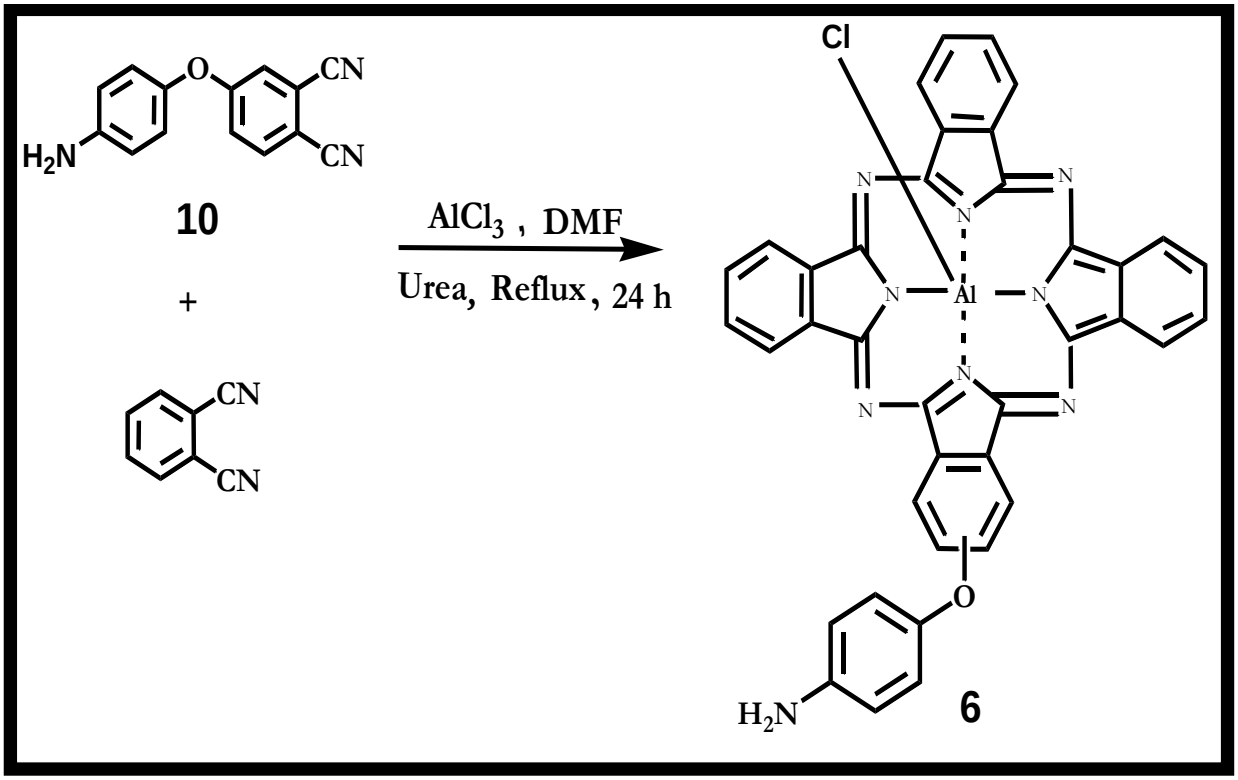

Scheme 3.2. Synthesis of ClAlMAPPc (6) derivative.

3.2.3. Synthesis and characterization of 7 and 8 containing mercaptosuccinic acid

The synthesis of complexes **7** and **8** (Scheme 3.3) occurred under similar conditions except that the amount of urea used was smaller for **7** than for **8.** Low amounts of urea resulted in the absence of one of the bridging nitrogen atoms and thus resulting in the formation of compound **7.** The complexes were successfully obtained after extensive washing with solvents and chromatographic separation. The complexes were characterized by UV/vis, FT-IR and MALDI TOF spectroscopies and by elemental analysis, all of which were in agreement with the predicted structures as detailed in the experimental section. The electronic spectra of the complexes measured before conjugation to the QD displayed a characteristic absorption in the Q band region with a maximum absorption wavelength of 673 nm for compound **7**

and 672 nm for compound **8** in DMSO:H_2O (3:2, v/v), Fig. 3.7. The split Q band is due to unsymmetric substitution. Complex **7** displayed a split and broad Soret band between 404 - 456 nm. The sharp nature of the Soret band is characteristic of triazatetrabenz-corrole complexes **[207].**

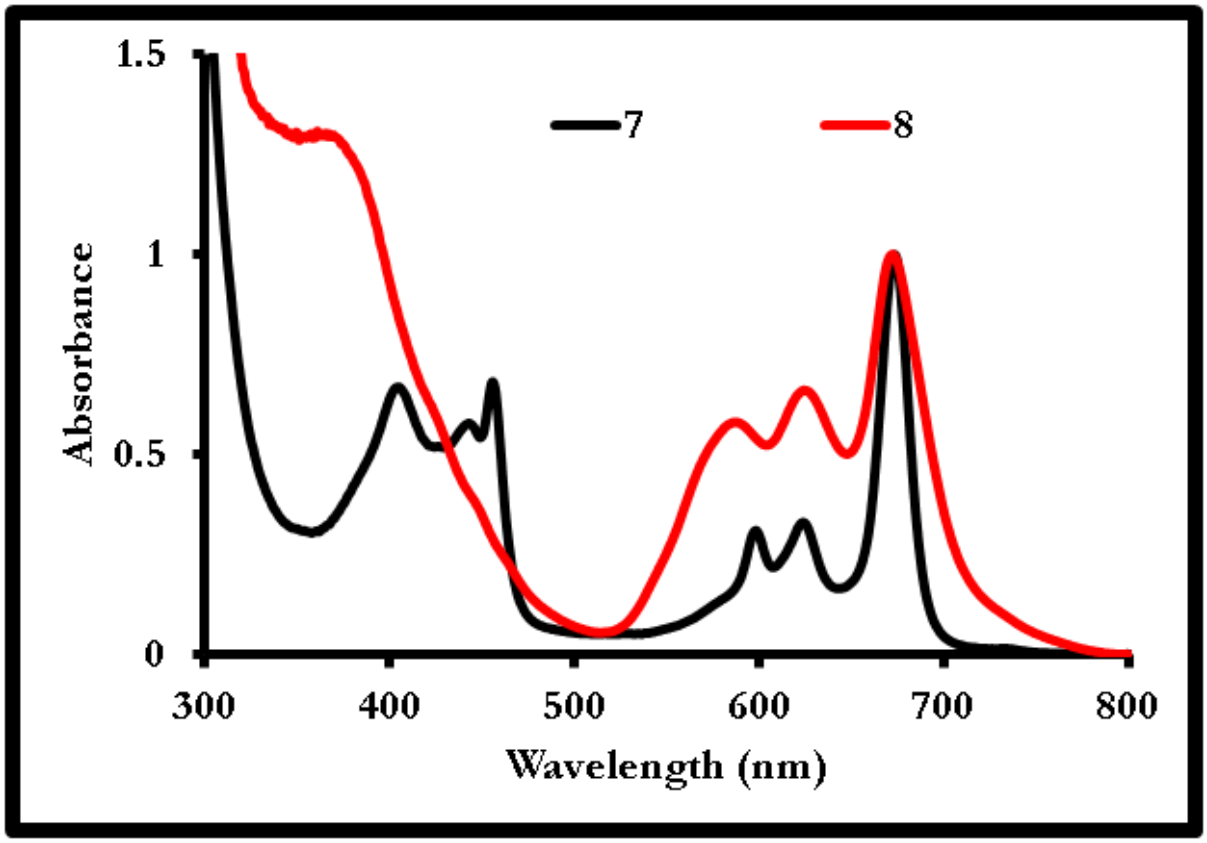

Fig. 3.7. UV/vis absorption spectra of as-synthesized 7 and 8 in DMSO:H_2O (3:2, v/v).

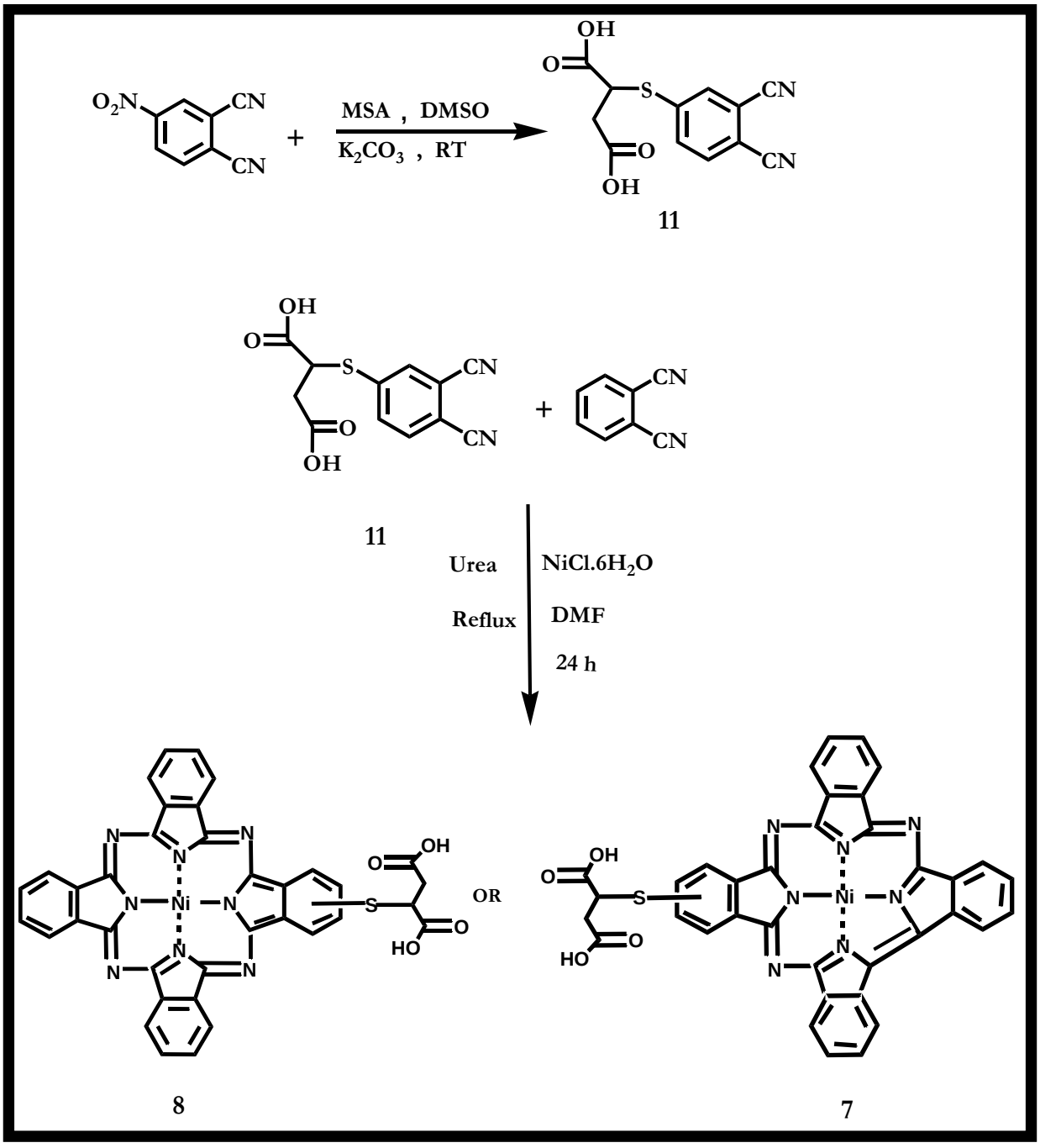

Scheme 3.3. Synthesis of 4-mercaptosuccinic acid phthalonitrile (10) and the corresponding NiMMSATBC (7) and NiMMSAPc (8) complexes.

3.3. MPc-QDs conjugates

QDs were conjugated to amino-containing Pcs (**1 – 6**) by activation of the COOH group of the QDs using EDC and NHS as coupling agents. For compounds **7** and **8**, the COOH groups of the compounds were activated and bonded to the amino group of the QDs. Hence, an amide bond between the QDs and the Pc complexes were formed as depicted in Scheme 3.4 (used as an example).

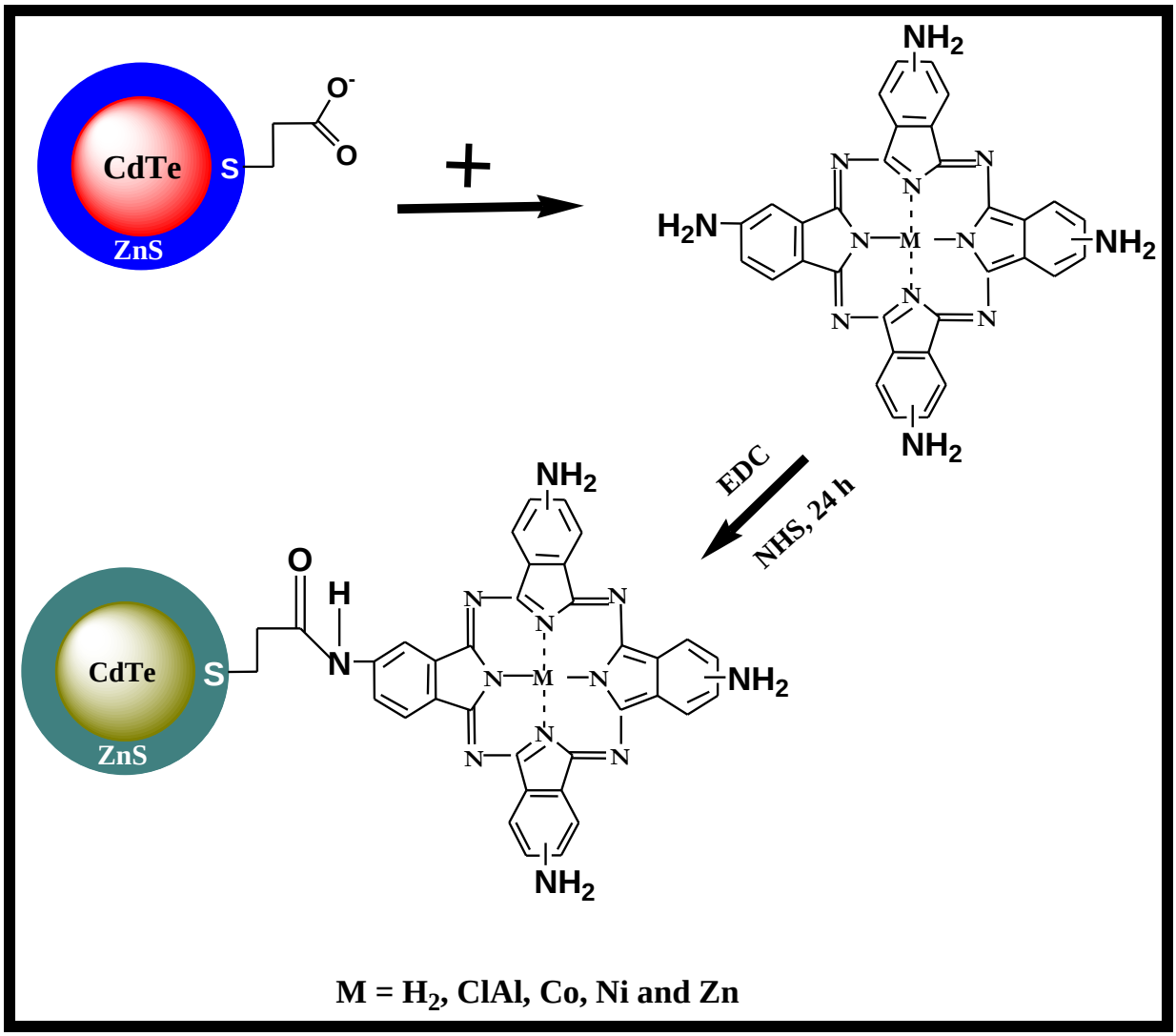

Scheme 3.4. Schematic representation showing the preparation of QDs-H_2, Al, Co, Ni and ZnTAPc nanoconjugate.

3.3.1. TEM analysis

The TEM images of the conjugates (Fig 3.8A – 3.8D using **5** and **6** as an example) shows that the MPc-QDs particles were interspersed showing some level of aggregation compared to the QDs alone, Fig 3.2. In addition, it was observed that the TEM images for GSH-CdSe@ZnS-**5** (Fig. 3.8C) and GSH-CdSe@ZnS-**6** (Fig. 3.8D) displayed an array of embedded particle and thus suggesting that the nature of the QDs capping conjugated to the **5** and **6** influences the surface morphology of the conjugates.

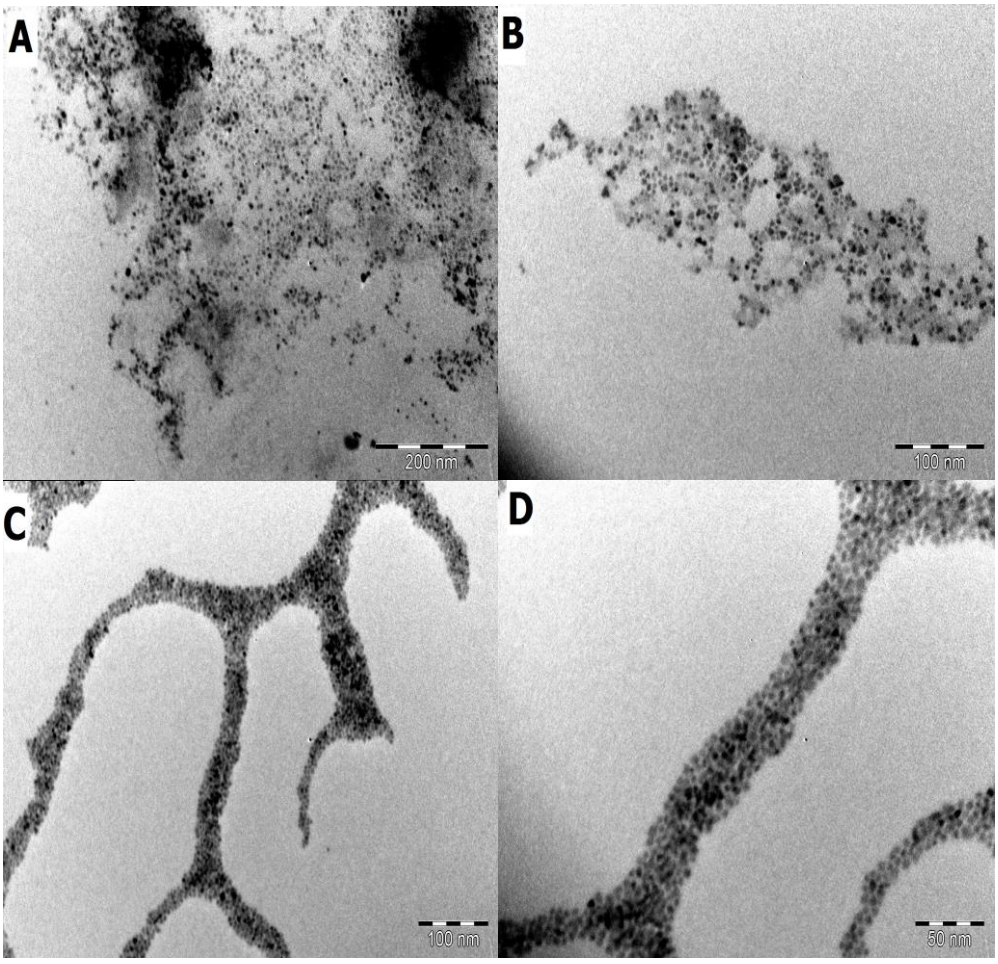

Fig. 3.8. TEM images for (A) MPA-CdSe@ZnS-5, (B) MPA-CdSe@ZnS-6, (C) GSH-CdSe@ZnS-5 and (D) GSH-CdSe@ZnS-6.

3.3.2. FT-IR analysis

To confirm the conjugation between the QDs and MPc complexes via the amide bond formation, FT-IR analysis was carried out. As an example, Fig. 3.9 shows the FT-IR spectra of (A) **5,** (B) GSH-CdSe@ZnS QDs, (C) MPA-CdSe@ZnS QDs, (D) MPA-CdSe@ZnS-**5** and (E) GSH-CdSe@ZnS-**5** respectively. For **5**, the peak at 1671 cm^{-1} is attributed to the $–NH_2$ bending mode of the Pc while the band at 3387 cm^{-1} may be assigned to the stretching mode of the $–NH_2$ group of the Pc. The bands at 1392 and 1586 cm^{-1} for the GSH-CdSe@ZnS and 1386 and 1557 cm^{-1} for MPA-CdSe@ZnS QDs may be assigned to the symmetric and asymmetric –COO functional group of the QDs. The corresponding band at 3277 cm^{-1} for GSH-QDs relates to the $–NH_2$ functional group while the band at 3213 cm^{-1} for MPA-QDs corresponds to the –OH functional group. The formation of 1^0 and 2^0 amide bonds in the conjugates were confirmed by the presence of the characteristic peaks at 1646 and 1567 cm^{-1} for MPA-CdSe@ZnS-**5** and 1653 and 1539 cm^{-1} for GSH-CdSe@ZnS-**5**.

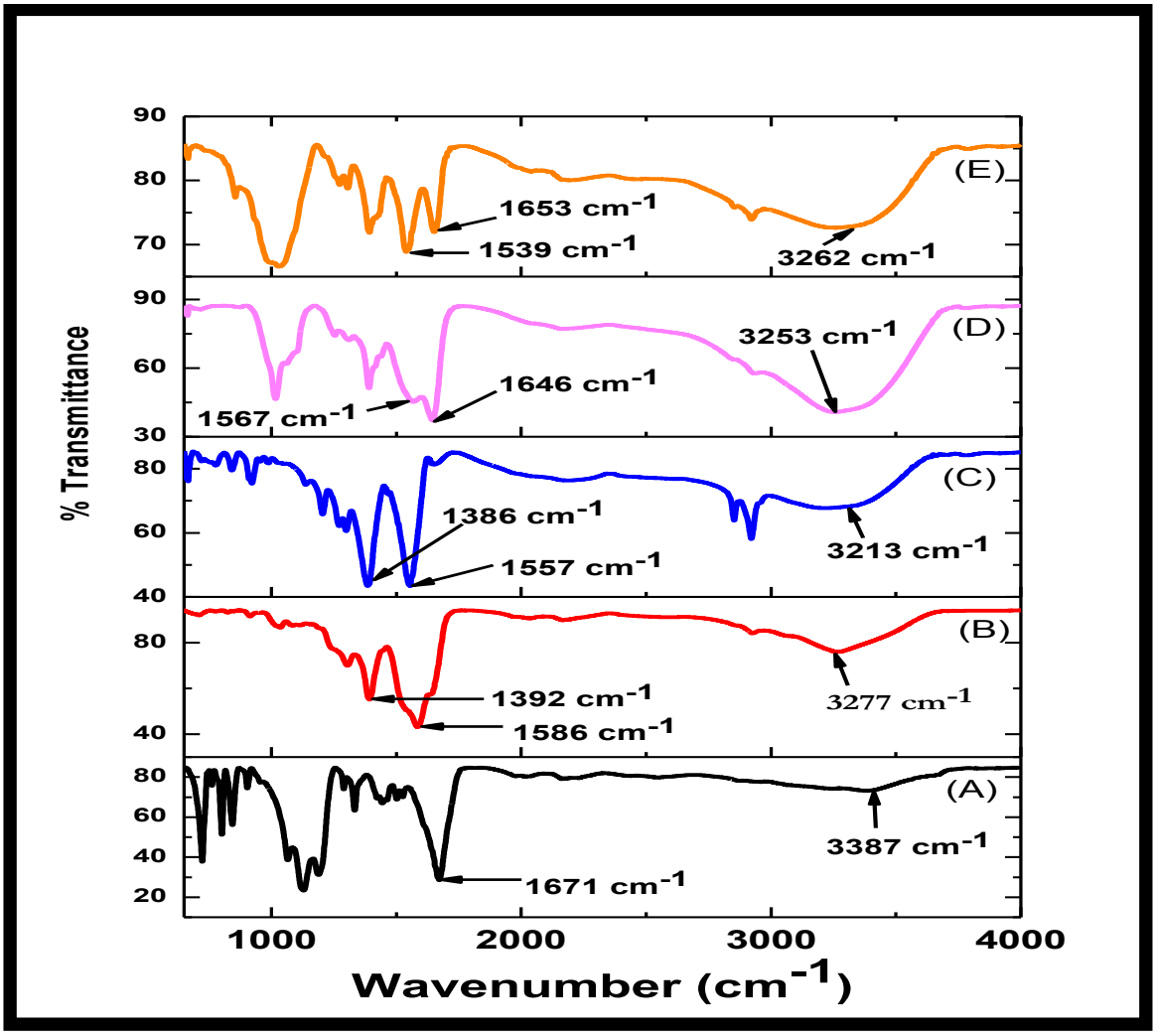

Fig. 3.9. FT-IR spectra of (A) complex 5 (used as an example), (B) GSH-CdSe@ZnS QDs, (C) MPA-CdSe@ZnS QDs, (D) MPA-CdSe@ZnS-5 and (E) GSH-CdSe@ZnS-5.

3.3.3. TGA analysis

Thermal properties of compound **2** and MPA-CdTe@ZnS-**2** (used an examples) were investigated using thermal gravimetric analysis (TGA) in order to gain useful insight into the stability of the QDs-MPc nanocomplexes compared to the MPc alone. Fig. 3.10 shows the thermal curves for **2**, MPA-CdTe@ZnS(3.1)-**2** and MPA-CdTe@ZnS(3.4)-**2**. It can be seen from Fig. 3.10 that as the temperature is increased,

the thermal decomposition of the **2** and QDs-**2** occurs at different decomposition steps. For **2**, the weight loss steps were in the range of 202 – 289 ^{o}C (propabaly due to solvent loss) and 289 – 542 ^{o}C. For both MPA-CdTe@ZnS(3.1)-**2** and MPA-CdTe@ZnS(3.4)-**2**, the TGA curves were very similar and thus displaying high degree of stability. Generally, from the respective TGA curves, it was observed that the QDs-**2** nanocomplexes have better thermal stability that the parent **2**.

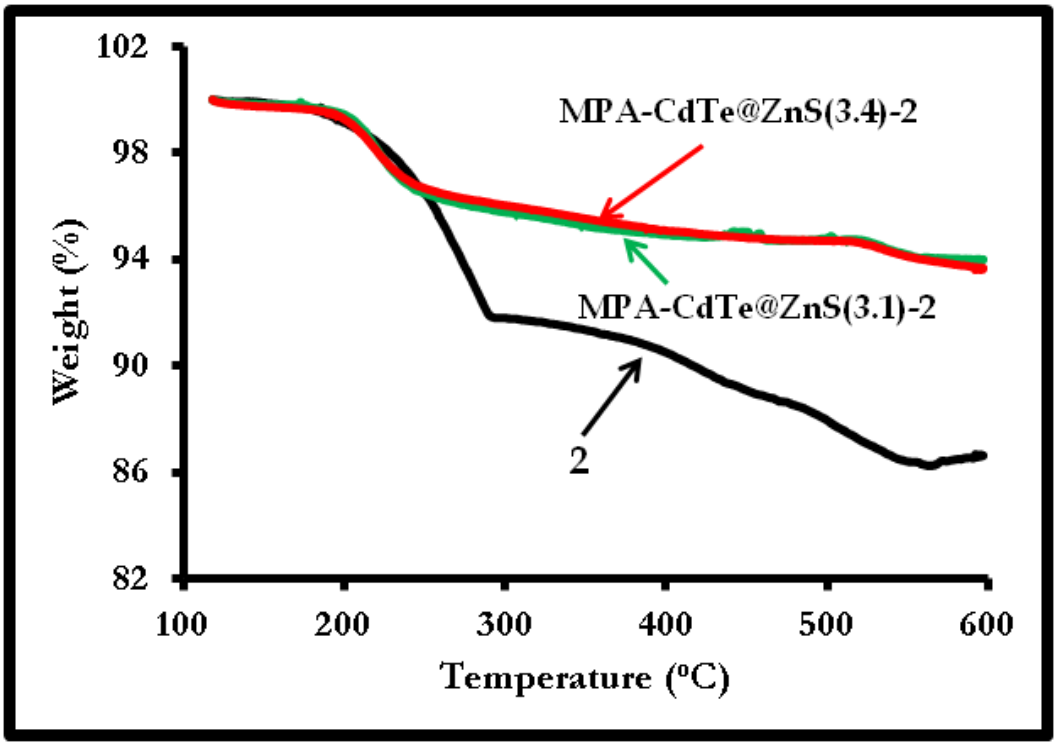

Fig. 3.10. TGA curves of thermal properties of compound 2, MPA-CdTe@ZnS(3.1)-2 and MPA-CdTe@ZnS(3.4)-2.

3.3.4. UV/vis absorption studies

As an example, the absorption spectra of the conjugates compared to the MPc alone are shown in Fig. 3.11 using **5** and **6** as examples. MPA-CdSe@ZnS(4.6)-**5** and GSH-CdSe@ZnS(4.7)-**5** conjugates (Fig. 3.11A) measured in DMF:PBS buffer (5:1, v/v)) displayed a combination of the absorption spectra of the QDs and MPc. The same

behaviour was observed for MPA-CdSe@ZnS(4.6)-**6** and GSH-CdSe@ZnS(4.7)-**6** conjugates (Fig. 3.11B). This gives a convincing affirmation that the MPc complexes have been successfully conjugated to the respective QDs. Similar pattern in the absorption spectra of the conjugates was also observed in PBS buffer pH 7.4 (as a colloidal solution) and for the other QDs conjugated to the respective MPc complexes. The increasing scattering background of the absorption spectra of the conjugates compared to the MPcs alone as observed in Fig 3.11A and 3.11B is due to to the very weak absorption tendencies of the QDs-MPc conjugates in the solvent medium due to the strong conjugation of the QDs to the MPc complexes.

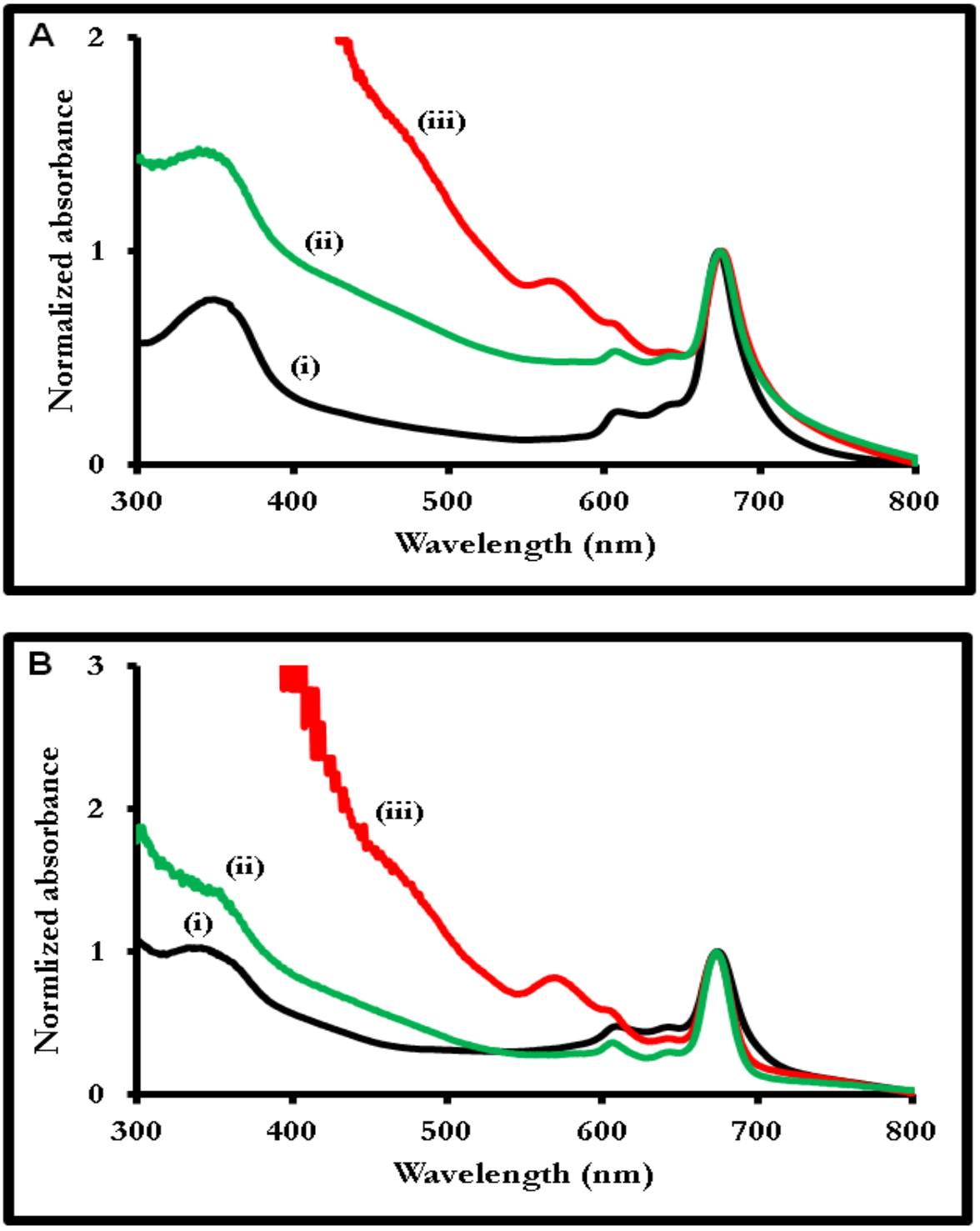

Fig. 3.11. UV/vis spectra of (A) 5 (i) [3 x 10^{-5} M], GSH-CdSe@ZnS(4.7)-5 (ii) [1 x 10^{-8} M] and MPA-CdSe@ZnS(4.6)-5 (iii) [3 x 10^{-7} M] and (B) 6 (i) [3 x 10^{-5} M], GSH-CdSe@ZnS(4.7)-6 (ii) [4 x 10^{-7} M] and MPA-CdSe@ZnS(4.6)-6 (iii) [1 x 10^{-7} M]. Solvent: DMF:PBS (5:1, v/v). Optimum concentrations of the conjugates were used.

3.3.5. Fluoresence behaviour of conjugates

The Φ_F of the QDs in the conjugates ($\Phi_{F(QD)}^{conjugate}$) were calculated according to Eq. 2.2. Binding of the Pcs to the QDs triggered an apparent fluorescence quenching of the QDs in the conjugate, Fig. 3.12B and 3.12C. Table 3.3 displays the observed Φ_F values of the conjugates. As expected, a decrease in the Φ_F of the conjugates was observed in comparison to the values of the QDs alone, due to FRET and other processes that deactivate the excited states. For FRET to occur there has to be overlap between the emission spectra of the QDs and the absorption spectra of the MPcs, as observed in Fig. 3.12A. An efficient way to verify the occurrence of FRET is to excite the QDs-MPc conjugate where the QDs absorb and Pcs do not in order to observe a stimulated energy transfer to the MPc. Fig. 3.12B and 3.12C shows the evidence of energy transfer from MPA-CdSe@ZnS(4.6) QDs and GSH-CdSe@ZnS(4.7) QDs to **5** (used as an example). The increase in the emission of **5** when excited at the wavelength (560 nm) where QDs absorb and Pc does not (Fig 3.6) resulted in stimulated emission for **5** due to FRET. There is also a corresponding decrease in the emission of the QDs.

The FRET efficiencies (Eff) were calculated from the quantum yield data using Eq. 3.2:

$$Eff = 1 - \frac{\Phi_{F(QD)}^{conjugate}}{\Phi_{F(QD)}} \qquad (3.2)$$

where $\Phi_{F(QD)}$ represents the fluorescence quantum yield of the QDs alone and $\Phi_{F(QD)}^{conjugate}$ is fluorescence quantum yield of the conjugates. $\Phi_{F(QD)}^{conjugate}$ values were calculated according to Eq. 2.2.. FRET efficiency values are an estimate since there

are other factors which could influence the decrease in QDs emission in addition to FRET. The *Eff* values for the conjugates are listed in Table 3.3. It was observed that the QDs with higher emission wavelength (considering the same QDs and capping agent) exhibited higher *Eff* values due to closer spectral overlap with the corresponding MPcs.

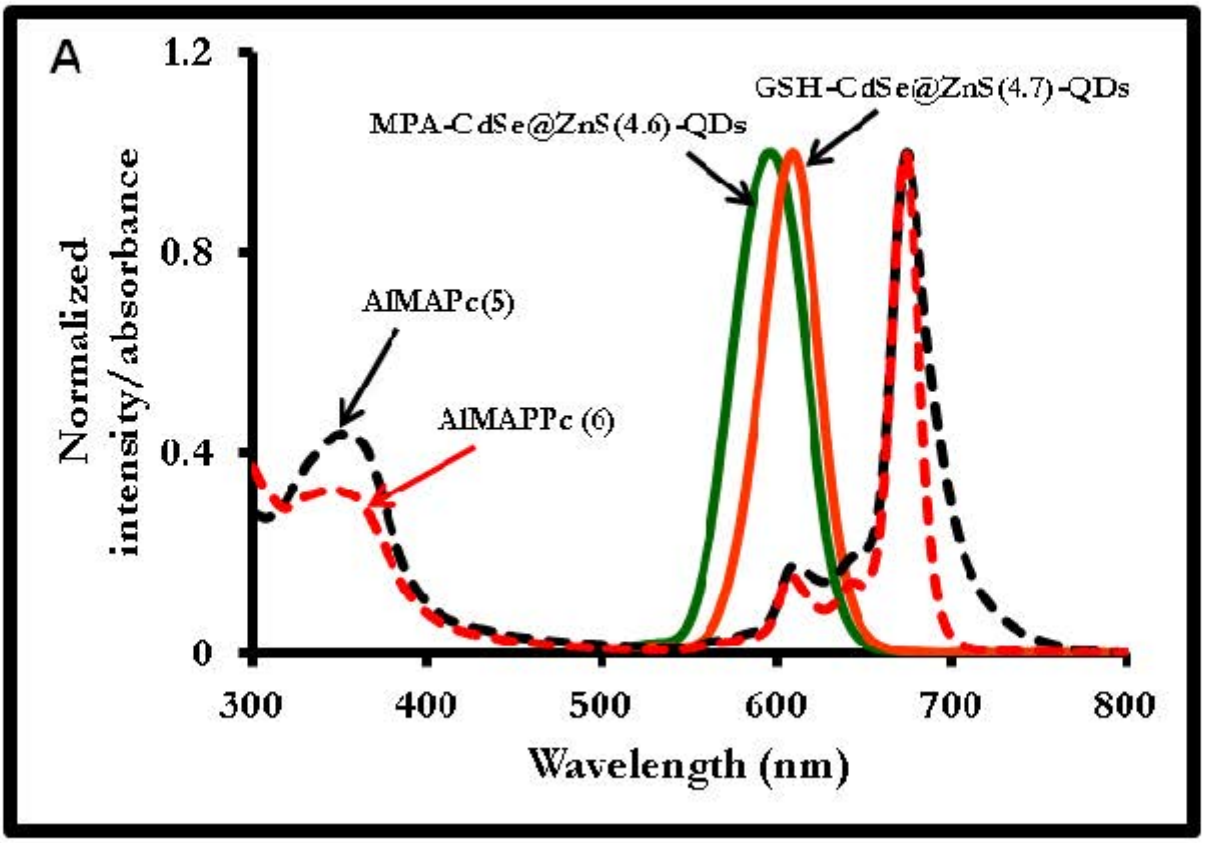
A
1.2
0.8
0.4
0
Normalized intensity/absorbance
GSH-CdSe@ZnS(4.7)-QDs
MPA-CdSe@ZnS(4.6)-QDs
AlMAPc(5)
AlMAPPc (6)
300
400
500
600
700
800
Wavelength (nm)

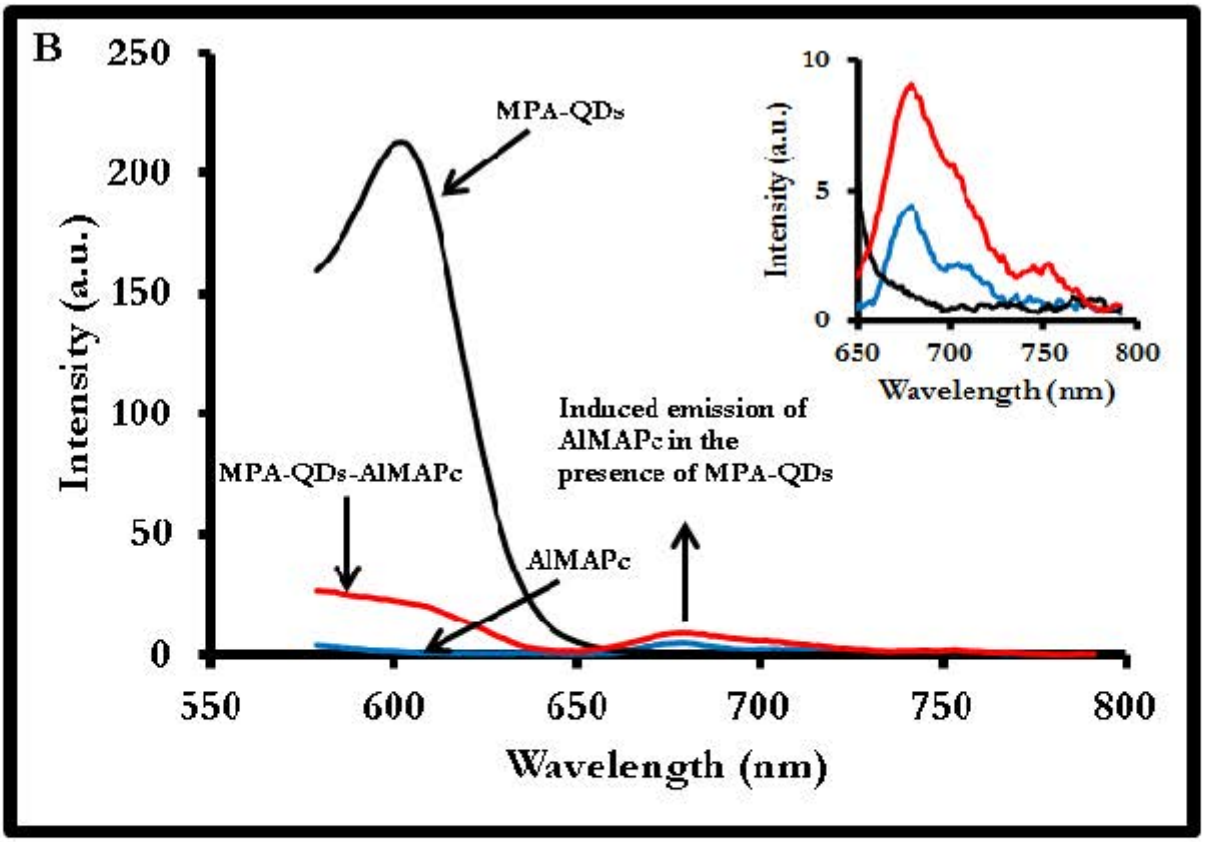
B
250
200
150
100
50
0
Intensity (a.u.)
MPA-QDs
MPA-QDs-AlMAPc
AlMAPc
Induced emission of AlMAPc in the presence of MPA-QDs
10
5
0
Intensity (a.u.)
650
700
750
800
Wavelength (nm)
550
600
650
700
750
800
Wavelength (nm)

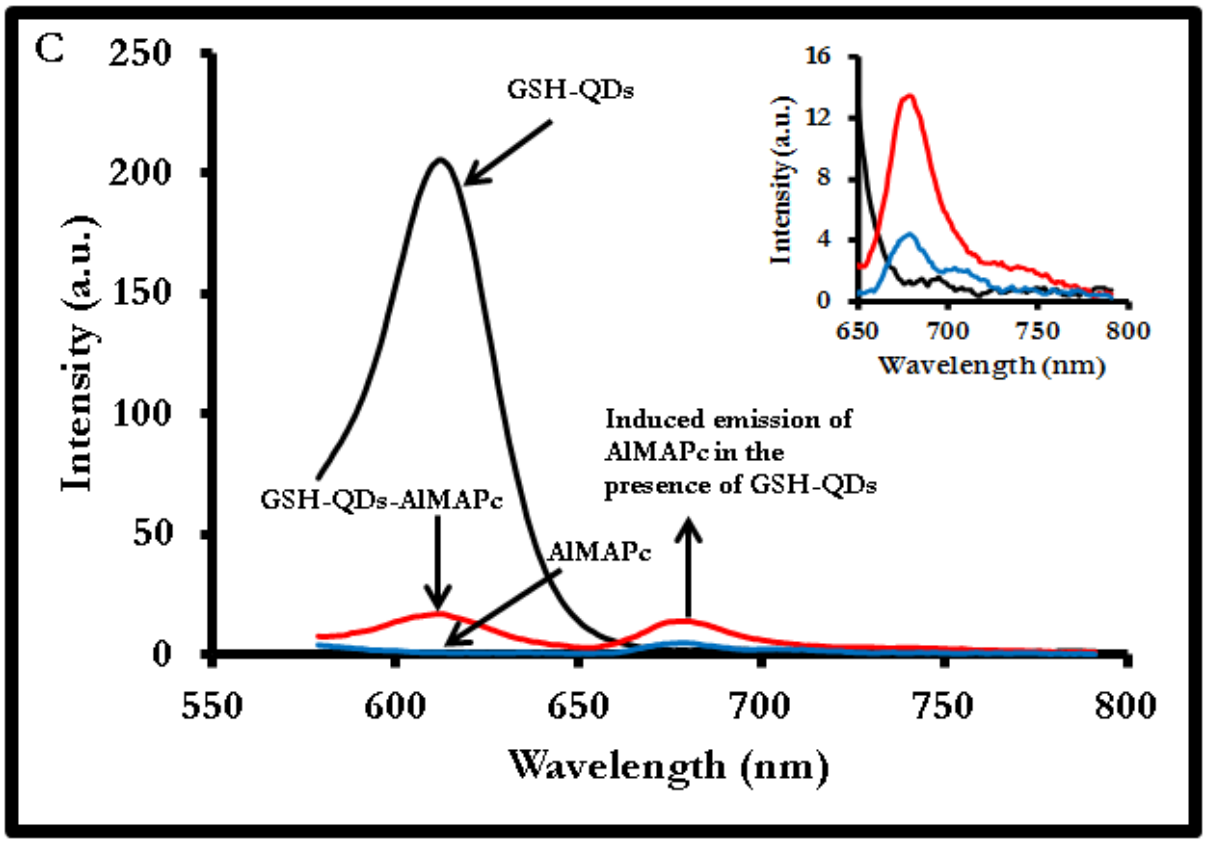

Fig. 3.12. (A) Normalized intensity/absorbance showing the overlap between MPA-CdSe@ZnS(4.6) QDs, GSH-CdSe@ZnS(4.7) QDs with compound 5 and 6. (B) Induced emission of 5 through energy transfer from MPA-CdSe@ZnS(4.6) QDs and GSH-CdSe@ZnS(4.7) QDs in the conjugate (used as a representative). Insets: Expanded view for induced emission. λ_{exc} = 560 nm. Solvent: PBS pH 7.4 buffer.

Table 3.3. Fluorescence quantum yields and FRET efficiencies (*Eff*) data for QDs-MPc and its related conjugates. The corresponding size and emission wavelengths of the QDs alone are included.

Conjugates	Φ_F (QDs alone)	Φ_F (QDs-conjugates)	*Eff*	[a]Emi max (nm)
MPA-CdTe@ZnS(3.0)-2	0.57	0.25	0.56	587
MPA-CdTe@ZnS(3.4)-2	0.46	0.05	0.89	626
MPA-CdTe@ZnS(3.0)-1	0.57	0.26	0.35	587
MPA-CdTe@ZnS(3.0)-3	0.57	0.10	0.69	587
MPA-CdTe@ZnS(3.0)-4	0.57	0.09	0.71	587
GSH-CdTe@ZnS(2.6)-3	0.62	0.38	0.39	562
GSH-CdTe@ZnS(3.4)-3	0.14	0.07	0.50	602
GSH-CdTe@ZnS(3.6)-3	0.07	0.02	0.71	619
MPA-CdSe@ZnS(4.6)-5	0.52	0.19	0.63	597
MPA-CdSe@ZnS(4.6)-6	0.52	0.27	0.48	597
GSH-CdSe@ZnS(4.7)-5	0.24	0.08	0.67	609
GSH-CdSe@ZnS(4.7)-6	0.24	0.05	0.69	609
GSH-CdSe@ZnS(4.7)-7	0.24	0.11	0.54	609
GSH-CdSe@ZnS(4.7)-8	0..24	0.06	0.75	609

[a]Emi max (nm) = Emission wavelength of the QDs alone.

3.4. QDs-4AT conjugate

QDs-4AT conjugate was formed by the covalent linking of the QDs to 4AT. The carboxylic group of the QDs was activated using EDC and thereafter coupled to the amino moiety of 4AT using NHS to form an amide bond (Scheme 3.5).

The XRD pattern of GSH-CdTe QDs-4AT complex is shown in Fig. 3.13B with peaks at 26.6^0, 43.9^0, 51.9^0, which are similar to those obtained for the QDs occurring at 26.5^o, 43.9^o, and 51.8^o (Fig. 3.13A). XRD analysis gives the crystal structure as cubic zinc blend and the (111), (220), and (311) planes being clearly distinguishable in the pattern. It could be seen that the diffraction peaks (Fig. 3.13B) became more intense and narrower compared to QDs alone. Also, as shown in Fig. 3.14, a considerable decrease in the fluorescence of the QDs was observed on coordination with 4AT.

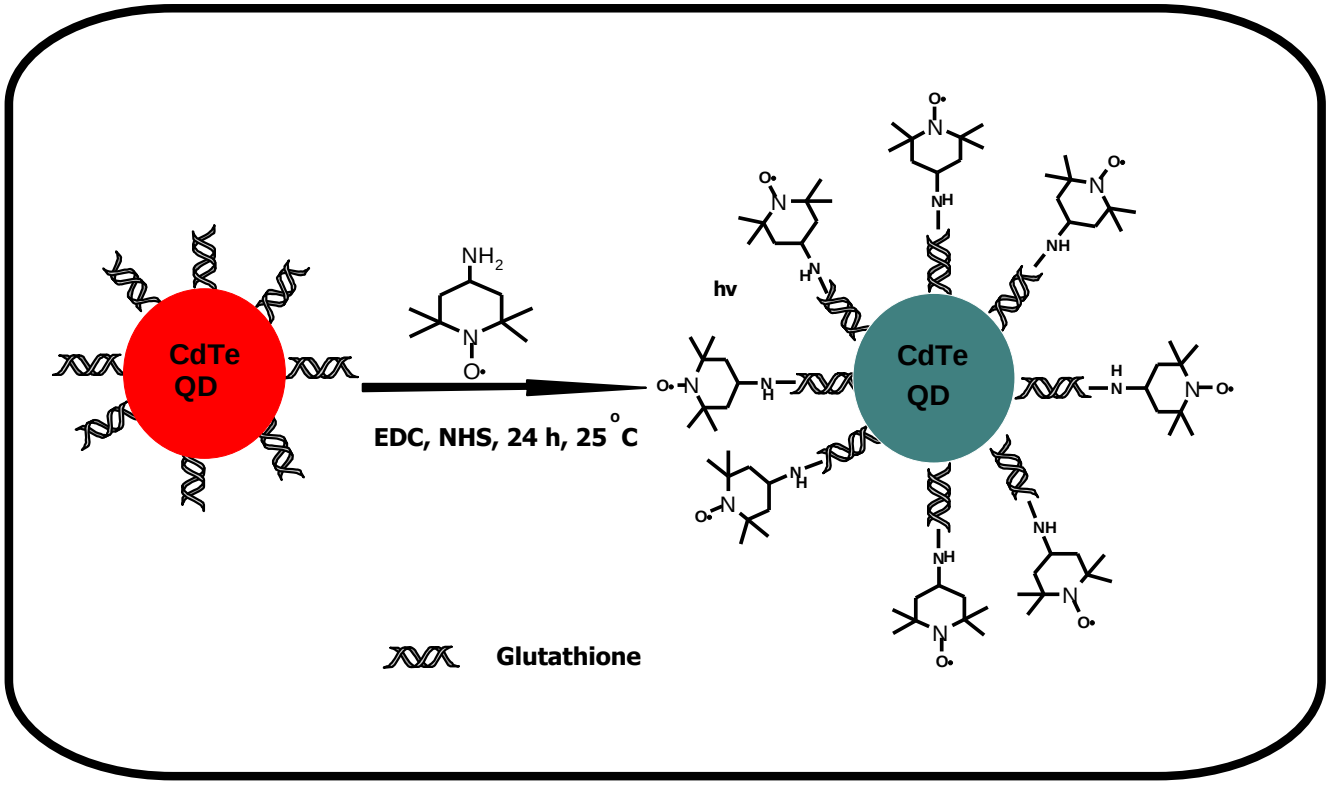

Scheme 3.5. Preparation of QDs-4AT nanoprobe.

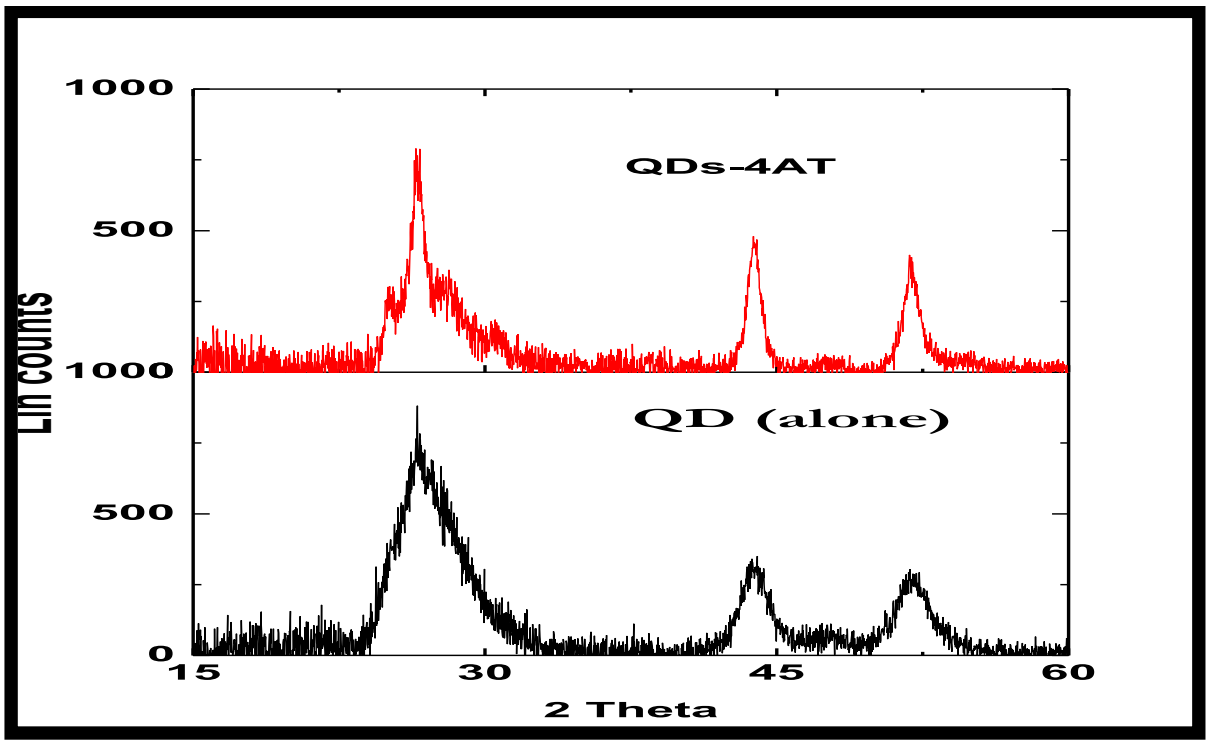

Fig. 3.13. Powder XRD spectra of the QD (alone) and QDs-4AT.

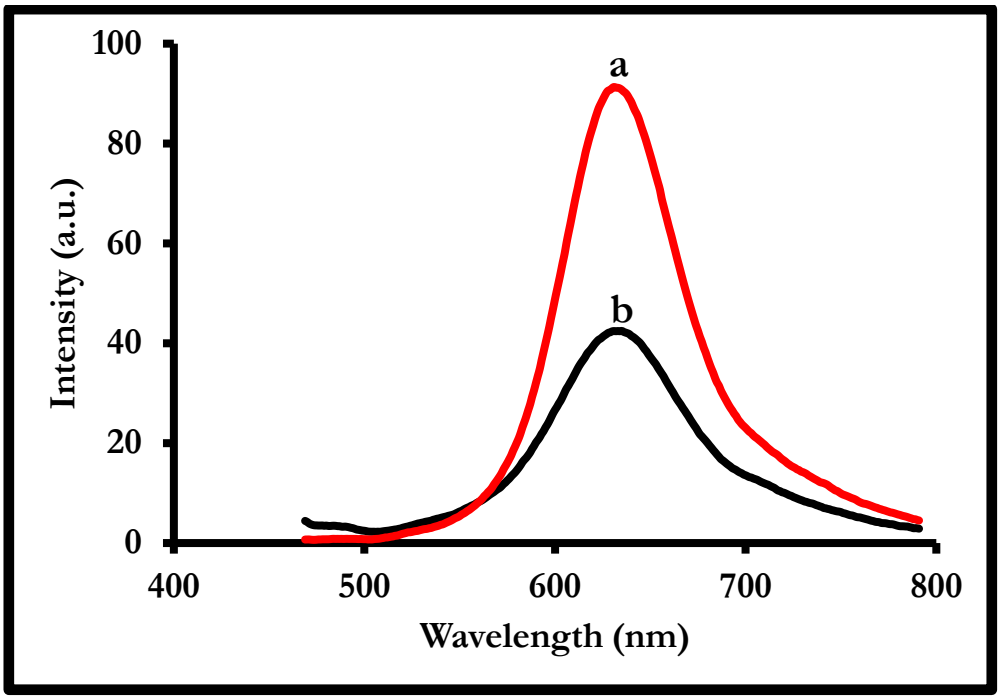

Fig. 3.14. Fluorescence spectra of GSH-CdTe QDs before conjugation (a) and GSH-CdTe QDs-4AT (b) in 50 mM Tris-HCl (pH 7.4). [QDs] = 1.0 mg/mL and [QDs-4AT] nanoprobe = 1.0 mg/mL.

4. DETECTION OF ANALYTES USING QDs ALONE

This chapter presents the quenching of the fluorescence of QDs (alone) by target analytes for use as a fluorescence probe for analyte sensing.

4.1. Interaction of TGA-CdTe QDs with DPPH•

Table 4.1 shows the list of QDs used in this chapter, together with the the analytes detected, linear range, limit of detection (LOD) and measuring signal.

This section reports that the fluorescence of CdTe QDs can be efficiently quenched by DPPH• at different concentrations. TGA-CdTe QDs was used as an example and the effects of the QDs size on the overall quenching will be explored. DPPH• (Scheme 4.1) is a stable paramagnetic free radical with an intense purple colour and has historically been used as a primary spin-concentration standard in electron paramagnetic resonance (EPR). Hence, it was chosen as a model radical for this study. Also, it is popularly known to be a good abstractor of hydrogen yielding its reduced counterpart 2,2-diphenyl-1-picrylhydrazine (DPPH-H) **[208].** The quenching of CdTe by DPPH• is investigated by combined steady state and time resolved fluorescence measurements and the effects of pH on the quenching process are explored. It is expected that the results will provide new fundamental insights into the process of fluorescence quenching of QDs by free radicals for development of QDs-based fluorescent probes for free radicals (as will be presented in later sections).

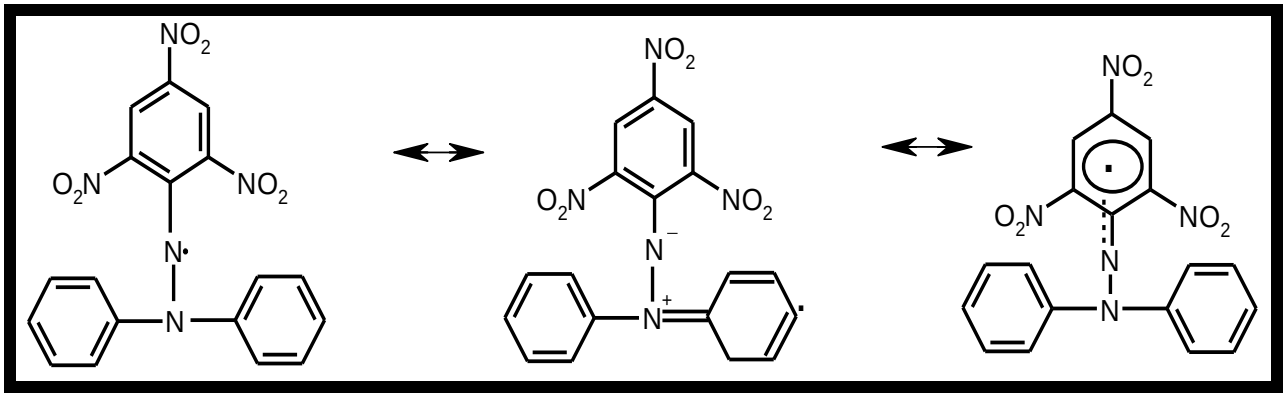

Scheme 4.1. The structure of the stable free radical DPPH•.

Table 4.1. List of QDs (alone) employed for fluorescence sensing using quenching processes. The sizes of the QDs, the analytes detected, linear range and limit of detection (LOD) are included.

QDs (size nm)	Analytes	Linear range (M)	LOD (M)
TGA-CdTe(2.2)	DPPH•	2.0×10^{-8} – 1.4×10^{-7}	4.8×10^{-8}
TGA-CdTe(2.6)	DPPH•	2.0×10^{-8} – 1.4×10^{-7}	5.3×10^{-8}
TGA-CdTe(2.3)	HO•	1.0×10^{-7} - 8.5×10^{-7}	9.7×10^{-8}
MPA-CdTe(2.7)	HO•	1.0×10^{-7} - 8.5×10^{-7}	2.5×10^{-7}
MPA-CdTe@ZnS(3.1)	HO•	1.0×10^{-7} - 8.5×10^{-7}	9.5×10^{-8}
GSH-CdTe@ZnS(3.0)	HO•	1.0×10^{-7} - 8.5×10^{-7}	8.5×10^{-8}
MPA-CdTe(2.7)	$ONOO^-$	5.0×10^{-8} - 4.0×10^{-7}	[a]7.24×10^{-8} [b]1.19×10^{-7}
MPA-CdTe@ZnS(3.1)	$ONOO^-$	5.0×10^{-8} - 4.0×10^{-7}	[a]1.26×10^{-8} [b]1.33×10^{-8}
GSH-CdTe@ZnS(3.0)	$ONOO^-$	5.0×10^{-8} - 4.0×10^{-7}	[a]1.77×10^{-8} [b]3.71×10^{-8}

[b]LOD at pH 9.4. [b]LOD at pH 12.

4.1.1. Fluorescence quenching

Factors such as pH **[209]**, electron donors/acceptors and ionic strength have been reported to have great influence on the fluorescence emission spectra of QDs. In order to study the effects of pH, the quenching of QDs emission by DPPH• was recorded at different pHs (4.8, 7.0 and 10.3). Fig. 4.1 shows the quenching of 2.2 nm and 2.6 nm TGA-CdTe QDs emission on addition of various amounts of DPPH• recorded at pH 7.0 (as a representative of the rest of the pHs). The fluorescence intensity decreased gradually with increasing concentration of DPPH•. No feasible change in the shape of the fluorescence spectra was observed upon quenching. The LOD which is defined as the smallest concentration of the analytes that is statistically distinguishable from the blank was evaluated according to the equation LOD = 3 δ/K, where δ is the standard deviation of blank measurement and K is the slope of the calibration graph. The linear range was between 2.0 x 10^{-8} – 1.4 x 10^{-7} M and the LOD was 4.8 × 10^{-8} and 5.3 × 10^{-8} M for 2.2 and 2.6 nm QDs respectively at pH 7.0, Table 4.1. The quenching of QDs fluorescence by DPPH•, may be represented by the Stern-Volmer equation (Eq. 4.1).

$$\frac{F_0}{F} = 1 + Ksv(Q) \qquad (4.1)$$

where F_0 and F are the steady-state fluorescence intensity in the absence and presence of the quencher (DPPH•); K_{SV} is the quenching rate constant and [Q] is the concentration of quencher (DPPH•). As shown in Fig. 4.1 insets, linear Stern-Volmer plots were obtained for all pH conditions (pH 4.8, 7.0, and 10.3), irrespective of the QDs size.

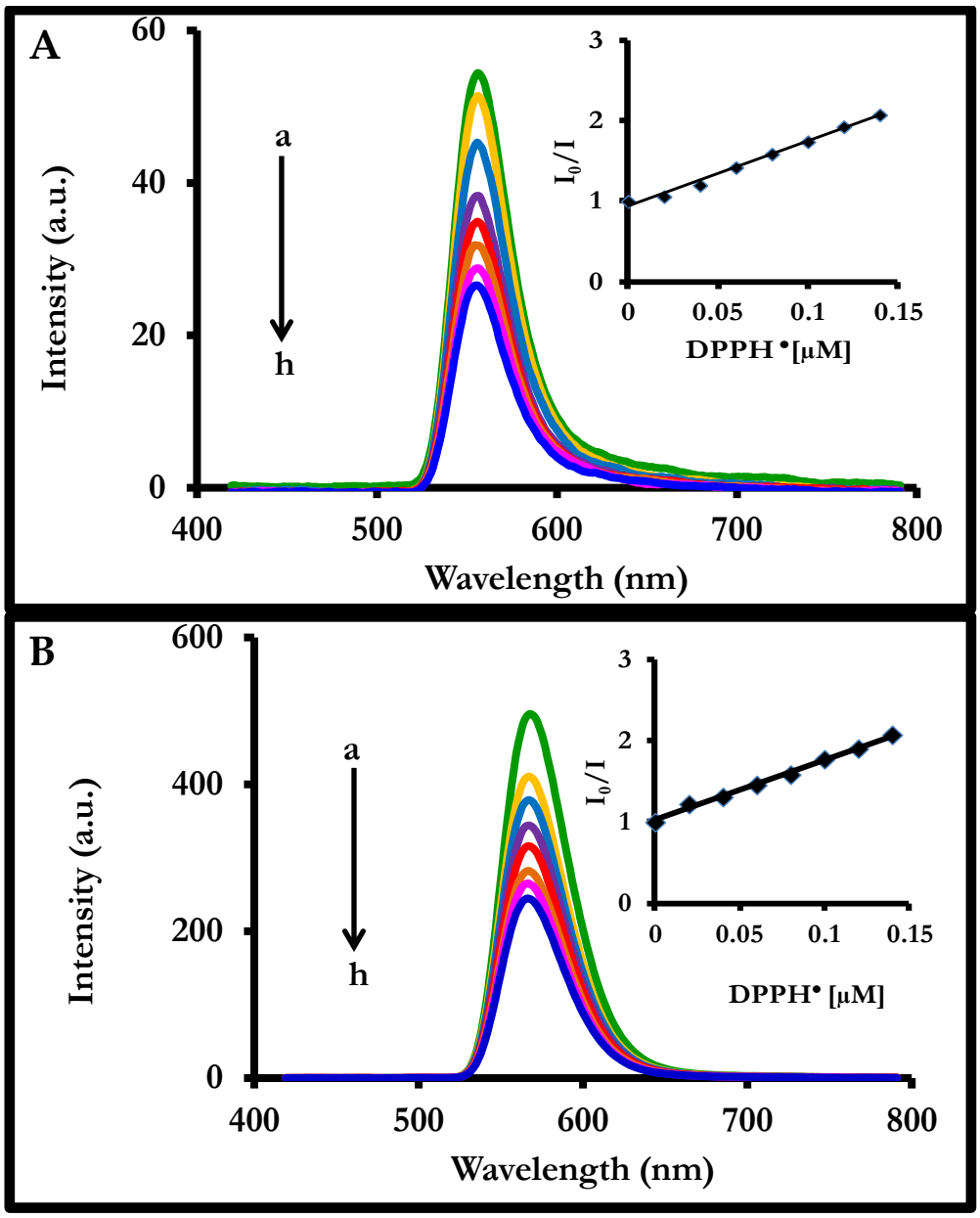

Fig. 4.1. Fluorescence spectra of 2.2 nm QDs (A) and 2.6 nm QDs (B) in the presence of increasing concentration of DPPH• in MeOH: Tris-HCl buffer solution at pH 7.0. a: absence of DPPH•, b-h: 0.02, 0.04, 0.06, 0.08, 0.1, 0.12 and 0.14 μM. Inset: corresponding Stern-Volmer plot.

Table 4.2 lists the K_{SV} values for both 2.2 nm and 2.6 nm QDs. From the high values of K_{SV} at low pH, it can be concluded that the QDs are more exposed to quenching than at high pH. As reported before **[210]**, the change of pH influences the surface of

the QDs. At low pH levels, capping agents may be removed from the surface of the QDs; hence exposing the QDs to more quenching and hence larger K_{SV} values. At high pH, the instability of DPPH• has been proposed **[208].** This may suggest the lower quenching efficiency observed in alkaline media in addition to pH effects on QDs. Linear or curved (upward or downward) Stern-Volmer plots obtained for static quenching, depends on the association constants **[211]**. Also, the pH dependence of the Stern-Volmer plots was more effective for the 2.2. nm QDs than for the 2.6 nm QDs which may be due to the larger surface area of the 2.2. nm QDs compared to the 2.6 nm QDs. Linear plots are usually observed for dynamic quenching and may also be obaserved for static quenching.

Fluorescence lifetime measurements are the most useful method for differentiating between static and dynamic quenching **[212]**. It is a vital tool used in luminescence technology in elucidating possible interactions between a fluorophore and sensing specie. It can provide key information on the recombination of photoinduced carriers in QDs. The QDs exhibit triexponential decay in the presence and absence of DPPH• and the lifetimes are listed in Table 4.3. No changes were observed in the fluorescence lifetimes in the presence of DPPH• and when increasing the concentration of DPPH•, Table 4.3. For dynamic quenching, the fluorescence lifetimes vary proportionally with the quencher concentration while in the case of static quenching the lifetimes are independent of quencher concentration **[213**]. The fact that the fluorescence lifetime values are virtually constant in Table 4.3, suggests that static quenching predominates.

Table 4.2. Static quenching rate constants (K_{SV}) at pH 4.8, pH 7.0 and pH 10.3 and first-order reaction rate constant (k) at pH 7.0 calculated from the fluorescence data of TGA-capped QD-DPPH• system for 2.2 and 2.6 nm QDs respectively. Solvent: MeOH:Tris-HCl buffer.

QD size (nm)	pH	K_{SV} (10^6 M^{-1})	k
2.2	4.8	8.43	-
	7.0	8.03	0.30
	10.3	6.71	-
2.6	4.8	7.41	-
	7.0	7.32	0.22
	10.3	7.29	-

Table 4.3. Fluorescence lifetime of TGA-capped CdTe QDs in the absence and presence of DPPH•. Solvent: MeOH:Tris-HCl buffer.

QD (nm)	[DPPH•] (μM)	τ_2 (ns) [a] (±0.15)	τ_2 (ns) [a] (±0.09)	τ_3 (ns) [a] (±0.01)	Mean lifetimes (ns) (±0.1)
2.2	0	20.1 (0.66)	6.1 (0.30)	0.9 (0.04)	9.0
	0.02	20.6 (0.67)	6.3 (0.28)	1.0 (0.05)	9.3
	0.04	20.4 (0.67)	6.3 (0.29)	1.0 (0.04)	9.2
	0.06	20.2 (0.67)	6.2 (0.29)	0.9 (0.04)	9.1
2.6	0	22.5 (0.75)	7.8 (0.23)	1.1 (0.02)	10.5
	0.02	22.4 (0.77)	7.8 (0.21)	1.1 (0.02)	10.5
	0.04	22.6 (0.77)	7.9 (0.21)	1.1 (0.02)	10.5
	0.06	22.4 (0.77)	7.7 (0.21)	1.0 (0.02)	10.4

4.1.2. Kinetics

There have been very few reports on the antioxidant activity and the catalytic ability of inorganic nanoparticles to scavenge free radicals **[214]**. To further understand the interaction between CdTe QDs and DPPH•, we have investigated the interaction of TGA-capped CdTe QDs with DPPH• free radicals. Fig. 4.2 presents UV-vis absorption spectral changes (with time) of DPPH• in the presence of CdTe QDs. On addition of QDs to DPPH•, there was evidence of enhancement of the absorption peaks due to DPPH• at wavelengths shorter than 400 nm, Fig. 4.2. The DPPH• peak at 350 nm is enhanced and also shifts with time confirming formation of a new product between DPPH• and QDs. This observation suggests static quenching. It could be seen that the absorption maximum at 547 nm due to DPPH•, decreased with time in the presence of a fixed concentration of the QDs. However, the decrease in absorbance was slow and strongly dependent on the nanoparticle size with the purple colour of the radical being bleached gradually. Notwithstanding, the decrease in absorbance was detectable within 15 minutes of the reaction and confirms an efficient scavenging of DPPH• and a possible reduction to 2,2-diphenyl-1-picrylhydrazine (DPPH-H), Scheme 4.2, at pH 7.

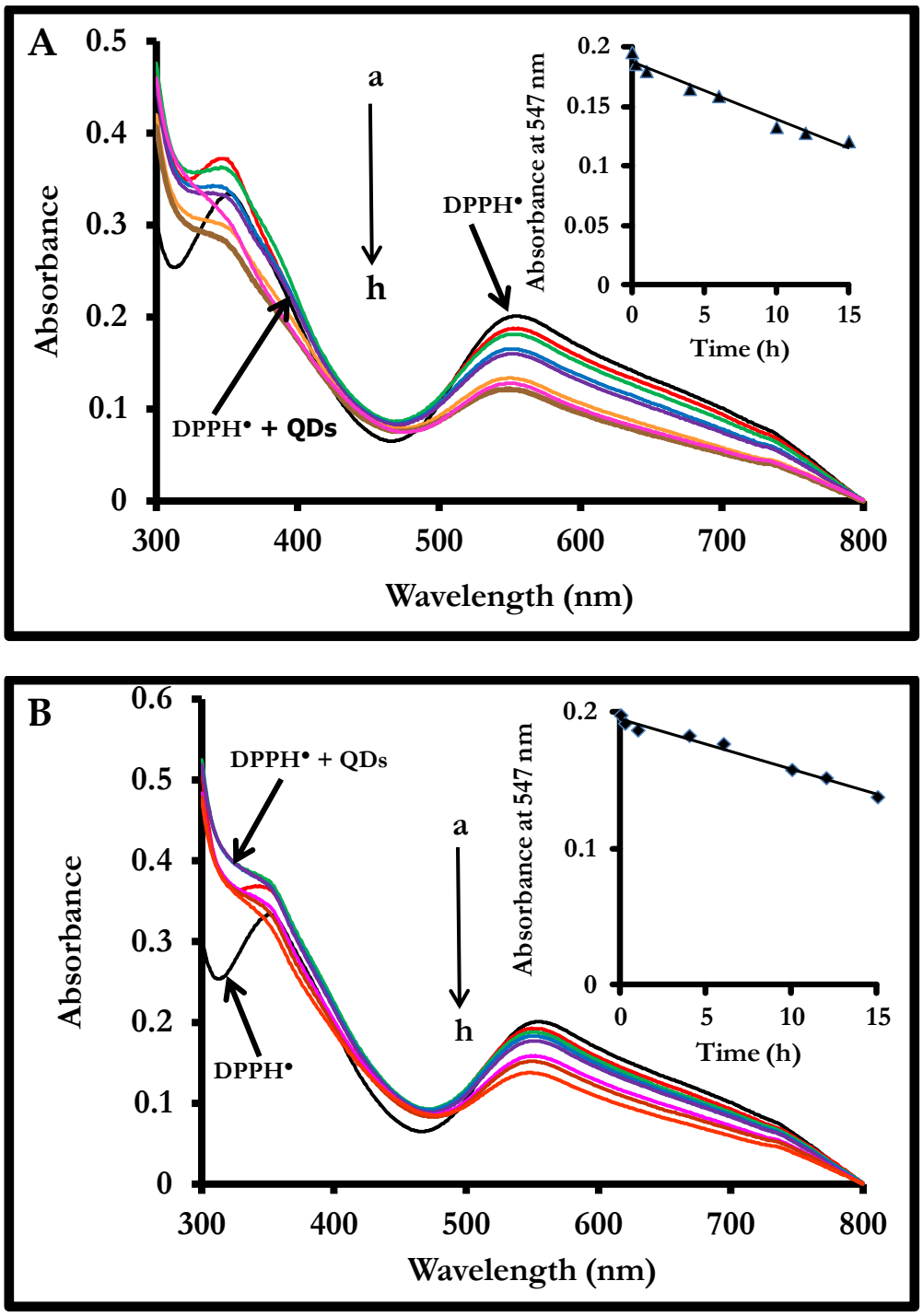

Fig. 4.2. UV-vis absorption spectral changes with time observed following addition of (A) 2.2 nm QDs (1.8 μM) and 2.6 nm QDs (1.8 μM) to solutions of 0.1 μM DPPH•; a: absence of QDs, b-h (DPPH• + QDs): 0.25, 1, 4, 6, 10, 12, 15 h). Insets: Corresponding plot of absorbance maximum at 547 nm against time for DPPH•. Solvent: MeOH:Tris-HCl buffer solution (pH 7.0).

Kinetics of the CdTe QDs-DPPH• system follows a first-order-reaction as shown in the insets of Fig. 4.2A and 4.2B. The first-order reaction rate constants (k) were evaluated from the slope of each line and are: 0.30 min^{-1} for 2.2 nm QDs and 0.22 min^{-1} for 2.6 nm QDs respectively, at pH 7.0. Thus, the smaller QDs react with DPPH• faster than the larger ones. Since TGA (used as capping agent) is also a known reducing agent **[215]**, experiments were performed where the capping agent (TGA) alone was added to DPPH•, and spectral changes similar to those in Fig. 4.2 were observed. Thus, the changes in the rate constants are related to the number of TGA capping agents which would be more for the smaller QDs, hence the larger rate constant compared with the larger QDs.

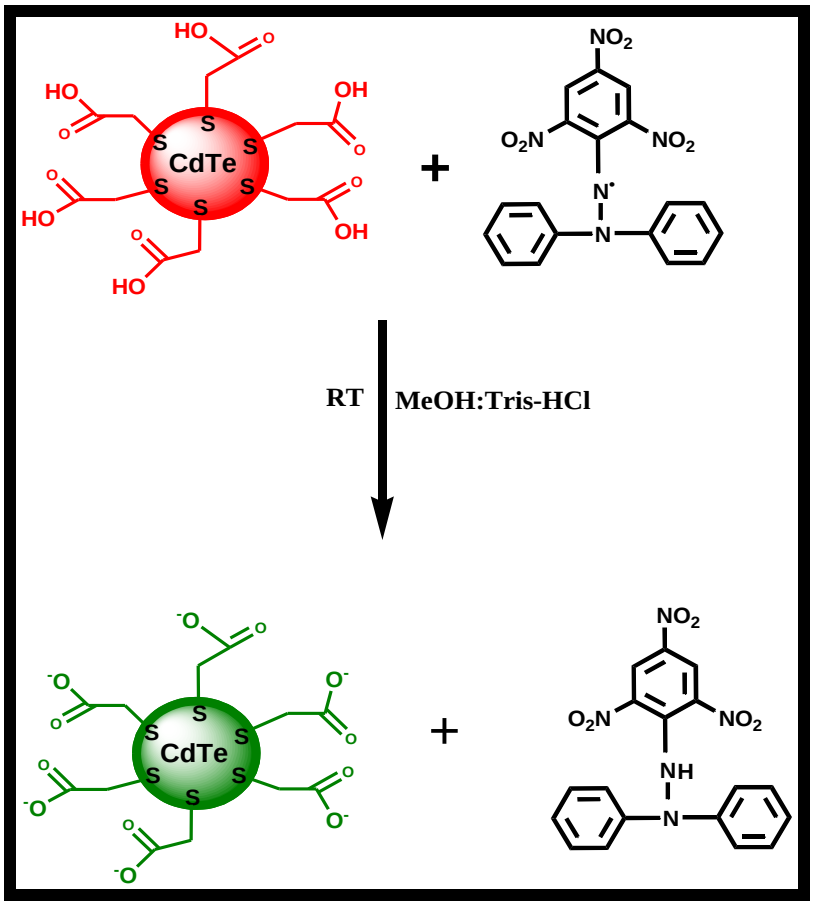

Scheme 4.2. Proposed reaction between DPPH• and TGA-CdTe QDs.

4.1.3. Conclusions

In this section, the interaction between TGA-capped CdTe QDs and DPPH• free radical has been studied by UV-visible absorption and by steady state and time resolved fluorescence measurements. The results show clearly that DPPH• effectively quenches the fluorescence of TGA-capped CdTe QDs (used as a representative) through formation of a ground state complex (static quenching) which was confirmed by fluorescence lifetime studies. The quenching behaviour was described by the Stern-Volmer relationship and a linear plot was observed. Time course absorption studies revealed that DPPH• could be reduced to its subsequent hydrazine form (DPPH-H) in the presence of CdTe QDs. The fact that QDs showed efficient fluorescent quenching sensitivity towards DPPH• radical investigated indicates that they hold promising application for development of probes as sensors for detection of free radicals as will be presented in later sections.

4.2. HO• sensing

For these studies, core (CdTe) and core-shell (CdTe@ZnS) QDs were employed as examples to compare their fluorescence sensing efficiency. The coating of the core with a higher bandgap material such as ZnS can be an effective tool for influencing the chemical, optical and photocatalytic properties of QDs. This can lead to an improvement in the photostability and enhancement in sensitivity and selectivity of the QDs**.** Hence, in this work, a sensor for HO• is developed and effects of different capping agents are investigated. QDs used are: TGA-CdTe(2.3 nm), MPA-CdTe(2.7 nm), MPA-CdTe@ZnS(3.1 nm) and GSH-CdTe@ZnS(3.0 nm).

4.2.1. Effect of pH and types of buffer

GSH-CdTe@ZnS(3.0 nm) QDs was chosen as a representative for all the QDs to optimize the HO• detection conditions. Different buffers such as, phosphate buffered solution (PBS), acetate buffer, phosphate buffer, citric acid-NaOH, tris-ethylenediaminetetraacetic acid (Tris-EDTA) and Tris-HCl were examined (all at pH 7.4) and our results showed that Tris-HCl (50 mM) was best suited because it resulted in the largest quenching of the QDs fluorescence on addition of HO•, Fig 4.3 inset. Thus, Tris-HCl was selected for further experiments. As explained in Section 2.7.3, it is possible that certain buffers does interfere with the detection of specific analytes, hence the same pheneomenon could be explained here that the lower fluorescence response experienced for the other buffer (with the exception of Tris-HCl) could be due to the fact that they interfered with the detection of HO•. pH could have a drastic influence on the fluorescence intensity of QDs, which could affect both the sensitivity and selectivity of target analytes **[216],** while the capping agent is also known to be protonated at the surface of the QDs in acidic pH**.** Hence, the effect of pH on the fluorescence intensity of aqueous QDs-HO• system was investigated at different pH values. Fig. 4.3 shows that there was more quenching of fluorescence of the QDs by HO• in the pH range 6.8 to 7.8. Therefore, pH 7.4, 50 mM Tris-HCl buffer was selected for further experiments.

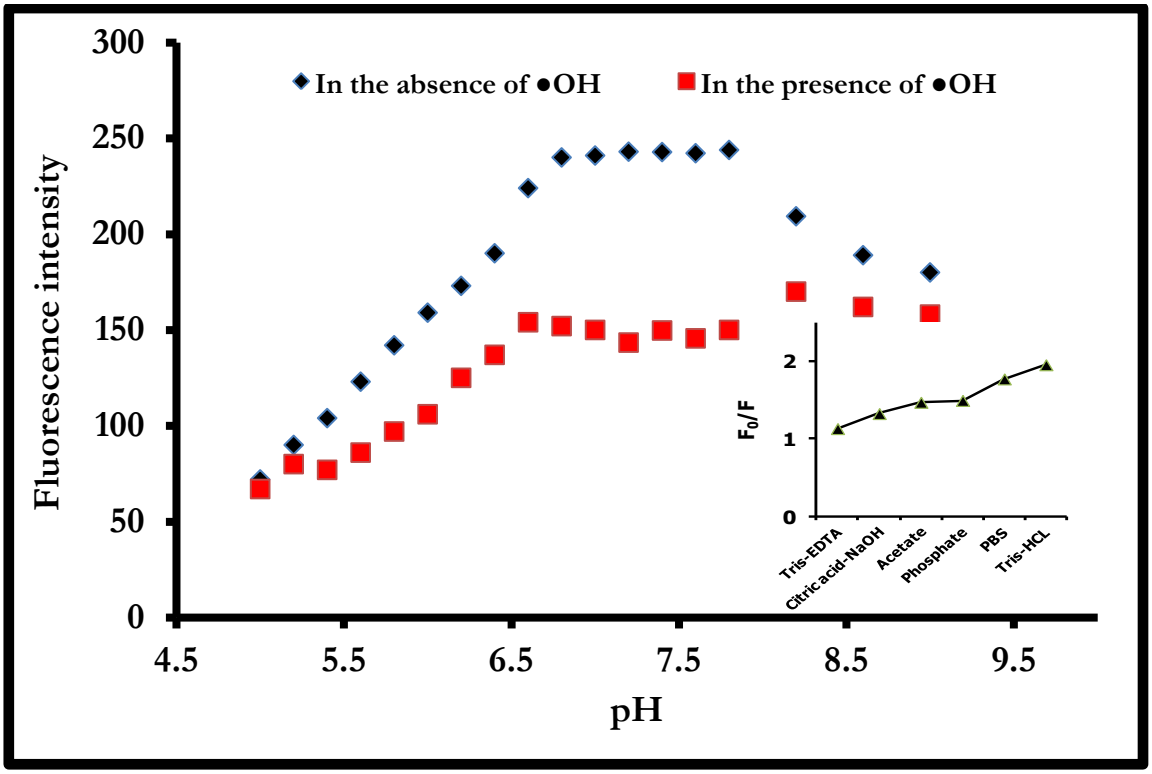

Fig. 4.3. Effects of pH on the fluorescence intensity of GSH-CdTe@ZnS(3.0 nm) QDs-HO• solution system ([QDs]: 6.7 x 10^{-7} M, [•OH]: 2.5 x 10^{-7} M s^{-1}, solvent: 50 mM Tris-HCl buffer). Inset: Effect of different buffers on the fluorescence intensity. F_0 and F are the fluorescence intensity of aqueous CdTe@ZnS QDs without and with •OH).

4.2.2. Fluorescence quenching

Under the optimum conditions, it was found that HO• quenched the fluorescence of CdTe and CdTe@ZnS QDs (Fig. 4.4) in a concentration-dependent manner that was best described by the linear Stern-Volmer relationship, Eq. 4.1.

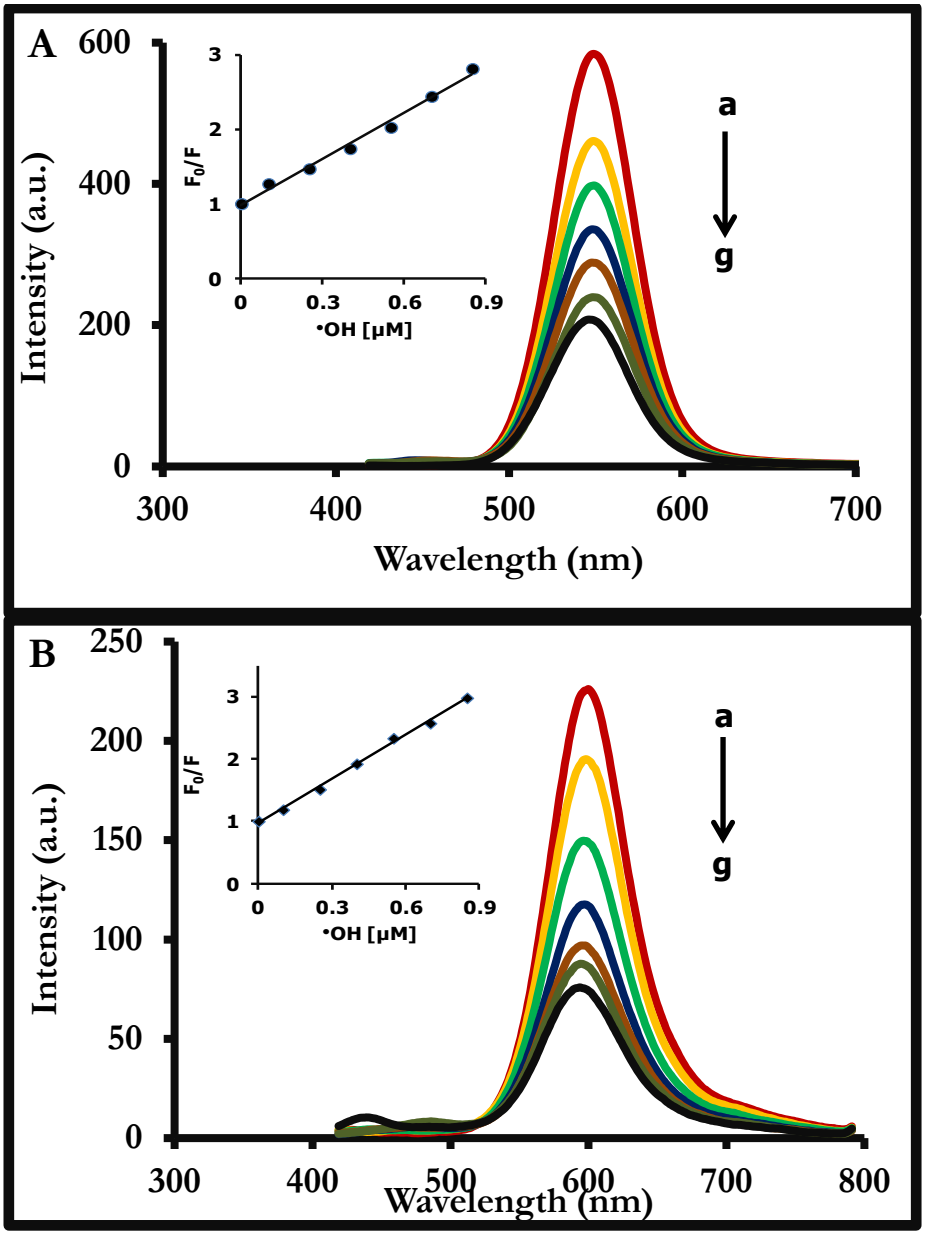

Fig. 4.4. Effects of addition of different concentrations of HO• on the fluorescence of (A) TGA-CdTe(2.3 nm) QDs and (B) GSH-CdTe@ZnS(3.0 nm) QDs shown as a representative. [HO•]: (a) 0, (b) 1.0 x 10^{-7}, (c) 2.5 x 10^{-7}, (d) 4.0 x 10^{-7}, (e) 5.5 x 10^{-7}, (f) 7.0 x 10^{-7} and (g) 8.5 x 10^{-7} M s^{-1}. Inset: corresponding Stern-Volmer plots. Solvent: 50 mM Tris-HCL buffer pH 7.4.

Based on the rate constant of 8 x 10^3 M^{-1} s^{-1} **[217],** which has been reported for Fe^{2+}/EDTA Fenton's reaction, the concentrations of HO• were calculated to be 1 x

10^{-7}, 2.5 x 10^{-7}, 4.0 x 10^{-7}, 5.5 x 10^{-7}, 7.0 x 10^{-7} and 8.5 x 10^{-7} M, in the presence of 4.2 x 10^{-7}, 1.0 x 10^{-6}, 1.7 x 10^{-6}, 2.3 x 10^{-6}, 2.9 x 10^{-6} and 3.5 x 10^{-6} M Fe^{2+}/EDTA respectively and 3 x 10^{-5} M H_2O_2 according to a method described by Maki et al **[218]**.

GSH-CdTe@ZnS(3.0 nm) QDs exhibited the best sensitivity (larger K_{SV}) for the detection of HO• while MPA-CdTe(2.7 nm) QDs showed the least sensitivity (comparing the K_{sv} values, Table 4.4). Also, the K_{SV} value was found to be higher for TGA-CdTe(2.3 nm) QDs than MPA-CdTe(2.7 nm) QDs when considering the same kind of QDs core. However, different sizes of the QDs will affect the results, Table 4.4. The core-shell CdTe@ZnS QDs were however more sensitive and are best suited for the detection of HO• than the core CdTe QDs, when comparing MPA-CdTe(2.7 nm) QDs and MPA-CdTe@ZnS(3.1 nm) QD containing the same capping agent even though the latter was slightly larger in size. This may be due to the fact that the coating of a secondary layer with a wider bandgap semiconductor such as ZnS has been reported to passivate the surface of the QDs and can increase the extent of fluorescence quenching in the presence of a quencher [**219**].

Also, it was noticed that the nature of the capping agent of the QDs influenced the sensitivity of the probe (Table 4.4). For example, GSH capping on CdTe@ZnS has a slightly larger K_{SV} value than when MPA is employed for the same core-shell QDs even though the sizes of these QDs differ only by 0.1 nm. This effect may be related to reports that GSH provides better surface passivation for QDs than other thiol ligands [**220**]. All results suggest that the differing degree of sensitivity of the core and coreshell QDs to HO• may depend on multiple factors. Capping agent, QD size, oxidative, photolytic and mechanical stability are individual and collective factors

that can influence the sensitivity of the QDs to HO•, hence the difference in sensitivity of core and coreshell QDs towards HO•.

The limit of detection (LOD) was evaluated according to the equation LOD = 3 δ/K, where δ is the standard deviation of blank measurement (n = 10) and K is the slope of the calibration graph. The LOD correlated favourably with the sensitivity of the probe and the best value of 8.5 x 10^{-8} M (Table 4.4) was obtained for GSH-CdTe@ZnS QDs with a correlation coefficient of 0.997.

Table 4.4. Quenching rate constant (K_{SV}) and LOD for different QDs used for the detection of HO•. Solvent: 50 mM Tris-HCl pH 7.4.

QDs(size nm)	Ksv (M^{-1})	LOD (M)
TGA-CdTe(2.3)	2..0 × 10^6	9.7 × 10^{-8}
MPA-CdTe(2.7)	1.5 × 10^6	2.5 × 10^{-7}
MPA-CdTe@ZnS(3.1)	2.1 × 10^6	9.5 × 10^{-8}
GSH-CdTe@ZnS(3.0)	2.4 × 10^6	8.5 × 10^{-8}

4.2.3. Selectivity studies

A high selectivity for the detection of HO• is needed for fluorescent probes. H_2O_2, $ONOO^-$ and HO• have been reported to quench the fluorescence of QDs **[221-223]**. As a result, we have evaluated the effect of different ROS ([O_2^{-}•] = 200 μM, [$ONOO^-$] = 300 μM, [H_2O_2], [TBHP] and [ClO_4^-] = 50 μM) on the fluorescence response of TGA-CdTe, MPA-CdTe and MPA-CdTe@ZnS and GSH-CdTe@ZnS QDs and the results showed that the fluorescence of TGA-CdTe, MPA-CdTe and MPA-

CdTe@ZnS and GSH-CdTe@ZnS QDs were sensitive to $ONOO^-$ and H_2O_2 but was more significantly quenched by HO• (Fig. 4.5A). This implies that the QDs probe can be used to detect similar ROS but with HO• displaying a more staggering effect. A tolerable error of ±5.0% in the relative fluorescence intensity was taken into consideration. The effect of co-existing ROS on the fluorescence of CdTe and CdTe@ZnS QDs were studied by mixing an equivalent concentration of HO• (0.85 μM s^{-1}) and an excess of interfering species. Fig. 4.5B, showed there was no significant effect on the fluorescence response of CdTe@ZnS QDs for the detection of HO•. However, for TGA-CdTe and MPA-CdTe QDs, a considerable decrease in fluorescence response was observed in the presence of $ONOO^-$ and H_2O_2 indicating that $ONOO^-$ and H_2O_2 interfered with the probe for CdTe QDs. This makes MPA-CdTe@ZnS and GSH-CdTe@ZnS QDs more attractive for the selective recognition of HO• than CdTe QDs. Since there were negligible interferences by the tested species using CdTe@ZnS QDs, thus demonstrating that this probe has relatively high selectivity and can detect HO•. In addition, the presence of the Fenton reagents ([ascorbic acid], $[Fe^{3+}]$, $[Fe^{2+}]$ and [EDTA] = 100 μM) had no effect on the detection of HO• (Fig. 4.5C).

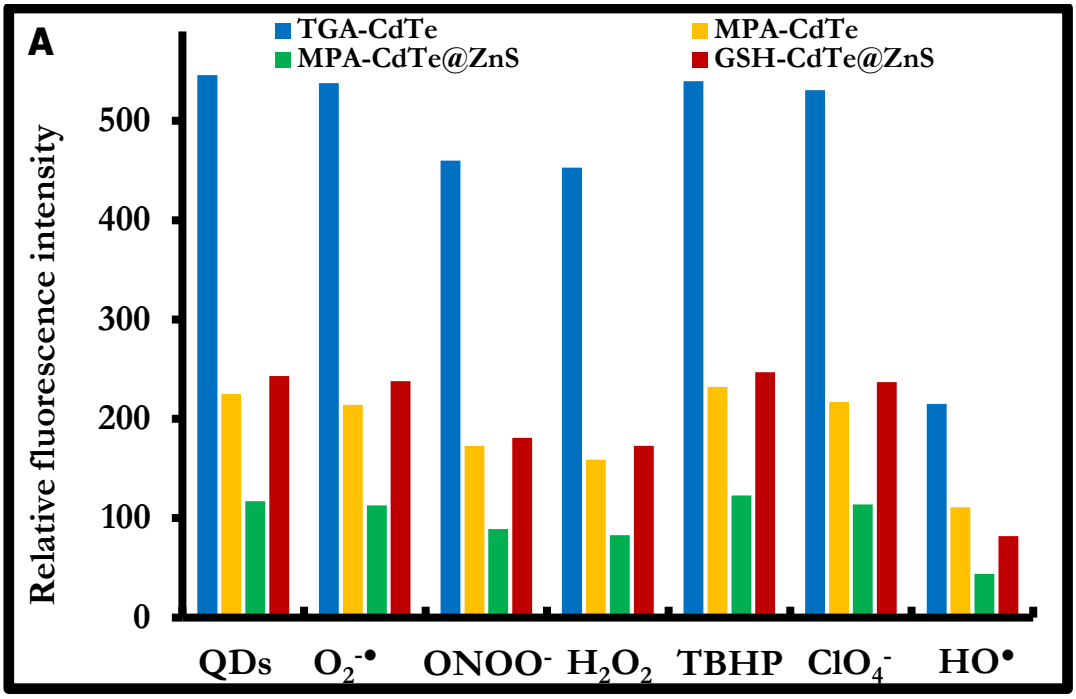
A
TGA-CdTe
MPA-CdTe
MPA-CdTe@ZnS
GSH-CdTe@ZnS
Relative fluorescence intensity
0
100
200
300
400
500
QDs
$O_2^{-\bullet}$
$ONOO^-$
H_2O_2
TBHP
ClO_4^-
$HO^\bullet$

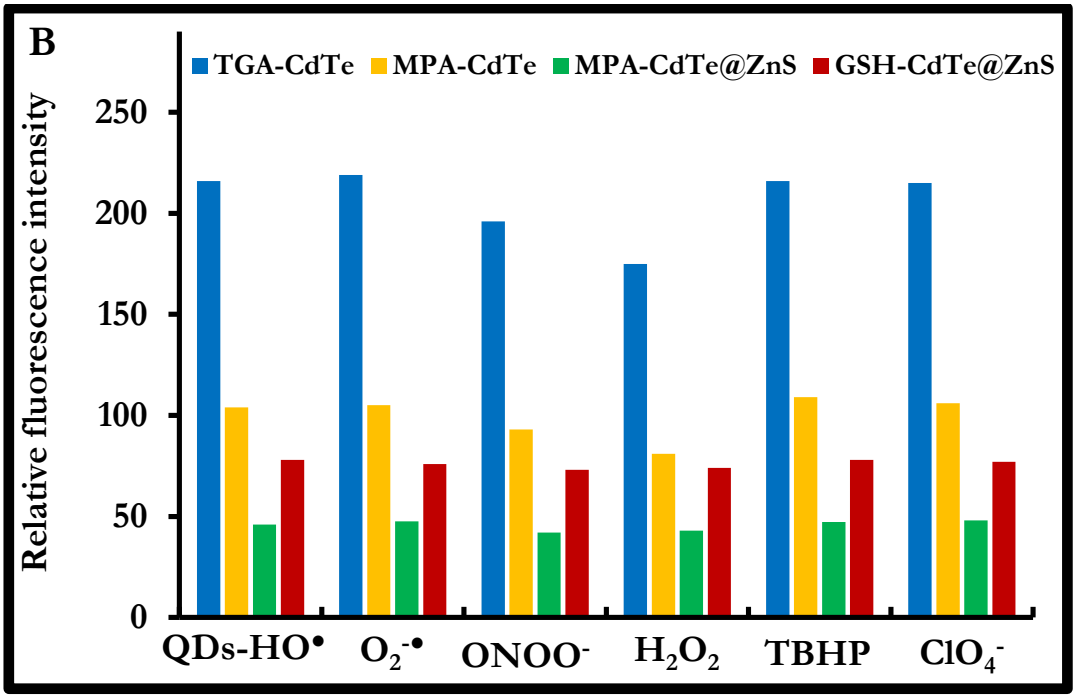
B
TGA-CdTe
MPA-CdTe
MPA-CdTe@ZnS
GSH-CdTe@ZnS
Relative fluorescence intensity
0
50
100
150
200
250
QDs-$HO^\bullet$
$O_2^{-\bullet}$
$ONOO^-$
H_2O_2
TBHP
ClO_4^-

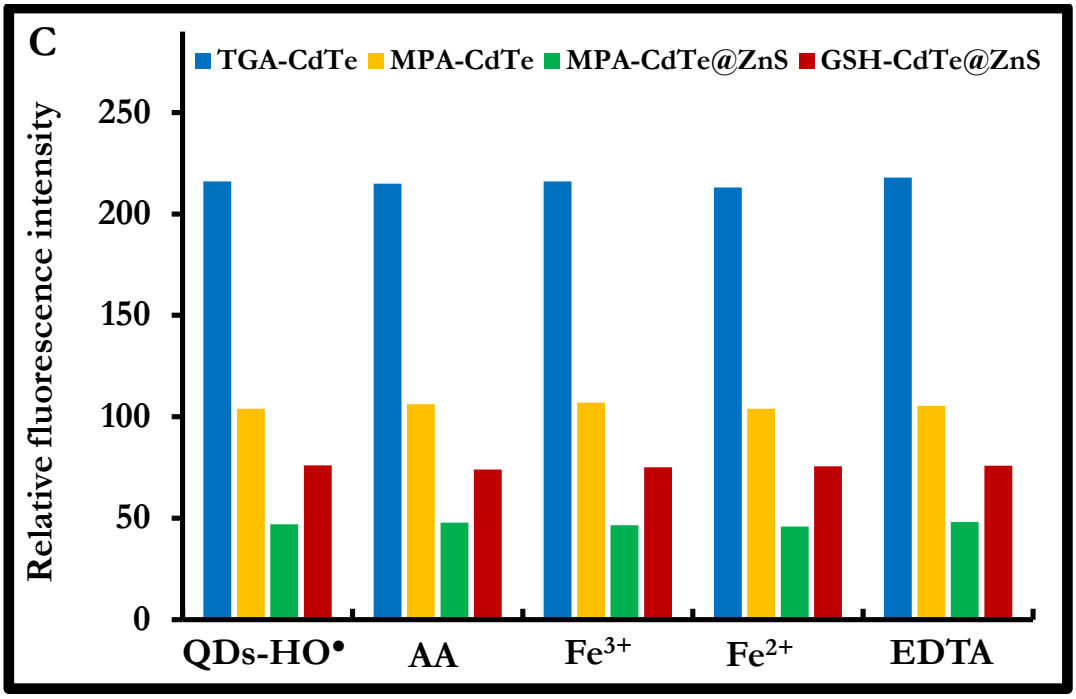

Fig. 4.5. (A) Effect of ROS on the fluorescence of TGA-CdTe, MPA-CdTe and MPA-CdTe@ZnS and GSH-CdTe@ZnS QDs (B) Effect of co-existing ROS and (C) Fenton reactants and products as tested interferences on the detection of HO• by the proposed QDs-based fluorescent probe. Ascorbic acid is abbreviated as AA. Solvent: 50 mM Tris-HCl buffer pH 7.4.

4.2.4. Proposed quenching mechanism

In order to elucidate the mechanism for HO• detection, we carried out fluorescence lifetime measurements on CdTe and CdTe@ZnS QDs. Fig. 4.6 shows the decay curves of CdTe and CdTe@ZnS QDs in the presence of HO•. As shown in Table 4.5, the fluorescence lifetime evaluated from the triexponential decay curve of CdTe and CdTe@ZnS QDs decreased on addition HO• relative to value of the QDs in the absence of HO•, Table 4.5. For dynamic quenching; the fluorescence lifetimes vary with the quencher concentration while in the case of static quenching; the lifetimes

are independent of quencher concentration **[224,225].** The fact that there is a change in the lifetime with at a fixed concentration of HO• indicates that the interaction is mainly dynamic, possibly involving electron transfer (ET) processes. ET from the conduction band of GSH-capped CdTe QDs to HO• (to form hydroxyl ion) has previously been proposed **[221].** We assume that since the presence of the Fenton reactants and products did not interfere with the fluorescence of QDs-HO• probe (as shown in Fig. 4.5C), then HO• is mainly responsible for the quenching of the fluorescence of CdTe and CdTe@ZnS QDs due to its strong electron accepting ability (Scheme 4.3).

Table 4.5. Comparison of the best-fit fluorescence lifetime values for a triexponential fit of CdTe and CdTe@ZnS QDs in the absence and presence of an equivalent of HO• in 50 mM Tris-HCl buffer, pH 7.4.

QDs(size nm)	[HO•] ($\mu M\ s^{-1}$)	τ_1 (ns) ±0.1	τ_2 (ns) ±0.07	τ_3 (ns) ±0.03
TGA-CdTe(2.3)	0	24.0(0.79)	7.3(0.19)	0.9(0.02)
	0.1	22.8(0.80)	7.0(0.18)	0.8(0.02)
MPA-CdTe(2.7)	0	29.0(0.83)	7.0(0.15)	0.8(0.02)
	0.1	28.0(0.83)	6.4(0.15)	0.5(0.02)
MPA-CdTe@ZnS(3.1)	0	33.8(0.68)	12.0(0.30)	1.4(0.02)
	0.1	31.2(0.72)	10.0(0.25)	0.9(0.03)
GSH-CdTe@ZnS(3.0)	0	60.6(0.89)	16.0(0.09)	1.5(0.02)
	0.1	58.1(0.90)	13.3(0.08)	1.3(0.02)

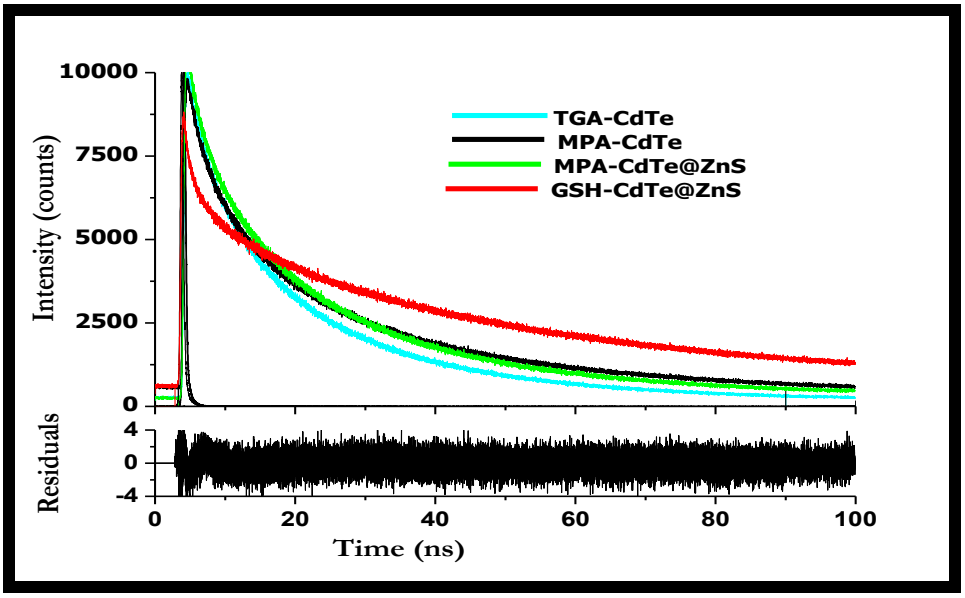

Fig. 4.6. Fluorescence decay curves of CdTe and CdTe@ZnS QDs in the presence of 1.0 x 10^{-7} M s^{-1} HO•. Solvent: 50 mM Tris-HCL pH 7.4 buffer.

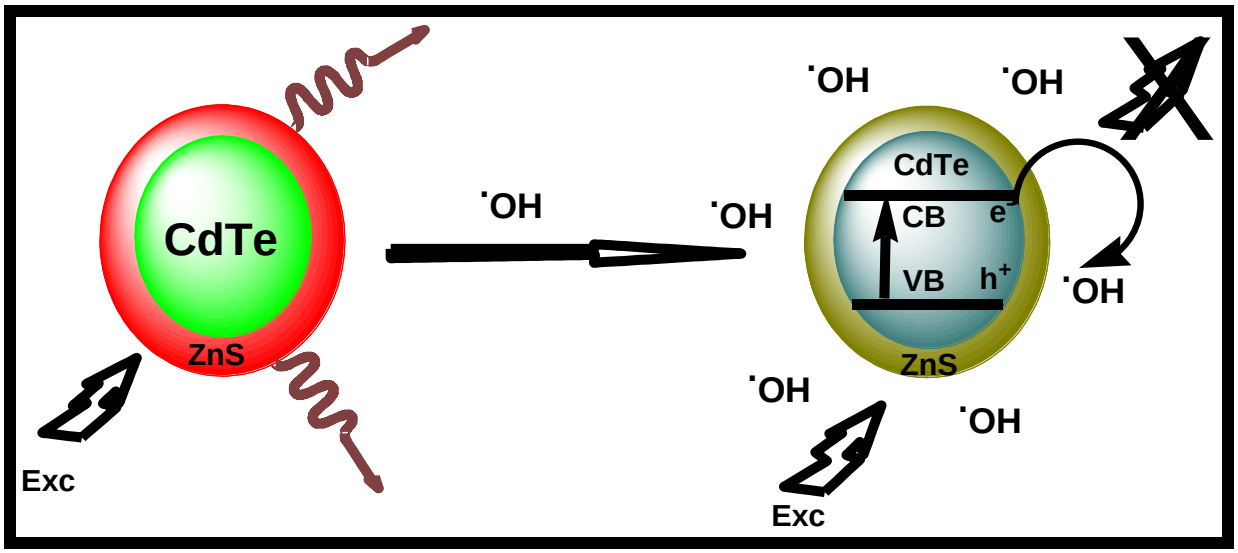

Scheme 4.3. The detection mechanism induced by electron transfer from QDs to HO•.

4.2.5. Conclusions

New QDs probe has been proposed for the sensitive and selective determination of $HO^{\bullet}$ in aqueous media by comparative studies between different thiol-capped CdTe and CdTe@ZnS QDs. The results showed that the type of capping agent and QDs influenced the sensitivity and selectivity of the probe with GSH-CdTe@ZnS giving the best sensitivity. The mechanisms of fluorescence quenching of the QDs is by dynamic quenching, yet static quenching was observed for $DPPH^{\bullet}$. This could be due to differences in electron accepting abilities. Moreover, the proposed probe offered a LOD as low as 8.5×10^{-8} M using GSH-CdTe@ZnS QDs. Interferences from foreign ROS and the Fenton reactants and products were negligible for CdTe@ZnS QDs but CdTe QDs were not very selective towards $HO^{\bullet}$.

4.3. $ONOO^-$ sesnsing

This section reports on the detection of $ONOO^-$ using MPA-CdTe (2.7 nm), MPA-CdTe@ZnS (3.1 nm) and GSH-CdTe@ZnS (3.0 nm) QDs as luminescent probes. The kinetics and mechanism of the reaction are studied.

Fig. 4.7 shows that the shape of the absorption spectrum of as-synthesized $ONOO^-$ is consistent with literature **[222,226]** and thus confirming we have successfully synthesized $ONOO^-$.

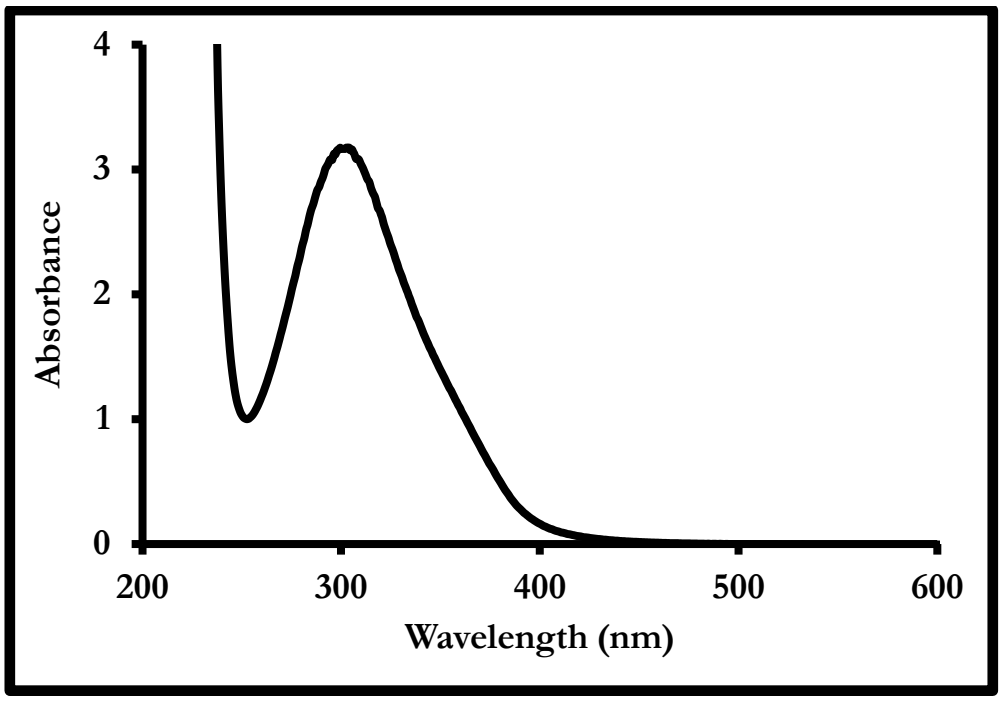

Fig. 4.7. UV/vis absorption spectrum of as-synthesized $ONOO^-$.

4.3.1. Fluorescence quenching

Under the optimum conditions, the fluorescence of CdTe and CdTe@ZnS QDs were quenched by $ONOO^-$ at pH 9.4 and 12. At pH 9.4, a 53% quenching of the fluorescence intensity of MPA-CdTe QDs was observed for a 4 x 10^{-7} M of $ONOO^-$, whereas at the same $ONOO^-$ concentration, 81% and 87% quenching was obtained for GSH-CdTe@ZnS and MPA-CdTe@ZnS QDs respectively, Fig 4.8. At pH 12, a similar trend in quenching pattern was observed for the QDs with $ONOO^-$. This gives a strong indication that CdTe QDs are far less sensitive to $ONOO^-$ than CdTe@ZnS QDs as observed above for $HO^{\bullet}$. An attempt was made to detect $ONOO^-$ at physiological pH 7.4, but due to the fast decomposition rate of $ONOO^-$ at this pH, it was difficult for us to obtain a stable fluorescence signal.

Table 4.6. K_{SV} and LOD for CdTe and CdTe@ZnS QDs used for the detection of $ONOO^-$ at pH 9.4 and pH 12 respectively. Solvent: 50 mM phosphate buffer.

QDs(size nm)	Ksv (M^{-1}) (pH 9.4)	Ksv (M^{-1}) (pH 12)	LOD (nM) (pH 9.4)	LOD (nM) (pH 12)
[a]MPA-CdTe@ZnS(3.1)	1.58×10^7	1.50×10^7	12.6	13.3
[b]GSH-CdTe@ZnS(3.0)	1.13×10^7	5.39×10^6	17.7	37.1
[c]MPA-CdTe(2.7)	2.76×10^6	1.68×10^6	72.4	119.0

Optimum concentration of QDs: [a]7.0×10^{-7} M, [b]6.7×10^{-7} M and [c]1.0×10^{-5} M

MPA-CdTe@ZnS(3.1) QDs exhibited the best sensitivity for the detection of $ONOO^-$ while MPA-CdTe QDs showed the least sensitivity (comparing the K_{SV} values at pH 9.4 and 12, Table 4.6). From Table 4.6, it can be seen that CdTe@ZnS QDs are more sensitive and are best suited for the detection of $ONOO^-$ than the core CdTe QDs when comparing K_{SV} values of MPA-CdTe(2.7) QDs and MPA-CdTe@ZnS(3.1) QD containing the same capping ligand. It was noticed that the nature of the capping ligand of the QDs influenced the sensitivity of the probe as was the case for $HO^\bullet$ (Table 4.4). For example, MPA capping on CdTe@ZnS has a larger K_{SV} value than when GSH is employed. As stated above, the coating of a secondary layer with a wider bandgap semiconductor such as ZnS, passivates the surface of the CdTe core and can increase the efficiency of fluorescence quenching in the presence of a quencher**.** The LOD was evaluated at pH 9.4 and pH 12 and the values of 12.6, 17.7 and 72.4 nM (Table 4.6) were obtained for MPA-CdTe@ZnS, GSH-CdTe@ZnS and MPA-CdTe QDs at pH 9.4 respectively, which are much lower as compared to the

values at pH 12 (Table 4.6). This gives an indication that pH 9.4 is most suitable for the detection of $ONOO^-$ using our method and was afterward selected for further studies.

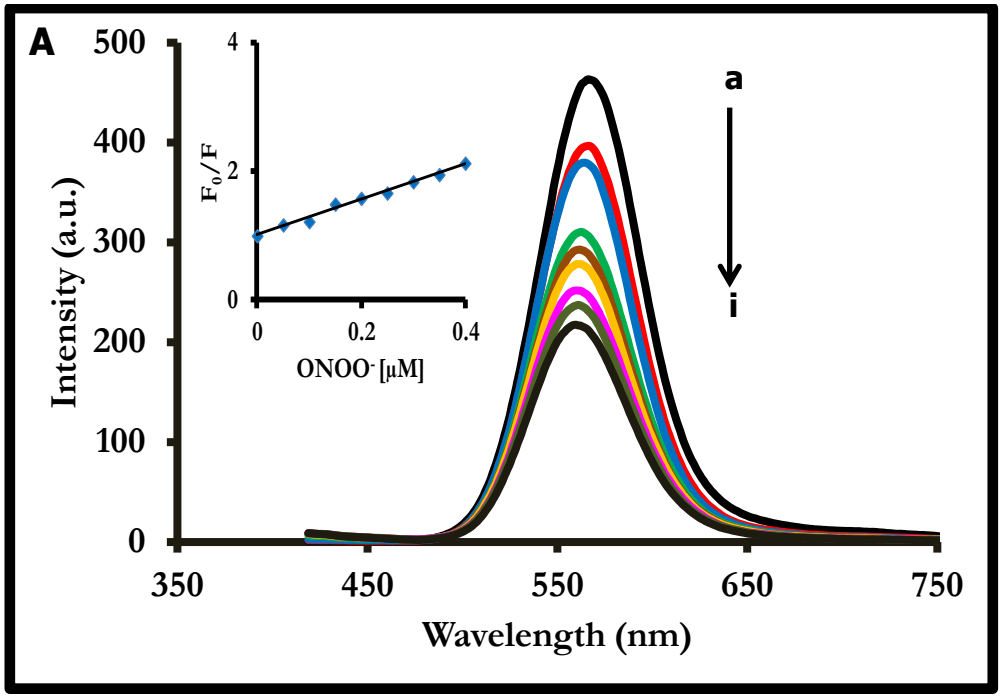
A
Intensity (a.u.)
Wavelength (nm)
a
i
F0/F
ONOO- [μM]

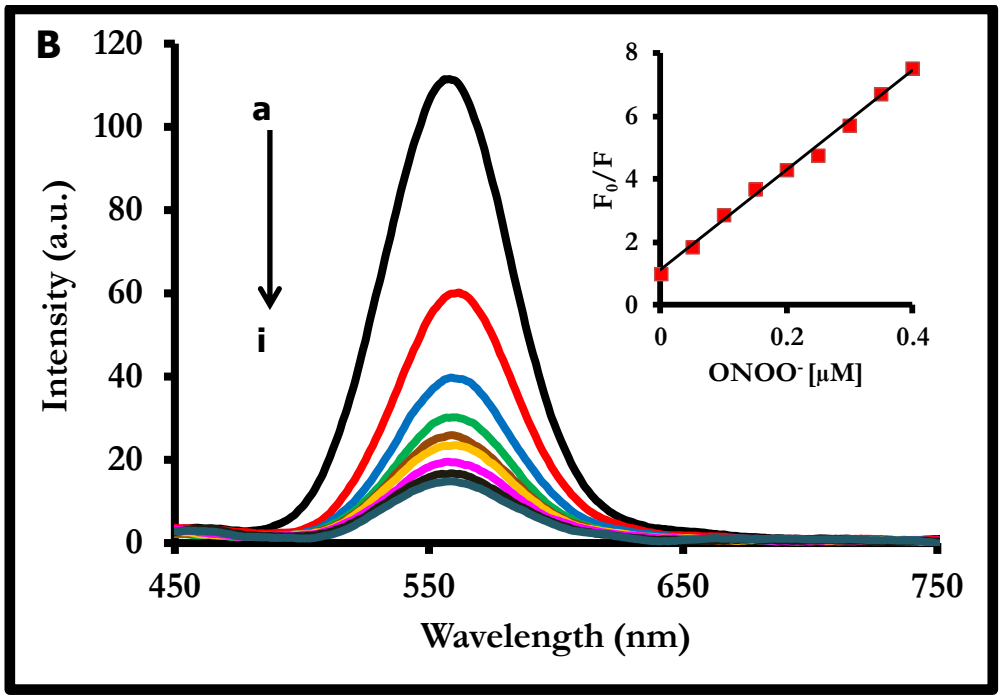
B
Intensity (a.u.)
Wavelength (nm)
a
i
F0/F
ONOO- [μM]

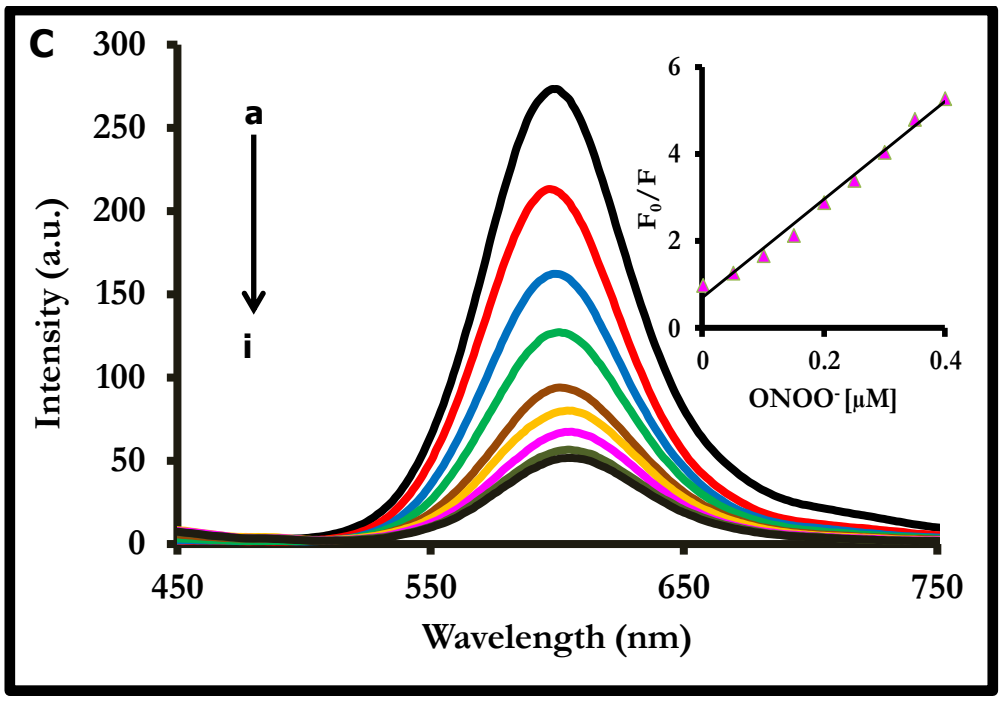

Fig. 4.8. Quenching of different concentrations of $ONOO^-$ on the fluorescence of (A) MPA-CdTe(2.7) (B) MPA-CdTe@ZnS(3.1) and (C) GSH-CdTe@ZnS(3.0) QDs at pH 9.4. Concentrations of $ONOO^-$: (a) 0, (b) 5.0 x 10^{-8}, (c) 1.0 x 10^{-7}, (d) 1.5 x 10^{-7}, (e) 2.0 x 10^{-7}, (f) 2.5 x 10^{-7}, (g) 3.0 x 10^{-7}, (h) 3.5 x 10^{-7} and (i) 4.0 x 10^{-7} M. Inset: Corresponding linear curves. Solvent: 50 mM phosphate buffer, pH 7.4.

4.3.2. Selectivity studies

It is commonly known that the selective detection of $ONOO^-$ in biological system is a big challenge because of the elusive nature of $ONOO^-$ which precludes its detection and direct isolation as well as the difficulty in discriminating between the biological effects of $ONOO^-$ versus that of its precursors **[227]**. As a result, a high selectivity for the detection of $ONOO^-$ is needed for fluorescent probes. As reported before **[228]**, the presence of nitrite does often interfere or complicate studies on the reactivity of $ONOO^-$. Therefore, it is imperative to probe the effect of nitrite (NO_2^-) as well as

nitrate (NO_3^-) (which are decomposition products of $ONOO^-$) on the fluorescence of the QDs. Hence, we studied the effects of these species and other possible ROS interferents on the direct detection of $ONOO^-$ in aqueous media using the CdTe and CdTe@ZnS QDs probes. Table 4.7 (Fig. 4.9), presents the effects of 20-fold excess of ROS and decomposition products of $ONOO^-$ on the fluorescence response of CdTe and CdTe@ZnS QDs for the detection of 5×10^{-8} M $ONOO^-$. A tolerable error of ±5.0% in the relative fluorescence intensity was taken into consideration. It can be seen from Table 4.7 (Fig. 4.9) that the fluorescence of MPA-CdTe QDs was significantly quenched by the presence of H_2O_2, $HO^\bullet$ and NO. Thus, $HO^\bullet$ interferes with $ONOO^-$ detection and as observed above, the later also interferes with $HO^\bullet$ detection when using core CdTe QDs. Comparing MPA-CdTe@ZnS(3.1) with MPA-CdTe(2.7) QDs, there was less decrease in fluorescence intensity in the presence of interferents in the former (with the exception of $O_2^{-\bullet}$ and NO). Thus, the coreshell MPA-CdTe@ZnS(3.1) is more suited than MPA-CdTe(2.7) QDs for the detection of $ONOO^-$ in the presence of studied interferents as was the case for $HO^\bullet$ detection. We further compared the effects of these species on the fluorescence response of the two coreshell QDs: MPA-CdTe@ZnS(3.1) and GSH-CdTe@ZnS(3.0), Table 4.7 (Fig. 4.9). Generally, there is a larger decrease in percentage fluorescence intensity of MPA-CdTe@ZnS(3.1) than for GSH-CdTe@ZnS(3.0), with the exception of hydrogen peroxide. Thus, GSH-CdTe@ZnS(3.0) is more suited for $ONOO^-$ detection in the presence of all interferents studied than MPA-capped QDs. It is possible that steric restrictions due to the size of the GSH molecule will preclude or reduce the oxidative attack of the interfering species on the selective detection of $ONOO^-$, making GSH-

CdTe@ZnS(3.0) QDs a more attractive candidate for the selective recognition of $ONOO^-$ in aqueous media. As shown in Table 4.7 (Fig. 4.9), decomposition products of $ONOO^-$ (NO_2^- and NO_3^-) did not interfere with the probes and thus making us to conclude that the QDs were highly selective for $ONOO^-$ over these products using our method.

Table 4.7. Percentage fluorescence intensity (% FI) change of co-existing ROS and $ONOO^-$ decomposition products on the detection of 5.0 x 10^{-8} M $ONOO^-$ by the proposed QDs-based fluorescent probe. Concentration of interfering species = 1 x 10^{-6} M.

Species	MPA-CdTe(2.7) (% FI change)	MPA-CdTe@ ZnS(3.1) (% FI change)	GSH-CdTe@ ZnS(3.0) (% FI change)
H_2O_2	6.1	2.1	3.6
$O_2^{\bullet-}$	4.8	5.3	1.3
TBHP	5.0	4.7	0.4
HO●	8.8	3.8	1.6
NO	8.9	5.4	1.9
NO_2^-	1.2	0.7	0.5
NO_3^-	0.8	0.4	0.3

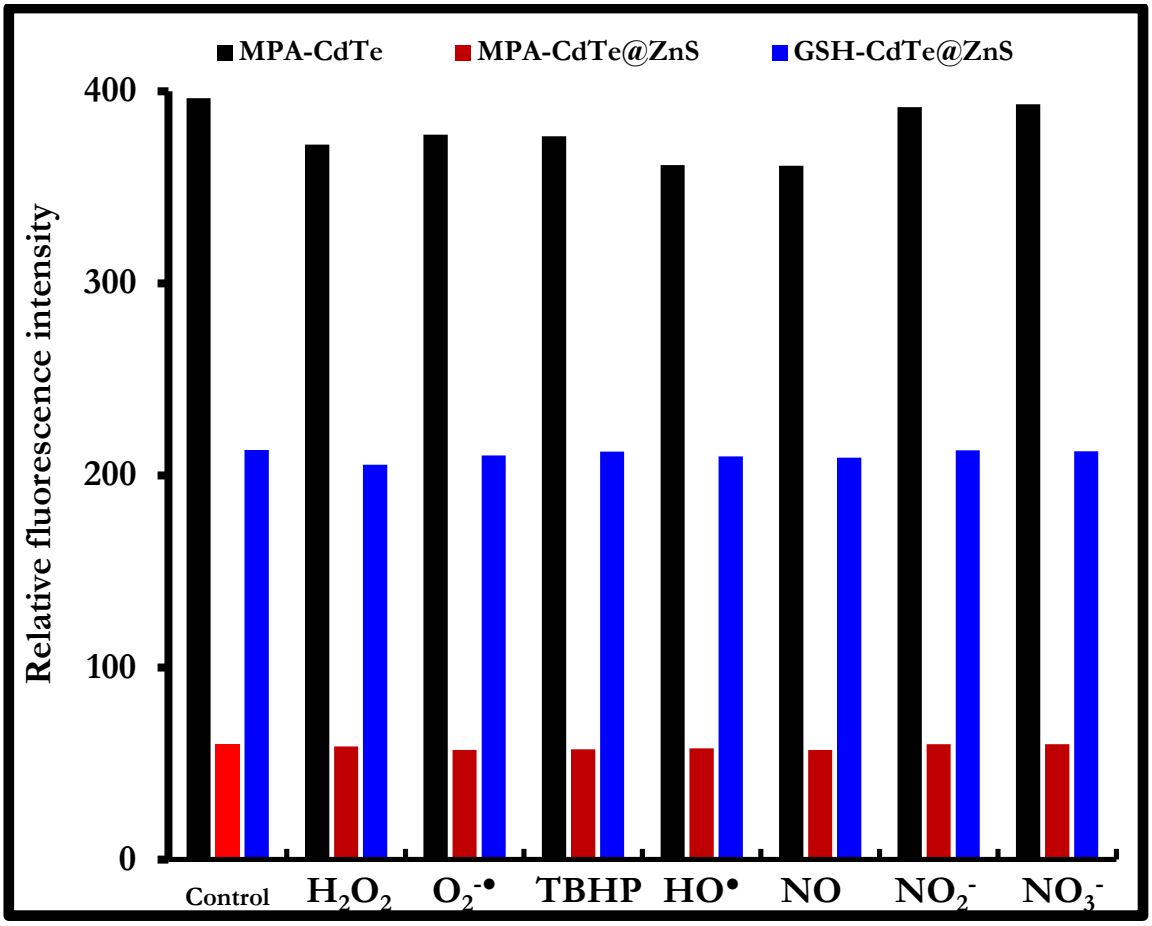

Fig. 4.9. Effects of co-existing ROS as tested interferences on the detection of $ONOO^-$ by the proposed QDs-based fluorescent probe. (Concentration of species = 1 x 10^{-6} M, $ONOO^-$ = 5 x 10^{-8} M, MPA-CdTe(2.7) = 1.0 x 10^{-5} M, MPA-CdTe@ZnS(3.1) = 7.0 x 10^{-7} M GSH-CdTe@ZnS(3.0) = 6.7 x 10^{-7} M). Control = QDs + $ONOO^-$. t-Butyl hydroperoxide is abbreviated as TBHP. Solvent: 50 mM phosphate buffer at pH 9.4. Optimum concentration of respective QDs was used.

4.3.3. First-order decay kinetics

In order to gain an insight into the interaction of $ONOO^-$ with CdTe and CdTe@ZnS QDs, the decay kinetics of $ONOO^-$ was monitored at room temperature by following the changes in its absorbance at 302 nm with time, Fig. 4.10. As shown in Fig. 4.10A

and the corresponding insets, the decay profiles, follows first order kinetics with a half life of 41.0 min for $ONOO^-$ (alone), (Table 4.8). The half-life value obtained for $ONOO^-$ (alone) using our method is comparable with the value of 45.6 min reported in literature **[221]**. In the presence of MPA-CdTe(2.7) QDs a significant blue shift (32 nm) of the decay profile of $ONOO^-$ was observed (Fig. 4.10B) and the corresponding rate constant doubled while the half-life decreased by 55% to a value of 18.6 min, Table 4.8. However, in the presence of MPA-CdTe@ZnS(3.1) QDs, less blue shift (16 nm) in the absorption spectra of $ONOO^-$ was observed (Fig. 4.10C). The half-life of $ONOO^-$ was more for GSH-CdTe@ZnS(3.0) QDs than when MPA-CdTe@ZnS(3.1) QDs is employed. This gives an indication that the type of capping ligand on the coreshell QDs influenced the reactivity of $ONOO^-$ as discussed above.

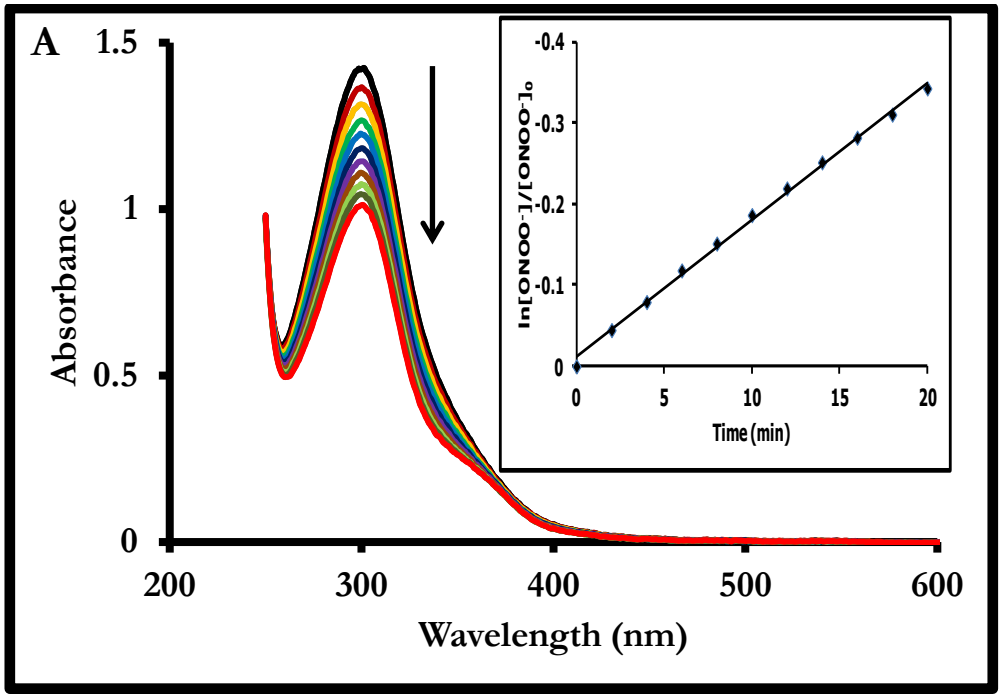
A
1.5
1
0.5
0
Absorbance
200
300
400
500
600
Wavelength (nm)
-0.4
-0.3
-0.2
-0.1
0
ln[ONOO-]/[ONOO-]o
0
5
10
15
20
Time (min)

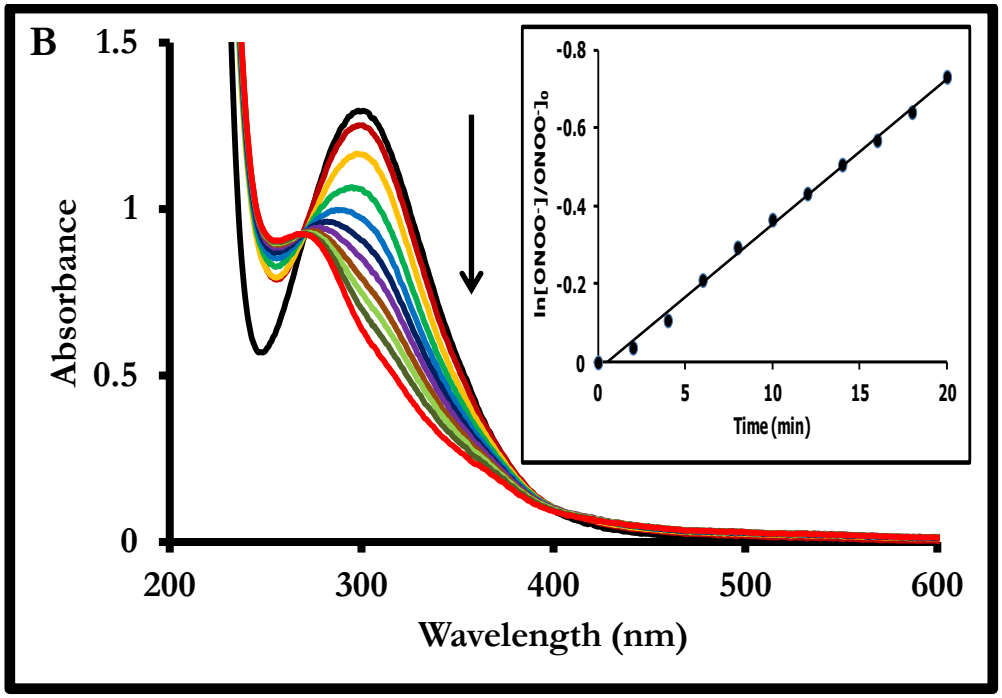
B
1.5
1
0.5
0
Absorbance
200
300
400
500
600
Wavelength (nm)
-0.8
-0.6
-0.4
-0.2
0
ln[ONOO-]/ONOO-]o
0
5
10
15
20
Time (min)

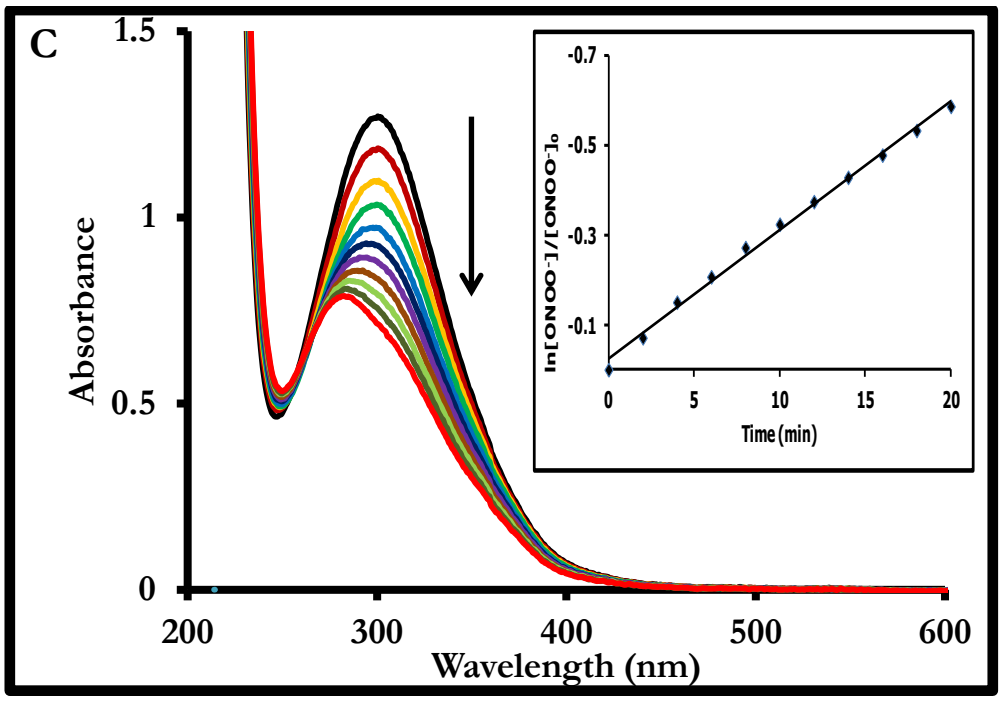

Fig. 4.10. UV/vis plot of the decay of $ONOO^-$ against time at 302 nm for (A) $ONOO^-$ alone, (B) $ONOO^-$ + MPA-CdTe QDs and (C) $ONOO^-$ + MPA-CdTe@ZnS QDs. Insets: First order decay plot of $\ln[ONOO^-]/[ONOO^-]_0$ against time for each case. Here $[ONOO^-]$ and $[ONOO^-]_0$ denotes the concentration of peroxynitrite present initially (t = 0 min) and after a certain time, t, respectively.

Table 4.8. First order decay kinetics of $ONOO^-$ in the absence and presence of different QDs at pH 9.4 and 25 ^{o} C.

Samples	Rate constant (k/min^{-1})	Half-life ($t_{½}$/min)
$ONOO^-$ alone	1.7×10^{-2}	41.0
$ONOO^-$ + MPA-CdTe(2.7)	3.7×10^{-2}	18.6
$ONOO^-$ + MPA-CdTe@ZnS(3.1)	2.9×10^{-2}	24.2
$ONOO^-$ + GSH-CdTe@ZnS(3.0)	1.6×10^{-2}	43.5

4.3.4. Mechanism

In order to further elucidate the mechanism for $ONOO^-$ detection, we carried out fluorescence lifetime measurements on CdTe and CdTe@ZnS QDs**.** A decay curve similar to Fig 4.6 was obtained. As shown in Table 4.9, the fluorescence lifetimes evaluated from the triexponential decay curve of CdTe and CdTe@ZnS QDs remained virtually constant on addition of $ONOO^-$ when compared to the QDs in the absence of $ONOO^-$. The lack of changes in the lifetimes of the QDs on addition of $ONOO^-$, indicate that the interaction is static in nature which also implies that either a complex or a binding formation exist between $ONOO^-$ and the QDs. Our result is in agreement with literature for the interaction of L-cysteine CdTe with $ONOO^-$ **[222].**

Oxidation of fluorescent probes by $ONOO^-$ has been used as a tool to interpret the mechanism of $ONOO^-$ detection **[222,227].** It is note-worthy that the oxidation of various substrates by $ONOO^-$ can take place via multiple reaction pathways which include: direct oxidation of the substrate by $ONOO^-$, decomposition of $ONOO^-$ to highly reactive species which subsequently hydroxylates or oxidizes the substrate **[226].** In the present study, it is proved through selectivity studies that neither decomposition products (NO_3^- and NO_2^-) of $ONOO^-$ mediated the fluorescence quenching of the QDs. There is an existence of Cd^{2+}-thiolate complex on the surface of the QDs since MPA or GSH were used as capping ligands. As reported before, $ONOO^-$ can interact with Cd^{2+}-thiolate, resulting in the detachment of the capping agent from the QDs surface which in turn would result in fluorescence quenching **[222,229]**. It also appears that the presence of the shell around the core of the QDs

influenced the sensitivity of the QDs to $ONOO^-$, while the overall extent of this quenching was dependent of the type of capping ligand attached to the coreshell QDs (comparing the K_{SV} values, Table 4.6). This may be further explained in terms of bond strength of the coordination linkage between QDs and the capping ligand. This implies that the QD-thiolate bond is much stronger in CdTe than CdTe@ZnS QDs and thus, the breaking of the QD-thiolate bond by the oxidative effect of $ONOO^-$ is more favourable for CdTe@ZnS than CdTe QDs.

Table 4.9. Best-fit fluorescence lifetime values for a triexponential fit of MPA-CdTe(2.7), MPA-CdTe@ZnS(3.1) and GSH-CdTe@ZnS(3.0) QDs in the absence and presence of an equivalent of [$ONOO^-$] in 50 mM phosphate buffer, pH 9.4.

QDs	[$ONOO^-$] (μM)	τ_1 (ns) ±0.1	τ_2 (ns) ±0.05	τ_3 (ns) ±0.03
MPA-CdTe(2.7)	0	26.2(0.73)	8.3(0.24)	1.5(0.03)
	5.0×10^{-8}	26.1(0.72)	8.4(0.25)	1.5(0.03)
MPA-CdTe@ZnS(3.1)	0	34.8(0.86)	7.1(0.12)	1.5(0.02)
	5.0×10^{-8}	34.5(0.72)	7.0(0.24)	1.5(0.04)
GSH-CdTe@ZnS(3.0)	0	55.1(0.93)	11.0(0.06)	1.0(0.01)
	5.0×10^{-8}	55.0(0.90)	11.2(0.09)	1.2(0.01)

4.3.5. Conclusions

We have successfully probed the sensitive and selective detection of $ONOO^-$ using QDs capped with MPA or GSH as a fluorescent probe for the first time. The sensitivity of the proposed probe (based on LOD) followed the order: MPA-CdTe@ZnS(3.1) > GSH-CdTe@ZnS(3.0) > MPA-CdTe(2.7) QDs and the selectivity

followed the order: GSH-CdTe@ZnS(3.0) > MPA-CdTe@ZnS(3.1) > MPA-CdTe(2.7) QDs. LOD for $ONOO^-$ at pH 9.4 was much lower than the values obtained at pH 12. The varying degree of sensitivity of the proposed probe has been explained based on the oxidative effect of $ONOO^-$ on the QD-thiolate bond as well as the type of capping ligand attached to the surface of the QDs. Steric hindrance caused by the size of the GSH molecule on the coreshell QDs can prevent oxidative attack from co-existing species in solution making it attractive for the selective recognition of $ONOO^-$. Decay kinetic studies provided supportive evidence that the reactivity of $ONOO^-$ was influenced by the type of QDs and capping ligand attached to it. Time resolved fluorescence measurement indicates the interaction between $ONOO^-$ and the QDs was static in nature.

4.4. General conclusions for the chapter

In general, it can be seen that the interaction of the QDs with $DPPH^•$ and $ONOO^-$ was static in nature while electron transfer processes between the QDs and $HO^•$ was observed. The differences in quenching interaction of the QDs with these analytes may suggest that the surface chemistry of QDs is being influenced by the type of analytes that it interacts with.

Judging from the LOD values obtained for the detection of $HO^•$ and $ONOO^-$, it was generally observed that the core-shell QDs were more sensitive than their core counterpart. For the detection of $HO^•$, core QDs with TGA capping was more sensitive than the MPA capping while core-shell QDs with GSH capping was more sensitive than MPA capping, whereas, for the detection of $ONOO^-$, core-shell QDs

with MPA capping was more sensitive than for GSH capping. Hence, the varying degree of sensitivity of the core and coreshell QDs to HO• and $ONOO^-$ may depend on multiple factors derived from their inherent physicochemical properties such as capping agents, QD size, oxidative, photolytic and mechanical stability, which are individual and collective factors that can influence the sensitivity of the QDs to these analytes.

For the selectivity studies for the detection of HO• and $ONOO^-$, it was observed that when using core QDs, $ONOO^-$ interfered with the detection of HO•, while HO• interfered with the detection of $ONOO^-$. Such interferences observed for the core QDs may suggest that they exhibit lesser shielding power from the oxidative effects from interfering species. The coating of the secondary shell (ZnS) on the core as observed in this work, proved to exhibit higher shielding power as judged by their better selectivity towards interfering species.

5. Fluorescence detection of analytes using QDs-4AT

This chapter reports on the detection of bromide ion using QDs-4AT nanoprobe.

5.1. Optimization of Br^- detection conditions on QDs-4AT nanoprobe

The effect of pH in a range 5.2 – 9.0 was investigated. It was found that in the presence of Br^-, the fluorescence intensity of QDs-4AT nanoprobe was effectively enhanced (Fig 5.1) and the fluorescence enhancement was related to the solution pH (Fig 5.2), nature of the buffer and QDs-4AT concentration. Maximum and stable fluorescence was obtained between pH 7.2 – 7.8. Therefore, pH 7.4 was selected in order to develop a sensitive and rapid spectrophotometric method for the determination of bromide ion using QDs-4AT nanoprobe.

Different buffers, for example, PBS, acetate buffer, phosphate buffer, citric acid-NaOH and Tris-HCl were examined and our results showed that Tris-HCl (50 mM) was best suited and was selected for further experiments.

Also, the dependence of the relative fluorescence intensity on the concentration of QDs-4AT nanoprobe ranging from 0.1 – 1.0 μM was investigated in the presence of a fixed concentration of Br^- (0.1 μM) (plot not shown). The relative fluorescence intensity increased with increase in the concentration of QDs-4AT and reached equilibrium when the concentration was more than 0.7 μM. Therefore, we chose 0.7 μM as the concentration of QDs-4AT in this work.

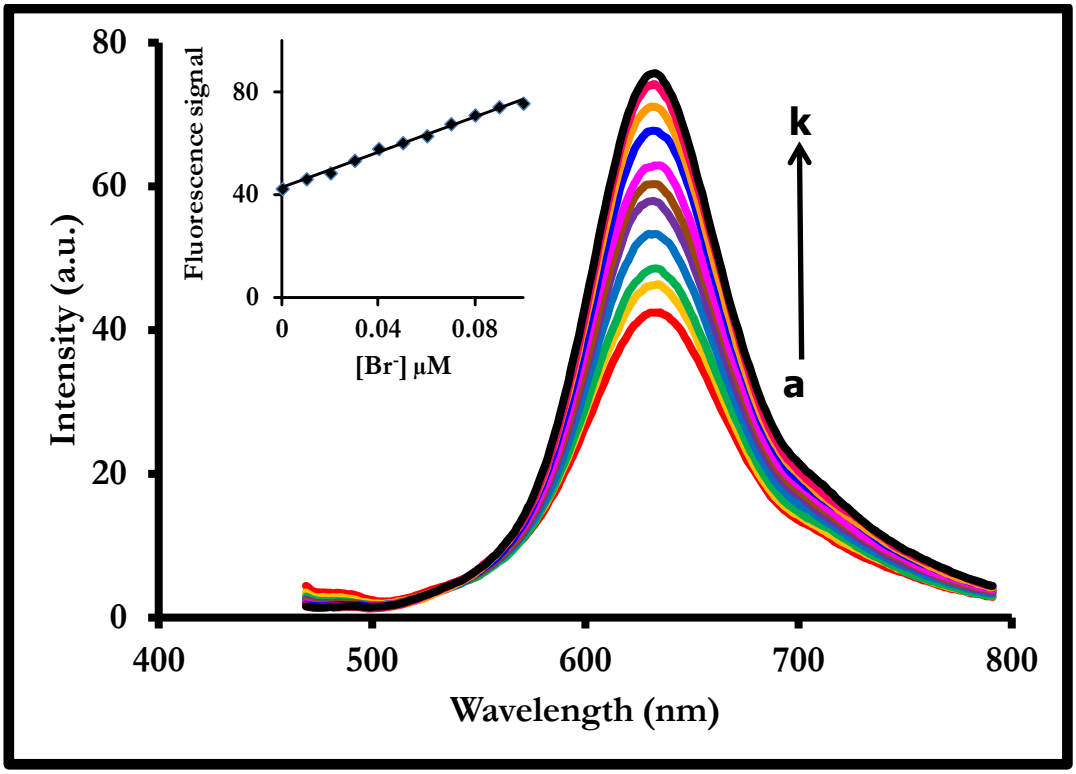

Fig. 5.1. Fluorescence emission spectra of QDs-4AT in the presence of various concentrations of bromide ion. The addition sequence of the reagents: probe solution (0.7 µM of QDs-4AT), Tris-HCl buffer solution (50 mM, pH 7.4), and bromide ion (a-k; 0, 0.01, 0.02, 0.03, 0.04, 0.05, 0.06, 0.07, 0.08, 0.09 and 0.1 µM). Inset: the linear relationship between fluorescence intensity and the concentrations of Br^- in the range of 0 – 0.1 µM.

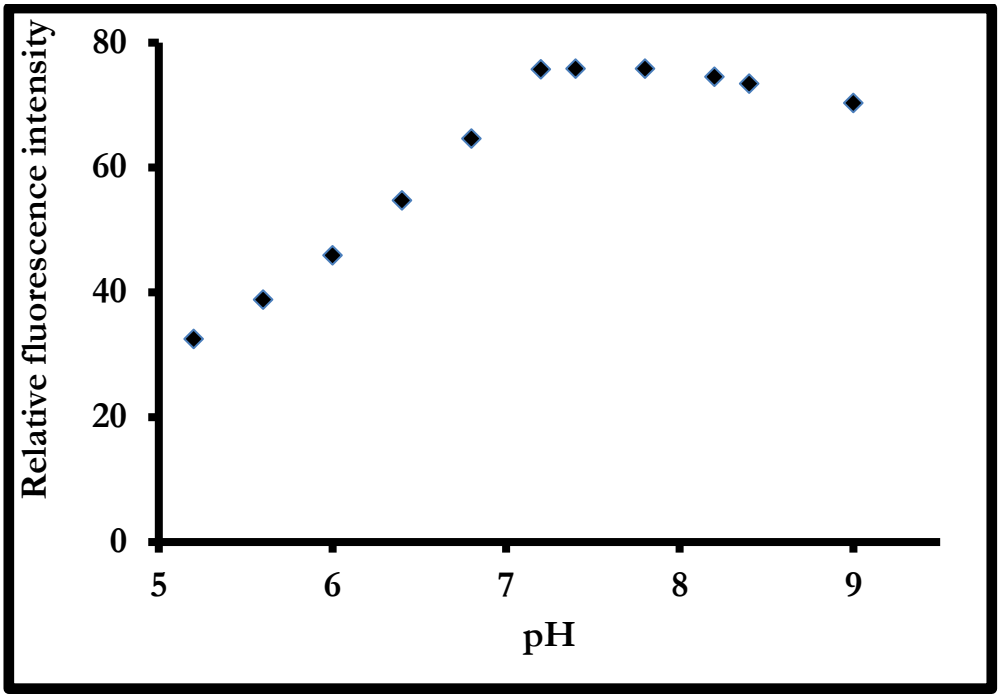

Fig. 5.2. Effect of pH on the fluorescence of the reaction condition of 0.7 μM QDs-4AT nanoprobe and 0.1 μM Br^-.

5.2. Selectivity studies

In order to evaluate the selectivity of the QDs-4AT nanoprobe toward Br^-, the fluorescence response in the presence of other environmental metal ions, such as K^+, Na^+, Mg^{2+}, Al^{2+}, Fe^{3+}, Ni^{3+}, Cr^{3+}, Zn^{2+}, I^-, CO_3^{2-}, Ac^-, SO_3^{2-}, SO_4^{2-}, NO_3^-, Cl^- and F^- were investigated under optimum conditions. A tolerable error of ±5.0% in the relative fluorescence intensity was taken into consideration. As shown in Fig. 5.3, the fluorescence intensity of the QDs-4AT nanoprobe remained almost the same in the presence of K^+, Na^+, Mg^{2+}, Al^{2+}, I^-, CO_3^{2-}, Ac^- , Br^-, SO_3^{2-}, SO_4^{2-}, NO_3^-, Cl^- and F^- even with concentrations 100 fold higher than that of bromide ion. This gives a strong indication of a high selectivity of the nanoprobe for bromide ion over other ions. In the presence of transitional metals ions of Fe^{3+}, Ni^{3+} and Cr^{3+}, the fluorescence of the

nanoprobe was effectively quenched (Fig. 5.3). This result indicates that the nanoprobe was highly selective towards Br^-, but the quenching effect of transitional metal ions of Fe^{3+}, Ni^{3+} and Cr^{3+} could affect the selectivity of the nanoprobe towards Br^- detection. In general, the nanoprobe can specifically detect Br^- based on fluorescence enhancement.

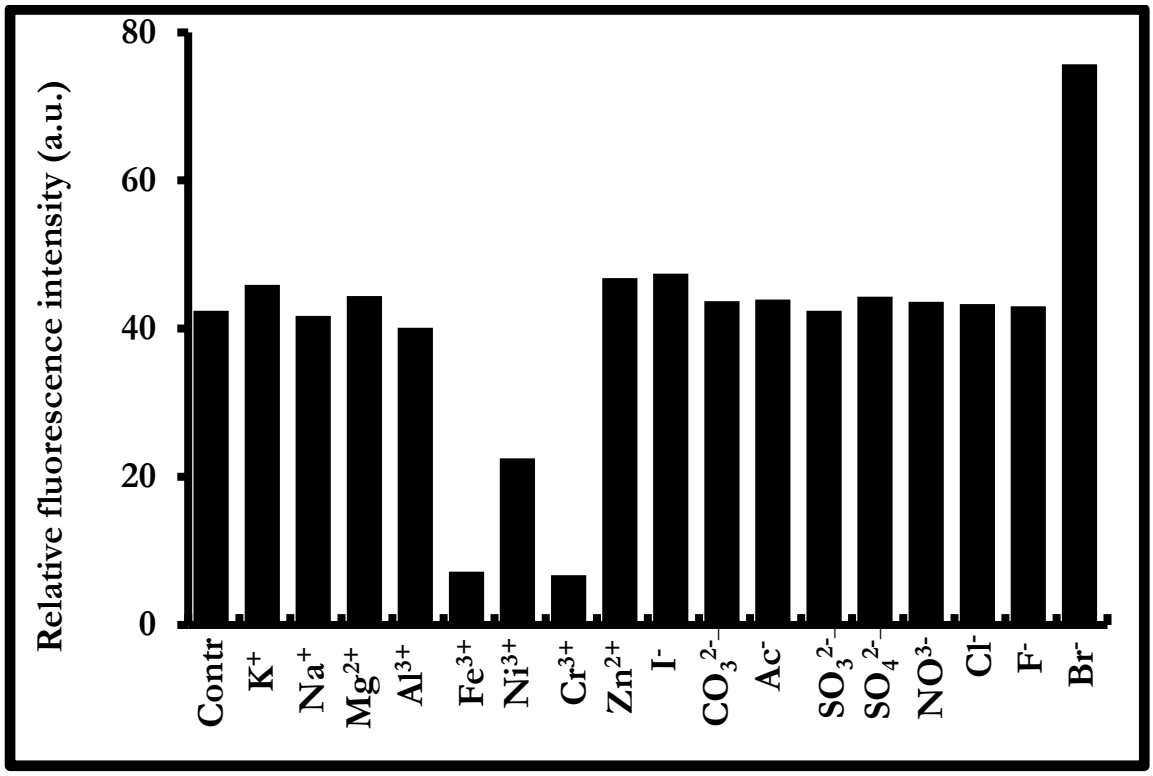

Fig. 5.3. Relative fluorescence response of QDs-4AT nanoprobe (0.7 μM) in the presence of Br^- (0.1 μM), Cr^{3+} and Fe^{3+} (1.0 nM) and other ions (1.5 μM) at pH 7.4, 50 mM Tris HCl.

5.3. Sensitivity of bromide ion towards QDs-4AT nanoprobe

It was observed that the fluorescence intensity of QDs-4AT nanoprobe was gradually enhanced in the presence of various concentrations of Br^- (Fig. 5.1). No

emission peak shift was observed even at relatively high concentrations of Br^- (Fig. 5.1). A calibration curve of fluorescence signals versus the concentrations of Br^- was plotted (Inset: Fig. 5.1). The LOD was evaluated and the value of 0.6 nM was obtained, Table 5.1. The linear range was between 0.01 – 0.13 μM and corresponded to a correlation coefficient of 0.995. In comparison with the few reported methods for Br^- detection [**230-236**], this method provides an improvement in sensitivity, selectivity, simplicity and rapidity for Br^- detection (Table 5.1).

Table 5.1. Comparison of the sensitivity of the proposed QDs-4AT nanoprobe with some published analytical techniques for Br^- detection.

Technique	Detection limit	Linear range	References
Fluorescence enhancement	**0.6 nM**	**0.01 – 0.13 μM**	**This work**
Electromagnetic fields	**2.0×10^{-5} M**	**1.0×10^{-1} – 3.2×10^{-5} M**	**[229]**
Ion chromatography	**3.0 μg/L**	**-**	**[230]**
Ion chromatography	**4.5 mg/L**	**-**	**[231]**
Ion chromatography	**0.1 μg/L**	**-**	**[232]**
Ion chromatography	**0.058 mM**	**0.010 -0.10 mM**	**[233]**
Ion chromatography	**2.0 μg/L**	**-**	**[234]**
Flow injection	**6.0×10^{-3} M**	**1.0×10^{-3} -1.0×10^{-2} M**	**[235]**

5.4. Reaction mechanism

The fluorescence decay curve of the QDs-4AT in the absence and presence of Br^- is shown in Fig. 5.4. As shown in Table 5.2, in the presence of varying concentrations of

Br^-, the fluorescence lifetime of the QDs-4AT nanoprobe decreased and thus suggests dynamic quenching processes. Since 4AT quenches the fluorescence of the QDs we assume the relative fluorescence enhancement in the presence of Br^- may be ascribed to electron transfer (ET) from the Br^- to QDs-4AT **[237]**. As shown in Scheme 5.1, Br^- is converted to bromine molecule due to electron loss, while the nitroxyl radical moiety of the QDs-4AT nanoprobe acts as an electron acceptor.

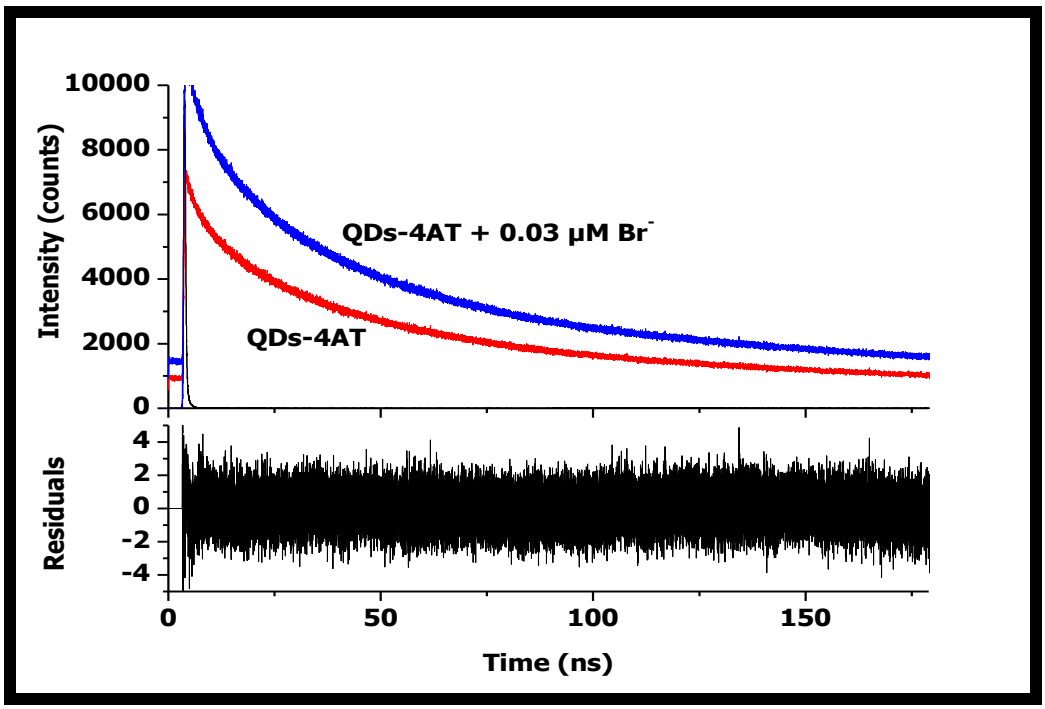

Fig. 5.4. Fluorescence decay curves of QDs-4AT in the absence (red) and presence (blue) of 0.03 µM bromide ion in 50 mM Tris-HCl pH 7.4.

Table 5.2. Best-fit fluorescence lifetime values for a triexponential fit of QDs-4AT nanoprobe with bromide ion concentrations in 50 mM Tris-HCl buffer pH 7.4.

Nanoprobe	[Br^-] (μM)	τ_1 (ns) ±0.1	τ_2 (ns) ±0.06	τ_3 (ns) ±0.05
QDs-4AT	0	70.8(0.87)	17.0(0.12)	2.4(0.01)
	0.01	69.7(0.87)	16.3(0.12)	2.3(0.01)
	0.02	66.6(0.88)	15.0(0.11)	2.0(0.01)
	0.03	62.5(0.90)	12.7(0.09)	1.7(0.01)

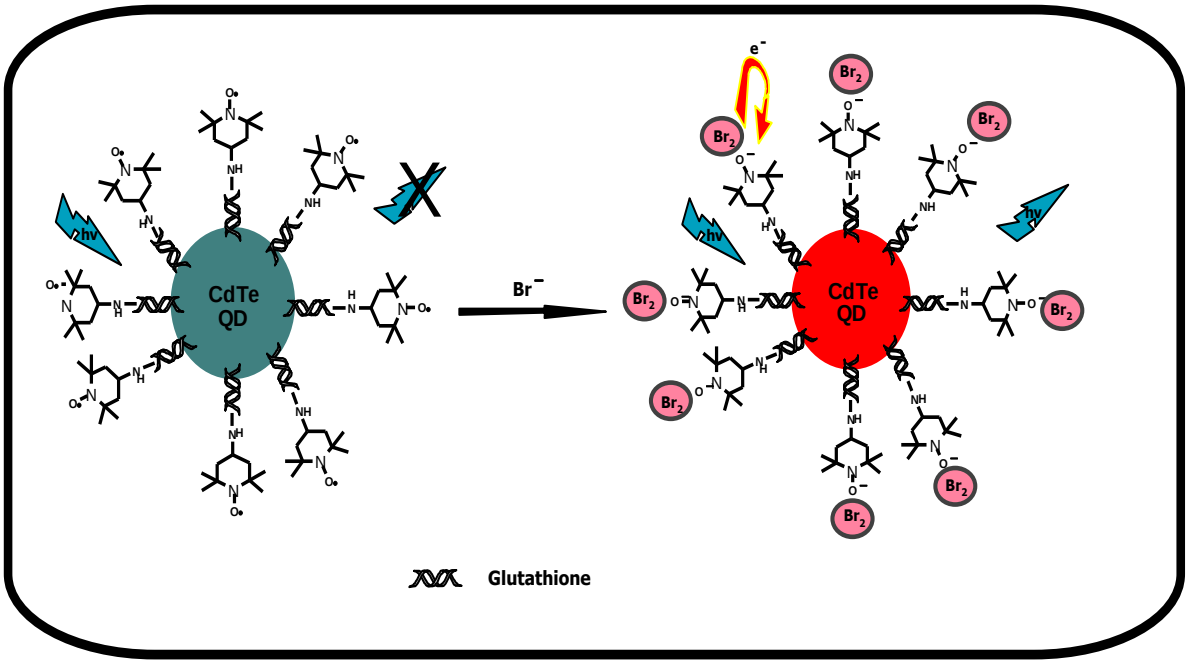

Scheme 5.1. Proposed mechanism of interaction between QDs-4AT nanoprobe and bromide ion.

5.5. EPR measurements

EPR investigations on the interaction between 4AT and CdTe QDs as well as QDs-4AT nanoprobe and Br^- have been carried to further elucidate the ET reaction mechanism as proposed above. EPR spectra of 4AT in 50 mM Tris-HCl pH 7.4,

shows the three characteristic ^{14}N hyperfine splitting in Fig. 5.5A (blue line), as previously reported in literature **[238,239].** Addition of 0.7 μM CdTe QDs to a solution of 4AT led to a slight broadening of the EPR signal of the peak (Fig. 5.5A, red line) accompanied by a decrease in the peak-to-peak height. This observation is consistent with literature **[238].** As reported before **[238],** the broadening arises as a result of restricted mobility and slow tumbling of the nitroxide due to attachment to the QD surface. Apart from the broadening, a shift in the EPR signal to lower field on addition of CdTe QDs was observed. One possible reason for the observed shift may be due to the size effect of the QDs. No shifting of EPR signal was observed in literature for interaction of hydrophobic CdSe QDs with 4AT **[238].** Thus, the surface properties of GSH-capped CdTe QDs used in this work are expected to be different due to solubility, surface ligands, synthetic conditions and particle size. To probe the fluorescence recovery of QD-4AT nanoprobe in the presence of Br^-, EPR studies were carried out. CdTe QDs did not show any signal in the EPR spectrum. Therefore, we expect that if electron from Br^- was transferred to the nitroxyl radical moiety of QD-4AT nanoprobe and was irreversible, a diminution in the EPR signal would occur. The EPR spectrum of the QDs-4AT nanoprobe in 50 mM Tris-HCl pH 7.4 in Fig. 5.5B (black line) shows a narrower and sharper signal and a higher peak-to-peak height at high, central and low fields respectively as compared to 4AT alone (Fig 5.5A, blue line). The absence of a broadening for QD-4AT may suggest that the mobility of the nitroxide (conjugated via an amide bond to the QD) is not restricted and hence can accept electron. Upon addition of Br^- to the QD-4AT nanoprobe solution, a significant decrease of the EPR signal was observed as shown in Fig. 5.5B (green

line) indicating that part of the nitroxide has been transformed to a nonparamagnetic specie. In the presence of Br^-, a complete loss of the EPR signal was not observed, therefore, we can conclude that QD-4AT reduction could be due to electron transfer from the bromide ion to the nitroxyl moiety of QD-4AT nanoprobe (Scheme 5.1).

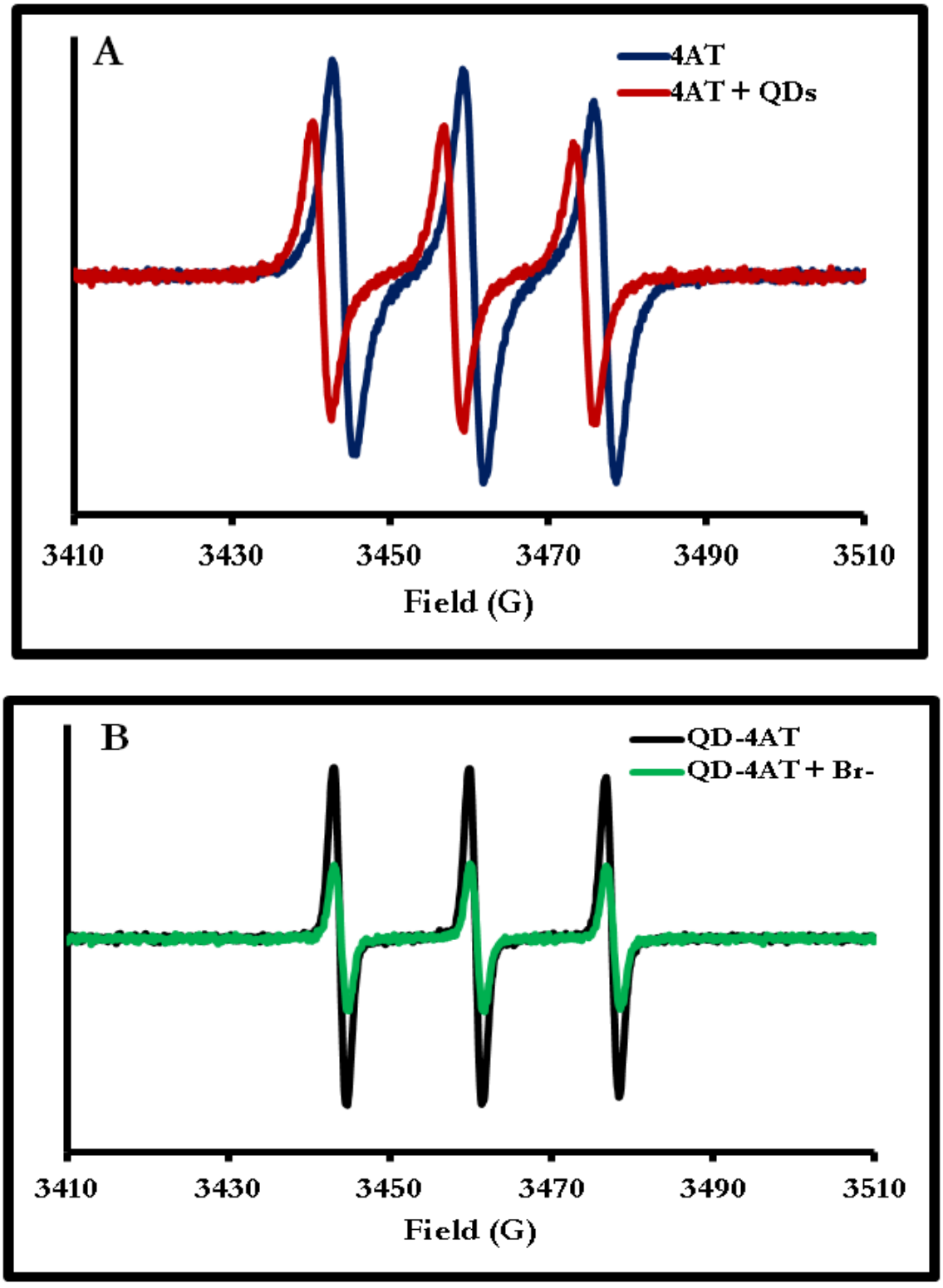

Fig. 5.5. EPR spectra of (A) 4AT (4 mM) and upon successive addition of 0.9 µM CdTe QDs. (B) QD-4AT nanoprobe (0.7 µM) and addition of 0.1 µM bromide ion. Solvent: 50 mM Tris-HCl buffer pH 7.4.

5.6. Conclusions

In summary, QDs-4AT was utilized as a luminescent nanoprobe for Br^- sensing. This work proposed a sensitive and selective determination of bromide ion based on the fluorescence enhancement of QDs-4AT nanoprobe and the LOD obtained was 0.6 nM. This method is advantageous to practical applications from the perspectives of detection sensitivity and selectivity.

6. QDs-MPc conjugates for analyte detection

This chapter reports the use of QDs conjugated to MPc for use as fluorescence probes for analyte sensing. The effects of the central metal, substituents on the MPc ring and mechanism of interaction are reported.

6.1. Effects of central metals using MTAPc

This study presents an investigation into the efficiency of sensing of H_2O_2 (used as a test molecule) using MPA-CdTe@ZnS QDs (3.0 nm) linked to (Cl)AlTAPc (**1**), NiTAPc (**3**) and ZnTAPc (**4**). The QDs were also linked to metal free (H_2)TAPc to test its efficiency for sensing of H_2O_2 in comparison to the MTAPcs. The general purpose of this study is to elucidate the effect of the central metal of the MPc on the overall sensor sensitivity and selectivity towards H_2O_2. Table 6.1 shows a list of all the QDs-conjugates employed in this work together with their corresponding LOD and linear range.

Table 6.1. List of QDs-conjugates employed for fluorescence sensing using enhancement processes. The sizes of the QDs, the analytes detected, linear range and LOD are included. Solvent: pH 7.4 buffer.

QDs-conjugates	Analytes	Linear range (M)	LOD (M)
MPA-CdTe@ZnS(3.0)-1	H_2O_2	1.0×10^{-9} - 1.6×10^{-8}	9.8×10^{-9}
MPA-CdTe@ZnS(3.0)-3	H_2O_2	1.0×10^{-9} - 1.6×10^{-8}	4.4×10^{-9}
MPA-CdTe@ZnS(3.0)-4	H_2O_2	1.0×10^{-9} - 1.6×10^{-8}	2.2×10^{-9}
GSH-CdTe@ZnS(3.6)-2	GSH	2.0×10^{-9} - 4.8×10^{-8}	3.34×10^{-10}
GSH-CdTe@ZnS(3.6)-2	Cysteamine	6.5×10^{-9} - 1.6×10^{-7}	1.71×10^{-9}
GSH-CdTe@ZnS(3.6)-2	TBHP	4.5×10^{-8} - 5.4×10^{-7}	4.44×10^{-9}
GSH-CdTe@ZnS(3.6)-2	ClO_4^-	6.5×10^{-8} - 1.6×10^{-7}	8.15×10^{-9}
GSH-CdTe@ZnS(3.6)-2	$HO^{\bullet}$	4.2×10^{-9} - 2.8×10^{-8}	1.98×10^{-10}
MPA-CdTe@ZnS1(3.0)-2	$O_2^{-\bullet}$	1.0×10^{-7} - 1.0×10^{-6}	2.1×10^{-9}
MPA-CdTe@ZnS2(3.4)-2	$O_2^{-\bullet}$	1.0×10^{-7} - 1.0×10^{-6}	2.4×10^{-9}
GSH-CdTe@ZnS1(2.6)-3	Br^-	1.0×10^{-9} - 4.8×10^{-8}	1.62×10^{-10}
GSH-CdTe@ZnS2(3.4)-3	Br^-	1.0×10^{-9} - 4.8×10^{-8}	2.14×10^{-10}
GSH-CdTe@ZnS3(3.6)-3	Br^-	1.0×10^{-9} - 4.8×10^{-8}	2.54×10^{-10}
MPA-CdSe@ZnS(4.6)-5	F^-	1.5×10^{-9} - 1.2×10^{-7}	2.30×10^{-10}
MPA-CdSe@ZnS(4.6)-6	F^-	1.5×10^{-9} - 1.2×10^{-7}	1.04×10^{-10}
GSH-CdSe@ZnS(4.7)-5	F^-	1.5×10^{-9} - 1.2×10^{-7}	1.78×10^{-10}
GSH-CdSe@ZnS-6	F^-	1.5×10^{-9} - 1.2×10^{-7}	1.42×10^{-10}

GSH-CdSe@ZnS-7	**Hg^{2+}**	**1.2×10^{-9} - 3.8×10^{-8}**	**2.0×10^{-10}**
GSH-CdSe@ZnS-8	**Hg^{2+}**	**1.2×10^{-9} - 3.8×10^{-8}**	**5.7×10^{-11}**

6.1.1. Fluorescence "turn ON" for the detection of H_2O_2

We explore the possibility of the fluorescence of the linked QDs being "turned ON" when interacted with H_2O_2. The presence of different MTAPc covalently linked to the QDs could have a significant influence on the sensitivity of the nanoprobe. Hence, a comparative investigation using, H_2TAPc, **1**, **3** and **4** was carried out. Upon addition of H_2O_2 to QDs-**1** (Fig. 6.1A), QDs-**3** (Fig. 6.1B) and QDs-**4** (Fig. 6.1C) nanoprobe, the fluorescence of the linked QDs was progressively recovered with the successive increase in H_2O_2 concentration. However, for QDs-H_2TAPc (Fig. 6.1D), there was no significant fluorescence enhancement in the presence of varying concentrations of H_2O_2. This implies that H_2O_2 does not have any direct interaction with the emission of QDs-H_2TAPc and thus gives a strong indication that the presence of the central metal attached to the MPc, plays a major role in determining the fluorescence property of the QDs-MTAPc on interaction with targeted species.

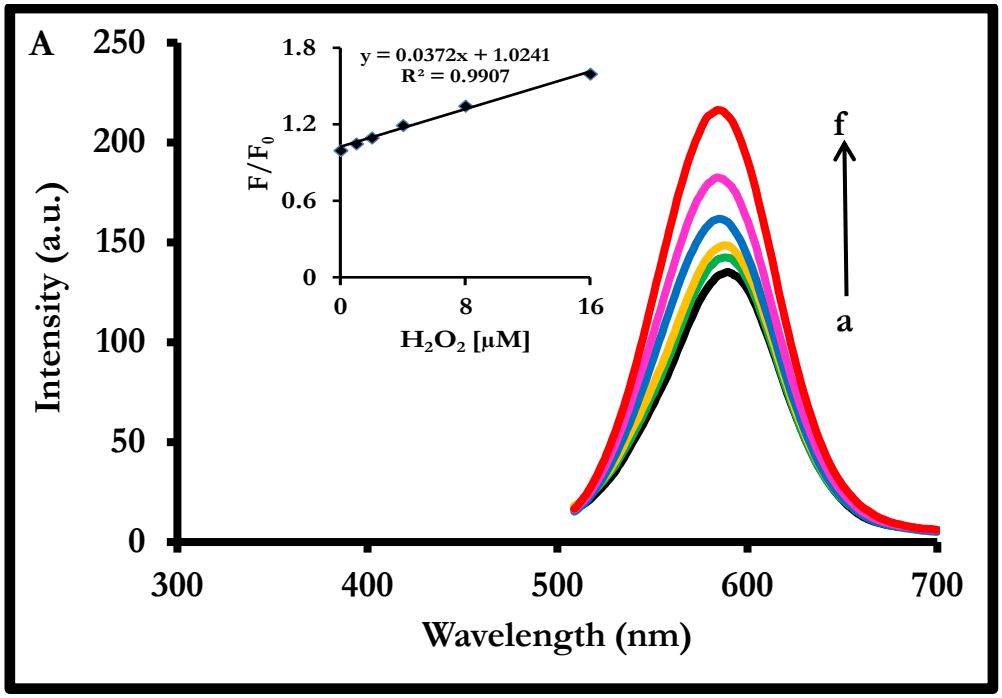
A
Intensity (a.u.)
Wavelength (nm)
y = 0.0372x + 1.0241
R² = 0.9907
F/F0
H2O2 [µM]
f
a

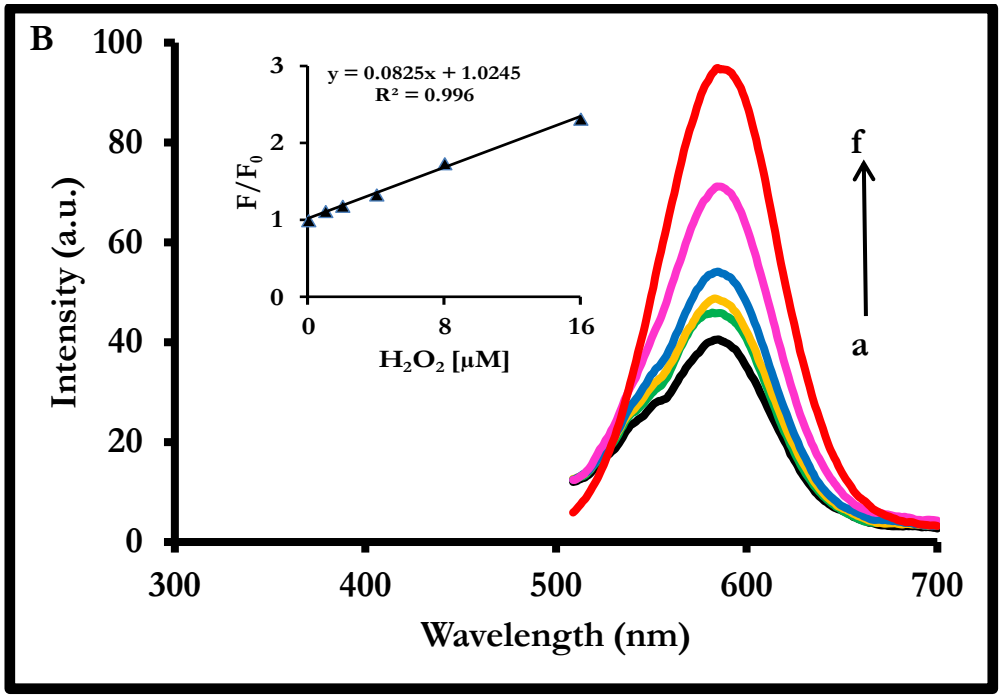
B
Intensity (a.u.)
Wavelength (nm)
y = 0.0825x + 1.0245
R² = 0.996
F/F0
H2O2 [µM]
f
a

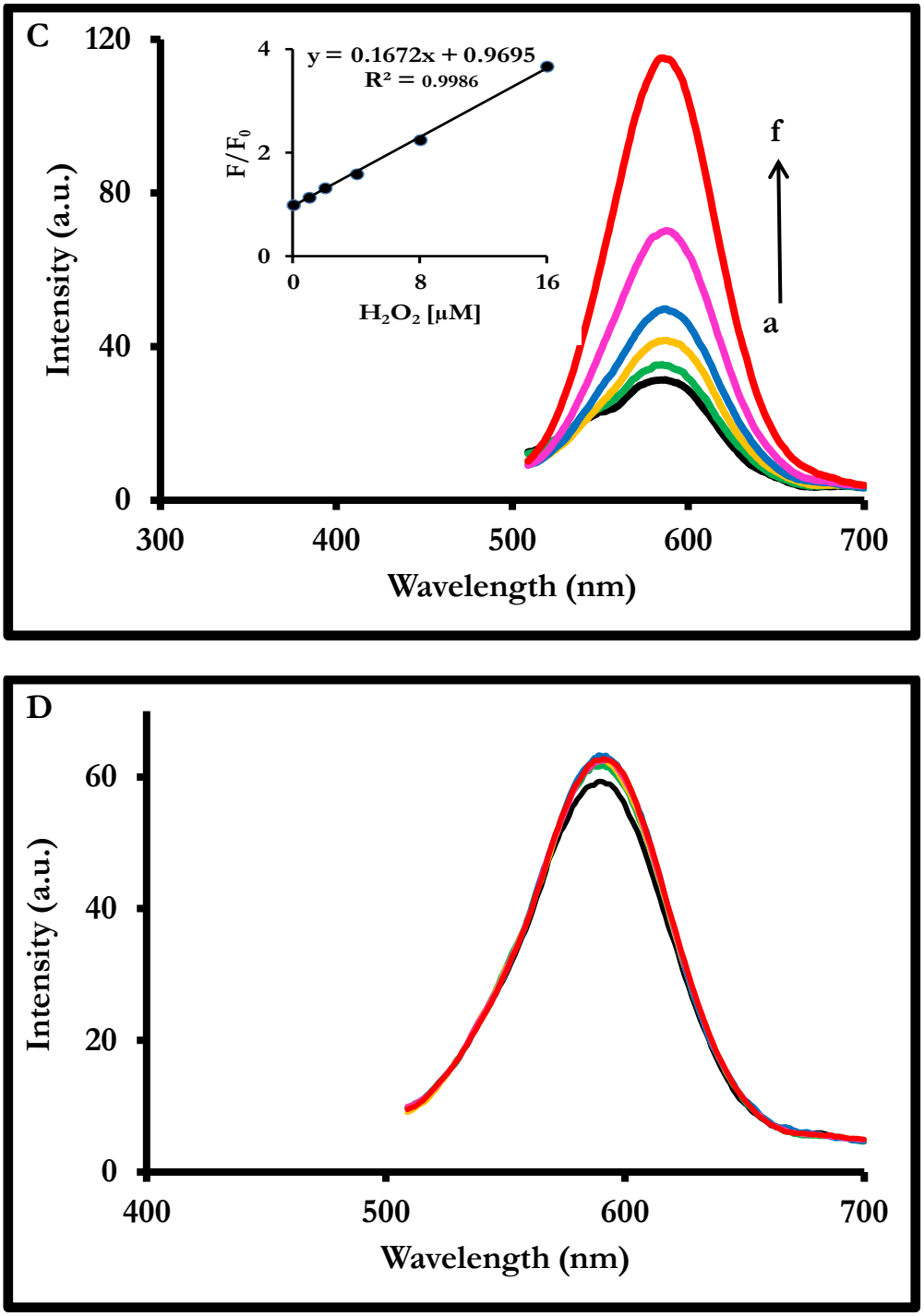

Fig. 6.1. Fluorescence emission spectra of (A) QDs-1, (B) QDs-3, (C) QDs-4 and (D) QDs-H_2TAPc upon addition of varying concentration of H_2O_2. Inset: calibration curve of F/F_0 versus H_2O_2 concentration. [H_2O_2], a-f: 0, 1.0 x 10^{-9}, 2.0 x 10^{-9}, 4.0 x 10^{-9}, 8.0 x 10^{-9} and 1.6 x 10^{-8} M. λ_{exc} = 490 nm.

It is worth noting that the QDs alone could not detect H_2O_2 with a stable fluorescence signal at the same concentration (of H_2O_2) used for the QDs-MTAPc complexes. Hence, H_2O_2 can only be detected at a much higher concentration by quenching (not enhancement reported here) of the fluorescence of the QDs alone as compared to lower concentrations detected by the QDs-MTAPc. Hence, the QDs-MTAPc nanoprobe shows higher sensitivity.

In order to evaluate the fluorescence enhancement sensitivity of the probe, the fluorescence intensities of the QDs-MTAPc in the absence (F_0) and presence (F) of H_2O_2 was investigated using Eq. 6.1.

$$\frac{F}{F_0} = 1 + K[H_2O_2] \qquad (6.1)$$

Please note that Eq. 6.1 relates to F/F_0 (due to enhancement of fluorescence) instead of F_0/F usually employed for quenching of fluorescence (Eq. 4.1). As displayed in the insets of Fig. 6.1A – 6.1C, plots of F/F_0 against H_2O_2 concentrations were linear. Using the value of K as a measure of degree of sensitivity of the nanoprobe, the sensitivity followed the order: QDs-**4** > QDs-**3** > QDs-**1** (Table 6.2). Thus, the rate is faster for Zn followed by Ni. Quantitative analysis of this method showed a good LOD for H_2O_2 (Table 6.3) and followed the order of sensitivity of the nanoprobe. To the best of our knowledge, there are no reports on H_2O_2 detection using QDs-macrocyclic complexes. Hence, we compared our LOD values with other QDs based probe for H_2O_2 **[240-242]** and results showed our system offered an improvement in the LOD (Table 6.3).

Table 6.2. Sensitivity values (*K*) for the QDs-MTAPc nanoprobe and fluorescence lifetimes for a triexponential fit of QDs (alone) and QDs-MTAPc nanoprobe in the absence and presence of H_2O_2 in 50 mM PBS buffer, pH 7.4.

Samples	H_2O_2[M]	τ_1 (ns) ±0.1	τ_2 (ns) ±0.1	τ_3 (ns) ±0.02	K(M^{-1})
QDs	0	42.6(0.56)	13.8(0.39)	2.6(0.05)	-
	1.6×10^{-8}	42.6(0.57)	13.8(0.37)	2.5(0.06)	
QDs-1	0	24.7(0.57)	8.3(0.37)	1.6(0.06)	3.72×10^{7}
	1.6×10^{-8}	46.1(0.61)	8.9(0.37)	2.0(0.02)	
QDs-3	0	31.2(0.56)	7.9(0.36)	1.6(0.08)	8.25×10^{7}
	1.6×10^{-8}	46.9(0.48)	15.2(0.45)	3.0(0.07)	
QDs-4	0	31.2(0.54)	6.5(0.38)	0.8(0.08)	1.67×10^{8}
	1.6×10^{-8}	42.7(0.59)	13.5(0.36)	2.2(0.05)	

Table 6.3. Comparison of the LOD of the proposed nanosensor with some published data for H_2O_2 detection using the QDs-MTAPc nanoprobe. Solvent: 50 mM PBS pH 7.4.

QDs Probe	LOD	References
QDs-AlTAPc	9.8 nM	This work
QDs-NiTAPc	4.4 nM	This work
QDs-ZnTAPc	2.2 nM	This work
CdSe@ZnS-Horseradish	284 nM	[240]
CdS-FePt dimer	18.7 μM	[241]
CdTe-Hemoglobin	2230 nM	[242]

6.1.2. Fluorescence lifetime measurement

Fig. 6.2 shows the fluorescence decay curve of QDs-**1** (used as an example) in the absence and presence of a fixed concentration of H_2O_2. As shown in Table 6.2, the tri-exponential decay lifetimes of the QDs-MTAPc complexes were substantially increased when H_2O_2 was added. When the same equivalent concentration of H_2O_2 was added to the QDs alone, no change in the fluorescence lifetime of the QDs was observed (Table 6.2).

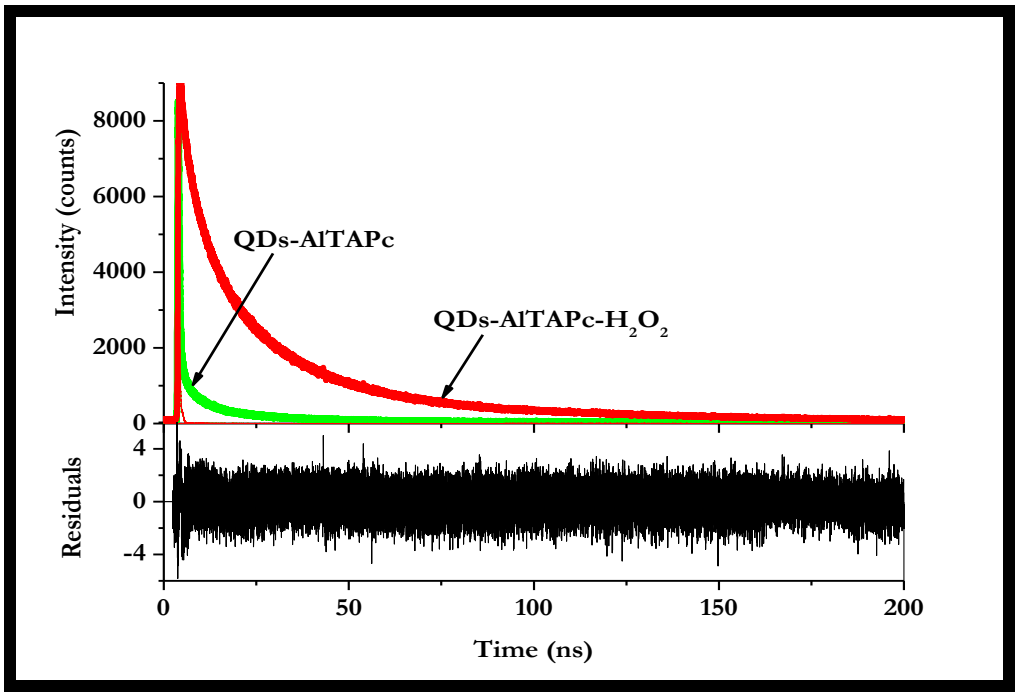

Fig. 6.2. Overlay of the fluorescence decay curves of QDs-1 (as a representative) in the absence and presence of 1.6 x 10^{-8} M H_2O_2.

Based on the data discussed above, the reaction mechanism can be generalised by means of an "off/on" fluorescence principle in which the QD transfers its energy to MTAPc through FRET. This then led to a radiationless deactivation of the excited

state of the QDs and the fluorescence is quenched. Upon addition of H_2O_2, the FRET process is interrupted and the fluorescence of the QDs is switched on.

Additionally, since H_2O_2 is a known oxidant, it is also possible that oxidation by MTAPc-H_2O_2 complex switched on the fluorescence of the QDs **[243].** Soh et al **[243],** have previously shown that oxidation by H_2O_2 switches on the fluorescence of 7-hydroxy-2-oxo-N-(2-(diphenylphosphino) ethyl)-2 H-chromene-3-carboxamide.

6.1.3. Selectivity studies

Since it is ideal for an efficient fluorescent probe to combine both sensitivity and selectivity for its efficacy, the proposed QDs-MTAPc nanosensor selectivity towards H_2O_2 was investigated. The fluorescence intensity change of a fixed concentration of QDs-MTAPc was studied in the presence of 200-fold excess of co-existing biological active species such as: cysteamine (cys), ClO_4^-, GSH, urea, NO_2^-, NO_3^-, $_L$-cysteine ($_L$-cys), $HO^\bullet$, TBHP, $O_2^{\bullet-}$ and $ONOO^-$. A tolerance error of ±5% in fluorescence intensity (FI) change was taken into consideration. As shown in Table 6.4, the fluorescence response of all co-existing species to the proposed nanosensor varied, depending on the nature of the nanoprobe. Generally, it can be seen from Table 6.4 that even though QDs-**4** showed excellent sensitivity towards H_2O_2 as previously discussed, it suffered from severe interferences from species like, ClO_4^-, GSH, $HO^\bullet$, TBHP and $O_2^{\bullet-}$. It is important to note that H_2O_2 interfered with $HO^\bullet$ sensing when using QDs alone, chapter 4. Hence this QDs-**4** probe is not very selective towards H_2O_2. For QDs-**1** the fluorescence of all co-existing species was rather slight except for TBHP but for QDs-**3**, the effects of all co-existing species were negligible and thus

make QDs-**3** the most selective nanoprobe for H_2O_2. Therefore, the order of selectivity of the nanoprobe is: QDs-**3** > QDs-**1** > QDs-**4**. Thus, the order of selectivity of the nanoprobe did not follow the same trend with the sensitivity (QDs-**4** > QDs-**3** **>** QDs-**1)**. As previously discussed, the order of sensitivity of a probe towards ROS may not follow similar trends with its selectivity because steric effects and oxidative shielding of the probe may differ in the presence of co-existing species. In order to prove the selectivity, DFT calculations showed that there is more electron density on the ring for **3** (0.208) (Fig. 6.3)**,** followed by **1** (0.206) and **4** (0.188) probably due to the stronger coordination of the amino substituents to the central metal through the nitrogen atoms. The trend in electron density of the MTAPc was the same with the selectivity trend of the nanoprobe. This may suggest that steric effect and shielding from oxidative attack was more for QDs-**3** than for the other nanoprobes. Since a mutual balance between sensitivity and selectivity need to be achieved for an efficient probe, QDs-**3** is the most effective nanoprobe for H_2O_2.

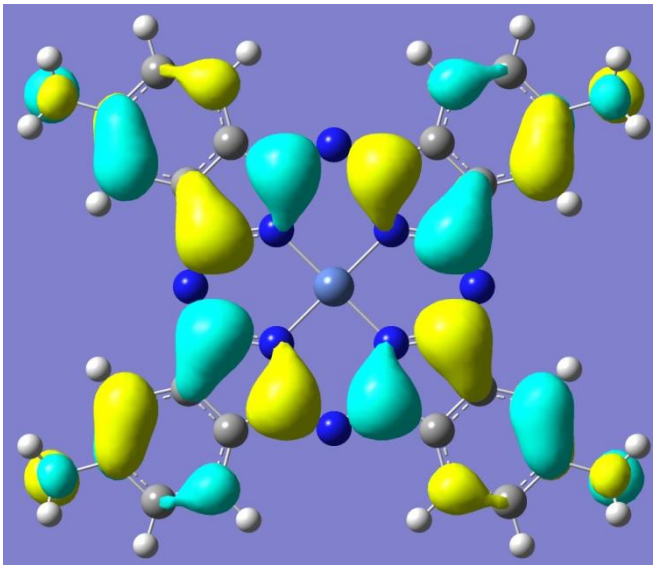

Fig. 6.3. Frontier molecular orbital structure of compound 3 (as a representative) used for DFT calculation.

Table 6.4. Percentage fluorescence intensity (% FI) change of co-existing biological active species on the detection of 4.0 x 10^{-9} M H_2O_2 by the proposed QDs-MTAPc nanoprobe. Concentration of interfering ions = 8.0 x 10^{-7} M. Solvent: 50 mM PBS pH 7.4.

Species	QDs-1 (%FI)	QDs-3 (%FI)	QDs-4 (%FI)
Cysteamine	+3.6	+2.2	+1.8
ClO_4^-	-0.3	-2.1	-10.9
GSH	+4.0	-0.8	-9.2
UREA	-0.1	-0.6	-2.4
NO_2^-	-3.3	-2.6	-2.0
NO_3^-	+1.9	-2.1	-5.0
L-cysteine	+1.4	-2.0	-5.1
HO●	-3.7	-4.8	-8.2
TBHP	-5.1	-1.3	-11.9
$O_2^{\bullet-}$	-2.3	-1.4	-9.4
$ONOO^-$	+1.9	+1.6	+4.8

6.1.4. Conclusions

We have demonstrated in this work that MPcs containing amino substituent can be covalently linked to QDs to form a QDs-MTAPc nanoconjugate which can be

applied as a luminescence nanosensor for ROS detection with varying degree of sensitivity and selectivity. Experimental results showed that interaction between the QDs and MTAPc occurred through FRET which in turn "turned OFF" the fluorescence of the QDs. In the presence of varying concentrations of H_2O_2, the fluorescence of the QDs was "turned ON" and the degree of sensitivity/LOD followed the order: QDs-**4** > QDs-**3** > QDs-**1**. The selectivity of the proposed nanosensor followed the order: QDs-**3** > QDs-**1** > QDs-**4**. However, unmetallated Pc showed no change in fluorescence intensity in the presence of H_2O_2.

6.2. Survey of analyte detection on QDs-CoTAPc probe

The purpose of this study is to compare the efficiency of sensing different analytes using QDs-MPc probe as an attempt to: (1) explain why some analytes are detected with more specificity than others and (2) to elucidate the reaction mechanism in more detail, in the presence of the different analytes. CoTAPc (**2**) was selected as an example because the effects of different metals presented in section 6.1 showed that the fluorescence enhancement occurs regardless of the central metal attached to the Pc ring. CoTAPc (**2**) was linked to GSH-CdTe@ZnS(3.6) QDs (as an example) and employed as a probe for the screening of different analytes ($ONOO^-$, GSH, cysteamine, L-cysteine, TBHP, ClO_4^-, $HO^\bullet$, NO_2^-, NO_3^-, $O_2^{-\bullet}$, Br^-, F^-, $DPPH^\bullet$ and urea) of biological importance.

6.2.1. Fluorescence quenching vs enhancement

Among the different analytes screened, an enhancement of the fluorescence emission of the QDs-**2** nanoprobe was observed for $ONOO^-$, GSH, cysteamine, TBHP, ClO_4^-, $HO^\bullet$, $O_2^{-\bullet}$, Br^- and F^-. Figures similar to Fig. 6.1A - 6.1C were obtained. Thus, the fluorescence "ON mode" of the QDs in the conjugate was activated and showed a linear regression. However, analytes such as NO_2^-, NO_3^- and L-cysteine and urea showed no enhancement of fluorescence of the QDs-**2** nanoprobe. Analytes such as NO_2^- and NO_3^- have been reported [**244**] not to restore the quenched fluorescence of QDs-Ni^{2+} system due to their weaker interaction with Ni^{2+}. $DPPH^\bullet$ on the other hand, showed continued quenching of the QDs fluorescence (Figure not shown). The LOD was determined and the variations in the LOD values and linear range are listed in Table 6.5 for selected analytes that "turned on" the fluorescence of the nanoprobe.

Table 6.5. Linear range and LOD values for the fluorescence "turn ON" of QD-2 nanoprobe in the presence of different analytes.

Analytes	Linear range (M)	LOD (M)
GSH	2.0×10^{-9} - 4.8×10^{-8}	3.34×10^{-10}
Cysteamine	6.5×10^{-9} - 1.6×10^{-7}	1.71×10^{-9}
TBHP	4.5×10^{-8} - 5.4×10^{-7}	4.44×10^{-9}
ClO_4^-	6.5×10^{-8} - 1.6×10^{-7}	8.15×10^{-9}
$^\bullet OH$	4.2×10^{-9} - 2.8×10^{-8}	1.98×10^{-10}

6.2.2. Possible mechanism of QDs-CoTAPc-based "turn-ON" sensor

In order to further deduce the mechanism of the analytes response towards QDs-MPc probe, the absorption spectrum of the nanoconjugate was studied in the presence of each analytes. As reported before **[154],** the QDs emission is "turned on" when the free motion of the surface substituents of the QDs is suppressed. This gives rise to an ordered orientation or improved rigidity of the surface substituent, which may suppress the QDs quenching and thus enhance the fluorescence intensity. Axial ligation to **2** could change the rigidity of its motion. As shown in Fig. 6.4A, the addition of each analyte to the solution of QDs-**2** caused an increase in the aggregation and a decrease in aggregation for GSH (Fig. 6.4B). Aggregation is judged by the enhancement of the high energy peak (Fig. 6.4A) and disaggregation by the decrease in this peak relative to the monomer peak in Fig. 6.4B. The enhancement of the aggregate was also observed for DPPH• where quenching of fluorescence was continued. The aggregate (dimer)-monomer equilibrium in Pcs is affected by many factors including ionic strength **[245]** and the nature of ring substituents. In the case of GSH, the bulky nature of the analyte could have resulted in the disaggregation of the loosely bound "H" aggregates as seen in Fig. 6.4B. Thus, axial ligation of the analytes to QDs-**2** could not be proved due to aggregation. Hence, the studies for axial ligation of analytes were done for unlinked **2**, since it showed no aggregation (Fig. 6.5). Slight changes in the Q band on addition of the analytes are typical of axial ligation **[246].** The spectral changes (blue shift) observed in the Q Band, Table 6.6 and Fig. 6.5, when cysteamine, $ONOO^-$, HO•, $ClO4^-$ and TBHP, were added to **2** solution suggest axial ligation to **2 [246].** Similar behaviour

(blue shift) was also observed for $O_2^{-\bullet}$, Br^- and F^-. For GSH (Fig. 6.5), a red shift was observed, Table 6.6. We propose in this work that cysteamine, $ONOO^-$, ClO_4^-, TBHP, •OH, GSH, $O_2^{-\bullet}$, Br^- and F^- may change the orientation of **2** via axial ligation resulting in enhancement of fluorescence (Scheme 6.1). For NO_2^-, NO_3, urea and L-cysteine, there was no shift in the Q band corresponding to no response in the fluorescence intensity.

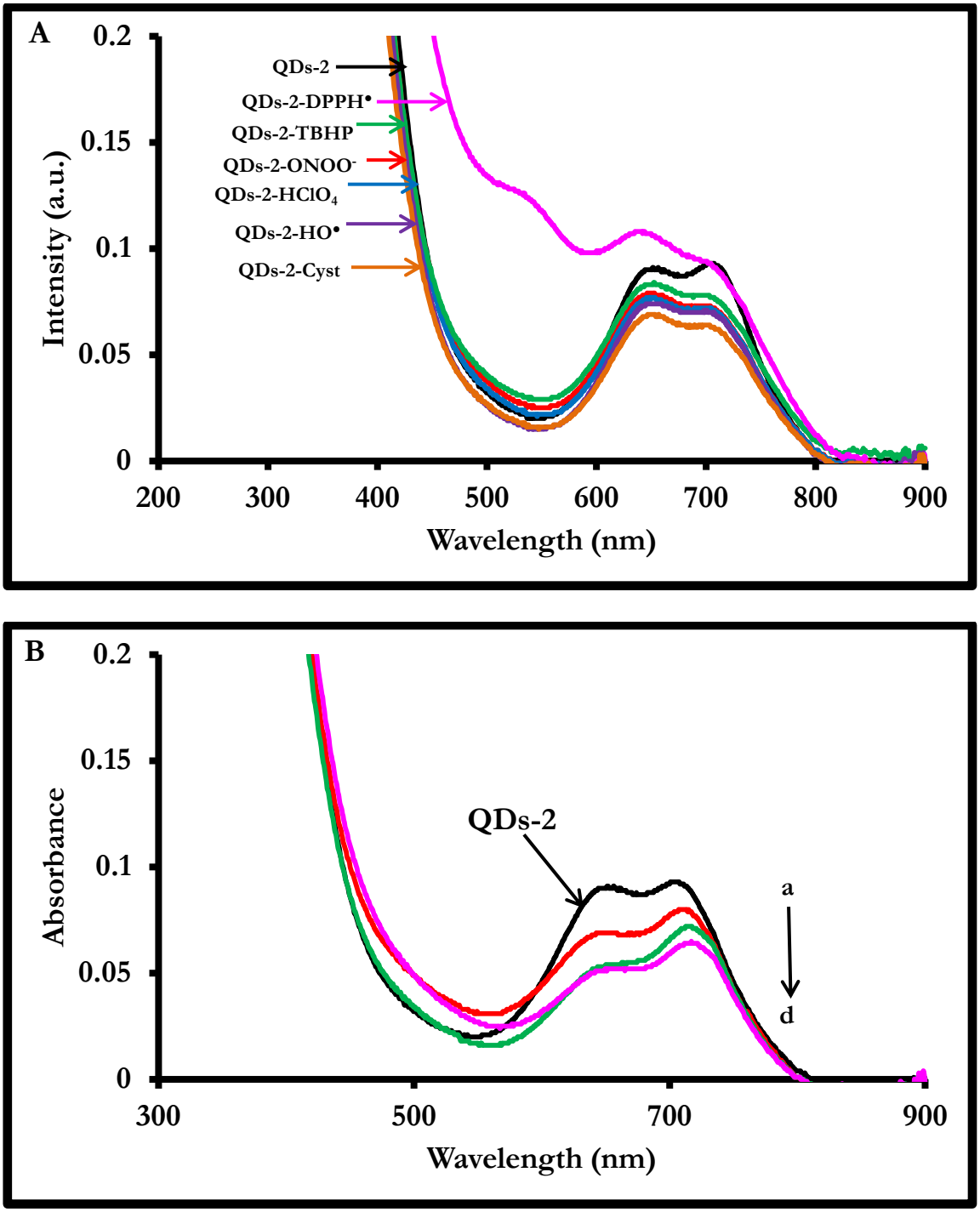

Fig. 6.4. UV/vis absorption spectra of QDs-2 upon addition of (A) 5.4 x 10^{-7} M [DPPH•] or [TBHP], 1.6 x 10^{-8} M [$ONOO^-$], 1.6 x 10^{-6} M [$HClO_4$], 2.8 x 10^{-8} M [•OH] and 1.6 x 10^{-7} M [Cysteamine] and (B) (a) [GSH] (a-d); 0, 2.0 x 10^{-9}, 6.0 x 10^{-9} M, 1.2 x 10^{-8} M. [QDs-2] = 6.1 x 10^{-7} M. PBS buffer, pH 7.4.

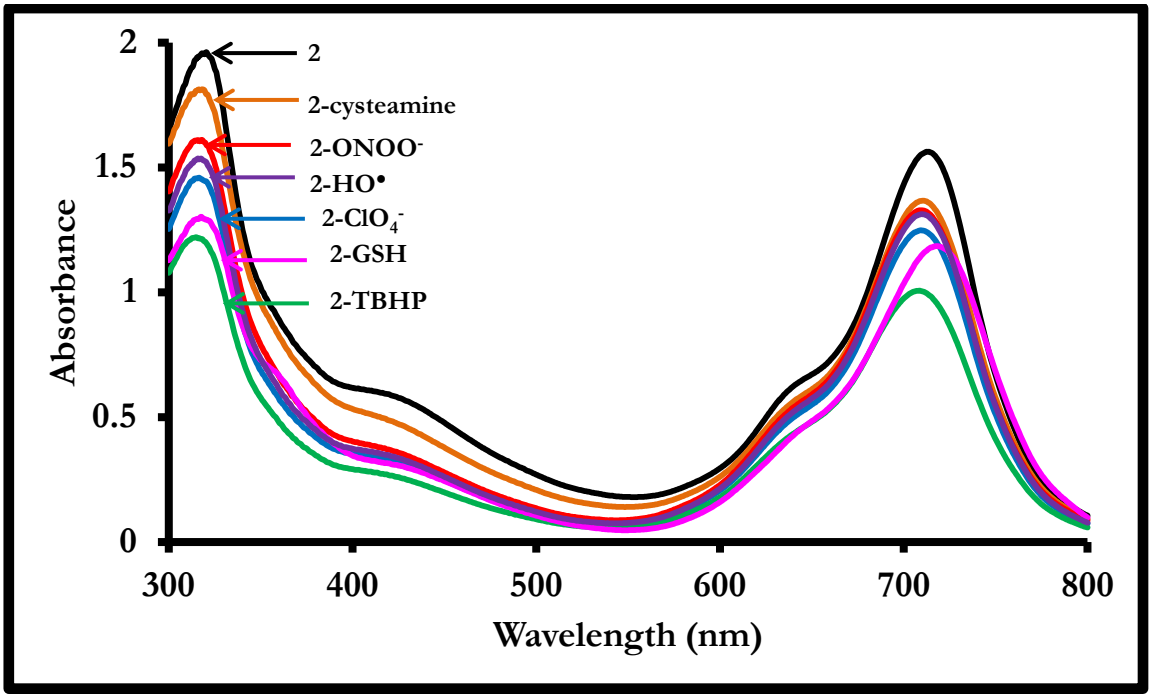

Fig. 6.5. UV/vis absorption spectra of 2 upon addition of selected analytes. [Cysteamine] = 1.6 x 10^{-7} M, [$ONOO^-$] = 1.6 x 10^{-8} M, [•OH] = 2.8 x 10^{-8} M, [ClO_4^-] = 1.6 x 10^{-6} M, [GSH] = 1.2 x 10^{-8} M, [TBHP] = 5.4 x 10^{-7} M and [2] =8.1 x 10^{-6} M. Solvent: DMF:PBS buffer (3:1, v/v).

Table 6.6. Fluorescence lifetime data for QDs-2 nanoprobe in the absence and presence of some selected analytes. The absorption wavelengths of the Q band position of the different analytes upon interaction with QDs-2 nanoprobe are also included.

Samples	Analyte	Q-band (nm) in DMF:PBS buffer	Amount added [M]	τ_1 (ns) ±1.0	τ_2 (ns) ±0.4	τ_3 (ns) ±0.1	Mean Lifetime (ns)
QDs	No analyte	-	8.1×10^{-7}	66.1(0.86)	11.7(0.12)	0.8(0.08)	26.2
QDs-2	No analyte	704	6.1×10^{-7}	22.7(0.44)	3.5(0.32)	0.3(0.24)	8.8
	Cysteamine	698	1.6×10^{-7}	57.7(0.82)	8.6(0.16)	0.5(0.02)	22.3
	$ONOO^-$	698	1.6×10^{-8}	60.7(0.83)	11.2(0.15)	0.9(0.02)	24.3
	GSH	718	4.8×10^{-8}	87.7(0.89)	15.3(0.10)	1.2(0.01)	34.7
	ClO_4^-	700	1.6×10^{-6}	86.0(0.87)	16.4(0.12)	1.5(0.01)	34.6
	TBHP	698	5.4×10^{-7}	57.5(0.82)	8.6(0.15)	0.6(0.03)	22.2
	•OH	700	2.8×10^{-8}	90.5(0.87)	16.2(0.11)	1.2(0.02)	40.0
	DPPH•	701	1.4×10^{-8}	16.7(0.49)	3.1(0.33)	0.2(0.18)	6.7

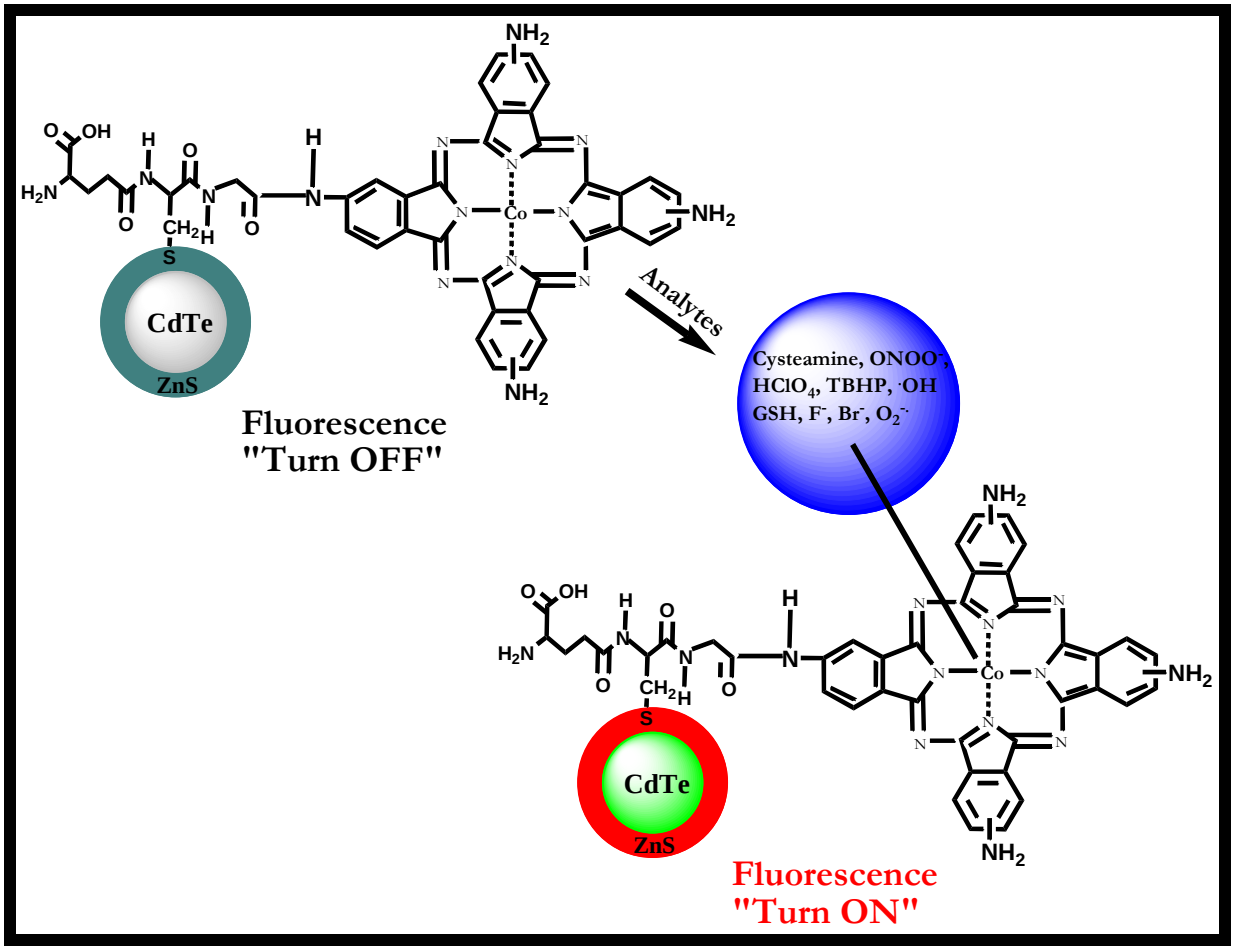

Scheme 6.1. Schematic representation of the fluorescence "turn ON" for different analytes using the QDs-2 nanoprobe.

6.2.3. Fluorescence life-time measurements

From Table 6.6, it can be seen that the mean triexponential fluorescence lifetimes of QDs-**2** nanoprobe decreased (in the absence of the analytes) remarkably when compared to QD_{619} alone. The decrease in lifetimes of QDs-**2** nanoprobe provides further answers to the observed fluorescence quenching of the QDs when conjugated to **2** as discussed above. However, the most important observation is the significant increase in the mean fluorescence lifetime of the QDs-**2** nanoprobe on interaction with a fixed concentration of some selected analytes (cysteamine, $ONOO^-$, GSH,

ClO_4^-, TBHP and •OH) that "turned ON" the fluorescence of the nanoprobe. Therefore, the fluorescence lifetime data compliments the fluorescence enhancement effects of the nanoprobe on interaction with cysteamine, $ONOO^-$, GSH, ClO_4^-, TBHP and •OH. In the presence of DPPH•, a staggering decrease in the mean lifetime of the nanoprobe was observed. This further corroborates the fluorescence quenching effect of the nanoprobe on interaction with DPPH•. For other analytes: NO_2^-, NO_3^-, L-cysteine and urea, there were no changes in the fluorescence lifetimes.

6.2.4. Conclusions

GSH-CdTe@ZnS(3.0) QDs were conjugated to **2** to form a QDs-**2** nanoconjugate system. Different analytes of biological importance were screened for their fluorescence response on the nanoprobe. The results showed that some analytes have the tendencies to either "turn on", others further quench or show no effect on the fluorescence property of the nanoprobe. The results presented here indicate that QDs decorated with Pcs have huge prospect for the construction of versatile fluorescent nanosensors for "turn on" sensing of biological active analytes, depending on their interaction with the probe.

A selection (O_2^-•, Br^- and F^-) of the analytes which enhanced the fluorescence of the nanoprobe are studied in detail below.

6.3. Detailed studies on the detection of superoxide anion

MPA-CdTe@ZnS (3.0 nm) and MPA-CdTe@ZnS (3.4 nm) QDs were chosen in this study since MPA-CdTe@ZnS QDs were found to be superioir for $ONOO^-$ detection

(section 4.3). Co was chosen as a central metal for the Pc because Co tetrasulphonated-phthalocyanine (CoTSPc) has been reported to mimic the activity of Cytochrome c **[247**]. Cytochrome c is known to be selective towards $O_2^{\bullet-}$ when coupled with QDs **[248].** We chose Co as a central metal for the TAPc ring and investigated its ability to selectively recognise $O_2^{\bullet-}$ when coupled to the QDs. Compound **2** can be covalently linked to QDs forming a stable amide bond. Hence, **2** was employed in this work instead of CoTSPc. The QDs were either chemically linked to **2** or mixed (without a chemical bond). The studies were done in DMF:PBS mixture to enhance solubility of the conjugates.

6.3.1. Time-resolved fluorescence measurements

Fluorescence lifetime measurement was employed to further understand the interaction between the QD and MPc. The decay curves for QDs-**2** revealed triexponential decay kinetics (Table 6.7) as discussed above for other QDs-MPc conjugates. The average lifetimes are listed in Table 6.7. It was observed that the fluorescence lifetime of the QDs in the conjugates showed shorter lifetimes compared to the lifetime of the QDs before conjugation to **2** (Table 6.7). The decrease in the lifetime of the QDs in the conjugate may be attributed to FRET (and other processes stated above that decrease fluorescence) in QDs-**2 [249]**. In general, it can be seen from Table 6.7 that the fluorescence lifetime of the QDs in the conjugate (linked) increased on interaction with a fixed concentration of $O_2^{\bullet-}$. This gives an indication that $O_2^{\bullet-}$ can switch on the fluorescence of the QDs in the conjugate. The overall trend suggests that the covalent linking of the QDs to **2** plays a crucial role

for the molecular recognition of $O_2^{\bullet-}$, as judged by the increment of lifetimes in the presence of $O_2^{\bullet-}$. When mixed with no chemical bond, the lifetimes in the presence of $O_2^{\bullet-}$ decreased, Table 6.7.

Table 6.7. Fluorescence lifetimes values QDs-2 nanoconjugates in the absence and presence of $O_2^{\bullet-}$. The fluorescence lifetime values for the QDs-2 (mixed) is also included. Solvent DMF:PBS (3:1) pH 7.4.

Samples	$O_2^{\bullet-}$ [M]	τ_1 (ns) ±0.1	τ_2 (ns) ±0.07	τ_3 (ns) ±0.02	Mean lifetime (ns) (±0.1)
MPA-CdTe@ZnS(3.0)	0	43.8(0.50)	14.9(0.44)	2.8(0.06)	20.5
	3.0×10^{-7}	43.7(0.52)	14.5(0.42)	2.7(0.06)	20.3
MPA-CdTe@ZnS(3.4)	0	46.4(0.62)	15.8(0.34)	2.9(0.04)	21.7
	3.0×10^{-7}	46.3(0.62)	15.9(0.34)	2.9(0.04)	21.7
MPA-CdTe@ZnS(3.0)-2-$_{linked}$	0	41.9(0.56)	12.2(0.38)	2.3(0.06)	18.8
	3.0×10^{-7}	45.6(0.58)	14.9(0.37)	2.5(0.05)	21.0
MPA-CdTe@ZnS(3.4)-2-$_{linked}$	0	32.2(0.60)	8.5(0.35)	1.8(0.05)	14.2
	3.0×10^{-7}	45.7(0.65)	15.6(0.31)	2.7(0.04)	21.3
MPA-CdTe@ZnS(3.0)-2-$_{mixed}$	0	27.4(0.54)	6.8(0.41)	1.7(0.05)	12.0
	3.0×10^{-7}	15.0(0.54)	4.4(0.41)	1.1(0.05)	6.8
MPA-CdTe@ZnS(3.4)-2-$_{mixed}$	0	38.0(0.65)	11.8(0.31)	2.4(0.04)	17.4
	3.0×10^{-7}	33.8(0.65)	9.4(0.31)	2.3(0.04)	15.2

6.3.2. EPR studies

The $O_2^{\bullet-}$ generated in alkaline DMSO is known to be stable **[196,197].** Also, $O_2^{\bullet-}$ has been shown to be highly stable when detected under physiological condition **[198]**. However, it is important to note that water content results in the accelerated decay of $O_2^{\bullet-}$. Since DMF:PBS solvent mixture was employed in this study, EPR spectroscopy was used to study the stability of $O_2^{\bullet-}$ in alkaline DMSO and in DMF:PBS pH 7.4 (3:1). Fig. 6.6A shows the EPR spectrum of $O_2^{\bullet-}$ in alkaline DMSO and thus confirming this specie was successfully generated. When a solution of DMF:PBS pH 7.4 (3:1) (which was used for measurements) was added to $O_2^{\bullet-}$, the EPR spectra recorded at 0 min (Fig. 6.6B) and after 2.5 h (Fig. 6.6C) showed no decomposition when compared to the spectrum of $O_2^{\bullet-}$ (without the solvent mixture). This gives a strong indication that $O_2^{\bullet-}$ was highly stable in this solvent medium and over time, which is necessary, since its detection (as discussed below) was finished within 2.5 h.

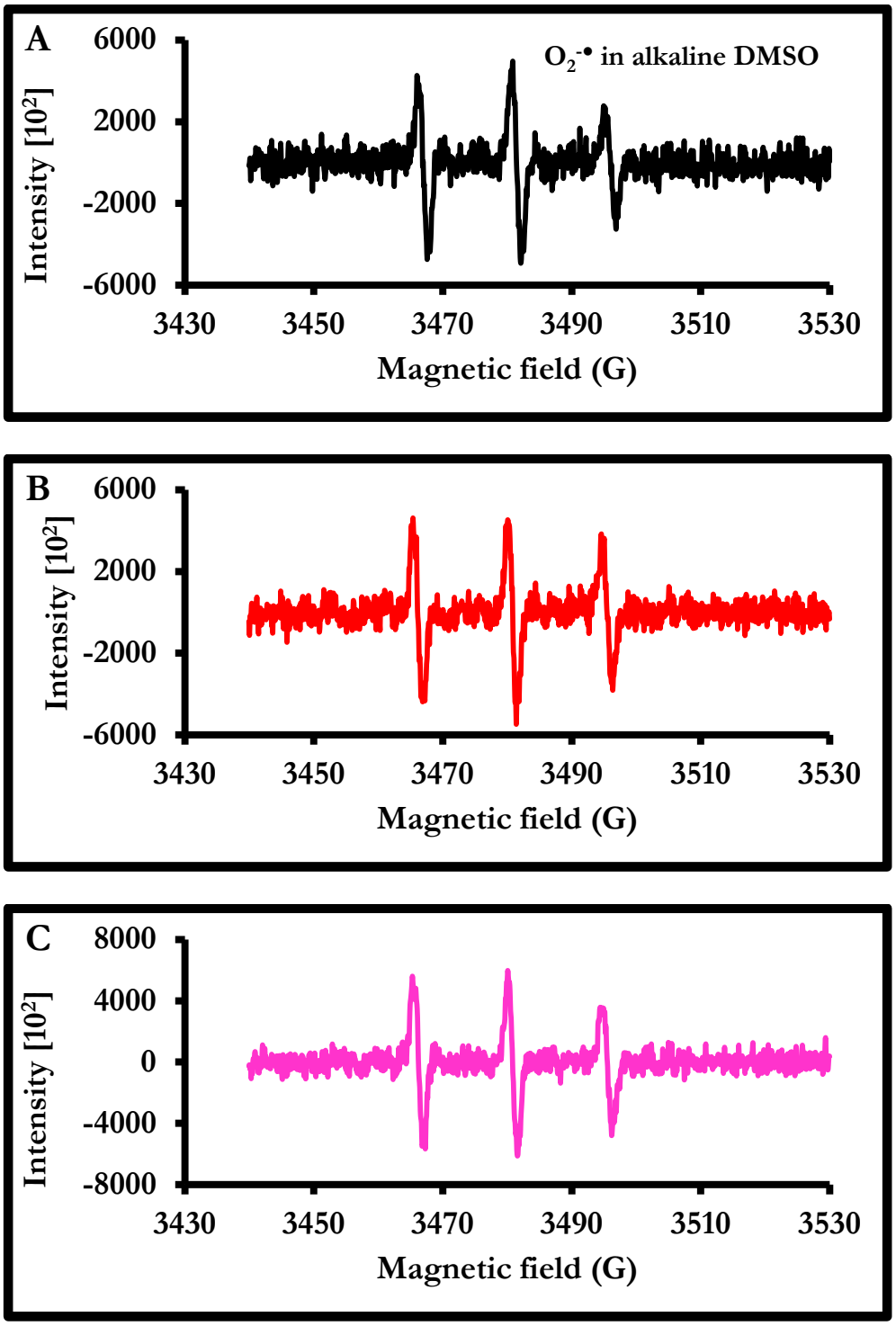

Fig. 6.6. EPR spectra showing the stability of $O_2^{\bullet-}$ formed in alkaline DMSO (A), $O_2^{\bullet-}$ formed in alkaline DMSO + DMF:PBS pH 7.4 (3:1) at 0 min (B) and after 2.5 h (C).

6.3.3. Fluorescence enhancement

Steady state fluorescence response of the QDs-**2** in the presence of varying concentration of $O_2^{\bullet-}$ was examined. With an increase in $O_2^{\bullet-}$ concentration, the fluorescence signal of MPA-CdTe@ZnS(3.0)-**2** (Fig. 6.7A) and MPA-CdTe@ZnS(3.4)-**2** (Fig. 6.7B) was markedly enhanced (as observed in Fig 6.1 A – 6.1C), giving a linear regression as indicated in the corresponding insets. For MPA-CdTe@ZnS(3.0)-**2**, there was no shift in the fluorescence signal of the linked QDs in the presence of increasing concentrations of $O_2^{\bullet-}$, but for MPA-CdTe@ZnS(3.4)-**2**, a red shift in the fluorescence signal on increasing the concentration of $O_2^{\bullet-}$. The red shift may be associated with increased aggregation. It is reasonable to believe that the covalent linking of **2** to CdTe@ZnS QDs played a crucial role in the molecular recognition of $O_2^{\bullet-}$. Since the fluorescence of the QDs in the conjugates was enhanced in the presence of $O_2^{\bullet-}$ (Fig. 6.7) and the fluorescence of the QDs (alone) was quenched in the presence of $O_2^{\bullet-}$ (figure not shown), we propose that compound **2** stabilized the QDs against quenching by the radical. It has been shown before that **2** stabilized CdTe QDs against oxidative disintegration **[250].**

It is important to note that the quenching of the luminescence of the QDs (alone) in the presence of $O_2^{\bullet-}$ observed in our work, is consistent with literature **[251]**. The corresponding LOD for $O_2^{\bullet-}$ detection was calculated and the value for MPA-CdTe@ZnS(3.0)-**2** was 2.1 nM and that for MPA-CdTe@ZnS(3.4)-**2** was 2.4 nM, Table 6.1. The former is more sensitive for the optical recognition of $O_2^{\bullet-}$ as judged from the lower LOD value probably due to its smaller size. Compared with the few

literature LOD values for $O_2^{\bullet-}$ **[252,253]** (10^{-8} to 10^{-7} M range), the use of our system offers an improvement in the LOD.

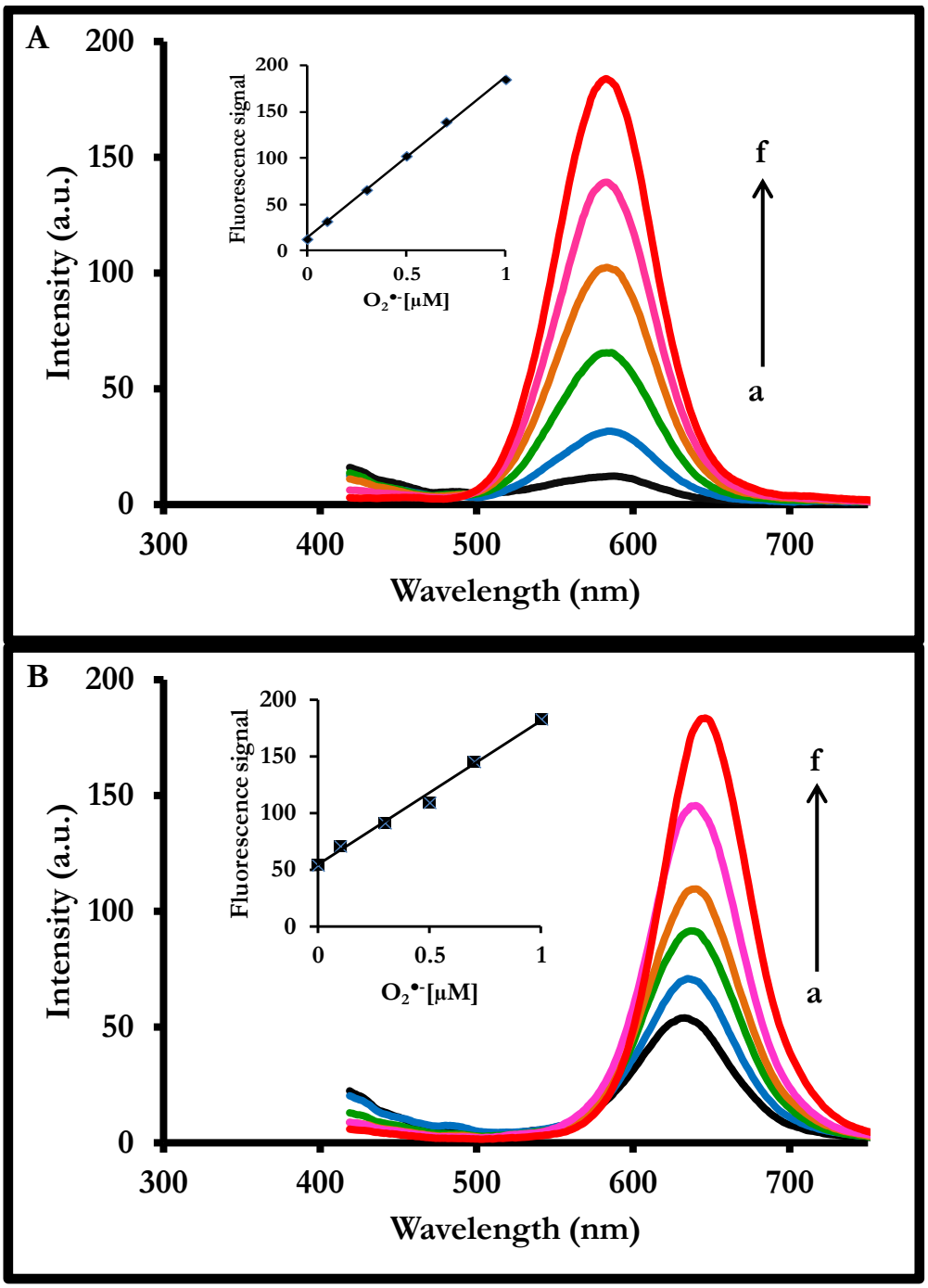

Fig. 6.7. Effect of addition of different concentrations of $O_2^{\bullet-}$ on the fluorescence of (A) MPA-CdTe@ZnS(3.0)-2 and (B) MPA-CdTe@ZnS(3.4)-2. Concentration of $O_2^{\bullet-}$: (a) 0, (b) 1.0 x 10^{-7}, (c) 3.0 x 10^{-7} (d) 5.0 x 10^{-7}, (e) 7.0 x 10^{-7}, (f) 1.0 x 10^{-6}. Inset: corresponding fluorescence signal vs $[O_2^{\bullet-}]$. λ_{exc} = 400 nm.

6.3.4. Selectivity of QDs-CoTAPc nanoconjugates

The fluorescence signal of QDs-**2**-$O_2^{\bullet-}$ system in the presence of various possible co-existing interfering species (TBHP, $ONOO^-$, $HO^{\bullet}$, ClO_4^-, NO_3^-, NO_2^-, L-cysteine, cysteamine, GSH, and urea) was carried out to investigate the selectivity of the proposed nanosensor. Fig. 6.8, shows the effect of 1 x 10^{-3} M excess of relevant species on the luminescence signal of 3 x 10^{-7} M of $O_2^{\bullet-}$ with the QDs-**2** nanoconjugates. A tolerable error of ±5.0% in the relative fluorescence signal was taken into consideration. It can be seen from Fig. 6.8, that the fluorescence of the respective QDs-**2**-$O_2^{\bullet-}$ was unaffected, with none of the species causing any significant interference. That is, there was no change in fluorescence (enhancement or decrease) when these interfering specie were added to QDs-**2**-$O_2^{\bullet-}$, meaning that QD-**2** was highly selective towards $O_2^{\bullet-}$. Therefore, the distinct discrimination between $O_2^{\bullet-}$ and other species makes it possible for QDs-**2** to detect $O_2^{\bullet-}$ in the presence of co-existing species with no interference. We can conclude that the QDs-**2** is highly selective towards $O_2^{\bullet-}$.

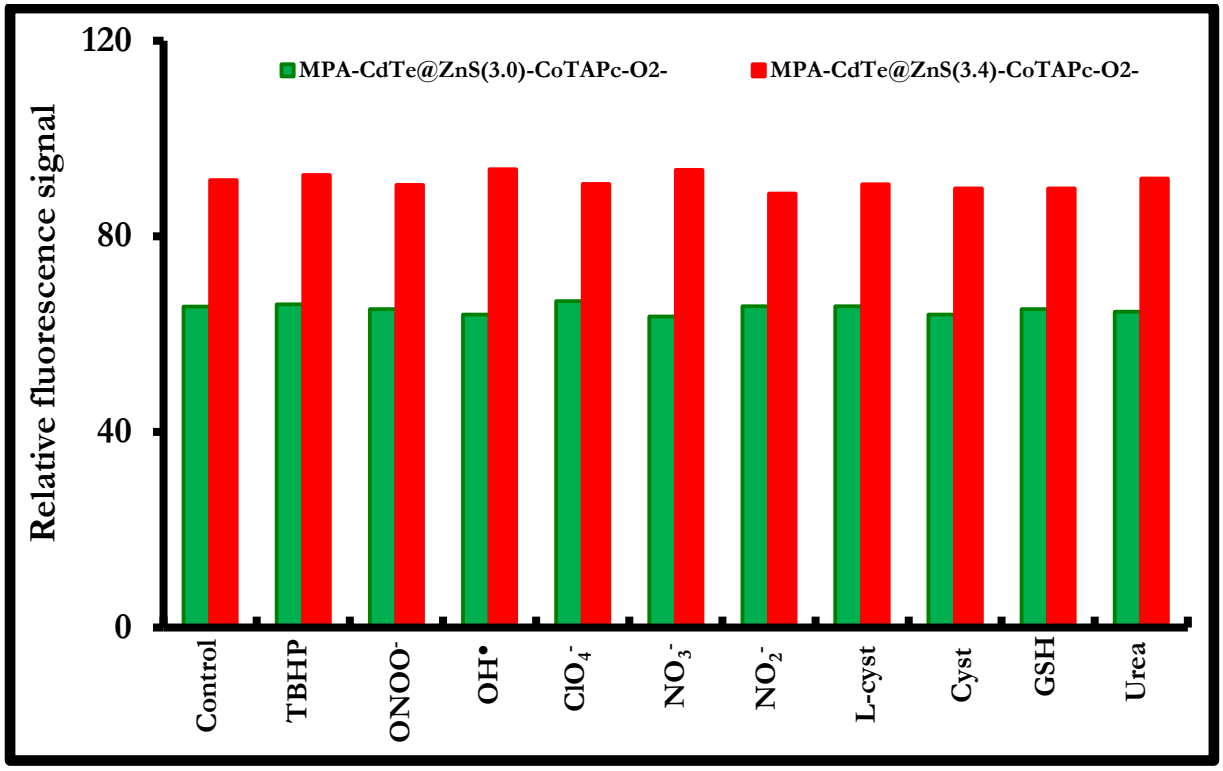

Fig. 6.8. Co-existing effects of different interfering species on the fluorescence of the QDs-2-$O_2^{\bullet-}$ system. Concentration of $O_2^{\bullet-}$ = 3 x 10^{-7} M. Other species = 1 x 10^{-3} M. Control = QDs-2 + $O_2^{\bullet-}$.

6.3.5. Conclusions

The nanocomplex of QDs-**2** was successfully examined for its ability to optically recognize $O_2^{\bullet-}$ in aqueous solution. Based on this success, the proposed nanosensor approach, presents great promise for further development of sensors based on QDs-MPc conjugates.

6.4. Detailed studies on the detection of bromide ion using GSH-CdTe@ZnS-NiTAPc

GSH-CdTe@ZnS-NiTAPc nanoconjugates were employed for the detection of Br^-. Since the photoluminescence properties of QDs are dependent on their size,

different-sized; GSH-CdTe@ZnS (2.6 nm), GSH-CdTe@ZnS (3.4 nm) and GSH-CdTe@ZnS (3.6 nm) were conjugated to **3** to study the size-dependent properties of the conjugates towards Br^- detection.

6.4.1. Fluorescence studies

As explained in the above section, the covalent binding of the different-sized QDs to **3** induced the fluorescence "turn OFF" (quenching) of the linked QDs possibly due to FRET and other processes which deactivate the excited state. The fluorescence of the QDs in the conjugate was "turned ON" upon interaction with Br^- as judged by the enhancement in fluorescence with figures similar to Fig. 6.1A – 6.1C. It is expected that the presence of differently sized QDs, covalently linked to **3** could have a varying effect on the sensitivity of the nanoprobe. Hence, a comparative investigation using QDs(2.6)-**3**, QDs(3.4)-**3** and QDs(3.6)-**3** were carried out for Br^- recognition. It was observed that the optimum concentration of each QDs-**3** nanoprobe used for the experiment varied with the size of the QDs. Therefore, the ratio of each QDs-**3** to Br^- to induce the highest fluorescence enhancement at the optimum concentration of the former was: QDs(2.6)-**3**:Br^- (1:2.7), QDs(3.4)-**3**:Br^- (1:6.3) and QDs(3.6)-**3**:Br^- (1:12.7).

In addition, when the same concentration of Br^- was added to the QD alone (plots not shown), there was quenching of fluorescence (not enhancement), but only higher concentrations (micromolar range) of Br^- (as observed above for $O_2^{-\bullet}$) could be detected and hence demonstrating the superior sensitivity of the QDs-**3** nanoprobe. When the QDs were mixed with **3** without a chemical bond, there was quenching of

fluorescence of the former, but addition of Br^- did not result in enhancement ("turn ON") of fluorescence observed when there is a chemical bond between QDs and **3**.

In order to evaluate the fluorescence enhancement sensitivity of the nanoprobe, the fluorescence signal of the nanoprobe was plotted against varying concentrations of Br^-. A good LOD for Br^- (Table 6.1) were obtained for these plots. We observed that the LOD values displayed in Table 6.8 varied slightly, depending on the size of the QDs conjugated to **3** and followed the order: QDs(2.6)-**3** > QDs(3.4)-**3** > QDs(3.6)-**3**. We noted that as the size of the QDs increased, the sensitivity of the nanoprobe towards Br^- decreased and thus demonstrating the versatile quantum size effect of nanocystal QDs. The fact that the smaller QDs showed improved sensitivity could be related to the large surface area due to the size.

6.4.2. Mechanism of the fluorescence "turn-ON" probe

Time resolved fluorescence measurements were carried out and the luminescence decay curves in the absence and presence of a fixed concentration of Br^- were similar to Fig 6.2. As displayed in Table 6.8, the tri-exponential fluorescence lifetimes of QDs(2.6)-**3** nanocomplex were significantly increased when a fixed concentration of Br^- was added. When the same equivalent concentration of Br^- was added to the QDs alone, a significant decrease in the fluorescence lifetime of the QDs was observed (Table 6.8). Alternatively, when QDs are mixed with **3** without a chemical bond, there was no significant enhancement of fluorescence observed. In fact, there was shortening of fluorescence lifetimes.

Table 6.8. Fluorescence lifetimes for a triexponential fit of GSH-CdTe@ZnS1 QDs (alone) and GSH-CdTe@ZnS1-3 nanoprobe (as a representative) in the absence and presence of Br^- in 10 mM PBS buffer, pH 7.4.

Samples	Br^-[M]	τ_1 (ns) ±0.09	τ_2 (ns) ±0.07	τ_3 (ns) ±0.03
GSH-CdTe@ZnS(2.6)	0	45.6(0.54)	15.7(0.40)	2.6(0.06)
	6.0×10^{-9}	38.6(0.51)	12.3(0.41)	1.8(0.08)
GSH-CdTe@ZnS(2.6)-3-$_{linked}$	0	38.3(0.52)	12.2(0.41)	1.7(0.07)
	6.0×10^{-9}	65.6(0.59)	19.6(0.37)	3.5(0.04)
GSH-CdTe@ZnS(2.6)-3-$_{mixed}$	0	42.5(0.62)	11.4(0.33)	1.7(0.05)
	6.0×10^{-9}	40.2(0.66)	9.7(0.29)	1.4(0.05)

As stated above, it has been suggested that the emission of QDs is enhanced when the free motion of the substituents on the surface of QDs are suppressed **[154]**. This results in an ordered orientation or improved rigidity of the surface substituent, which may suppress the QDs quenching and thus increase the luminescence intensity. We suggest in this study that Br^- may affect the orientation of compound **3** via axial ligation as discussed above, Scheme 6.1. Based on the above hypothesis, the reaction mechanism can be summarised by means of an "OFF/ON" fluorescence principle in which GSH-CdTe@ZnS QDs transfers its energy to **3** as a result of FRET. This then led to a radiationless deactivation of the excited state of the QDs, and the fluorescence is quenched. Upon interaction of QDs-**3** with Br^-, the FRET process is

interrupted and the fluorescence of the QD is "turned on". This occurs only when there is a chemical bond between the QDs and **3**.

6.4.3. Selectivity of the proposed nanoprobe

To explore the selective performance of the proposed nanoprobe, the effects of excess co-existing cation and anion [1.5 x 10^{-6} M] of Na^+, K^+, Mg^{2+}, Ca^{2+}, Fe^{3+}, Ni^{2+}, Cr^{3+}, Zn^{2+}, SO_4^{2-}, NO_3^-, NO_2^-, OAc^- (acetate), CO_3^{2-}, I^-, F^- and Cl^- were studied. The co-existing ions were mixed with a fixed concentration of QDs-**3**-Br^- system. The concentration of Br^- used was 4.8 x 10^{-8} M. Comparing the effects of the co-existing ions on the different-sized nanoprobe, Table 6.9 shows that the metal ions did not pose any significant effect on the fluorescence of QDs(2.6)-**3**-Br^-, hence this probe was highly selective for Br^- detection. For QDs(3.4)-**3**-Br^-, the probe suffered from interference from ions such as: Na^+, I^-, F^- and Cl^-, hence this probe was partially selective for Br^- detection. It turned out that QD_{621}-**3**-Br^- probe suffered severe interference from co-existing ions of: K^+, Mg^{2+}, Fe^{3+}, Ni^{2+}, Cr^{3+}, Zn^{2+}, NO_3^-, NO_2^-, CO_3^{2-}, I^-, F^- and Cl^-, hence this probe is not selective for Br^- detection. Table 6.9 shows that the smaller QDs gave the lowest %FI values and the largest QDs gave the largest %FI values. In addition, the effects of familiar anions of Cl^-, F^- and I^- were individually studied on the fluorescence of QDs(3.4)-**3** (used as a representative) and their fluorescence effects were compared with Br^-. As shown in Fig 6.9, it was observed that Cl^-, F^- and I^- could enhance the fluorescence of the nanoprobe but their effect was very minimal at the same concentration used for Br^-. Hence, developing a probe for Cl^-, F^- and I^- using this method will require higher linear range and LOD

when compared to Br^-. This implies that this nanoprobe can be used to detect similar anions with varying LOD. Such varying interactions and sensitivity of similar anions **[254]** and cations **[255]** on the fluorescence of QDs have previously been reported. This study demonstrates the feasibility of using QDs-**3** for anion sensing in which Br^- was purposely chosen as a model anion. Also, the purity of KCl (99 – 100.5 %), KI (99 %), NH_4F (≥ 98 %) used in this work indicates that trace amount of Br^- may not be present in these salts, meaning this anions on their own can interact with the nanoprobe. In summary, the selectivity of the nanoprobe (QDs(2.6)-**3** > QDs(3.4)-**3** > QDs(3.6)-**3**) followed the same trend with the sensitivity of the probe and thus demonstrating in this work that the fluorescence response of QDs in luminescence sensor technology depends on their size.

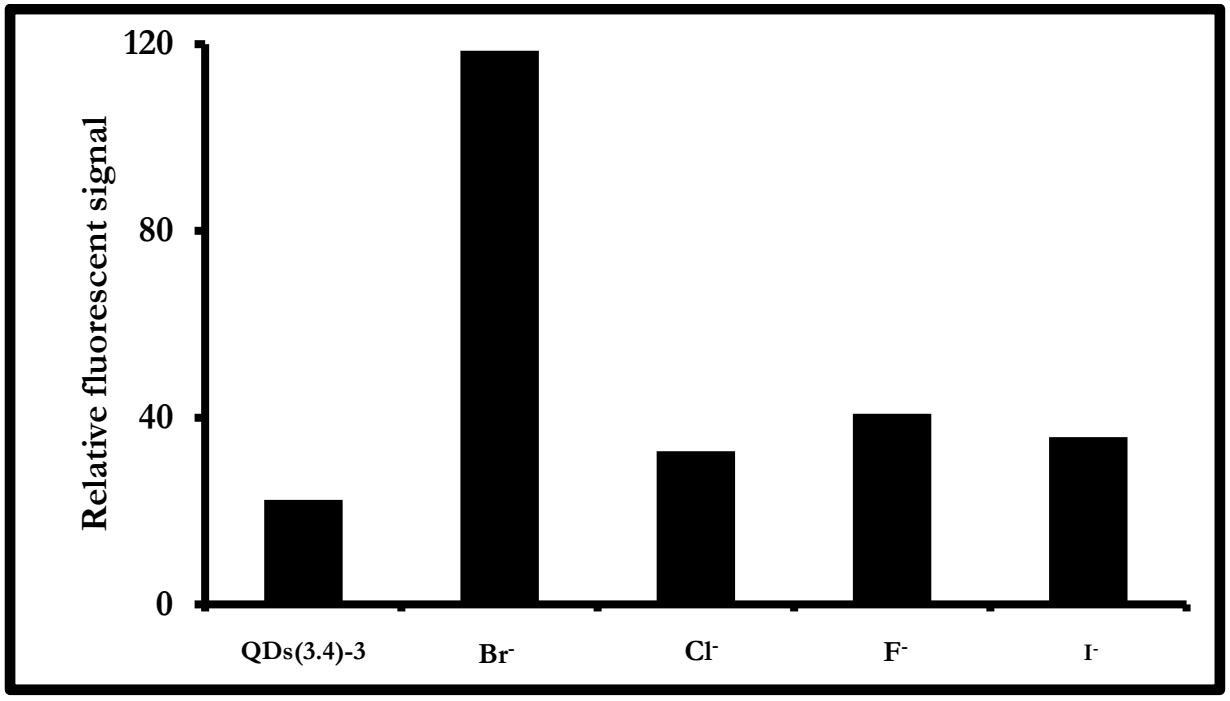

Fig. 6.9. Comparative effects of samiliar anions on the fluorescence of QDs(3.4)-3 (as a representative). Concentration of Br^-, Cl^-, F^-, and I^- = 4.8 x 10^{-8} M.

Table 6.9. Percentage fluorescence intensity (% FI) change of co-existing interferent ions on the fluorescence detection of 4.8 x 10^{-8} M Br^- by the proposed GSH-CdTe@ZnS QDs-3 nanoprobe. Concentration of interfering ions = 1.5 x 10^{-6} M. Solvent: 10 mM PBS pH 7.4.

Ions	QDs(2.6)-3 (%FI)	QDs(3.4)-3 (%FI)	QDs(3.6)-3 (%FI)
Na^+	+1.1	+4.8	+1.6
K^+	+0.5	+0.4	+8.3
Mg^{2+}	+0.3	-1.4	-13.6
Ca^{2+}	-0.2	+0.6	-1.8
Fe^{3+}	+2.1	-0.5	+12.4
Ni^{2+}	-0.3	+2.5	-5.4
Cr^{3+}	-0.3	-1.4	+3.7
Zn^{2+}	+1.1	+0.8	-4.1
SO_4^{2-}	-0.1	-0.6	0.2
NO_3^-	-2.0	+1.2	-3.6
NO_2^-	+0.3	-2.1	+7.3
OAc^-	+1.0	-0.5	-3.1
CO_3^{2-}	+0.7	+0.4	+4.1
I^-	+0.8	-7.6	-6.4
F^-	+1.4	-4.3	-11.0
Cl^-	+0.9	+5.5	+7.0

6.4.4. Conclusions

We have demonstrated in this study that GSH-capped CdTe@ZnS QDs of different sizes can be covalently linked to NiTAPc and applied as a luminescence nanosensor for anion sensing. Br^- was chosen as a model anion. Experimental results showed that the overall sensor sensitivity and selectivity was dependent on the size of the modified QDs and followed the order: GSH-CdTe@ZnS(2.6)-**3** > GSH-CdTe@ZnS(3.4)-**3** > GSH-CdTe@ZnS(3.6)-**3**.

6.5. Detection of fluoride ion using QDs-AlMAPc(5) and QDs-AlMAPPc(6) conjugates

To ensure that only one reactive substituent of the MPc is linked to the QDs, this section reports on the chemical coordination of newly synthesized unsymmetrical substituted ClAlMAPc (**5**) and ClAlMAPPc (**6**) conjugated MPA-CdSe@ZnS (4.6 nm) and GSH-CdSe@ZnS (4.7 nm) QDs for application as a fluorescence-based sensor. The use of mono-substituted MPc complexes allows for a more defined conjugation to the QDs, unlike the previously used tetrasubstituted MPc (presented in the previous sections). Al, as an example, was chosen as central metal for the Pc complexes because it could udergo axial ligand exchange reactions with the analyte. Fluoride ion (F^-) was chosen as a test ion because selective screening of different anions (as discussed later) showed that F^- was among the ions that could "turn ON" the fluorescence of the QDs-5 or 6 nanoprobe. The effects of the nature of ring substituents on the overall sensor sensitivity will be presented. In addition, the application of the nanosensor for F^- detection in tap water and in cell culture medium (Dulbecco's modified Eagle medium (DMEM)) is presented.

6.5.1. Selective screening of different anions

In order to study the effects of different anions on the fluorescence response of the nanoprobe, a series of experiments were carried out using MPA-CdSe@ZnS-**6** as a representative probe to evaluate the fluorescence "turn ON" effect of various anions. Fig. 6.10 shows the effects of these anions (at the same concentration, 1.4 x 10^{-8} M). As it can be observed, anions such as NO_3^-, NO_2^-, CO_3^{2-}, SO_3^{2-}, PO_4^{3-} and OAc^- further quenched the fluorescence of the nanoprobe and thus indicating that these anions cannot interact with the probe to "turn ON" the fluorescence. Anions such as SO_4^{2-}, Cl^- and I^-, displayed a slight fluorescence increment on the nanoprobe while the effect of Br^- and F^- were much higher. In general, F^- gave the largest fluorescence increment. This implies that this nanoprobe has a strong affinity for detecting similar anions. Fig 6.9, shows that the fluorescence of GSH-CdTe@ZnS(3.4)-**3** in the presence of Br^- was more enhanced than F^- while Fig. 6.10 shows that F^- was more enhanced than Br^- using MPA-CdSe@ZnS(4.6)-**6.** This implies that the selectivity of the sensor depends on the size and nature of the QDs.

As previously explained, the QDs fluorescence emission is "turned ON" when the free motion of the surface substituents is suppressed which gives rise to an ordered orientation or improved rigidity of the surface substituent. This may suppress the QDs quenching and thus enhance the fluorescence intensity. We propose that change in axial ligation on ClAlPc could influence the rigidity of its motion. F^- has a high electronegativity and may replace Cl^- in the axial position in ClAlPc (Scheme 6.2). The exchange of Cl^- for F^- was proved spectroscopically by adding F^- to ClAlPc solutions. A slight blue shift (2 nm) in Q band wavelength (Fig. 6.11) of compound **6**

was observed for F^- and thus confirming a possible axial ligand exchange **[246]**), while there were no noticeable changes for other ions (CO_3^{2-}, NO_3^- and SO_4^{2-}) that did not enhance the fluorescence. The electronic effect of the axial substituents is also known to play a major role in determining the degree of ruffling (distortion) in porphyrins **[256]** which will also be the case with Pcs. This may suggest that the linked Pc interacts strongly with F^- than for the other anions and thus "turn ON" the fluorescence of the linked QDs. In addition, the substantial fluorescence increment by other anions (such as Cl^-, I^- and SO_4^{2-}) suggests that this probe can be employed to detect these anions with varying sensitivity as often observed by other QDs-based probe **[254].** However, to test the efficacy of the nanoprobe in this study, F^- was selected as the test anion.

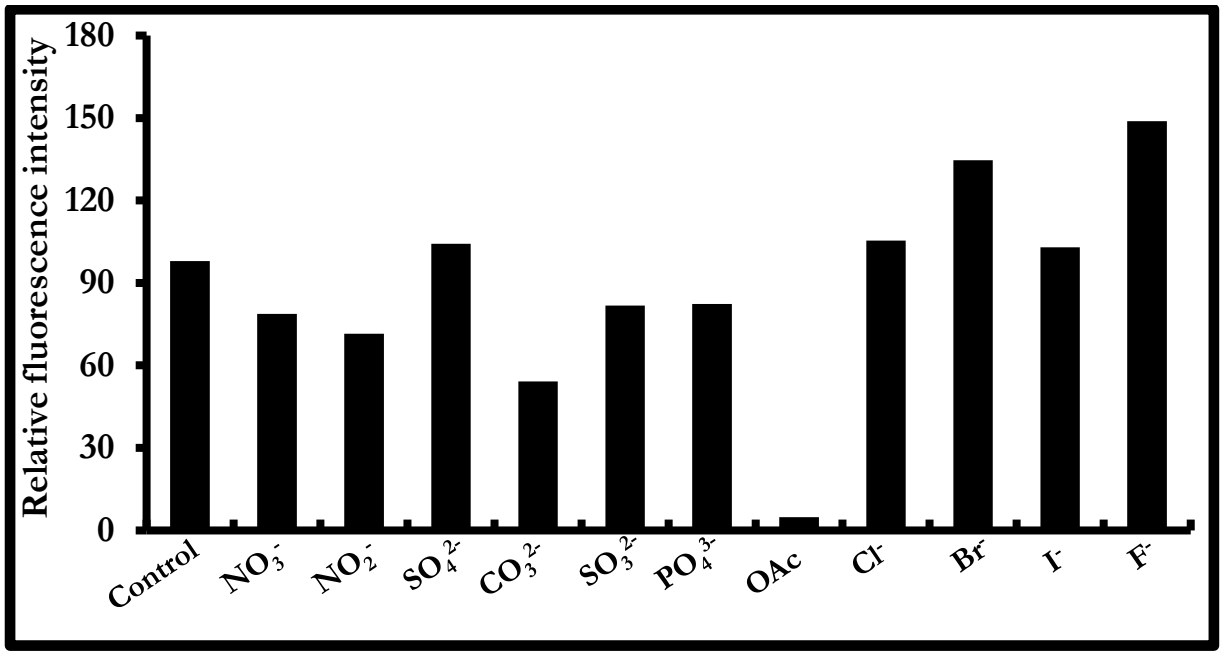

Fig. 6.10. Effect of different anions on the fluorescence response of MPACdSe@ZnS-6 (used as a control) nanoprobe. Concentration of anions = 1.4 x 10^{-8} M.

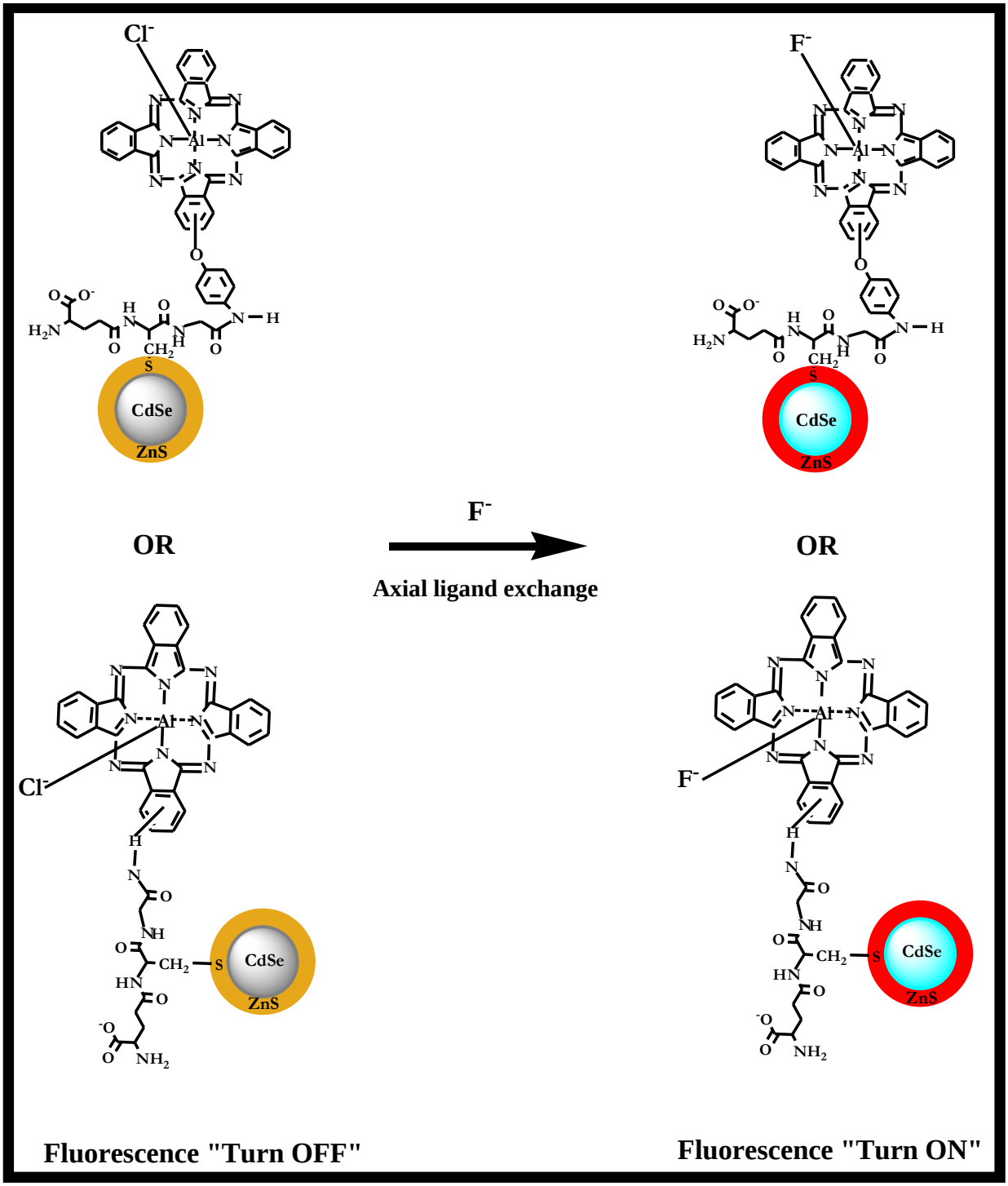

Scheme 6.2. Schematic representation for the detection mechanism of F^- using the proposed nanoprobe. GSH-CdSe@ZnS-5 and GSH-CdSe@ZnS-5 nanoconjugates are shown as representatives.

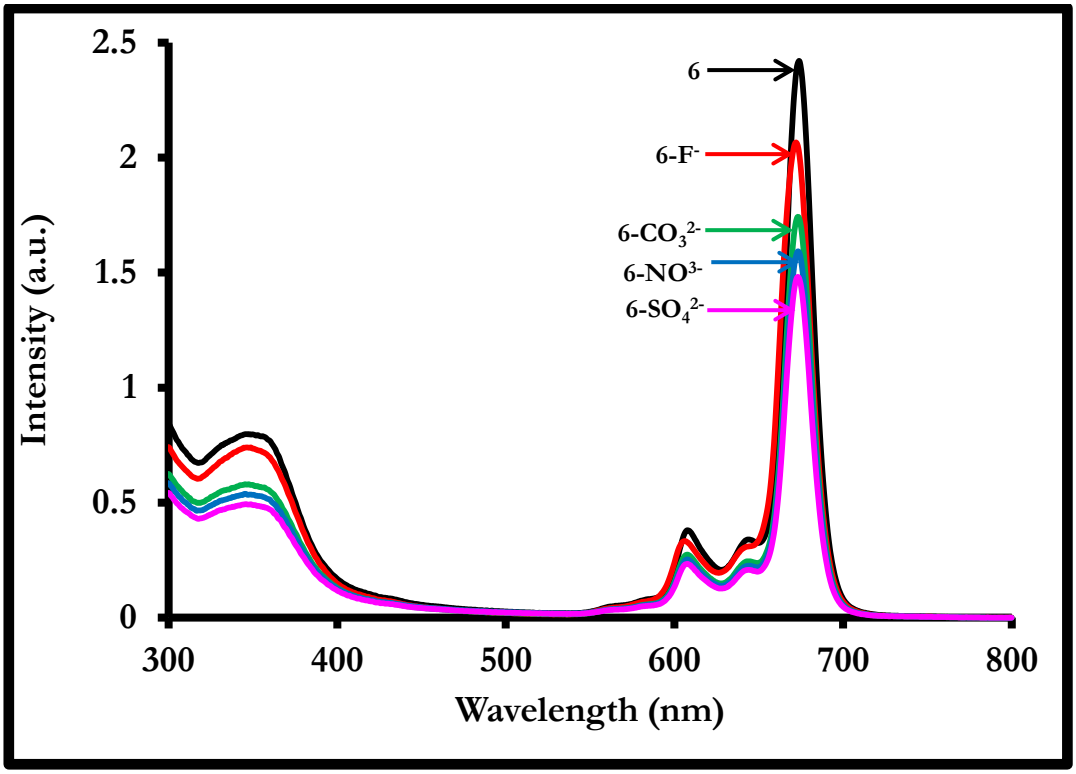

Fig. 6.11. Effect of anions of the absorption spectrum of 6 (used as a representative). Concentration of ions [4.5 x 10^{-8} M].

6.5.2. Fluorescence recognition of fluoride ion in aqueous media

The detection of F^- was studied using MPA-CdSe@ZnS(4.6)-**5**, MPA-CdSe@ZnS(4.6)-**6**, GSH-CdSe@ZnS(4.7)-**5** and GSH-CdSe@ZnS(4.7)-**6** nanoprobes (as examples) in aqueous media. As observed for other analytes in the presence of QDs-MPc (Fig 6.1A – 6.1C), the fluorescence of the nanoprobe was enhanced in the presence of increasing concentration of F^-. At the optimum concentration of F^- (1.2 x 10^{-7} M), a 77.6% fold increase in fluorescence intensity was observed for MPA-CdSe@ZnS-**5**, 80.6% for MPA-CdSe@ZnS-**6**, 78.8% for GSH-CdSe@ZnS-**5** and 88.1% for GSH-CdSe@ZnS-**6**. Under the optimum conditions, the fluorescence signal correlated linearly with the concentration of F^-. As shown in Table 6.10, good LOD values for F^-

were obtained, but were dependent on the nature of the MPc conjugated to the QDs. This may be related to the electronic and distortion effects of the ring substituents. A better LOD, which was obtained for MPA or GSH-CdSe@ZnS-**6** conjugates could be related to the effect of the aminophenoxy substituent (which is more electron donating than the amino substituent) on the stabilization of the Pc. Comparison of the sensitivity of our new system for F^- detection with other QDs-based probe [**257-259**] showed that our system offers an improvement in the detection performance (Table 6.10).

Table 6.10. Comparison of the detection performance of the proposed QDs-MPc nanoprobe with some published QD-based probe for F^- detection based on fluorescence enhancement.

Probe	LOD	Linear range	References
MPA-CdSe@ZnS(4.6)-5	**2.30×10^{-10} M**	**1.5×10^{-9} - 1.2×10^{-7} M**	**This work**
MPA-CdSe@ZnS(4.6)-6	**1.04×10^{-10} M**	**1.5×10^{-9} - 1.2×10^{-7} M**	**This work**
GSH-CdSe@ZnS(4.7)-5	**1.78×10^{-10} M**	**1.5×10^{-9} - 1.2×10^{-7} M**	**This work**
GSH-CdSe@ZnS(4.7)-6	**1.42×10^{-10} M**	**1.5×10^{-9} - 1.2×10^{-7} M**	**This work**
Gemini-CdSe@ZnS	**6.8×10^{-7} M**	**1.5×10^{-4} - 3.0×10^{-3} M**	**[257]**
Cysteamine-CdTe	**5.0×10^{-5} M**	**0 - 1.2×10^{-2} M**	**[258]**
AuNPs-CdTe	**5.0×10^{-8} M**	**5.0×10^{-6} - 4.5×10^{-5} M**	**[259]**

6.5.3. Time-resolved fluorescence measurements

The optical performance of the QDs-MPc nanoprobe towards F^- was further complemented using time-resolved fluorescence measurement and the decay curves were similar to Fig. 6.2. As shown in Table 6.11, MPA-CdSe@ZnS QDs exhibited a fast tri-exponential decay, with an average lifetime of 6.2 ns. CdSe@ZnS QDs obtained after ligand exchange are known to decay very fast **[260].** For MPA-CdSe@ZnS(4.6)-**5** and MPA-CdSe@ZnS(4.6)-**6** (in the absence of F^-), the average fluorescence lifetime decreased substantially (relative to the QDs alone) which could be attributed to FRET from the QDs to the Pc or other processes which decrease the fluorescence of QDs as discussed already. In the presence of F^-, an increase in the mean fluorescence lifetime was observed and thus confirming that the radiative electron-hole recombination pair of the linked QDs was activated.

Table 6.11. Fluorescence lifetimes for a triexponential fit of MPA-CdSe@ZnS QDs, MPA-CdSe@ZnS-5 and MPA-CdSe@ZnS-6 nanoprobe (as a representative) in the absence and presence of F^- in 10 mM PBS buffer, pH 7.4.

Samples	F^-[M]	τ_1 (ns) ±0.1	τ_2 (ns) ±0.07	τ_3 (ns) ±0.04	Mean Lifetime (ns)
MPA-CdSe@ZnS(4.6)	No Analyte	13.5(0.53)	4.4(0.38)	0.7(0.9)	6.2
MPA-CdSe@ZnS(4.6)-5	0 4.5×10^{-8}	12.3(0.51) 13.2(0.45)	2.7(0.30) 3.6(0.38)	0.6(0.19) 0.7(0.16)	5.2 5.8
MPA-CdSe@ZnS(4.6)-6	0 4.5×10^{-8}	10.6(0.44) 13.4(0.59)	2.2(0.34) 3.9(0.29)	0.5(0.22) 0.7(0.12)	4.4 6.0

6.5.4. Detection of F^- in simulated biological fluid and tap water

The evaluation and usability of the proposed QDs-MPc nanoprobe for the detection of F^- in real biological sample was carried out in DMEM cell culture medium. DMEM contains various components such as glucose, amino acids, vitamins, inorganic salts and other cell components and has been reported to be used as a medium to determine zinc ion using a QDs probe by spiking with a known concentration of the ion **[260]**. In this work, DMEM (diluted in a 10:1 with PBS buffer, pH 7.4) and tap water were spiked with a known concentration of F^- (50 nM and 62 nM, respectively for DMEM and tap water). F^- concentration in DMEM and tap water were measured three times using GSH-CdSe@ZnS-**6** as a representative nanoprobe. The results listed in Table 6.12 showed that the concentration of F^- determined using "turn ON" fluorescence was close to the amount added. The recoveries were in the range of 99 – 102% and an excellent reproducibility of ≤2 % was obtained. The results obtained demonstrate the practicability and reliability of our sensor.

Table 6.12. Application of QDs-MPc nanoprobe (GSH-CdSe@ZnS(4.7)-6 used as a representative probe) for the detection of F^- in simulated biological fluid and tap water (n = 3). Mean values presented.

Samples	Spiked (nM)	Found (nM)	Recovery (%)	RSD (%)
DMEM:PBS(10:1)	62.0	63.3	102	1.50
	50.0	50.1	101	0.67
Tap water	62.0	62.8	101	1.16
	50.0	49.5	99	0.45

6.5.5. Conclusions

This work shows that unsymmetrical substituted MPcs bearing amino substituents and conjugated to thiol-capped CdSe@ZnS QDs can be employed as luminescent nanosensors for anion sensing. Compounds **5** and **6** were successfully conjugated to MPA or GSH-capped CdSe@ZnS QDs. The fluorescence enhancement effect of F^- on the proposed nanoprobe was influenced by the type of substituent anchored onto the MPc ring. In general, the nanoprobe was highly sensitive to F^-. The results presented here would be beneficial in the design of substituent-dependent conjugates which could have a positive bearing on the sensitivity and efficacy of QD-MPc based probes.

6.6. Detection of mercury ion using QDs-NiMMSATBC(7) and QDs-NiMMSAPc(8) conjugates

While we have shown that symmetrical and unsymmetrically substituted MPc-QDs conjugates can be used for the fluorescence sensing of analytes, this study compares the effect of the nature of the macrocyclic ring (TBC versus Pc) by conjugating GSH-CdSe@ZnS QDs (4.7 nm) to unsymmetrically substituted NiMMSATBC (**7**) and NiMMSAPc (**8**) for the detection of Hg^{2+}. Selective screening of the conjugates in the presence of different cations showed that Hg^{2+} (discussed below) could induce the most selective "turn ON" of the sensor.

6.6.1. Selective screening of different cations

The selective screening of different cations was performed using the proposed GSH-CdSe@ZnS-**7** and GSH-CdSe@ZnS-**8** nanoprobes. The following cations: Na^+, Mg^{2+},

Ca^{2+}, Fe^{3+}, Co^{2+}, Mn^{2+}, Cd^{2+}, Cu^{2+}, Ni^{2+}, Sn^{2+}, Pb^{2+}, Ag^{+}, Cr^{3+} and Hg^{2+} were examined at the same concentration level to determine their fluorescence response to the nanoprobe. A tolerable error of ±5.0% in relative fluorescence intensity was taken into consideration. As shown in Fig. 6.12, Hg^{2+} induced a significant fluorescence "turn ON" of the sensor, while other cations further quenched the fluorescence except Pb^{2+}. The results imply that the proposed nanosensor can detect both Hg^{2+} and Pb^{2+} but with a greater sensitivity for Hg^{2+} than for Pb^{2+}. Hence, Hg^{2+} was selected as the ion of interest.

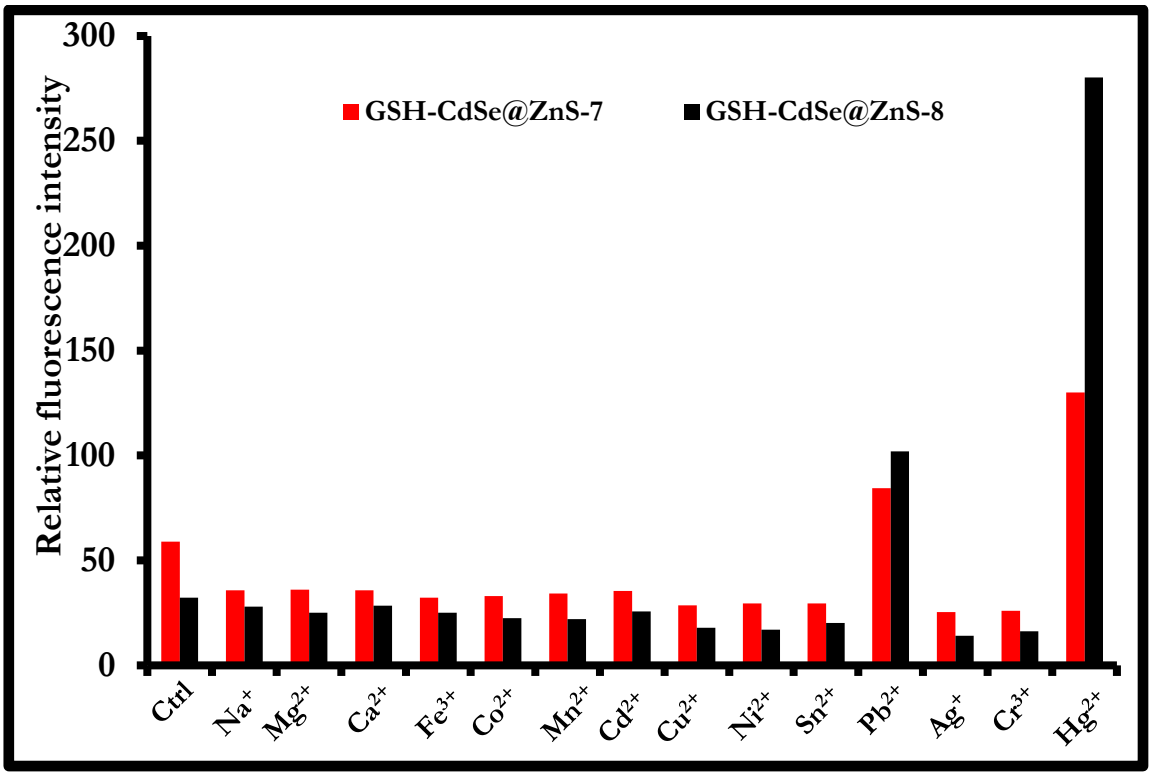

Fig. 6.12. Effects of different cations on the fluorescence response of GSH-CdSe@ZnS(4.7)-7 and GSH-CdSe@ZnS(4.7)-8 nanoprobe. Concentration of ions = 8.0 x 10^{-8} M.

6.6.2. Fluorescence recognition of mercury ion

The fluorimetric detection of Hg^{2+} was performed using the proposed GSH-CdSe@ZnS-**7** and GSH-CdSe@ZnS-**8** nanoprobes in pH 7.4 PBS buffer. The enhancement of QDs fluorescence on increasing concentration of Hg^{2+} was similar to those shown in Fig. 6.1A – 6.1C. The fluorescence signal increased linearly with the concentration of Hg^{2+} within the linear concentration range of 1.2×10^{-9} – 3.8×10^{-8} M, Table 6.13. The LOD obtained were 2.0×10^{-10} M for QDs-**7** and 5.7×10^{-11} M for QDs-**8** nanoprobe, Table 6.13. This gives a good indication that **7** can be employed as molecular recognition sensor for ion sensing when coupled to QDs but with a much lower sensitivity as compared to GSH-CdSe@ZnS-**8** nanoprobe. Thus Pcs are better than TBCs. Comparison of our proposed detection system with some mercury-based QDs probes **[70,261-263]** showed an improvement in the detection sensitivity.

Table 6.13. Fluorescence lifetimes for a triexponential fit of GSH-CdSe@ZnS QDs, GSH-CdSe@ZnS-7 and GSH-CdSe@ZnS-8 nanoprobe in the absence and presence of Hg^{2+} in 50 mM PBS buffer, pH 7.4. LOD also included.

Samples	Hg^{2+}[M]	τ_1 (ns)[a] ±0.1	τ_2 (ns)[a] ±0.06	τ_3 (ns)[a] ±0.02	Mean Lifetime (ns)	LOD
GSH-CdSe@ZnS	-	19.1(0.58)	6.3(0.34)	1.3(0.8)	8.9	-
GSH-CdSe@ZnS-7	0 3.8×10^{-8}	15.6(0.53) 18.2(0.53)	4.5(0.37) 5.6(0.36)	1.2(0.10) 1.3(0.11)	7.1 8.4	2.0×10^{-10} M
GSH-CdSe@ZnS-8	0 3.8×10^{-8}	14.7(0.52) 19.1(0.55)	3.9(0.32) 6.3(0.36)	1.2(0.16) 1.3(0.09)	6.6 8.9	5.7×10^{-11} M

6.6.3. Time-resolved fluorescence measurements

The activation of the radiative fluorescence enhancement effect of Hg^{2+} on the proposed nanoprobe was further analyzed using time-resolved fluorescence measurements, exhibiting decay curves similar to those shown in Fig 6.2. A triexponential fluorescence lifetime was obtained as detailed in Table 6.13. It was observed that the mean fluorescence lifetime of the conjugates decreased relative to the mean lifetime of the QDs alone. This may be due to FRET or other processes which deactivate the excited state of the QDs as discussed above. In the presence of a known concentration of Hg^{2+}, the mean fluorescence lifetime of the conjugates increased and thus confirming the fluorescence "turn ON" effect of Hg^{2+} on the proposed nanoprobe.

6.6.4. Proposed mechanism of interaction

We propose that the fluorescence "turn ON" effect of Hg^{2+} on the proposed nanoprobe may be due to binding of Hg^{2+} to the sulfur groups of **7** and **8** ring attached to the QDs. The presence of the sulfur atoms on the Pc rings gives the opportunity to bind soft transition metal ions such as Ag^{+}, Pd^{2+}, Pb^{2+} and Hg^{2+} **[264]**. In fact, it has been demonstrated by Zhou *et al*. **[265]** that Hg^{2+} specifically binds to sulfur groups of a cationic triazatetra-benzcorrole sensor. Hence, the same principle can be applied in this work as depicted in Scheme 6.3, in which Hg^{2+} binds specifically to the sulfur groups of the TBC or Pc ring and in turn influences the fluorescence "turn ON" mode of the QDs. Therefore, we propose that the differences in sensing abilities for Hg^{2+} compared to the other ions is related to its superior

binding ability, which affects the motion of the Pc or TBC and hence enhance the fluorescence of the QDs. Fig. 6.12, shows that there is less enhancement of fluorescence for complex **7** compared to **8**, suggesting that the motion of the former (with one aza nitrogen lost) is less affected by coordination of Hg^{2+} relative to **8**.

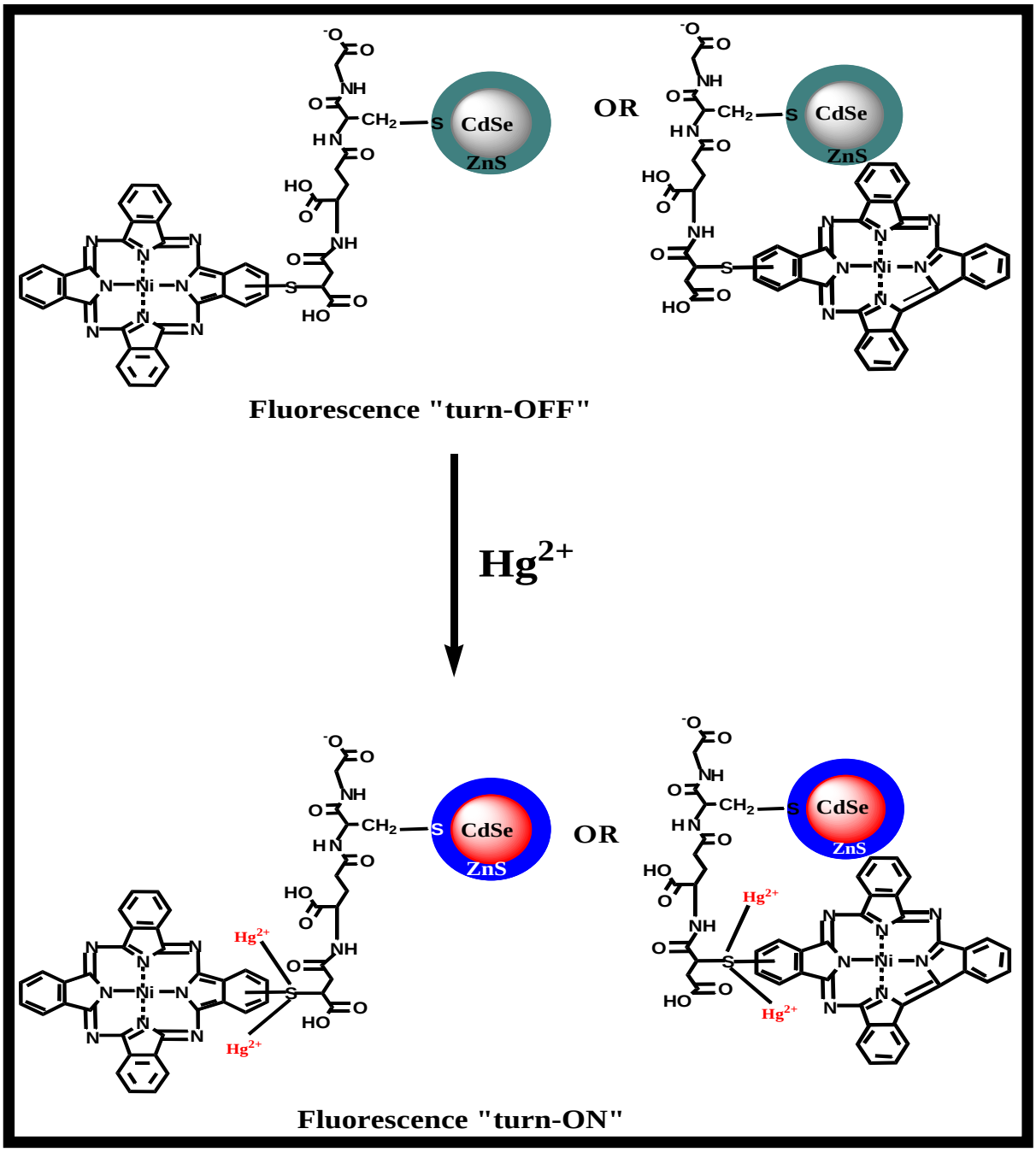

Scheme 6.3. Schematic representation for the detection mechanism of Hg^{2+} using the GSH-CdSe@ZnS-7 and GSH-CdSe@ZnS-8 nanoprobe.

6.6.5. Conclusions

The work presented here shows that both metallo-triaazatetra-benzcorrole and phthalocynanine complexes hold great promise as molecular recognition sensors when coordinated to QDs with the later showing a greater sensitivity. The nature of the ring could suggest that, TBC which is already distorted is less affected by analytes relative to the Pc.

7. GENERAL CONCLUSIONS AND FUTURE PROSPECTS

This chapter gives a summary of the work presented in this thesis and its future prospect.

7.1. General Conclusions

The luminescent sensing of different analytes using thiol-capped core and core-shell QDs on their own and when conjugated to an organic radical and macrocylic compounds such as metallo-phthalocyanines and a triazatetra-benzcorrole has been presented in this work. Interaction studies between core CdTe and DPPH• showed that QDs can be employed as excellent fluorescent probes for free radical sensing using fluorescence quenching processes. To determine the efficiency for ROS sensing, different thiol-capping of core CdTe and core-shell CdTe@ZnS QDs were investigated for their sensitivity towards •OH and $ONOO^-$ detection. Comparative studies showed that the overall sensitivity and selectivity of the sensor depends on the type of capping and QDs used, with CdTe@ZnS QDs showing superior sensitivity than the core.

Furthermore, QDs-4AT was highly selective towards bromide ion detection. Hence, a sensor for bromide ion was constructed based on the ability of bromide ion to "turn ON" the fluorescence of QDs-4AT probe. Elucidation of the reaction mechanism using EPR measurements showed that bromide ion transferred its electron to the nitroxyl moiety of QDs-4AT nanoprobe.

The conjugation of macrocylic compound such as MPcs on the surface of QDs to form QDs-MPc nanoprobes for analyte sensing was attempted in this work with success. Different symmetrically-substituted tetra-amino MPcs were conjugated to CdTe@ZnS QDs to detect various analytes. Results showed that the QDs-MPc sensor exhibited superior sensitivity when compared with other conventional QDs-based probe. Investigation of the effect of the central metal showed that the sensor could be

formed regardless of the central metal within the Pc ring but with varying sensitivity. Metal-free Pc did not show any sensitivity towards analyte sensing. The mechanism of the QDs-MPc sensor was investigated with result showing that axial ligation of the analytes to the MPc ring was responsible for the "turned ON" effect of the probe.

Finally, the conjugation of QDs to unsymmetrical substituted MPcs showed that it can be employed for analyte sensing with superior sensitivity. However, the sensitivity of the sensor was dependent on the substituent attached to the Pc ring. Also, the efficiency of sensing using QDs-MPc probe versus QDs-TBC probe was investigated with result showing that TBC can be incorporated into the family of macrocyclic compound as host-molecule sensor but showed a lower sensitivity for analyte sensing when compared with QDs-MPc probe.

7.2. Future Prospects

Despite the success of using QDs-MPc probes for analyte sensing, analyte-specific subtsituents are needed to be attached onto the MPc ring in order to develop more selective QDs-MPc sensors.

REFERENCES

1. M. Ishikawa, V. Biju, *Prog. Mol. Transl. Sci*, **104** (2011) 53.
2. O. Salata, *J. Nanobiotech.* **2** (2004) 3.
3. K.K. Jain, *Clin. Chim. Acta* **358** (2005) 37.
4. H.M.E. Azzazy, M.M.H. Mansour, S.C. Kazmierczak, *Clin. Biochem.* **40** (2007) 917.
5. R. Rossetti, L. Brus, *J. Phys. Chem.* **86** (1982) 4470.
6. T. Pons, H. Mattousi, *Ann. Biomed. Eng*. **37** (2009) 1934.
7. W.C.W. Chan, D.J. Maxwell, X. Gao, R.E. Bailey, M. Han, S. Nie, *Curr. Opin. Biotech.* **13** (2002) 40.
8. R.J. Byers, E.R. Hitchman, *Prog. Histochem. Cytoc*. **45** (2011) 201.
9. T. Jamieson, R. Bakhshi, D. Petrova, R. Pocock, M. Imani, A.M. Seifalian, *Biomaterials* **28** (2007) 4717.
10. A.F.E. Hezinger, J. Teßmar, A. Göpferich, *Eur. J. Pharm. Biophram.* **68** (2008) 138.
11. D.R. Larson, W.R. Zipfel, R.M. Williams, S.W. Clark, M.P. Bruchez, F.W. Wise, W.W. Webb, *Science* **300** (2003) 1434.
12. V. Biju, S. Mundayoor, R.V. Omkumar, A. Anas, M. Ishikawa, *Biotechnol. Adv*. **28** (2010) 199.
13. X.H. Gao, Y.Y. Cui, R.M. Levenson, L.W.K. Chung, S. Nie, *Nat. Biotechnol*. **22** (2004) 969.
14. W.B. Cai, D.W. Shin, K. Chen, O. Gheysens, Q.Z. Cao, S.X. Wang, S.S. Gamnhir, X. Chen, *Nano Lett.* **6** (2006) 669.
15. A.P. Alivisatos, W. Gu, C. Larabell, *Annu. Rev. Biomed. Eng.* **7** (2005) 55.
16. M.P. Bruchez, *Curr. Opin. Chem. Biol.* **9** (2005) 533.

17. X. Michalet, F.F. Pinaud, L.A. Bentolila, J.M. Tsay, S. Doose, J.J. Li, g. Sundaresan, A.M. Wu, S.S. Gambhir, S. Weiss, *Science* **307** (2005) 538.

18. M. Geszke-Moritz, M. Moritz, *Mater. Sci. Eng., C* **33** (2008) 1008.

19. K.K. Jain, *Expert Rev. Mol. Diagn.* **3** (2003) 153.

20. L. Shi, V. De Paoli, N. Rosenzweig, Z. Rosenzweig, J. Am. Chem. Soc. **128** (2006) 10378.

21. D.M. Willard, L.L. Carillo, J. Jung, A. Van Orden, *Nano Lett.* **1** (2001) 469.

22. S.V. Dezhurov, I.Y. Volkova, M.S. Wakstein, *Bioconjugate Chem.* **22** (2011) 338.

23. X. Huang, J. Wang, H. Liu, T. Lan, J. Ren, *Talanta* **106** (2013) 79-84.

24. Q. Zhao, X. Rong, H. Ma, G. Tao, *J. Hard. Mater*. **250-251** (2013) 45.

25. S.P. Wang, N. Mamedova, N.A. Kotov, W. Chen, J. Studer, *Nano Lett.* **2** (2002) 817.

26. S. Hohng, T. Ha, Chem. Phys. Chem. **6** (2005) 956.

27. S.A. McKinney, A.C. Declais, D.M.J. Lilley, T. Ha, *Nat. Struct. Biol.* **10** (2003) 93.

28. I.L. Medintz, A.R. Clapp, H. Mattoussi, E.R. Goldman, B. Fisher, J.M. Mauro, *Nat. Mater.* **2** (2003) 630.

29. I.L. Medintz, A.R. Clapp, F.M. Brunel, T. Tiefenbrunn, H.T. Uyeda, E.L. Chang, J.R. Deschamps, P.E. Dawson, H. Mattousi, *Nat. Mater.* **5** (2006) 581.

30. E. Chang, J.S. Miller, J.T. Sun, W.W. Yu, V.L. Colvin, R. Drezek, J.L. West, *Biochem. Biophys. Res. Commun.* **334** (2005) 1317.

31. C.J. Xu, B.G. Xing, H.H. Rao, *Biochem. Biophys. Res. Commun.* **344** (2006) 931.

32. D. Gerion, W.J. Parak, S.C. Williams, D. Zanchet, C.M. Micheel, A.P. Alivisatos, *J. Am. Chem. Soc.* **124** (2002) 7070.

33. L.Y. Lee, S.L. Ong, J.Y. Hu, W.J. Ng, Y.Y. Feng, X.L. Tan, S.W. Wong, *Appl. Environ. Microbiol.* **70** (2004) 5732.

34. E.B. Voura, J.K. Jaiswal, H. Mattoussi, S.M. Simon, *Nat. Med*. **10** (2004) 993.

35. K-W. Huang, C-J. Yu, W-L. Tseng, *Biosens. Bioelectron.* **25** (2010) 984.

36. D. Thomas, L. Lonappan, L. Rajith, S.T. Cyriac, K.G. Kumar, *J. Fluoresc.* **23** (2013) 473.

37. H. Zhou, J. Dong, V.K. Deo, E.Y. Park, J. Lee, *Sens. Actuators, B* **178** (2013) 192.

38. K-t. Yong, W-C. Law, I. Roy, Z. Jing, H. Huang, M.T. Swihart, P.N. Prasad, *J. Biophotomics* **4** (2011) 9.

39. A. L. Rogach, T. Franzl, T. A. Klar, J. Feldmann, N. Gaponik, V. Lesnyak, A. Shavel, A. Eychmuller, Y. P. Rakovich, J. F. Donegan, *J. Phys. Chem. C* **111** (2007) 14628.

40. B. T. Nguyen, J. E. Gautrot, C. Ji, P.-L. Brunner, M. T. Nguyen, X. X. Zhu, *Langmuir* **22** (2006) 4799.

41. S. Mazumder, R. Dey, M.K. Mitra, S. Mukherjee, G.C. Das, J. *Nanomater.* (2009) Article ID 815734.

42. C. Y. Zhang, H. Ma, S.M. Nie, Y. Ding, L. Jin, D. Y. Chen, *Analyst*, **125** (2000) 1029.

43. S. Pathak, S.-K. Choi, N. Arnheim, M. E. Thompson, *J. Am. Chem. Soc.* **123** (2001) 4103.

44. Y. A. Wang, J. J. Li, H. Chen, X. Peng, *J. Am. Chem. Soc.* **124** (2002) 2293.

45. H. Skaff, T. Emrick, *Chem. Commun*. ***9*** (2003) 52.

46. B. Dubertret, P. Skourides, D.J. Norris, V. Noireaux, A.H. Brivanlou, A. Libchaber, *Science* **298** (2002) 1759.

47. R.M. Raab, *Biotechnol. Bioeng.* **88** (2004) 21.

48. M. Kuno, D.P. Fromm, S.T. Johnson, A. Gallagher, D.J. Nesbitt, *Phys. Rev. B* **67** (2003) 67.

49. P. Reiss, M. Protière, L. Li, *Small* **5** (2009) 154.

50. A. Piryatinski, S.A. Ivanov, S. Tretiak, V.I. Klimov, *Nano Lett.* **7** (2007) 108.

51. L.H Qu, X.G. Peng, *J. Am. Chem. Soc.* **124** (2002) 2049.

52. A. van Dijken, J. Makkinje, A. Meijerink, *J. Lumin.* **92** (2001) 323.

53. R.G. Xie, U. Kolb, J.X. Li, T. Basche, A. Mews, *J. Am. Chem. Soc.* **127** (2005) 7480.

54. F. Wu, J.Z. Zhang, R. Kho, R.K. Mehra, *Chem. Phys. Lett.* **330** (2000) 237.

55. H. Liu, P. Guyot-Sionnest, *J. Phys. Chem. C* **114** (2010) 14860.

56. Z. Yuan, A. Zhang, Y. Cao, J. Yang, Y. Zhu, P. Yang, *J. Fluoresc.* **22** (2010) 121.

57. H.S. Chen, M. Ando, N. Murase, *Mater. Lett.* **65** (2011) 3146.

58. J. Britton, E. Antunes, T. Nyokong, *J. Photochem. Photobiol. A: Chem* **210** (2010) 1.

59. M.A. Jhonsi, R. Renganathan, *J. Colloid Interf. Sci.* **344** (2010) 596-602.

60. J.B. Delehanty, K. Susumu, R.L. Manthe, W.R. Algar, I.L. Medintz, *Anal. Chim. Acta* **720** (2012) 63.

61. S. Jagadeeswari, M.A Jhonsi, A. Kathiravan, R. Renganathan, *J. Lumin.* **131** (2011) 597.

62. M. van de Weert, L. Stella, *J. Mol. Struct.* **998** (2011) 144.

63. Y. Zhang, T-H. Wang, *Theranostics* **7** (2012) 631.

64. J. Li, F. Mei, W-Y. Li, X-W. He, Y-K. Zhang, *Spectrochim. Acta Part A* **70** (2008) 811.

65. W.R. Algar, U.J. Krull, *Anal. Chim. Acta* **581** (2007) 193.

66. M. Hou, J. Na, *Anal. Bioanal. Chem.* **397** (2010) 3589.

67. J. Li, D. Bao, X. Hong, D. Li, J. Li, Y. Bai, T. Li, *Colloids Surf A* **267** (2005) 257.

68. C. Bo, Z. Ping, *Anal. Bioanal. Chem.* **381** (2005) 986.

69. H. Li, X. Wang, *Sens. Actuators B* **134** (2008) 238.

70. M. Koneswaran, R. Narayanaswamy, *Sens. Actuators B* **139** (2009) 91.

71. F-C. Liu, Y-M. Chen, J-H. Lin, W-L. Tseng, *J. Colloid Interf. Sci.* **337** (2009) 414.

72. S. Chen, X. Zhang, Q. Zhang, X. Hou, Q. Zhou, J. Yan, W. Tan, *J. Lumin*. **131** (2011) 947.

73. H. Xu, R. Miao, Z. Fang, X. Zhong, *Anal. Chim. Acta* **687** (2011) 82.

74. Y. Xia, C. Zhu, Analyst **133** (2008) 928.

75. M.J. Rueda-Rama, E.A.H. Hall, *Analyst* **133** (2008) 1556-1566.

76. W. J. Jin, J.M. Costa-Fernández, R. Pereiro, A. Sanz-Medel, *Anal. Chimica. Acta* **522** (2004) 1.

77. W. Zhao, Y. Fung, O. Waisum, MP.L. Cheung, *Anal. Sci* **26** (2010) 879.

78. J.F. Sun, C.L. Ren, L.H. Liu, X.G. Chen, *Chin. Chem. Lett.* **19** (2008) 855.

79. Y. Chen, Z. Chen, Y. He, H. Lin, P. Sheng, C. Liu, S. Luo, Q. Cai, *Nanotechnology* **21** (2010) 1.

80. S. Raichlin, E. Sharon, R. Freeman, Y. Tzfati, I. Willner, *Biosens. Bioelectron.* **26** (2011) 4681.

81. C. Carrillo-Carrión, B.M. Simonet, M. M. Valcárcel, *Biosens. Bioelectron.* **26** (2011) 4368.

82. C. Carrillo-Carrión, B. Lendl, B.M. Simonet, M. Valcárcel, *Anal. Chem.* **83** (2011) 8093.

83. K-E. Kim, T.G. Kim, Y-M. Sung, *J. Nanopart. Res.* **14** (2012) 1179.

84. W. Dong, H-B. Shen, X-H. Liu, M-J. Li, L-S. Li, *Spectrochim. Acta Part A* **78** (2011) 537.

85. C. Carrillo-Carrión, S. Cárdenas, B.M. Simonet, M. Valcárcel, *Anal. Chem.* **81** (2009) 4730.

86. Z. Liu, P. Yin, H. Gong, P. Li, X. Wang, Y. He, *J. Lumin,* **132** (2012) 2484.

87. H. Liu, D. Liu, G. Fang, F, Liu, C. Liu, Y. Yang, S. Wang, *Anal. Chim. Acta* **762** (2013) 76.

88. R.Q. Aucélio, A.I. Peréz-Cordovés, J.L.X. Lima, A.B.B. Ferreira, A.M.E. Guas, A.R. da Silva, *Spectrochim. Acta Part A* **100** (2013) 155.

89. J. Yuan, W. Guo, J. Yin, E. Wang, *Talanta* **77** (2009) 1858.

90. J. Peng, X. Hu, *J. Lumin.* **131** (2011) 952.

91. W.E. Mahmoud, S.J. Yaghmour, A.M. AlAmri, *J. Lumin.* **134** (2013) 429.

92. G-L. Wang, H-J. Jiao, X-Y. Zhu, Y-M. Dong, Z-J. Li, *Talanta* **93** (2012) 398.

93. S. Huang, Q. Xiao, R. Li, H-L. Guan, J. Liu, X-R. Liu, Z-K. He, Y. Liu, *Anal. Chim. Acta* **645** (2009) 73.

94. M. Algarra, B.B. Campos, F.R. Aquiar, J.E. Rodriguez-Borges, J.C.G.E. de Silva, *Mater. Sci. Eng. C* **32** (2012) 799.

95. X. Wang, J. Wu, F. Li, H. Li, *Nanotechnology* **19** (2008) 205501.

96. J. Tian, H. Zhao, M. Liu, Y. Chen, X. Chen, *Anal. Chim. Acta* **723** (2012) 83.

97. S. Ge, J. Lu, M. Yan, F. Yu, J. Yu, X. Sun, *Dyes Pigments* **91** (2011) 304.

98. Z. Liu, S. Liu, P. Yin, Y. He, *Anal. Chim. Acta* **745** (2012) 78.

99. M. Li, X. Zhou, S. Guo, N. Wu, *Biosens. Bioelectron.* **43** (2013) 69.

100. Z. Liu, S. Liu, X. Wang, P. Li, Y. He, *Sens. Actuators B* **176** (2013) 1147.

101. R. Gui, X. An, W. Huang, *Anal. Chim. Acta* **767** (2013) 134.

102. R.E. Galian, M.D.L. Guardia, *Trac-Trends Anal. Chem.* **28** (2009) 279.

103. G.I. Likhtenstein, K. Ishii, S. Nakatsuji, *Photochem. Photobiol.* **83** (2007) 871

104. M.G. Ivan, J. C.Scaiano, *Photochem. Photobiol.* **78** (2003) 416.

105. C. Coenjarts, O. Garcia, L. Llauger, J. Palfreyman, A.L. Vinette, J.C. Scaiano, *J. Am. Chem. Soc.* **125** (2003) 620.

106. V.Y. Nagy, I.M. Bystryak, A.I. Kotelnikov, G.I. Likhtenshtein, O.M. Petrukhin, Y.A. Zolotov, L.B. Voloarskii, *Analyst* **115** *(*1990) 839.

107. E. Hideg, T. Ka´lai, P.B. K´os, K. Asada, K. Hideg, *Photochem. Photobiol.* 82 *(*2006) 1211.

108. P. Meineke, U. Rauen, H. de Groot, H.G. Korth, R. Sustmann, *Chem. Eur. J.* **5** (1999) 1738.

109. Z.-Y. Bian, X.-Q. Guo, Y.-B. Zhao, J.-O. Du, *Anal. Sci.* **21** (2005**)** 553.

110. G.M. Rosen, S. Pou, B.E. Britigan, M.S. Cohen, *Methods Enzymol.* **233** (1994) 105.

111. Y. Tang, F. He, M. Yu, S. Wang, Y. Li, D. Zhu, *Chem. Mater.* **18** *(*2006) 3605.

112. C. Tansakul, E. Lilie, E.D. Walter, F. Rivera III, A. Wolcott, J.Z. Zhang, G.L. Millhauser, R. Braslau, *J. Phys. Chem. C* **114** (2010) 7793.

113. V. Maurel, M. Laferrière, P. Billone, R. Godin, J.C. Scaiano, *J. Phys. Chem. B* **110** (2006) 16353.

114. K. Xu, H. Chen, H. Wang, J. Tian, J. Li, Q. Li, N. Li, B. Tang, *Biosens. Biolectron.* **26** (2011) 4632

115. C.C. Leznoff, A.B.P. Lever, (eds.): Phthalocyanines Properties and Applications. VCH, Weinheim (1989–1996).

116. C.W. Tang, *Appl. Phys. Lett.* **48** (1986) 183.

117. G. Chintakula, S. Rajaputra, V.P.Singh, *Sol. Energy Mater. Sol. Cells* **94** (2010) 34.

118. F. Dumoulin, M. Durmus, V. Ahsen, T. Nyokong, *Coord. Chem. Rev.* **254** (2010) 2792.

119. X-F. Zhang, Y. Wang, L. Niu, *J. Photochem. Photobiol. A* **209** (2010) 232.

120. Z. Xu, G. Zhang, Z. Cao, J. Zhao, H. Li, *J. Mol. Catal. A* **318** (2010) 101.

121. K. Sakamoto, E. Ohno-Okumura, *Materials* **2** (2009) 1127.

122. R. Hirohashi, K. Sakamoto, E. Okumura, (eds.): Phthalocyanines as Functional Dyes. Industrial Publishing & Consulting, Inc., Tokyo (2004).

123. G. de la Torre, P. Vazquez, T. Torres, *Chem. Rev.* **104** (2004) 3723.

124. R.J. Mortimer, A.L. Dyer, J.R. Reynolds, *Displays* **27** (2006) 2.

125. C.G. Claessens, U. Hahn, T. Torres, *Chem. Rec.* **8** (2008) 75.

126. J.D. Spikes, *Photochem. Photobiol.* **43** (1986) 691.

127. A. Henrikson, M. Soundbom, *Theor*. Chim. Acta **27** (1972) 213.

128. L. Edwards, M. Gouterman, *J. Mol. Spectrosc.* **33** (1970) 292.

129. M. Gouterman, in *The Porphyrins, Part A. Physical Chemistry*, D. Dolphin (Ed) Academic Press, New York, Vol. 3 (1978) P1-165.

130. A. Wang, L. Long, C. Zhang, *Tetrahedron* **68** (2012) 2433-2451.

131. M.S. Rodríguez-Morgade, G. de la Torre, T. Torres, in The Porphyrin Handbook, K.M. Kadish, K.M. Smith, R. Guilard (Eds.), Academic Press, Elsevier Science, Vol. 15 (2003) Chapter 99.

132. W.A. Nevin, W. Liu, S. Greenberg, M.R. Hempstead, S.M. Marcuccio, M. Melnik, C.C. Leznoff, A.B.P. Lever. *Inorg. Chem.* **26** (1987) 891.

133. A.M. Paoletti, G. Pennesi, G. Rossi, A. Generosi, B. Paci, V.R. Albertini, Sensors, **9** (2009) 5277.

134. J.M. Vanderkooi, G. Maniara, T.J. Green, D.F. Wilson, *J. Biol. Chem.* **262** (1987) 5476.

135. A. Hassan, T. Basova, S. Tuncel, F. Yuksel, A.G. Gürek, V. Ahsen, *Procedia Engr.* **25** (2011) 272.

136. X. Liu, C. Qi, T. Bing, X. Cheng, D. Shangguan, *Anal. Chem.* **81** (2009) 3699.

137. J. Spadavecchia, G. Ciccarella, L. Valli, R. Rella, *Sens. Actuators B* **113** (2006) 516.

138. A.b. El-Bosaty, T.A. El-Brolossy, S. Abdalla, S. Negm, R.A. Abdella, H. Talaat, *Egypt. J. Solids* **29** (2006) 121.

139. J. Spadavecchia, G. Ciccarella, L. Valli, R. Rella, *Sens. Actuators B* **100** (2004) 88.

140. B.N. Achar, G.M. Fohlen, J.A. Parker, J. Keshavayya, *Polyhedron* **6** (1987) 1463.

141. X.L. Chen, Z.B. Li, Y.X. Zhu, J.G. Xu, *Anal Chim Acta* **505** (2004) 505 283.

142. X-L. Chen, D-H. Li, H-H. Yang, Q-Z. Zhu, H. Zheng, J-G. Xu, *Analyst* **126** (2001) 523.

143. T. Mugadza, T. Nyokong, *Electrochim. Acta* **54** (2009) 6347.

144. M.P. Siswana, K.I. Ozoemena, D.A. Geraldo, T. Nyokong, *J. Solid State Electrochem.* **14** (2010) 1351.

145. X-F. Zhang, X. Li, L. Niu, L. Sun, L. Liu, *J. Fluoresc.* **19** (2009) 947.

146. S. D'Souza, E. Antunes, C. Litwinski, T. Nyokong, *J. Photochem. Photobiol. A: Chem.* **220** (2011) 11.

147. S. D'Souza, E. Antunes, T. Nyokong, *Inorg. Chim. Acta* **367** (2011) 173.

148. C. Han, H. Li, *Anal. Bioanal. Chem.* **397** (2010) 1437.

149. C-Y. Chen, C-T. Cheng, C-W. Lai, P-W. Wu, K-C. Wu, P-W. Wu, K-C. Wu, P-T. Chou, Y-H. Chou, H-T. Chiu, *Chem. Commun.* (2006) 263.

150. H. Li, C. Han, *Chem. Mater.* **20** (2008) 6053.

151. H. Li, Y. Zhang, X. Wang, D. Xiong, Y. Bai *Mater. Lett.* **61** (2007) 1474.

152. T. Jin, F. Fujii, H. Sakata, T. Mamoru, M. Kinjo, *Chem. Commun.* (2005) 4300.

153. H. Li, F. Qu, *Chem. Mater.* **19** (2007) 4148.

154. H. Li, F. Qu, *J. Mater. Chem.* **17** (2007) 3536.

155. H. Li, X. Wang, *Photochem. Photobiol. Sci.* **7** (2008) 694.

156. C. Han, H. Li, *Chin. Chem. Lett.* **19** (2008) 215.

157. R. Freeman, T. Finder, L. Bahshi, I. Willner, *Nano Lett.* **9** (2009) 2073.

158. Z.b. Shang, S. Hu, Y. Wang, W.J. Jin, *Luminescence* **26** (2011) 585.

159. X. Ai, L. Niu, Y. Li, F. Yang, X. Su, *Talanta* **99** (2012) 409.

160. S. Banerjee, S. Kar, S. Santra, *Chem. Commun.* (2008) 3037.

161. M.F. Frasco, V. Vamvakaki, N. Chaniotakis, *J. Nanopart. Res.* **12** (2010) 1449.

162. A. Ivanisevic, A.B. Ellis *Langmuir* **16** (2000) 7852.

163. J. Szejtli, *Chem. Rev.* **98** (1998) 1743.

164. D. Vlascici, E.F. Cosmas, E.M. Pica, V. Cosma, O. Bizerea, G. Mihailescu, L. Olenic, *Sensors* **8** (2008) 4995.

165. A.V. Isarov, J. Chrysochoos, *Proc Indian Acad Sci Chem Sci* **110** (1998) 277.

166. J.P. Kehrer, *Crit. Rev. Toxicol.* **23** (1993) 21.

167. M. Valko, M. Izakovic, M. Mazur, C.J. Rhodes, J. Telser, *Mol. Cell. Biochem.* **266** (2004) 37.

168. H.M. Shen, C.Y. Shi, Y. Shen, C.N. Ong, *Free Rad. Biol. Med.* **2** (1996) 139.

169. N.B. Ames, M.K. Shigenaga, T.M. Hagen, *Proc. Natl. Acad. Sci. USA* **90** (1993) 7915.

170. M. Kleerekoper, **27** (1998) 441.

171. H. Matsui, M. Morimoto, K. Horimoto, Y. Nishimura, *Toxicol. in Vitro* **21** (2007) 1113.

172. T. Nobukawa, S. Sanukida, *Wat. Res.* **35** (2001) 4293.

173. W. Buijs, S. Van der Gen., G.R. Mohn, D.D. Breimer, *Mutat. Res.* **141** (1984) 11.

174. M.A. Warne, D. Osborn, J. C. Lindon, J. K. Nicholson, *Chemosphere* **38** (1999) 3357.

175. US EPA, Regulatory Impact Analysis of the Clean Air Mercury Rule, EPA-452/R-05-003, Research Triangle Park, NC, 2005.

176. D.A. Beckman, J.J. Mullin, F.K. Assadi, *Tetratology* **58** (1998) 96.

177. R. Hong, G. Han, J.M. Fernandez, B.J. Kim, N.S. Forbes, V.M. Rotello, *J. Am. Chem. Soc.* **128** (2006) 1078.

178. Frisch MJ, Trucks GW, Schlegel HB, Scuseria GE, Robb MA, Cheeseman JR, Montgomery JA, Vreven JrT, Kudin KN, Burant JC, Millam JM, Iyengar SS, Tomasi J, Barone V, Mennucci B, Cossi M, Scalmani G, Rega N, Petersson GA, Nakatsuji H, Hada M, Ehara M, Toyota K, Fukuda R, Hasegawa J, Ishida M, Nakajima T, Honda Y, Kitao O, Nakai H, Klene M, Li X, Knox JE, Hratchian HP, Cross JB, Bakken V, Adamo C, Jaramillo J, Gomperts R, Stratmann RE, Yazyev O, Austin AJ, Cammi R, Pomelli C, Ochterski JW, Ayala PY, Morokuma K, Voth GA, Salvador P, Dannenberg JJ, Zakrzewski VG, Dapprich S, Daniels AD, Strain MC, Farkas O, Malick DK, Rabuck AD, Raghavachari K, Foresman JB, Ortiz JV, Cui Q, Baboul AG, Clifford S, Cioslowski J, Stefanov BB, Liu G, Liashenko A, Piskorz P, Komaromi I, Martin RL, Fox DJ, Keith T, Al-Laham MA, Peng CY, Nanayakkara A, Challacombe M, Gill PMW, Johnson B, Chen W, Wong MW, Gonzalez C, Pople JA (2004) Gaussian 03, Revision E.01. Gaussian, Inc., Wallingford CT.

179. X. Yun-Sheng, Z. Chang-Qing, *Microchim. Acta* **164** (2009) 29.

180. J. Tian, R. Liu, Y. Zhao, Q. Xu, S. Zhao, *J. Colloid Interface Sci.* **336** (2009) 504.

181. Y. Liu, J. Yu, *J. Colloid Interface Sci.* **351** (2010) 1.

182. M. Noh, T. Kim, H. Lee, C-K. Kim, S-W. Joo, K. Lee, *Colloids Surf., a: Physicochem. Eng. Aspects* **359** (2010) 39.

183. W. Dong, H-B. Shen, X-H. Liu, M-J. Li, L-S. Li, *Spectrochim. Acta, Part A*, **78** (2011) 537.

184. A. Saha, S. Goldstein, D. Cabelli, G. Czapski, *Free Radical Bio. Med.* **24** (1998) 653.

185. D. Li, R. Yan, H. Luo, G. Zou, *Biochemistry (Moscow)* **70** (2005) 1423.

186. D. Wöhrle, M. Eskes, K. Shigehara, A. Yamada, *Synthesis* (1993) 194.

187. S. Khene, S. Moeno T. Nyokong, *Polyhedron* **30** (2011) 2162.

188. W. Chidawanyika, C. Litwinski, E. Antunes, T. Nyokong, *J. Photochem. Photobiol. A* **212** (2010) 27.

189. G. Xu, M.R. Chance, *Chem. Rev.* **107** (2007) 3514.

190. M.A Packer, J.L. Scarlett, S.W. Martin, *Gen. Pharmac.* **31** (1998) 179.

191. Y. Wang, Z. Chen, *Talanta* **82** (2010) 534.

192. J. Huang, D. Li, J. Diao, J. Hou, J. Yuan, G. Zou, *Talanta* **72** (2007) 1283.

193. K. Dai, A.G. Vlessidis, N.P. Evmiridis, *Talanta* **59** (2003) 55.

194. C.N. Frankenfeld, M.R. Rosenbaugh, B.A. Fogarty, S.M. Lunte, *J. Chromatogr. A* **1111** (2006) 147.

195. R. Radi, G. Peluffo, M.N. Alvarez, M. Naviliat, A. Cayota, *Free Radical Bio. Med.* **30** (2001) 463.

196. K. Hyland, C. Auclair, *Biochem. Biophys. Res. Commun.* **102** (1981) 531.

197. R.F. Haseloff, B. Ebert, W. Damerau, *Anal. Chim. Acta.* **218** (1989) 179.

198. J. Di, S. Bi, M. Zhang, *Biosens. Bioelectron.* **19** (2004) 1479.

199. S. Fery-Forgues, D. Lavabre, *J. Chem. Ed*. **76** (1999) 1260.

200. J.R. Lakowicz (1999) Principles of Fluorescence Spectroscopy. Plenum Press, New York

201. R. Jenkins, R.L. Synder, Introduction to X-ray diffractometry (Wiley and Sons, New York) (1996).

202. Y-F. Liu, J-S. Yu, *J. Colloid Interf. Sci.* **333** (2009) 690.

203. L. M. Maestro, C. Jacinto, U. Rocha, M. C.Iglesias-de la Cruz, F. Sanz-Rodriguez, A. Juarranz, J. G. Solé, D. Jaque, *J. Appl. Phys.* **111** (2012) 023513.

204. X. Wang, L. Qu, J. Zhang, X. Peng, M. Xiao, *Nano Lett*. **3** (2003) 1103.

205. M. Sanz, M.A. Correa-Duarte, L.M. Liz-Marzan, A. Douhal, **196** (2008) 51.

206. Z. Yuan, A. Zhang, Y. Cao, J. Yang, Y. Zhu, P. Yang, *J. Fluoresc.* **22** (2012) 121.

207. Z. Song, F. Zhang, X. Li, C. Shek-Kiu, F. Zhao, Y. Tang, J. Porphyr. Phthalocya. **6** (2002) 484.

208. P. Ionita, *Chem. Pap.* **59** (2005) 11.

209. Y. Jipei, G. Weiwei, W. Erkang, *Anal. Chim. Acta* **630** (2008) 174.

210. A. Mandal, N. Tamai, *J. Phys. Chem. C* **112** (2008) 8244.

211. E. Blatt, A.W.H. Mau, W.H.F. Sasse, W.H. Sawyer, *Aust. J. Chem.* **41** (2008) 127.

212. M.A. Jhonsi, R. Renganathan, *J. Colloid Interface Sci*. **344** (2010) 596.

213. X. Wang, L. Qu, J. Zhang, X. Peng, M. Xiao *Nano Lett*. **3** (2003) 1103.

214. K.E. Geckeler, S. Samal, *Fullerene Sci. Technol.* **9** (2001) 17.

215. F. Demirhan, G. Taban, M. Baya, C. Dinoi, J-C. Daran, J. Organomet. Chem. **691** (2006) 648.

216. B. Han, J. Yuan, E. Wang, *Anal. Chem.* **81** (2009) 5569.

217. H.C. Sutton, C.C. Winterbourn, *Free Radical Bio. Med.* **6** (1989) 53.

218. T. Maki, N. Soh, T. Fukaminato, H. Nakajima, K. Nakano, T. Imato, *Anal. Chim. Acta* **639** (2009) 78-82.

219. M. Green, *J. Mater. Chem.* **20** (2010) 5797.

220. C. Tortiglione, A. Quarta, A. Tino, L. Manna, R. Cingolani, T. Pellegrino *Bioconjugate Chem.* **18** (2007) 829.

221. P. Wu, Y. Li, X-P. Yan, *Anal. Chem.* **81** (2009) 6252.

222. A. Priyam, S.C. Bhattacharya, A. Saha, *Phys. Chem. Chem. Phys.* **11** (2009) 520.

223. R. Gill, L. Bahshi, R. Freeman, I. Willner, *Angew Chem. Int. Ed.* **47** (2008) 1676.

224. D.S. Biradar, J. Thipperudrappa, S.M. Hanagodimath, *J. Lumin.* **126** (2007) 339.

225. M. Swaminathan, N. Radha, *Spectrochim. Acta Part A* **60** (2004) 1839.

226. X. Yang, X. Guo, Y. Zhao, *Talanta* **57** (2002) 883.

227. S. Pfeiffer, A.C.F. Gorren, K. Schmidt, E.R. Werner, B. Hansert, D.S. Bohle, B. Mayer, J. Biol. Chem. **272** (1997) 3465.

228. S. Goldstein, G. Czapski, J. Lind, G. Merényi, *Chem. Res. Toxicol.*. **12** (1999) 132-136.

229. A. Priyam, A. Chatterjee, S. C. Bhattacharya and A. Saha, *J. Cryst. Growth* **304** (2007) 416.

230. M. Shamsipur, S. Rouhani, A. Mohajeri, M.R. Ganjali, P. Rashidi-Ranjbar, *Anal. Chim. Acta.* **418** (2000) 197.

231. E. Salhi, U.V. Gunten, *Wat. Res.* **33** (1999) 3239.

232. A. Suzuki, L. Wah Lim, T. Hiroi, T. Takeuchi, *Talanta* **70** (2006) 190.

233. S. Seefeld, U. Baltensperger, *Anal. Chim. Acta.* **283** (1993) 246.

234. W. Hu, S. Cao, M. Tominaga, A. Miyazaki, *Anal. Chim. Acta.* **322** (1996) 43.

235. B. Zhu, Z. Zhong, J. Yao, *J. Chromatogr.* **1118** (2006) 106.

236. T. Masadome, Y. Asano, T. Nakamura, *Talanta.* **50** (1999) 595.

237. R. Giri, *Spectrochim. Acta, Part A*. **60** (2004) 757-763.

238. C. Tansakul, E. Lilie, E.D. Walter, F. Rivera III, A. Wolcott, J.Z. Zhang, G.L. Millhauser, R. Braslau, *J. Phys. Chem. C* **114** (2010) 7793.

239. V. Maurel, M. Laferrière, P. Billone, R. Godin, J.C. Scaiano, *J. Phys. Chem. B* **110** (2006) 16353.

240. Z. Wang, Q. Xu, H-Q. Wang, Q. Yang, J-H. Yu, Y-D. Zhao, *Sens. Actuators B* **138** (2009) 278.

241. Z. Yue, W. Zhang, C. Wang, G. Liu, W. Niu, *Mater. Lett.* **74** (2012) 180.

242. Q. Xu, J-H. Wang, Z. Wang, H-Q. Wang, Q. Yang, Y-D. Zhao, *Anal. Lett.* **42** (2009) 2496.

243. N. Soh, O. Sakawaki, K. Makihara, Y. Odo, T. Fukaminato, T. Kawai, M. Irie, T. Imato, *Bioorg. Med. Chem.* **13** (2005) 1131.

244. Y. Xia, J. Wang, Y. Zhang, L. Song, J. Je, G. Yang, K. Tan, *Nanoscale* **4** (2012) 5954.

245. N. Sh. Lebedeva, *Russian Chem. Bull. Intern. Ed.* **53** (2004) 2674.

246. M.J. Stillman, T. Nyokong, in C.C. Leznoff, A.B.P. Lever (Eds), Phthalocyanine: Properties and Applications, vol 1, VCH Publisher, New York, 1989.

247. H. Przywarska-Boniecka, L. Ostropolska, *J. Inorg. Biochem.* **16** (1982) 183.

248. C. Stoll, C. Gehring, K. Schubert, M. Zanella, W. J. Parak and F. Lisdat, *Biosens. Bioelectron.* **24** (2008) 260.

249. C. Park, T.H. Yoon, *Colloids Surf., B: Biointerfaces* **75** (2010) 472.

250. S. Khene, T. Nyokong, *Microchem. J.* **99** (2011) 478.

251. L. Qin, W. Ma, D. Li, Y. Li, X. Chen, H. Kraatz, T.D. James, Y. Long, *Chem. Eur. J.* **17** (2011) 5262.

252. B. Tang, L.Zhang, J. Hu, P. Li, H. Zhang, Y. Zhao, *Anal. Chim. Acta.* **502** (2004) 125.

253. X. Wang, M. Han, J. Bao, W. Tu, Z. Dai, *Anal. Chim. Acta* **717** (2012) 61.

254. Y. Xia, J. Wang, Y. Zhang, L. Song, J. Je, G. Yang, K. Tan, *Nanoscale* **4** (2012) 5954 .

255. J. Chen, A. Zheng, Y. Gao, C. He, G. Wu, Y. Chen, X. Kai, C. Zhu, *Spectrochim. Acta Part A* **69** (2008) 1044.

256. K. Akiba, R. Nadano, W. Satoh, Y. Yamamoto, S. Nagase, Z. Ou, X. Tan, K.M. Kadish, *Inorg. Chem.* **40** (2001) 5553.

257. B. Paramanik, S. Bhattacharyya, A. Patra, *Chem. Eur. J.* **19** (2013) 5980-5987.

258. J. Liu, X. Yang, K. Wang, R. Yang, H. Ji, L. Yang, C. Wu, *Chem. Commun.* **47** (2011) 935.

259. M. Xue, X. Wang, L. Duan, W. Gao, L. Ji, B. Tang, *Biosensen. Bioelectron.* **36** *(*2012) 168-173.

260. H. Xu, Z. Wang, Y. Li, S. Ma, P. Hu, X. Zhong, *Analyst* **138** (2013) 2181.

261. M-r. Chao, Y-Z. Chang, J-L. Chen, *Biosens. Bioelectron.* **42** (2013) 397.

262. G. Fang, M. Xu, F. Zeng, S. Wu, *Langmuir* **26** (2010) 17764.

263. A.N. Lang, L. Wang, H-Q. Chen, B-B. Qian, B. Ling, J. Fu, *Talanta* **81** (2010) 438.

264. C.F. van Nostrum, F.B.G. Benneker, H. Brussaard, H. Kooijman, N. Veldman. A.L. Spek, J. Schoonman, M.C. Feiters, J.M Nolte, *lnorg. Chem.* **35** 959.

265. Y. Zhou, M. Deng, Y. Du,S. Yan, R. Huang, X. Weng, C. Yang, X. Zhang, X. Zhou, *Analyst* **136** (2011) 955-961.